

# Biochemical and Cellular Studies of Vertebrate Globins

By

Shun Wilford Tse

Thesis submitted for the degree of  
Doctor of Philosophy  
School of Biological Sciences  
University of East Anglia  
September 2015

© This copy of the thesis has been supplied on condition that anyone who consults it is understood to recognise that its copyright rests with the author and that no quotations from the thesis, nor any information derived there-from may be published without the author's prior, written consent.

## Abstract

Human cytoglobin is a small heme-containing protein in the globin superfamily with a wide range of tissue and organ distribution. Although several cellular functions have been proposed for cytoglobin, the exact physiological function is still not fully defined. Recently, cytoglobin has been implicated to have a regulatory role in cancer cells to control cell proliferation and migration depending on cellular oxygen level. In order to gain a better understanding of a structure-to-function relationship of cytoglobin as a heme-protein and to evaluate its possible physiological function(s) in cancer cells, a combination of techniques, including protein engineering and advanced spectroscopies, was deployed. In this study, recombinant human cytoglobin purified from *E.coli* was purified as a monomeric protein, but displayed a dimeric property in solution. An intra-molecular disulphide bond is formed within the protein which has a redox potential at *ca* -280 mV. Advanced spectroscopic studies confirmed a low-spin bis-histidyl heme in cytoglobin in both ferric and ferrous state regardless of the state of the disulphide bond. Furthermore, nitrite reductase activity in globins was investigated in detail using myoglobin as a model to explore the biochemical basis of the distal histidine residue in determining activity. The distal histidine was demonstrated by both kinetics and advanced spectroscopic analyses that it stabilises the binding of nitrite ligand and directs the bound nitrite to a globin-specific nitrito, or *n*-bound orientation. Accessibility of nitrite to ferric cytoglobin is restricted by the distal histidine which may explain a rather slow nitrite reduction by cytoglobin. Probing the heme accessibility in cytoglobin using fluoride in the presence of GSH revealed a possible redox-linked control of the disulphide bond by GSH in the cells. Finally, a new method of pull-down assays using a strep-tagged cytoglobin were developed and performed in an attempt to search for any putative binding partner(s) of cytoglobin in renal cancer cells in which two potential protein partners are found to be co-eluted with cytoglobin in the experiments.

## **Acknowledgement**

First and foremost, I would like to express my sincere gratitude to my primary supervisor, Dr. Nick Watmough, who has never ceased to inspire me to think analytically and critically over the past four years. Equally, I would like to show my greatest appreciation to my secondary supervisor, Dr. Jelena Gavrilovic for her help, care and support throughout these years, especially at the time near the submission of this thesis. I would not be able to finish this thesis without their advice and guidance. It's been such a great pleasure working with them.

I would like to thank Dr. Myles Cheesman, Dr. Fraser Macmillan, Dr. Jason Crack (all from the School of Chemistry) and Dr. Damon Bevan (from the School of Biological Sciences) for their technical support, result interpretations and useful discussions on room-temperature MCD, Low-temperature X-band EPR, LCMS and qRT-PCR experiments, respectively. I would also like to thank Dr. Andy Gates for his contributions to the supervisory team.

Also, my life in UEA would not be so enjoyable without a bunch of great colleagues who are so friendly and helpful all the time, especially those from BIO 2.30. Pints and football in the union bar with them was always something I have enjoyed the most. So, thank you so much!

Special thanks go to my parents for allowing me to pursue my dream to become a scientist as well as their unlimited love, support and understanding throughout my life. No words can ever describe how much I love them! x

## Table of content

### Chapter 1: General Introduction

1.1 The Globin Family .....	1
1.1.1 Vertebrate Globins.....	1
1.1.2 Discovery of Cytoglobin.....	3
1.2 The Human <i>CYGB</i> gene.....	3
1.2.1 Organisation of <i>CYGB</i> gene .....	3
1.2.2 Promoter Sequence of <i>CYGB</i> gene.....	5
1.2.3 Regulation of <i>CYGB</i> gene Expression.....	5
1.2.4 Molecular Evolution of Cytoglobin .....	6
1.3 Protein Structure of Human Cytoglobin .....	9
1.3.1 Structural Overviews of Cytoglobin.....	9
1.3.2 Oligomeric State .....	11
1.3.3 Heme Coordination.....	12
1.3.4 Exogenous Ligand Binding.....	13
1.4 Distribution of Cytoglobin in Human Tissues .....	18
1.4.1 Physiology of Cytoglobin .....	18
1.4.2 Organ and Tissue Distribution .....	18
1.4.3 Subcellular Localisation.....	19
1.5 Putative Physiological Functions of Cytoglobin .....	20
1.5.1 A Role in Oxygen Storage and Delivery.....	20
1.5.2 A Role in Nitric Oxide Scavenging and Signalling.....	21
1.5.3 A Role in Cellular Oxidative Stress .....	22
1.5.4 A Role in Cellular Hypoxia .....	23
1.5.5 A Role in Collagen Synthesis.....	25
1.6 Cytoglobin as a Tumour Suppressor Gene in Cancer .....	27
1.6.1 A Link Between Cytoglobin and Cancer.....	27
1.6.2 Hypermethylation of the <i>CYGB</i> Promoter Region.....	27
1.6.3 Tumour Suppression Properties of Cytoglobin .....	28
1.6.4 Stress Responsive Properties of Cytoglobin in Cancer cells .....	29
1.7 Hypoxia .....	30
1.7.1 Hypoxia in Humans .....	30
1.7.2 Hypoxia Inducible Factor (HIF) .....	31

1.7.3 von Hippel Lindau Protein (pVHL) .....	31
1.7.4 Regulation of Hypoxia Inducible Factor .....	32
1. 8 Aims .....	35

## **Chapter 2: Materials and Methods**

2.1 Bacterial Cultivation and Strains.....	36
2.1.1 Culture Media and Antibiotics .....	36
2.1.2 Bacterial Strains .....	36
2.2 General Protein Biochemistry .....	37
2.2.1 Determination of Protein Concentration.....	37
2.2.2 Analysis of Proteins by SDS-PAGE and Non-Reducing SDS-PAGE .....	38
2.2.3 Liquid Chromatography Mass Spectrometry (LCMS) .....	40
2.2.4 Analytical Gel Filtration .....	40
2.3 General Molecular Biology Techniques .....	41
2.3.1 Plasmid DNA Extractions.....	41
2.3.2 Preparation of Competent <i>E.coli</i> Cells.....	41
2.3.3 Plasmid Transformations .....	42
2.3.4 Restriction Digestions.....	43
2.3.5 Site-directed Mutagenesis .....	43
2.3.6 Agarose Gel Electrophoresis .....	44
2.4 Expression Vectors of Recombinant Globins .....	45
2.4.1 Expression Vectors of Recombinant Human Cytooglobin .....	45
2.4.2 Expression Vectors of Recombinant Sperm Whale Myoglobin .....	47
2.4.3 Construction of Expression Vectors for the Cys38 and Cys83 Variants of Cytooglobin.....	47
2.4.4 Construction of Expression Vectors for the His81 Variants of Cytooglobin.....	49
2.4.5 Construction of Expression Vectors for the Strep-tagged Cytooglobin .....	49
2.4.6 Construction of Expression Vectors for the H93K Variant of Sperm Whale Myoglobin .....	53
2.5 Expression and Purification of Human Recombinant Cytooglobin and Variants... 54	
2.5.1 Expression of Recombinant Human Cytooglobin in <i>E.coli</i> .....	54
2.5.2 Extraction of Recombinant Human Cytooglobin .....	54
2.5.3 Heme Reconstitution of Apo-cytooglobin Protein in the Cell Lysate .....	55
2.5.4 Refolding and Reconstitution of Recombinant Cytooglobin from Inclusion	

Bodies .....	56
2.5.5 Purification of Recombinant Cytoglobin from Cell Lysate .....	56
2.5.6 Purification of Recombinant Cytoglobin from Inclusion Bodies.....	58
2.5.7 Expression and Purification of Recombinant Cytoglobin Variants .....	59
2.5.8 Expression and Purification of Strep-tagged Recombinant Cytoglobin.....	59
2.6 Expression and Purification of Sperm Whale Myoglobin and Variants .....	61
2.6.1 Expression of Sperm Whale Myoglobin in <i>E.coli</i> .....	61
2.6.2 Extraction of Sperm Whale Myoglobin.....	61
2.6.3 Purification of Sperm Whale Myoglobin.....	62
2.7 Spectroscopic Characterisation of Globins.....	64
2.7.1 Electronic Adsorption Spectroscopy .....	64
2.7.2 Stopped-Flow Spectroscopy.....	66
2.7.3 Magnetic Circular Dichroism (MCD) Spectroscopy.....	67
2.7.4 Electron Paramagnetic Resonance (EPR) spectroscopy .....	68
2.7.5 Data Handling.....	69
2.8 Independent Reduction of Heme and Disulphide Bond in Cytoglobin .....	71
2.8.1. Reduction of Heme in Cytoglobin .....	71
2.8.2. Reduction of Disulphide Bond in Cytoglobin.....	72
2.9 Verification of RCC4 cells.....	73
2.9.1 Cell Culture of RCC4 cells.....	73
2.9.2 MTT-Cell Viability Assay .....	74
2.9.3 Protein Quantification .....	74
2.9.4 Western Blot.....	75
2.9.5 Quantitative Reverse Transcription Polymerase Chain Reaction (qRT-PCR).....	76
2.10 Identification of Putative Binding Partner(s) of Cytoglobin in RCC4 Cells .....	77
2.10.1 Preparation of Cell Lysate .....	77
2.10.2 Pull Down Assay .....	78

### **Chapter 3: Characterisation of Human Recombinant Cytoglobin**

3.1 Introduction: .....	80
3.2 Results .....	83
3.2.1 Purification of Human Recombinant Cytoglobin .....	83
3.2.2 The State of the Disulphide Bond in Recombinant Cytoglobin .....	89

3.2.3 Analytical Gel Filtration of Recombinant Cytoglobin .....	91
3.2.4 Mid-point Potential of Disulphide Bond.....	96
3.2.5 Principle Redox States of Cytoglobin .....	99
3.3 Discussion.....	108

## **Chapter 4: Redox Linked Ligand Accessibility of Cytoglobin**

4.1 Introduction .....	114
4.2 Results .....	117
4.2.1 Spectroscopic Characterisation of Cytoglobin in the Ferrous State.....	117
4.2.2 Spectroscopic Characterisation on Cytoglobin C38S and C83S variants in the Ferric State .....	127
4.2.3 Spectroscopic Characterisation of Ferrous Cytoglobin with Different States of Disulphide Bond .....	132
4.2.4 Spectroscopic Characterisation of Carbomonoxy Cytoglobin and Cysteine Variants.....	138
4.2.5 Heme Accessibility for Exogeneous Ligands in Ferric Cytoglobin .....	141
4.2.6 Effect of GSH on the Heme Accessibility in Cytoglobin .....	145
4.3 Discussion.....	150

## **Chapter 5: Nitrite Reductase Activity of Globins**

5.1 Introduction .....	153
5.2 Results .....	155
5.2.1 Nitrite Reduction by Sperm Whale Myoglobin .....	155
5.2.2 Nitrite Binding to Ferric Myoglobin.....	161
5.2.3 Spectroscopic Analysis of Nitrite Binding to Wild-type Sperm Whale Myoglobin .....	165
5.2.4 Spectroscopic Analysis of the Nitrite-bound Forms of Representative Distal Pocket Variants (H64V and H64A) of Sperm Whale Myoglobin.....	168
5.2.5 Summary of Nitrite Binding to Myoglobin and H64 variants.....	176
5.2.6 Nitrite Reduction by Myoglobin H93K Variant.....	177
5.2.7 Spectroscopic Analysis of Nitrite Binding to Ferric H93K Variant.....	182
5.2.8 Nitrite Reductase Activity of Cytoglobin.....	188
5.2.9 Nitrite Binding to Ferric Cytoglobin .....	188
5.3 Discussion.....	193

## **Chapter 6: Putative Binding Partner(s) of Cytoglobin in Cancer Cells**

6.1 Introduction .....	197
6.2 Results .....	199
6.2.1 Verification of RCC4 Cells .....	199
6.2.2 Restoration of <i>CYGB</i> gene Expression in RCC4 Cells by 5-aza-2'- deoxycytidine.....	201
6.2.3 Validation of Strep-tagged Cytoglobin .....	209
6.2.4 Pull Down Assays in RCC4 Cells.....	216
6.3 Discussion.....	223

## **Chapter 7: General discussion**

7.1 Oligomeric State and Disulphide bond of Cytoglobin .....	228
7.2 S-glutathionylation of Cys83 and Oxidative Stress.....	230
7.3 Role of Cytoglobin in Metastasis .....	237

<b>References:</b> .....	240
--------------------------	-----

## **Appendix**

## Abbreviations

Cgb	Cytoglobin
CO	Carbon monoxide
Cys	Cysteine (also as C)
DTT	Dithiothreitol
EPR	Electron paramagnetic resonance
Gln	Glutamine (also as Q)
GSH	L-glutathione reduced
GSSG	Glutathione disulphide
HIF	Hypoxia inducible factor
His	Histidine (also as H)
H <sub>2</sub> O	Water molecule
LB	Luria Bertani broth
LCMS	Liquid chromatography mass spectrometry
Lys	Lysine (also as K)
MCD	Magnetic circular dichroism
MW	Molecular weight
NADH	Reduced nicotinamide adenine dinucleotide
NO	Nitric oxide
oxDTT	Trans-4,5-Dihydroxy-1,2,-dithiane (also as oxidised DTT)
PCA	Protocatechuate acid
PCD	Protocatechuate dioxygenase
PMS	Phenazine methosulfate
Ser	Serine (also as S)
rpm	Revolutions per minutes
RT	Room-temperature
TCEP	Tris-(2-carboxylethyl) phosphine
VHL	Von Hippel Lindau
WT	Wild-type



# Chapter 1: General Introduction

## 1.1 The Globin Family

### 1.1.1 Vertebrate Globins

Globins are small heme-containing globular proteins which can reversibly bind oxygen molecules via the heme iron. A typical globin, such as myoglobin, comprises seven or eight  $\alpha$ -helices linked by some non-helical segments and fold into a “three-over-three  $\alpha$ -helical sandwich” (Figure 1.1A) (Perutz, 1979). Globins have been identified in all three Kingdoms of Life (Hardison, 1996, Weber and Vinogradov, 2001). In the last fifteen years, more and more globins were identified which have unprecedented physiological functions. The diversity of the globin superfamily suggests that globins may have more diverse roles in cells than originally thought to deliver oxygen to support aerobic cellular metabolism (reviewed in Burmester and Hankeln, 2014).

To date, a total of eight different globins have been identified in vertebrate species, of which, five have been found in humans; haemoglobin (Hb), myoglobin (Mb), neuroglobin (Ngb), cytoglobin (Cgb) and androglobin (Adgb) (Burmester and Hankeln, 2014). The most intensively studied and best characterised vertebrate globins are haemoglobin which is a  $\alpha_2\beta_2$  tetramer found in red blood cells which transports oxygen within the circulatory system (Perutz, 1990) and myoglobin which is a monomeric protein predominantly found in cardiac and skeletal muscle cells where it facilitates oxygen diffusion to the cells and acts as an oxygen reservoir in the muscle cells (Wittenberg & Wittenberg, 1989). Both cytoglobin and neuroglobin were discovered within the last 15 years but their cellular functions remain unclear. Although, structure-wise, cytoglobin and neuroglobin are undoubtedly regarded as members of the globin family, they share only *ca* 20% sequence identity with myoglobin (Trent and Hargrove, 2002). Cytoglobin is ubiquitously expressed in many tissues, including heart, liver and kidney (Burmester et al., 2002 and Trent and Hargrove, 2002). Neuroglobin has a more specific expression profile and is predominately expressed in brain (Burmester et al., 2000) and retina

(Schmidt et al., 2003). The different expression patterns of individual globins in humans suggested a wide range of different physiological functions (Weber and Fago, 2004; Burmester and Hankeln, 2014). Despite the suggested physiological and functional differences, cytoglobin and neuroglobin are similar, to some extent, with other vertebrate globins in terms of the protein scaffold and the local architecture of the heme pocket. Some key amino acid residues which are essential to stabilising the heme cofactor in globins, such as PheCD1 which is the phenylalanine residue at the first position of the loop between helix C and D, HisE7 which is the histidine residue at the seventh position of E helix at the distal heme pocket and HisF8 which is the histidine residue at the eighth position of F helix at the proximal heme pocket are well conserved among them (Figure 1.1B).

The immediate environment of the heme cofactor varies within the globin family. For instance the coordination of the heme iron in haemoglobin and myoglobin is penta-coordinate in the absence of exogenous ligands; that is to say the heme iron is bound by four pyrrole nitrogen atoms in the same plane in the porphyrin ring and only one protein derived axial ligand leaving the opposite axial site in the distal heme pocket available for the binding of exogenous ligands (Figure 1.1B). In contrast, the heme iron in both cytoglobin and neuroglobin is hexa-coordinate with the heme iron being coordinated by two opposite axial ligands (de Sanctis et al., 2004; Dewilde et al., 2001; Sawai et al., 2003; Sugimoto et al., 2004). Although cytoglobin and neuroglobin were the first examples of the hexa-coordinated globins to be described in vertebrates, there had previously been described in plants, such as the non-symbiotic hemoglobin which transports oxygen in the plant tissues (Appleby et al., 1983; Hardison, 1998; Kundu et al., 2003). Subsequent examples of hexa-coordinate globins have also been described in lower animals and bacteria (Burmester et al., 2002; Burmester and Hankeln, 2014; Kakar et al., 2010; Kundu et al., 2003; Trent and Hargrove, 2002)

### **1.1.2 Discovery of Cytoglobin**

Cytoglobin was first identified in a proteomic screen of fibrotic liver in rats where its expression is up-regulated and was dubbed as “stellate cell activation-associated protein” (STAP) as it was postulated to play a pivotal role in development of fibrosis (Kawada et al., 2001). Later a human homologue of STAP of unknown function was discovered and shown to be present in almost all tissues (Burmester et al., 2002; Trent and Hargrove, 2002), and to be significantly up-regulated under low oxygen conditions (i.e. hypoxia) suggesting that cytoglobin expression is oxygen-dependent (Schmidt et al., 2004). The discovery of this new type of widely expressed globin, together with the subsequent discovery of other globin types, has allowed researchers to gain new insights into the evolution and physiological roles of globins in nature.

## **1.2 The Human *CYGB* gene**

### **1.2.1 Organisation of *CYGB* gene**

The human genome contains a single copy of *CYGB* gene which is 1.9 kb in length and located at chromosome 17q25.3. Sequencing results have showed that the *CYGB* gene contains four exons which contribute to an open reading frame of 573 base pairs and encode 190 amino acid residues. The organisation of the *CYGB* gene is different from other globins in which the *CYGB* gene is separated by three introns at position B12-2 (the 12<sup>th</sup> amino acid of Helix B, between codon position 2 and 3), G7-0 and HC11-2, instead of only two Introns at position B12-2 and G7-0 which are typically found in other globins (Burmester et al., 2002; Trent and Hargrove, 2002). Hence the 3<sup>rd</sup> intron at HC11-2 and the 4<sup>th</sup> exon which are close to the 3' end of the gene, are exclusively found in mammalian *CYGB* gene (Burmester et al., 2002; Burmester et al., 2004; Pesce et al., 2002). However, the origin and function of the additional fragment of the gene are still not clear (Figure 1.2A)

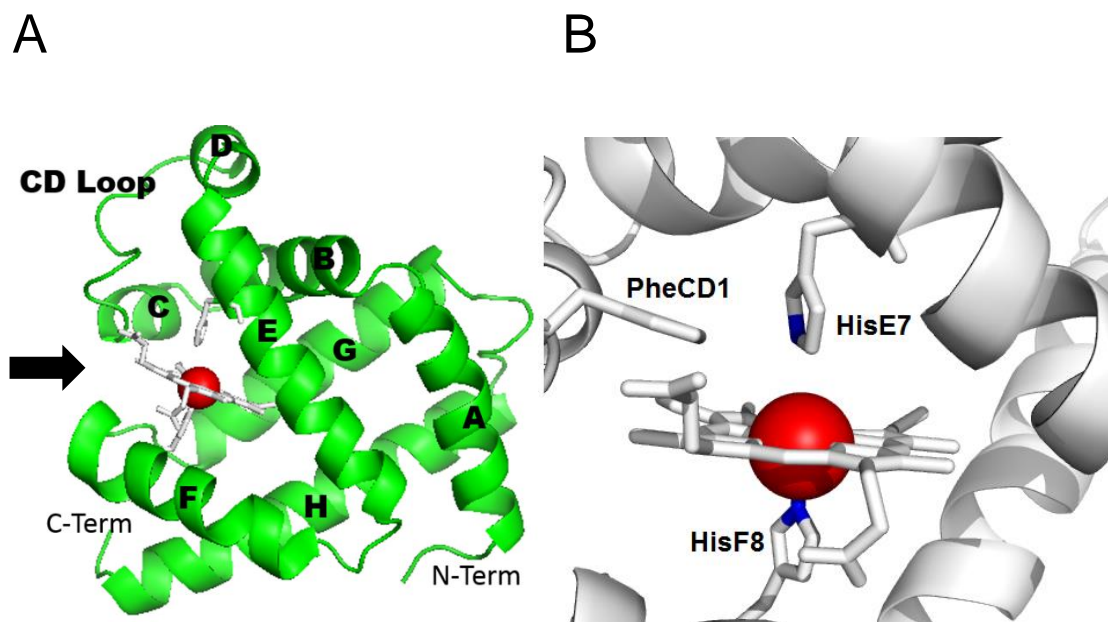


**Figure 1.1 The X-ray structure of myoglobin (A)** A cartoon representing the structure of myoglobin showing the characteristic “three-over-three  $\alpha$ -helical folding” in which core helices A, E and F were placed above helices B, G and H, or vice versa, seen from an angle as the same plane of the heme porphyrin indicated by a black arrow. The red sphere represents the heme iron. Helices are usually conventionally labelled from A to H starting from the N-terminus and linked by non-helical segments as shown as ribbon in the figure. **(B)** The key amino acid residues in the heme pocket of myoglobin which are conserved amongst the globin family. PheCD1 – the phenylalanine residue at the first position at loop region between helix C and D, HisE7 – the histidine residue at the seventh position on the helix E and HisF8 – the histidine at the eighth position on the helix F. (redrawn from PDB file 1A6K using Pymol v1.3)

### 1.2.2 Promoter Sequence of *CYGB* gene

Sequence analysis of the *CYGB* gene has revealed that *CYGB* gene promoter is a 1.4kb-long GC rich region in which no TATA box is found. The GC content of this region has been estimated to be around 60% (Burmester et al., 2002; Guo et al., 2006; Wystub et al., 2004). The minimal promoter region for transcription initiation of *CYGB* gene has been found to be between -1113 to -10 upstream from starting codon ATG (Guo et al., 2006). Several binding sites of different transcription factors were identified *in silico* and subsequently confirmed by reporter gene assays within the promoter region. These include Hypoxia responsive elements (HREs), binding sites for stimulatory protein 1 (SP1) as well as cellular erythroblastosis virus E26 homolog 1 (cETS-1). Moreover, several potential regulatory sequences for some other transcription factors, such as activator proteins (AP1 & AP2), nuclear factors (NFκB), CCAAT/enhancer binding protein (C/EBP), and Krüppel-like zinc finger proteins, have also been suggested to be present in both the promoter region and the non-coding sequences within the first intron of the *CYGB* gene (Figure 1.2B; Table 1.1) (Guo et al., 2006, 2007; Wystub et al., 2004).

### 1.2.3 Regulation of *CYGB* gene Expression

Since the promoter region of *CYGB* gene is well defined, it is clear that *CYGB* gene is a stress responsive gene that is up-regulated under various cellular stress conditions, such as hypoxia and oxidative stress. Reporter gene and DNA binding assays for c-ETS-1 and SP-1 proteins confirmed that binding of one cETS-1 and three SP1 proteins within the minimal promoter region is essential for activation of *CYGB* gene transcription (Guo et al., 2006). Under hypoxic conditions, a number of studies have demonstrated that *CYGB* gene expression is up-regulated both *in vitro* and *in vivo* (Fordel et al., 2004b; Gorr et al., 2011; Guo et al., 2007; Li et al., 2006; Schmidt et al., 2004; Shaw et al., 2009; Wystub et al., 2004). The up-regulation of *CYGB* gene expression during hypoxia was first suggested by the discovery of hypoxia responsive elements (HRE) motifs in the promoter sequence (Wystub et al., 2004).

Increased *CYGB* transcription under the control of the Hypoxia-inducible factor (HIF) pathway was further confirmed by real time PCR analysis *in vivo* study (Fordel et al., 2004a). Shortly after, site-directed mutagenesis, Chromatin immunoprecipitation (ChIP) assays and western blot showed that direct and precise binding of HIF-1 to the HRE motifs at positions -141, -144 and -488 within the promoter region is essential for the up-regulation of *CYGB* gene under hypoxia (Guo et al., 2007) (Figure 1.2).

#### **1.2.4 Molecular Evolution of Cytoglobin**

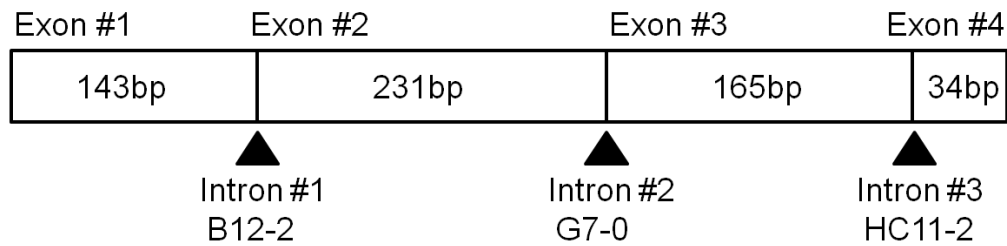
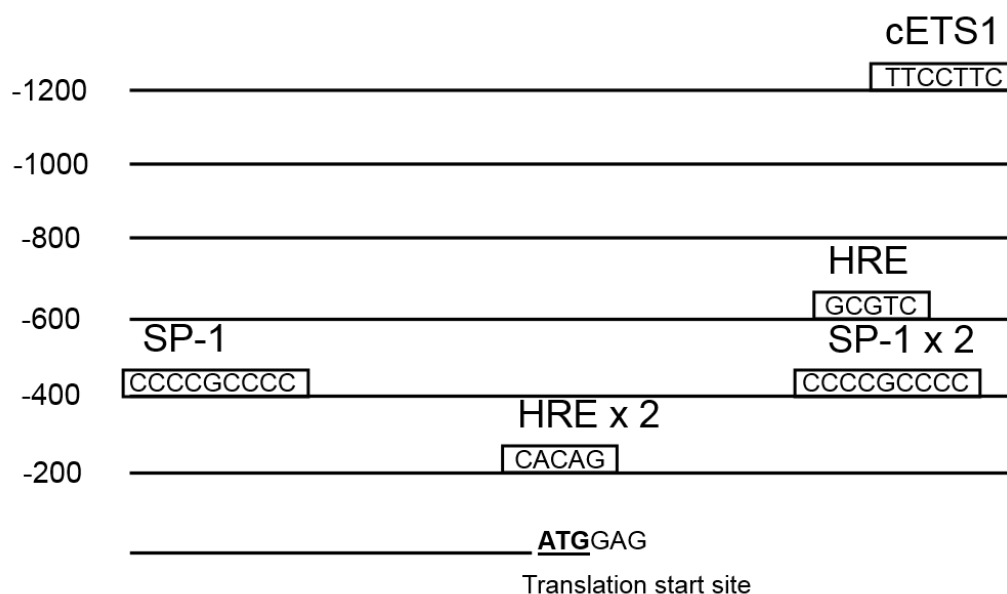
Cytoglobin is believed to be present in all vertebrates (Burmester and Hankeln, 2014). Amino acid sequence alignments between the human and mouse cytoglobin revealed that they share approximately 93% identity suggesting that the *CYGB* gene is very well conserved within mammals. However, only about 49% identity was found when human cytoglobin is compared to the zebrafish cytoglobin. The fourth exon of the gene was missing in zebra fish's *CYGB* gene suggesting that the additional exon sequence may have been acquired during evolution of tetrapod (Burmester et al., 2002). In the most recent model of vertebrate globin evolution proposed by Bumester and Hankeln, it is suggested that ancient vertebrates most likely possessed four distinctive types of globins; androglobin, neuroglobin, globin X and the one which is generally present in all the tissues. Cytoglobin is suggested to be of ancient origin which is separated from a common ancestor of haemoglobin and myoglobin during the development of vertebrates (Burmester and Hankeln, 2014).

Transcription factors	<b>SP1</b> <sup>1</sup>	<b>cETS-1</b> <sup>2</sup>	<b>HIF</b> <sup>3</sup>	<b>NFκB</b> <sup>4</sup>	<b>AP1</b> <sup>5</sup>
DNA Binding sites	Rich GC region/ GC box	5'-GGAW-3'*	5'-RCGTG-3' *	5'-GGGRNW YYCC-3' *	5'-TGAPTCA-3' *
Class of the regulatory elements	Sp/KLF family	ETS family	HIF family	NFκB family	Fos /Jun families
Cellular signal	Physiological and pathological stimuli	Upregulated by VEGF in response to hypoxia	Hypoxia	Oxidative stress; cytokines	Cytokines; bacterial and viral infection
Target genes' functions	Regulate nucleic acid biosynthesis, cell cycle, proliferation	Control tumor suppression, apoptosis, differentiation, angiogenesis and metastasis	Regulate metabolism, oxygen supply and other adaptive responses under hypoxia	Regulate cell proliferation, inflammatory response and immune response	Regulate cell proliferation, differentiation and apoptosis

**Table 1.1 Regulatory elements in promoter sequence of *CYGB* gene**

1. Refer to review article by Solomon et al. 2008
2. Refer to review article by Oikawa, 2004
3. Refer to review article by Semenza, 2000
4. Refer to review article by Gilmore, 2006
5. Refer to Zhou et al., 2005

\* For DNA residues, P = C/G, R = A/G, N = any nucleotide, W = A/T and Y = C/T.

**A****B**

**Figure 1.2 Representation of the organisation of the human *CYGB* gene. (A)** Diagram of the gene structure of *CYGB* gene shows that the *CYGB* gene is separated by three introns at position B12-2 (between the codon position 2 and 3 of the 12<sup>th</sup> amino acid residue of helix B), G7-0 (before the codon of the 7<sup>th</sup> amino acid residue of helix G) and HC11-2 (between the codon position 2 and 3 of the 11<sup>th</sup> amino acid residue after helix H) indicated by (▲) **(B)** Approximate locations of the regulatory elements on the promoter region about -1200 bp upstream of the translation start site of human *CYGB* gene. HRE (Hypoxia responsive elements); Sp1 (Stimulatory protein 1); cETS-1 (cellular erythroblastosis virus E26 homolog-1).

## 1.3 Protein Structure of Human Cytoglobin

### 1.3.1 Structural Overviews of Cytoglobin

The human cytoglobin is made up of 190 amino acids and has a molecular weight of about 21 kDa. Although the sequence identity of between cytoglobin and other vertebrate globins is low, key amino acid residues which help stabilizing the heme cofactor, such as the HisE7, HisF8 and PheCD1, are very well conserved within the family as shown in the Figure 1.3A. The overall structure of core region of cytoglobin also highly resembles other globins. Far-UV circular dichroism (CD) spectroscopy has indicated that the  $\alpha$ -helical content in cytoglobin is comparable to that of myoglobin (Sawai et al., 2003) which is also folded into the “three-over-three  $\alpha$ -helical sandwich” that has been described in various X-ray structures, although the X-ray structure of cytoglobin appears to be a dimer (Figure 1.3B and table 1.2).

Beside the core protein scaffold, amino acid sequence alignment has also revealed that the human cytoglobin is longer than other vertebrate globins in the family due to the presence of twenty amino acid sequence extensions at both N- and C- termini (Figure 1.3). The X-ray structure which includes the extended N- and C-termini in the human cytoglobin has been resolved at 1.68 Å by Makino and colleagues. In that X-ray structure the extended sequences at the N-terminal region is described to form a pre-A helical structure termed “Z helix” that was observed in one of the subunits (subunit B), while an ordered loop structure is found at the C-terminal region of the other subunit (subunit A) (Makino et al., 2006; refer to table 1.2). Globins having extended sequences at both or either ends of the protein are not uncommon. They have been found in some of the globins in primitive vertebrates, invertebrates and bacteria. However, the function of these extended sequences is still unknown (Bolognesi et al., 1997; Hardison, 1998).

<b>Authors:</b>	de Sanctis et al. 2004	Sugimoto et al. 2004	Makino et al. 2006	Makino et al. 2011	Gabba et al. 2013
<b>PDB file:</b>	1UT0	1V5H	2DC3	3AG0	4B3W
<b>Resolution:</b>	2.10 Å	2.40 Å	1.68 Å	2.60 Å	2.80 Å
<b>Protein:</b>	Human Cytoglobin variant (Cys38Ser and Cys83Ser double mutations)	6xHis-tagged human Cytoglobin wild-type	6xHis-tagged human Cytoglobin wild-type	6xHis-tagged human Cytoglobin wild-type	Human Cytoglobin variant (Cys38Ser, Cys83Ser and His81Gln triple mutations)
<b>Heme-coordination:</b>	Hexa- and Penta-coordination	Hexa-coordination	Hexa-coordination	Hexa-coordination	Penta-coordination
<b>Oxidation state:</b>	Ferric	Ferric	Ferric	Ferrous	Ferric
<b>Exogenous ligands?</b>	Nil	Nil	Nil	Carbon monoxide	Cyanide
<b>Quaternary structure:</b>	Homo-dimer	Homo-dimer	Homo-dimer	Monomer	Homo-dimer
<b>Dimerization:</b>	G-,H-helix and BC hinge region	Inter-subunit disulphide (B and E-helix)	Inter-subunit disulphide (B and E-helix)	N/A	Similar to 1UT0
<b>Remarks:</b>	1. 45% occupancy of subunit B displays “open” conformation (penta-coordination) 2. Disordered C- and N-terminals	1. A mixture of different oligomeric states present in the purified Cytoglobin in solution 2. Disordered C- and N-terminals	1. N-terminal was shown to be an additional helix – Z helix 2. C-terminal was shown to be an ordered loop structure	1. Cytoglobin was crystallised in the presence of sodium dithionite and under CO atmosphere 2. Conformational changes around the heme distal pocket	1. Cyanide ion doesn't coordinate to the heme iron. 2. Position of CD-loop and E-helix differ from those in 1UT0

**Table 1.2 X-ray structures of cytoglobin in the literature**

### 1.3.2 Oligomeric State

The physiologically relevant oligomeric state of cytoglobin has not yet been clearly defined. Reported results from crystallography studies were not always consistent with studies in protein solution. In the crystallography studies on ferric cytoglobin so far, all the X-ray structures of cytoglobin were resolved as a homo-dimer (Table 1.2). Moreover, different dimerization interfaces and interactions between the two subunits were described, either through a direct contact via two intermolecular disulphide bonds (Makino et al., 2006; Sugimoto et al., 2004) or via hydrophobic and electrostatic interactions between the dimerization surfaces (de Sanctis et al., 2004).

Studies of recombinant human cytoglobin in the solution also revealed a mixed results in the oligomeric states. Studies involving a combination of different chromatographic analyses suggested that the recombinant cytoglobin could exist as dimeric and multimeric states which linked are by inter-molecular disulphide bonds. Treatment of the dimer and multimer with reducing agents abolished the links between the multimeric states indicating the presence of inter-molecular disulphide bond (Sugimoto et al., 2004; Beckerson et al., 2014; Tsujino et al., 2014). On the other hand, in the study done by Hamdane and coworkers, the recombinant cytoglobin existed as a dimer, but neither reduction by reducing agents or dilution caused a transition to the monomeric form indicated that the dimerization was not via inter-subunit disulphide bond, but in an equilibrium (Hamdane et al., 2003).

However, Lechauve and colleagues showed that, using a combination of chromatographic and light scattering techniques, recombinant cytoglobin in the solution was detected predominately as monomer (95%) with the rest of the protein in the dimeric form in the absence of disulphide reducing agent. Moreover, they also explained that the apparent dimer-like behaviour of cytoglobin in the previously reported gel filtration experiments is probably due to the presence of the extended sequences at both N- and C-termini which affect the overall hydrodynamic radius of cytoglobin as the truncated form of recombinant cytoglobin

without the extensions at both ends seems to behave as a monomer in size exclusion chromatography (Hamdane et al., 2003; Lechauve et al., 2010).

### **1.3.3 Heme Coordination**

Comparison of the X-ray structure of human cytoglobin and myoglobin has shown that one of the major differences between the two globins is found at the distal heme pocket where the histidine residue (His81) on the E-helix in cytoglobin locates closer to the heme iron than that in myoglobin which coordinates to the heme iron at the axial position in the absence of exogenous ligands (Figure 1.4). The observed hexa-coordination in the X-ray structures of cytoglobin was confirmed by a number of advanced spectroscopic characterisations at the heme pocket. The absorption spectra of cytoglobin at both ferric and ferrous states are highly similar with other known globins that display hexa-coordinate heme, such as neuroglobin, and are different from their penta-coordinate counterparts, such as myoglobin (Dewilde et al., 2001; Trent and Hargrove, 2002). Furthermore, analyses of the microenvironment of the heme pocket by both resonance Raman spectroscopy and X-band EPR spectroscopy have revealed that the heme iron of the ferric cytoglobin is at a low-spin state with the distal His81 residue serves as the axial ligand occupying the sixth coordination site at the distal heme pocket in the absence of exogenous ligands (Sawai et al., 2003; Vinck et al., 2004; Van Doorslaer et al., 2004).

Interestingly, in the X-ray structure of cytoglobin described by de Sanctis and colleagues in which the two cysteine residues were replaced by serine residues, about half of the population of heme pockets in the monomeric subunit (B subunit) display an alternative “Open” conformation where the heme coordination is said to be penta-coordinate in the absence of any exogenous ligands. Comparison between the “Open” and the “Closed” conformation has revealed that the distal Histidine residue as well as a certain part of the E-helix was described to displace from its original position in the “Open” conformation (de Sanctis et al., 2004). A

similar alternative conformation was also described in a recent X-ray structure of cytoglobin which bears a histidine to glutamine mutation (H81Q) at the distal heme pocket (Gabba et al., 2013). However, in the X-ray structure reported by Makino and colleagues, the distal histidine in the carbon monoxide complex of cytoglobin displays a completely different orientation from the one described by de Sanctis and colleagues, in which the distal histidine is completely out of the distal heme pocket (Makino et al., 2010).

It is noteworthy that the two cysteine residues were replaced by serine in the de Sanctis's structure, thus neither an inter-molecular nor intra-molecular disulphide bond was formed. Whereas in the Makino's structure, the two cysteine residues were intact, thus the dimer was stabilised by the inter-molecular disulphide bond. Therefore, it may suggest that the heme coordination could be controlled by the state of the disulphide bond. Although the physiological significance of hexa-coordinate heme is unclear, it is proved by the kinetic studies that the hexa-coordinate globins, including cytoglobin and neuroglobin, have more complex ligand binding properties than their penta-coordinate counterparts.

#### **1.3.4 Exogenous Ligand Binding**

Small exogenous ligands, such as oxygen ( $O_2$ ), carbon monoxide (CO) and nitric oxide (NO) have been shown to bind to the heme iron of cytoglobin in the ferrous state. Ligand binding kinetic studies have suggested that cytoglobin has a higher oxygen association and lower oxygen dissociation rate compared to myoglobin, while the oxygen affinity is about the same as myoglobin (Trent and Hargrove, 2002). However, as shown in the figure 1.4 the major structural difference between the two globins is at the distal heme pocket, rather than the proximal pocket and the rest of the protein core. It is believed that such difference in the heme-coordination contributes to the differences in the exogenous binding equilibrium and the kinetics between cytoglobin and myoglobin (Sugimoto et al., 2004). The ligand binding parameters of both myoglobin and cytoglobin have been summarised in table 1.3.

A general mechanism for ligand binding to the hexa-coordinate heme was described by Trent and colleagues, which follows a biphasic ligand dissociation and association at the distal heme pocket (Trent et al., 2001). Since no such biphasic ligand binding mechanism has been observed in penta-coordinate heme, it is, therefore, believed that conformational changes in the heme pocket, especially at the distal side of the heme, are needed in order to allow the binding of exogenous ligands. A number of structural studies have shown that the distal heme pocket of cytoglobin could adopt a conformational transition between a hexa-coordinate form to an intermediate penta-coordinate form where the distal histidine is shifted away from the heme iron due to an upward and outward movement of the E-helix (de Sanctis et al., 2004; Sugimoto et al., 2004; Makino et al., 2010). Therefore, the scenario of the ligand binding when an exogenous ligand comes into contact with the heme iron at the distal site would be, first, dissociation of the endogenous distal His81 residue from the axial position together with an upward and outward movement of the E-helix from the heme pocket, and then followed by a competition for the distal heme binding site by both ligands. Consequently, the exogenous ligand will replace the distal His81 residue for the binding to the heme iron (Figure 1.5).

The intra-molecular disulphide bond in cytoglobin has been shown to regulate ligand binding by modulating affinity of the distal His81 residue (Hamdane et al., 2003). Based on the results of structural studies, a possible mechanism could be explained by a conformational change at the E-helix when the intra-molecular disulphide bond between Cys38 and Cys83 residues is formed which in turn modifies the position of the distal His81 residue and then modulates its to the heme iron (de Sanctis et al., 2004; Hamdane et al., 2003; Lechauve et al., 2010; Sawai et al., 2003; Sugimoto et al., 2004).



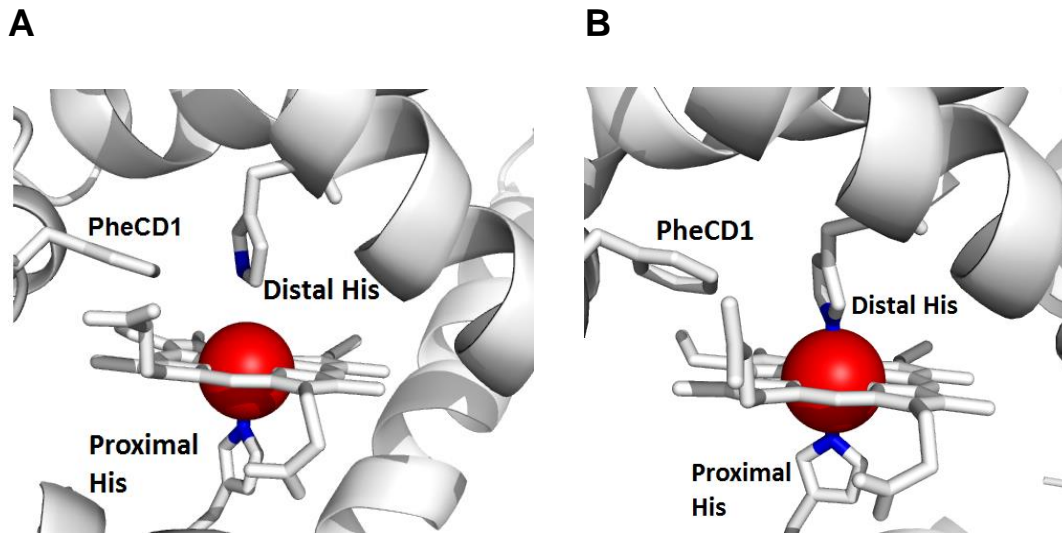


**Figure 1.4** Illustration of different heme coordination in globins. **(A)** penta-coordinate heme in myoglobin (redrawn from PDB file 1A6K). **(B)** hexa-coordinate heme in cytoglobin (redrawn from PDB file 2DC3, Chain b)

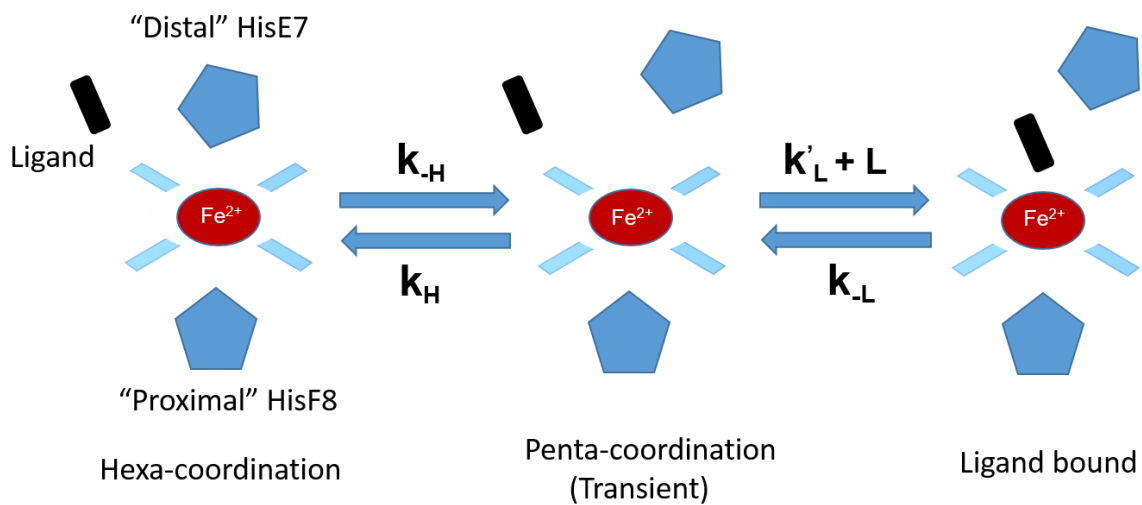


**Figure 1.5** Model of exogenous ligand binding to hexa-coordinate heme. Upon binding of exogenous ligand, the distal His residue has to be displaced from its original position creating a transient penta-coordinate state. The exogenous ligand is then competing with the distal His residue for the vacant binding site and form a ligand bounded complex eventually.

Vertebrate globins	$k_{\text{His}}$ ( $\text{s}^{-1}$ )	$k_{\text{His}}$ ( $\text{s}^{-1}$ )	$K_{\text{His}}$	$k'_{\text{O}_2}$ ( $\text{M}^{-1}\text{s}^{-1}$ )	$k_{\text{O}_2}$ ( $\text{s}^{-1}$ )	$K_{\text{O}_2}$ (M)	$k'_{\text{CO}}$ ( $\text{M}^{-1}\text{s}^{-1}$ )	$k_{\text{CO}}$ ( $\text{s}^{-1}$ )	$K_{\text{CO}}$ (M)
Human Mb	N/A	N/A	N/A	$19 \times 10^{-6}$	22	$1.1 \times 10^6$	$76 \times 10^{-6}$	0.02 2	289
swMb wild-type	N/A	N/A	N/A	$17 \times 10^{-6}$	15	$8.8 \times 10^5$	$51 \times 10^{-6}$	0.01 9	372
swMb H64F	N/A	N/A	N/A	$75 \times 10^{-6}$	10000	$1.3 \times 10^8$	$4.5 \times 10^{-6}$	0.05 4	$1.2 \times 10^4$
swMb H64Y	N/A	N/A	N/A	$6.7 \times 10^{-6}$	3200	$4.8 \times 10^8$	$50 \times 10^{-6}$	0.09 2	1840
Neuroglobin ^	8200	9800	1.2	$130 \times 10^{-6}$	0.3	$5 \times 10^3$	$5.6 \times 10^{-6}$	0.00 3	400
Cytoglobin ^	5	430	86	$30 \times 10^{-6}$	0.35	$1 \times 10^6$	$38 \times 10^{-6}$	0.00 7	$4.6 \times 10^4$

**Table 1.3 Ligand binding parameters of vertebrate globins with different heme coordinations**

\* Binding rate constants of both  $\text{O}_2$  and  $\text{CO}$  in Myoglobin and its mutants were obtained from Springer et al., 1994. Equilibrium binding constants were re-calculated and reported here as  $K_d$  ( $k_{\text{O}_2}/k'_{\text{O}_2}$  &  $k_{\text{CO}}/k'_{\text{CO}}$ ) since they were reported as  $K_a$  originally.

^ Values of rate constants for neuroglobin and cytoglobin were obtained from Trent et al., 2002; Histidine equilibrium constants ( $K_{\text{His}}$ ) of both proteins were calculated by ( $k_{\text{His}}/k_{-\text{His}}$ ); Values for oxygen and  $\text{CO}$  binding rate constants were calculated using the following equation:  $K_a = K_{\text{L, penta}} / (1 + K_{\text{His}})$ , where the value of  $K_{\text{L, penta}} = k_{\text{ligand}} / k_{-\text{ligand}}$ . The equation for calculating the  $K_a$  here for hexa-coordinate globins is different from that for myoglobin ( $K_a = K_{\text{on}} / K_{\text{off}}$ ), as the factor of  $K_{\text{His}}$  has to be taken into account for effective binding. Equilibrium binding constants were re-calculated and reported as  $K_d$  using equation:  $K_d = 1/K_a$ .

## **1.4 Distribution of Cytoglobin in Human Tissues**

### **1.4.1 Physiology of Cytoglobin**

Unlike other members in the vertebrate globin family, such as haemoglobin and myoglobin which show specific distribution in the body and are exclusively found in erythrocytes and muscle cells, respectively, cytoglobin, as its name suggested, however, showed a broad range of organ and tissue distributions which have been demonstrated by previous studies (Burmester et al., 2002; Trent and Hargrove, 2002). The expression level of cytoglobin varies in different organs, tissues and cell types and was estimated to be at a low  $\mu\text{M}$  range (Fago et al., 2004a; Fago et al., 2004b). However, due to its low sequence identities, distinct structural characteristics and ubiquitous expression in various organs and tissues compared to other globins, cytoglobin is believed to play different roles from neuroglobin, myoglobin and haemoglobin (Fago et al., 2004a; Weber and Fago, 2004).

### **1.4.2 Organ and Tissue Distribution**

Early studies detected *CYGB* mRNA in almost all major organs, such as heart, brain, lung, stomach, bladder, and kidney, (Burmester et al., 2002; Schmidt et al., 2004; Trent and Hargrove, 2002). The widespread distribution of cytoglobin in various tissues was further confirmed by immunohistochemistry studies on mammalian tissues using antibodies directly raised against human recombinant cytoglobin (Geuens et al., 2003; Ostojić et al., 2006; Shigematsu et al., 2008). In general, cytoglobin is detected in epithelial cells, cardio-myocytes, hepatic stellate cells in the liver as well as fibroblasts (Asahina et al., 2002; Schmidt et al., 2004; Shigematsu et al., 2008). Apart from the widespread distribution in the organs, cytoglobin was also found in myogenic progenitor cells which is suggested to play an important role in muscle regeneration (Singh et al., 2014), as well as in the tissues in the central nervous system in both developing and adult murine brain *in vivo* (Mammen et al., 2006).

### **1.4.3 Subcellular Localisation**

The subcellular localisation of cytoglobin in the cells is still not entirely clear and may be cell-specific. Although it has first been suggested that cytoglobin is very likely to be a cytoplasmic protein predicted by computational modelling (Burmester et al., 2002), different localisation patterns inside the cells have been reported in different cell types by several groups. The subcellular distribution of cytoglobin in cytoplasm was first observed in the fibroblasts and the related cell types (e.g. hepatic stellate cells) (Kawada et al., 2001; Man et al., 2008; Nakatani et al., 2004; Shigematsu et al., 2008) and mouse retinal neurons (Ostojic et al., 2006). However, some other studies demonstrated that nuclear localisation is also possible for cytoglobin (Geuens et al., 2003; Hodges et al., 2008; Man et al., 2008; Schmidt et al., 2004; Shigematsu et al., 2008; Singh et al., 2014). The ability of cytoglobin to localise to the nucleus in the cells implicates the possibility of a cell-specific function, such as gene regulation and cellular protection. Nonetheless, since cytoglobin lacks a signal peptide in the amino acid sequence, it is therefore rational to suggest that the nuclear translocation of cytoglobin could only be achieved by an interaction with a translocation partner. However, the nuclear translocation mechanism of cytoglobin and the exact function of cytoglobin in the nucleus in the cells remain unknown (Hodges et al., 2008; Oleksiewicz et al., 2011; Schmidt et al., 2004; Singh et al., 2014).

## **1.5 Putative Physiological Functions of Cytoglobin**

### **1.5.1 A Role in Oxygen Storage and Delivery**

One of the first proposed cellular functions for cytoglobin was as a carrier and a reservoir of oxygen in the cells. It was speculated that cytoglobin may involve in the general cellular oxygen metabolism similar to the role of myoglobin in the muscles cells which transports oxygen molecules to the mitochondria to support the oxidative respiration required for generation of energy. Such a speculation is supported by the facts that cytoglobin is evolutionarily related to myoglobin, and also cytoglobin has been shown to have a high affinity for oxygen molecules which is comparable to that of myoglobin (Pesce et al., 2002).

However, the physiological level of cytoglobin expression does not seem to support the proposed function in oxygen storage due to the fact that the cellular concentration of cytoglobin was only estimated to be at the range of a few micromolar (1-5  $\mu\text{M}$ ) which is far less than the concentration of myoglobin in muscle cells where a lot of oxygen is needed to maintain the oxidative respiration. Moreover, heme coordination of cytoglobin is said to be hexa-coordinate which is different from the penta-coordinate Myoglobin, it is therefore believed that the ligand binding properties of cytoglobin is different from penta-coordinate myoglobin (Trent et al., 2001; Trent and Hargrove, 2002; refer to table 1.3). Furthermore, cytoglobin was shown to be mainly expressed in specific cell types, such as fibroblasts and hepatic stellate cells (Schmidt et al., 2004). Hence, it is believed that oxygen storage and transport may not be a physiologically relevant function of cytoglobin as those cell types are considered not as metabolically active as muscle cells where myoglobin is found to be highly expressed. Therefore other alternative physiological functions, such as involvement in nitric oxide metabolism and reactive oxygen species scavenging, had been proposed for cytoglobin subsequently.

### 1.5.2 A Role in Nitric Oxide Scavenging and Signalling

Interaction with nitric oxide is believed to be an intrinsic ability among globins (Vinogradov and Moens, 2008). Nitric oxide is a potent intracellular second messenger in various organ and tissues systems such as the nervous system, cardiovascular system and immune system in which nitric oxide modulates various cellular responses (Gardner et al., 2001). Cytoglobin has been shown to scavenge nitric oxide (Halligan et al., 2009) by means of oxygen-dependent nitric oxide dioxygenation (NOD) which has also been reported in haemoglobin and myoglobin (Flögel et al., 2001). In the nitric oxide dioxygenation, oxy-ferrous cytoglobin interacts with the nitric oxide to convert it to nitrate with itself being oxidized to ferric cytoglobin. Indeed, Halligan and colleagues demonstrated that knocking down the *CYGB* gene in the rat fibroblast resulted in significant reduction in nitric oxide consumption and nitrate production and the cells were more susceptible to nitric oxide-mediated suppression of cellular respiration and proliferation. The situation can be restored by re-expressing the cytoglobin, thus, this confirmed that cytoglobin possesses NOD activity in cells and its localization in the vascular tissues indicated that cytoglobin may be critical to regulation of nitric oxide in the vascular wall (Halligan et al., 2009).

Recent biochemical studies have given a better understanding in the NOD activity of cytoglobin. Natural reductants such as ascorbate, cytochrome *b<sub>5</sub>* were shown to be capable of supporting the high NOD activity of cytoglobin by reducing ferric cytoglobin back to its ferrous state following a second order rate of reaction (Gardner et al., 2010). A later study using a mathematical approach has further delineated that the rate of NOD activity is actually oxygen-dependent and the reaction rate decrease dramatically under low oxygen tension which suggested that modulation of nitric oxide by cytoglobin occurs under hypoxia and the results further suggested the possible role of cytoglobin in regulating the vascular wall via regulating the nitric oxide concentration in the local tissue (Liu et al., 2012).

### 1.5.3 A Role in Cellular Oxidative Stress

Beside carrying diatomic gaseous ligands, some globins could have also been shown to perform several types of enzymatic activities *in vitro*, such as peroxidase, catalase and dismutase activities, towards reactive oxygen species (ROS). Cytoglobin has also been implicated to involve in cellular oxidative stress responses based on a number of observations in cultured cells. For examples, studies from Kawada and colleagues first discovered in rat hepatic stellate cells that a protein dubbed as stellate cell activation-associated protein (STAP), which was subsequently confirmed to be an analogue of cytoglobin, was up-regulated during chemically induced liver fibrosis (Kawada et al., 2001). Later on, a human ortholog was shown to be up-regulated in the same manner as in the rat, and the corresponding recombinant protein was shown to exhibit peroxidase-like activity toward hydrogen peroxide and lipid peroxide (Asahina et al., 2002). Moreover, cytoglobin's expression has been shown to be induced in response to exogenous insults by hydrogen peroxide *in vitro*, in which a set of genes, including *CYGB*, were found to be significantly up-regulated in the cultured cells under oxidative stress (Chua et al., 2009; Li et al., 2007). The up-regulation of cytoglobin was shown to be orchestrated by a transcription co-activator which promotes resistance to cell death by oxidative stress in cancer cells (Basu et al., 2012). Furthermore, the gene expression of cytoglobin was also shown to be up-regulated in the case of aging-related hearing loss in rat cochlea and suggested to be strongly correlated with damages caused by the oxidative stress (Tanaka et al., 2012). Thus, studies on differential expression of *CYGB* gene in different tissues and cell types has provided a lot of evidence to support the idea that cytoglobin plays a role in oxidative stress.

Although a detailed physiological function of cytoglobin under oxidative stress remains elusive, gain-and-loss of function studies on cytoglobin in cultured cells under oxidative stress has suggested that cytoglobin may act as a ROS scavenger which protects the cells against oxidative damages. The cell viability was shown to be significantly decreased when *CYGB* gene was deregulated by siRNA *in vitro* during oxidative stress (Fordel et al., 2007; Li et al.,

2007). On the contrary, the cell viability was significantly enhanced upon oxidative stress when the *CYGB* gene was over-expressed (Fordel et al., 2007). Besides promoting cell survival under oxidative stress, over-expression of *CYGB* gene has also been shown to be protective against oxidative DNA damage demonstrated in comet assays which suggested an ability to scavenge ROS by cytoglobin (Hodges et al., 2008; McRonald et al., 2012).

However, it is arguable that cellular protective effects by cytoglobin can be seen only under non-physiologically relevant concentrations (i.e. when it is over-expressed). Also, biochemical studies on recombinant cytoglobin did not seem to support any robust enzymatic activities of cytoglobin as a ROS scavenger as the performance of all the catalase, peroxidase, and dismutase activities were insignificant compared to the corresponding enzymes (Trandafir et al., 2007). Thus, the idea of cytoglobin being an authentic ROS scavenger to detoxify the ROS in cells under oxidative stress remains to be elucidated. However it would be worth exploring other possible roles of cytoglobin in the redox signalling cascade under oxidative stress.

#### **1.5.4 A Role in Cellular Hypoxia**

Early speculations on the physiological functions of cytoglobin have suggested that it may be involved in a cellular defence mechanism against oxygen deprivation. A similar function has been already observed in neuroglobin (Pesce et al., 2002) and non-symbiotic hemoglobins in plants, all of which also display hexa-coordinate heme (Hunt et al., 2002; Sowa et al., 1998). Coincidentally, *CYGB* gene expression was found to be up-regulated under hypoxia *in vitro* in cultured cells (Fordel et al., 2004a; Fordel et al., 2004b) and *in vivo* in certain organs, such as heart and liver (Fordel et al., 2004a; Fordel et al., 2004b; Schmidt et al., 2004). Furthermore, *CYGB* gene was also found to be up-regulated in various cultured cancer cells (Emara et al., 2010; Gorr et al., 2011; Shaw et al., 2009) subjected to hypoxic stress. The underlying gene regulation was shown to be under the control of the hypoxia inducible factor

(HIF-1 $\alpha$ ) pathway (Emara et al., 2010; Fordel et al., 2004a; Fordel et al., 2004b; Gorr et al., 2011; Shaw et al., 2009). Indeed, functional studies on the promoter sequence of the *CYGB* gene has revealed that it contains several hypoxia responsive elements (HRE) for the binding of transcription factor HIF-1 and also a hypoxia inducible protein binding site (HIPBS) for the stabilization of mRNA under hypoxia (Guo et al., 2006, 2007; Wystub et al., 2004). Since the promoter also harbours other binding sites for transcriptional factors involved in cellular oxygen homeostasis, these results strongly supported the notion that cytoglobin is a stress responsive protein which is up-regulated under hypoxia and oxidative stress.

Although it is well characterised that cytoglobin expression is up-regulated under hypoxia via HIF-1 $\alpha$  signalling pathway, the exact physiological role under hypoxia remains to be elucidated. A few suggestions on cellular oxygen storage and delivery under hypoxia had once been proposed. However, due to the low basal expression level of cytoglobin in certain tissues as well as being down-regulated in some cancer cells under epigenetic control, it is unlikely that cytoglobin serves this purpose. On the other hand, a few other studies have shown that under ischemic conditions, cytoglobin could promote cell survival (Fordel et al., 2004a; Fordel et al., 2007; Stagner et al., 2005) by scavenging ROS in the cells (Fordel et al., 2007). Taken together, the results again point to a cellular protective role during stress conditions, which needs to be further clarified.

### 1.5.5 A Role in Collagen Synthesis

Although a role as an oxygen carrier for oxidative respiration does not seem to be legitimate, a role in supporting enzymatic reactions would be more reasonable. Involvement of cytoglobin in regulation of collagen synthesis was first postulated when cytoglobin was first discovered in hepatic stellate cells, where its expression was correlated with the expression of both collagen  $\alpha 1(I)$  and  $\alpha 1(III)$  which were up-regulated during chemically induced liver fibrosis (Kawada et al., 2001). This idea was further supported by another study showing that expression of collagen  $\alpha 1(I)$  was significantly elevated by over-expression of cytoglobin in cultured NIH-3T3 mouse embryo fibroblast cells under the stimulation of transforming growth factor- $\beta 1$  (TGF- $\beta 1$ ) (Nakatani et al., 2004). Moreover, the presence of cytoglobin and the augmented collagen synthesis was in agreement with the tissue distribution pattern of cytoglobin, where it is predominantly detected in fibroblast of connective tissues which are actively producing collagen (Schmidt et al., 2004). Hence, these results suggested a possible regulatory role of cytoglobin in collagen synthesis.

However, the correlation between cytoglobin expression and collagen production is not necessarily positive. Collagen synthesis was found to be partially inhibited when expression of cytoglobin was over-expressed in several studies. When cytoglobin was over-expressed transiently in hepatic stellate cells treated with chemicals to induce fibrosis, collagen synthesis was found to be impaired compared with the control cells (Xu et al., 2006). A similar result in down-regulation of collagen synthesis was also observed in cancer cell lines where the gene expression of collagen  $\alpha 1(I)$  (*Col1A1*) was found to be down-regulated when cytoglobin was over-expressed in both lung and breast cancer cell lines, respectively (Shivapurkar et al., 2008). A clue for how cytoglobin-mediated represses collagen synthesis was provided by the study of Mimura and colleagues. They demonstrated that collagen production was unaffected in cultured kidney fibroblast cells when a mutation at the distal heme pocket of cytoglobin was introduced. Hence, the results implied that the repression of collagen production may not be due to any reaction at the heme pocket of cytoglobin (Mimura et al., 2010).

All of the results strongly suggested that a role in modulating collagen synthesis could be one of the physiological roles of cytoglobin, especially in the context of diseases, such as organ fibrosis and cancer. However, the exact mechanism of the regulating collagen synthesis by cytoglobin is still unclear and it seems to be dependent on cellular type, genetics and molecular environment in the cells (Oleksiewicz et al., 2011). Several hypotheses have been proposed which are worth investigating, for example, the cellular interplays between cytoglobin and nitric oxide since nitric oxide could inhibit the function of prolyl hydroxylases during collagen maturation leading to degradation of premature collagen (Cao et al. 1997).

## **1.6 Cytoglobin as a Tumour Suppressor Gene in Cancer**

### **1.6.1 A Link Between Cytoglobin and Cancer**

The link between cytoglobin and cancer was first established in a study that a 42.5kb minimal region was mapped out to be implicated in Tylosis with oesophageal cancer (TOC) syndrome on chromosome 17q25 which contains the entire *CYGB* gene and parts of two other putative genes, namely *FLJ22341* and *FM8* with unclear functions. These genes were identified as potential causative genes for sporadic oesophageal cancer (Langan et al., 2004; McRonald et al., 2006). It was shown that no TOC specific mutation was found within that minimal region. However, expression of *CYGB* gene was found to be significantly lower in biopsies from patient with tylosis than those without tylosis and the expression of *CYGB* gene was reduced about 70% (McRonald et al., 2006). Moreover, the expression of *CYGB* gene was also shown to be negatively correlated to the staging and grading of ovarian cancers with the later stage and high grade ovarian cancer showing less protein expression of Cytoglobin (Chen et al., 2014). Taken together, these results suggested that the down regulation of *CYGB* gene may be involved in the progression of certain type of cancers, including oesophageal and ovarian cancers.

### **1.6.2 Hypermethylation of the *CYGB* Promoter**

The cause of the down-regulation of *CYGB* gene was shown to be a result of an epigenetic alteration at the promoter of *CYGB* gene where it is said to be hypermethylated. It was first shown in both biopsies and cell lines in sporadic oesophageal carcinomas, while expression of both alleles of *CYGB* gene were equally repressed suggesting that the loss of *CYGB* gene expression is not due to mutation on one allele (McRonald et al., 2006). Such down-regulation of *CYGB* gene expression due to hypermethylation was further described by a number studies on various tumours tissues and tumour derived cancer cell lines, including

lung cancer (Shivapurkar et al., 2008; Xinarianos et al., 2006), breast cancer (Shivapurkar et al., 2008), head and neck cancer (Shaw et al., 2009) and Renal cell carcinoma (Gorr et al., 2011). Since hypermethylation of the promoters of tumour suppressor genes (TSG) would lead to transcriptional inactivation of the TSG which would ultimately promote tumourigenesis, thus it is suggested that cytoglobin could be a novel candidate TSG which may possess the ability to suppress cancer growth.

### **1.6.3 Tumour Suppression Properties of Cytoglobin**

The tumour suppression property of cytoglobin was first proposed and demonstrated in a study using non-small cell lung cancer cell lines in which the *CYGB* gene was subjected to a knockdown by RNA interference and over-expression by stable transfection of exogenous *CYGB* gene (Shivapurkar et al., 2008). The gain-and-loss of function study indicated that changes in *CYGB* gene expression, at both mRNA and protein levels, significantly affected colony formation with more colonies were formed by a *CYGB* gene knockdown lung cancer cell line and fewer colonies were observed by another *CYGB* gene over-expressed lung cancer cell line compared to their corresponding control cell lines. Recently, the TSG property of *CYGB* gene has been further described in other human malignancies, including lung adenocarcinoma and squamous cell lung carcinoma (Oleksiewicz et al., 2013) and ovarian cancer cell lines (Chen et al., 2014).

Investigations of downstream targets of *CYGB* gene regulation for its tumour suppression property have revealed that the expression level of six genes were significantly reduced in response to transient transfection of *CYGB* gene in lung and breast cancer cell lines (*COL1A1*, *PRPF40A*, *UCP2*, *DAPK*, *PYCARD* and *DNMT1*), three of which (*COL1A1*, *PRPF40A* and *UCP2*) were found to be consistently down-regulated in both cancer types while the others

were found to be down-regulated in either lung or breast cancer cell line which are suggested to be cell-specific targets under regulation of *CYGB* gene (Shivapurkar et al., 2008). More recently, cytoglobin was shown to regulate the expression of a cell cycle control protein, cyclin D1, which regulates the cell cycle in the ovarian cancer cell lines (Chen et al., 2014). Thus, these results strongly indicated the regulatory role of *CYGB* gene as a TSG and suggested that cytoglobin may regulate different genes expression in a cell-specific manner. Although the TSG property of *CYGB* gene was confirmed in a number of recent studies, the detailed molecular mechanism of the tumour suppression by cytoglobin remains to be elucidated.

#### **1.6.4 Stress Responsive Properties of Cytoglobin in Cancer cells**

Beside its role as a potential TSG, cytoglobin also exerts its effects on stress responses in many cancer cells which might be related to one of the causes of chemotherapy and radiotherapy resistance in cancer treatments. Several studies have already shown that gene expression of *CYGB* was up-regulated under cellular stresses, such as oxidation stress and hypoxia. *CYGB* gene expression was found to be up-regulated by the HIF-1 $\alpha$  pathway under hypoxia in head and neck cancer which is also found to be in strong correlation with some clinicopathological measures of tumour aggression in such cancer (Shaw et al., 2009). *CYGB* gene expression in neuroblastoma, glioblastoma, hepatocarcinoma and renal cell carcinoma cell lines were all shown to be upregulated under either anoxic or hypoxic conditions (Emara et al., 2010; Fordel et al., 2007; Gorr et al., 2011). Moreover, a recent study using prostate cancer cells has also revealed that *CYGB* gene expression was regulated by a transcription co-activator called LEDGF/p75, which is implicated in stress survival responses in the gain-and-loss-of-function experiment of LEDGF/p75 (Basu et al., 2012).

Interestingly, over-expression of cytoglobin in cancer cell lines showed reduced DNA

damages caused by reactive oxygen species suggesting that cytoglobin could play a role in cytoprotection against damages from oxidative stress caused by reperfusion injury following hypoxia (Hodges et al., 2008; McDonald et al., 2012).

Tumour hypoxia is a frequent event in the human cancers, and cancer cells that are under hypoxia are relatively more resistant to radiotherapy and chemotherapy treatments. Since cytoglobin expression has been shown to be up-regulated under such conditions, it is therefore suggested that cytoglobin may contribute to a pro-survival response in cancers under multiple stress-related conditions (Emara et al., 2010).

## **1.7 Hypoxia**

### **1.7.1 Hypoxia in Humans**

“Hypoxia” is a term that refers to an environmental condition where the oxygen partial pressure in the surrounding is lower than that in the atmosphere. Tissue hypoxia is a common physiological condition in our body as there is an oxygen gradient between tissues located close to a blood supply where it is saturated with oxygen and distant tissues where it is said to be highly hypoxic. In cancer, tumours are also subjected to hypoxia as vasculature development cannot come up with an uncontrolled growth of tumour cells. Lack of oxygen is lethal to the cells as it inhibits normal cellular metabolism, cell proliferation and could eventually lead to cell death.

However, there is an intrinsic adaptive mechanism in the cells to counteract the adverse effects due to the shortage of oxygen by activation of the Hypoxia inducible factor (HIF) and its subsequent signalling pathway which promotes a number of adaptive responses in the cells

under hypoxia, including promoting angiogenesis – the formation of new blood vessels – by producing vascular endothelial growth factor (VEGF) (Forsythe et al., 1996), and by promoting erythropoiesis – the production of red blood cells – by producing erythropoietin (EPO) (Semenza et al., 1991), and increasing glucose uptake by the cells by up-regulating the glucose transporter (Glut-1) expression (Hayashi et al., 2004).

### **1.7.2 Hypoxia Inducible Factor (HIF)**

The hypoxia signalling pathway which is activated under hypoxia is orchestrated by a transcription factor namely Hypoxia inducible factor (HIF) which binds onto the HREs in the promoter sequences of hypoxia responsive genes. HIF is a heterodimeric protein which is comprised of an  $\alpha$ -subunit (e.g. HIF-1 $\alpha$ ) which is stabilised and activated under hypoxia and a  $\beta$ -subunit (e.g. HIF-1 $\beta$ ) which is constitutively expressed and present in the cells. HIF belongs to a transcription factor family of basic helix-loop-helix- PAS (bHLH-PAS) proteins (Figure 1.6) (Wang et al., 1995) which includes three isoforms of the  $\alpha$ -subunit, namely HIF-1 $\alpha$ , HIF-2 $\alpha$  and HIF-3 $\alpha$ , and three paralogues of  $\beta$ -subunits, namely HIF-1 $\beta$ , HIF-2 $\beta$  and HIF-3 $\beta$ , also known previously as, Aryl Hydrocarbon Nuclear Translocator (ARNT). Among the three isoforms of the  $\alpha$ -subunit, HIF-1 $\alpha$ , a 120 kDa protein, has been extensively studied and well characterised and is believed to be the major mediator in cellular hypoxic responses. However, recent studies have shown that other isoforms (i.e. HIF-2 $\alpha$  and -3 $\alpha$ ) may have more specific expression patterns and functions under cellular hypoxia (reviewed in Loboda et al., 2010).

### **1.7.3 von Hippel Lindau Protein (pVHL)**

The *von Hippel-Lindau (VHL)* gene is located at chromosome 3q25 encoding two fully functional gene products at 19 kDa and 30 kDa, respectively. Both of the gene products,

termed as pVHL, are tumour suppressor proteins which suppress tumour growth. pVHL has been shown to play a crucial role in the regulation of HIF at the post-translational level. In renal clear cell carcinoma (RCC), mutations at the binding site or catalytic site of HIF on the pVHL cause the loss of function and promote tumour growth in kidney (Esteban et al., 2006).

#### **1.7.4 Regulation of Hypoxia Inducible Factor**

The  $\alpha$ -subunit of HIF is also believed to be expressed constitutively in cells, however, its stability is dependent on the availability of oxygen. Under normoxia, two Proline residues (Pro402 and Pro564) within the oxygen-dependent degradation domain (ODD) of the HIF-1 $\alpha$  (Figure 1.6) are hydroxylated in the presence of oxygen by a group of prolyl hydroxylases (PHDs). The hydroxylated HIF-1 $\alpha$  is then targeted by von Hippel Lindau protein (pVHL) which is a subunit of a E3 ubiquitin ligase complex including also Elongin B, Elongin C, Cul2 and Rbx 1 (known as VBC-CR complex). Consequently, the hydroxylated HIF-1 $\alpha$  is subjected to ubiquitylation and proteasomal degradation (Cockman et al., 2000; Maxwell et al., 1999). Moreover, transcriptional activity of HIF-1 $\alpha$  is also regulated by hydroxylation of an Asparagine residue (Asn 803) within a C-terminal transactivation domain (CAD) by an asparagyl hydroxylase, called factor inhibiting HIF (FIH-1) (Lando et al., 2002). Thus the hydroxylated asparagines residue prevents the transcriptional activity of the  $\alpha$ -subunit by not allowing the binding of a transcriptional coactivator p300 at the CAD. However, under hypoxia, due to the lack of oxygen for the hydroxylation of HIF-1 $\alpha$  by PHDs and FIH-1, HIF-1 $\alpha$  cannot be targeted by the E3 ubiquitin ligase complex, and thus the degradation of HIF-1 $\alpha$  is prevented. Hence, HIF-1 $\alpha$  is stabilised and translocated into the nucleus and dimerises with HIF-1 $\beta$  to induce the expression of several hypoxia inducible genes which contain HREs in their promoter regions (Figure 1.7).

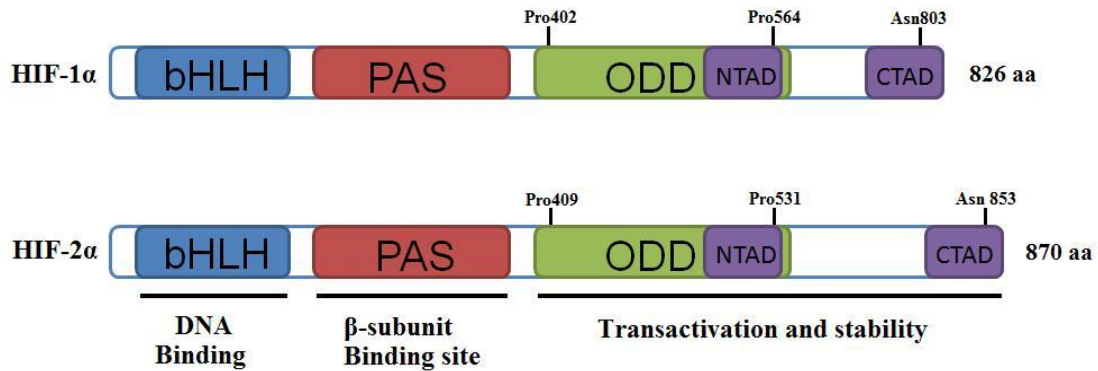


**Figure 1.6 Structure of HIF  $\alpha$ -subunits.** The functional domain on HIF $\alpha$ -subunits are basic helix-loop-helix domain (bHLH) for DNA binding, Per-AHR-ARNT-Sim homology domains (PAS) for binding with  $\beta$ -subunit, oxygen-dependent degradation domain (ODD) for hydroxylation by prolyl hydroxylase and subsequent proteasomal degradation, and transactivation domains (TAD, with C-terminal CAD and N-terminal NAD) for nuclear translocation.

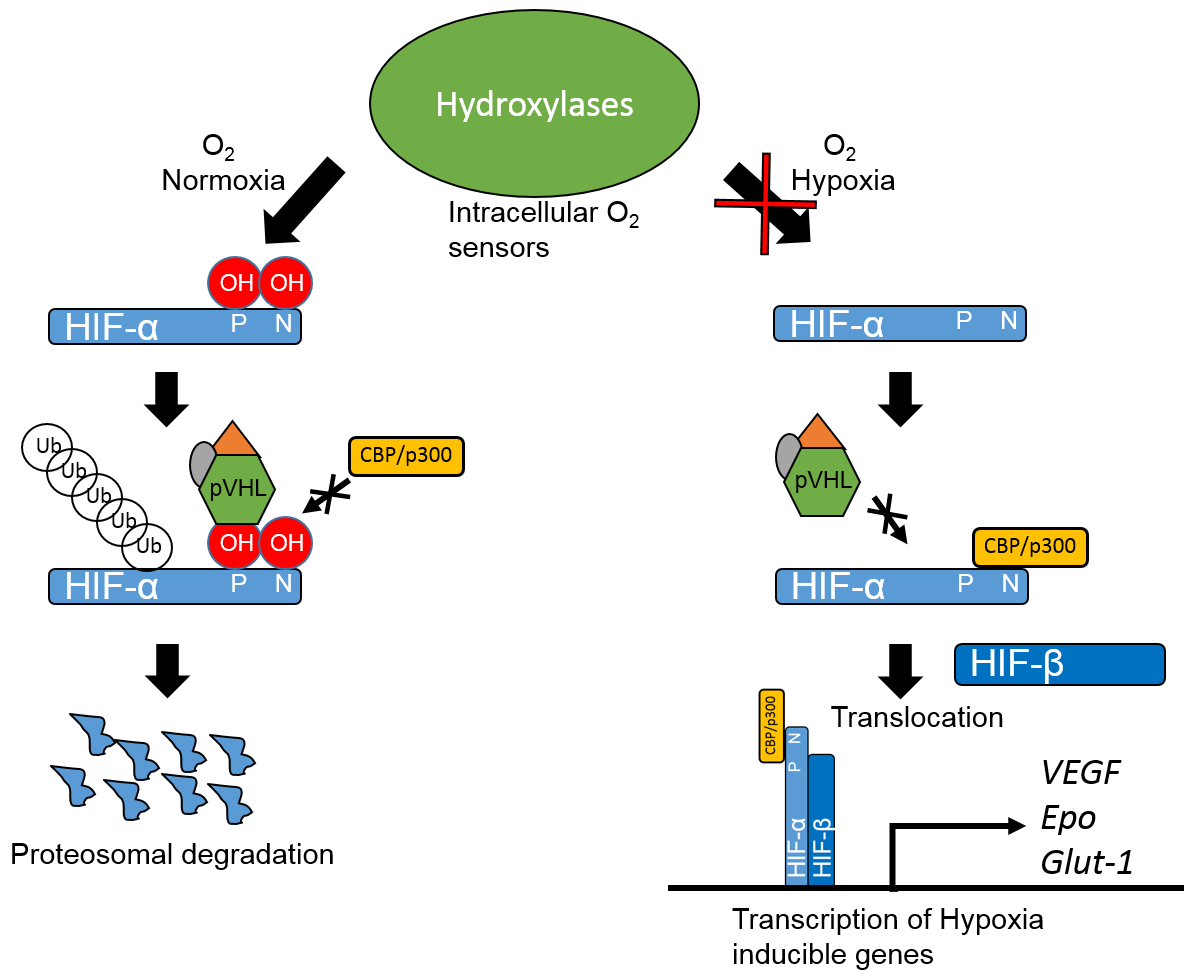


**Figure 1.7 Schematic representation of oxygen-dependent HIF-1α regulation in the cells.**

Under normoxic conditions, proline residues on HIF-1α are hydroxylated of by prolyl hydroxylases (PHDs) and the hydroxylated HIF-1α is targeted and ubiquitinyled by the pVHL E3 ubiquitin ligase system and eventually subjected to proteasomal degradation. Under hypoxic conditions, HIF-1α is stabilized and heterodimerizes with HIF-1β to regulate transcription of hypoxia inducible genes, such as VEGF, EPO, GLUT-1.

## 1. 8 Aims

The aim of this research is to elucidate the possible physiological roles of cytoglobin, as a tumour suppressor protein, in cancer cells. We aim to understand the molecular mechanism of how cytoglobin may function as a heme protein by characterising recombinant human cytoglobin purified from *E.coli*/BL21 (DE3) using a wide range of techniques, including protein engineering and advanced spectroscopies. We also aim to search for any putative protein partners in the cell signalling pathway which would confer the tumour suppresser function of cytoglobin and to test a hypothesis that such a protein-protein interaction is mediated via an unstructured C-terminus of cytoglobin by a newly discovered mechanism of coupled folding and binding of unstructured domain in proteins called fly casting. Understanding the molecular mechanism of tumour suppression by cytoglobin could allow an evaluation of potentially targeting cytoglobin in the context of diseases for therapeutic uses in the future.

## Chapter 2: Materials and Methods

### 2.1 Bacterial Cultivation and Strains

#### 2.1.1 Culture Media and Antibiotics

Bacteria (*E.coli*) were routinely cultured on sterile LB broth (10 g tryptone, 5 g yeast extract, 10 g NaCl per litre, pH 7.0). Solid LB medium was prepared with the addition of agar (1.5% (w/v)) to the liquid LB medium prior to autoclaving

All media used was supplemented with appropriate antibiotics according to the antibiotic resistant gene carried by the plasmids. This is essential to add antibiotics to the culture media to prevent the growth of bacterial strains other than the strain of interest. The antibiotics were made up by dissolving solid powders in distilled water which then passed through a sterile filter prior to use. For the growth of *E.coli* strains which carry the expression vectors of human cytoglobin, all the media used was supplemented with kanamycin at a final concentration of 50 µg ml<sup>-1</sup>. Whilst for the growth of *E.coli* strains which carry the expression vectors of sperm whale myoglobin, all the media used was supplemented with ampicillin and streptomycin at a final concentration of 100 µg ml<sup>-1</sup> and 50 µg ml<sup>-1</sup>, respectively.

#### 2.1.2 Bacterial Strains

The bacterial strains used in this work and their relevant characteristics are shown in Table 2.1.

Strains	Genotype	Source of Reference
<i>E.coli</i> DH5α	<i>fhuAΔ(argF-LacZ)U169, phoA, glnV44, Ø80Δ, (lacZ M15), gyrA496, recA1, relA1, endA1, thi-1, hsdR17</i>	Lab stock

<i>E.coli</i> BL21 (DE3)	F <sup>-</sup> , <i>ompT</i> , <i>gal</i> , <i>dcm</i> , <i>lon</i> <i>hsdS</i> (r <sub>B</sub> <sup>-</sup> , m <sub>B</sub> <sup>-</sup> ) λ DE3( <i>lacI</i> , <i>lacUV5</i> -T7 gene 1, <i>ind1</i> <i>sam7</i> <i>nin5</i> )	Lab stock
<i>E.coli</i> TB1	F <sup>-</sup> , <i>ara</i> Δ ( <i>lac-proAB</i> ) [Ø80 <i>dlac</i> Δ( <i>lacZ</i> )M15], <i>rpsL</i> (Str <sup>R</sup> ), <i>thi</i> , <i>hsdR</i>	Lab stock

**Table 2.1 List of Bacterial strains used in this study**

## 2.2 General Protein Biochemistry

### 2.2.1 Determination of Protein Concentration

The total protein concentration in solution was determined by the standard Bradford assay on a single wavelength colorimeter (Thermo Fisher Scientific) using 10 mm standard Poly (methyl-methacrylate) (PMMA) disposable cuvettes (Sigma Aldrich). Briefly, when the Bradford reagent (Bio-Rad, UK) which is an acidic solution of coomassie blue is added to the protein samples, binding of coomassie blue to the protein causes a visible colour change of the solution from brown to blue and a concomitant change in the absorption maxima at 595 nm. Hence, the intensity of the colour produced is proportional to the amount of protein in the solution.

Generally, a protein standard curve containing five different concentrations of protein standards was prepared using bovine serum albumin (BSA). The BSA solution was normally diluted to 0.5 mg ml<sup>-1</sup> from the stock solution (14 mg ml<sup>-1</sup>) and kept at 4 °C. Preparation of the BSA standard curve is shown in table 2.2. A total of 50 µl of BSA solution at each concentration was added to the cuvettes containing 1 ml of the Bradford reagent which had been diluted (1:4 dilution) in water prior to use. Protein solutions with unknown concentration were diluted 10 to 100 times in 500 µl with water prior to the detection. 50 µl of the diluted protein solution was

added to the cuvettes containing the diluted Bradford reagent for detection. The solutions in the cuvettes were gently mixed by pipette and allowed to incubate at room temperature for 5 minutes. The absorbance at 595 nm of the BSA standard and the protein samples was recorded and plotted in excel. The gradient of each standard curve was calculated and the protein concentration of the samples was determined.

BSA concentration (mg ml <sup>-1</sup> )	0.1	0.2	0.3	0.4	0.5
BSA (µl)	10	20	30	40	50
Water (µl)	40	30	20	10	0

**Table 2.2 Preparation of BSA standard for Bradford assay**

### **2.2.2 Analysis of Proteins by SDS-PAGE and Non-Reducing SDS-PAGE**

Sodium dodecyl sulfate polyacrylamide gel electrophoresis (SDS-PAGE) separates proteins based on their electrophoretic mobility. The SDS-PAGE (BioRad Mini Protean®-III system) was routinely used to analyse bacterial lysate, soluble fractions, purified protein from column chromatography and cancer cell lysate. Normally, 15% acrylamide gels were used for analyses of cytoglobin. Separation gels were prepared by the mixing the reagents stated in table 2.3 and then cast in the gel apparatus (1 mm thick). A small amount (1 ml) of isopropanol was applied on top of the gel. Once the separation gel was set, the layer of isopropanol was removed and then washed with water. Stacking gels were prepared by mixing the reagents stated in table 2.4 and then loaded into the gel apparatus on top of the separation gel, with combs placed at the top.

The protein samples were mixed with either conventional reducing sample loading buffer or non-reducing SDS-PAGE sample loading buffer in which the β-mercaptoethanol was

omitted in order to preserve the native state of disulphide bonds in the samples. The samples were boiled at 95 °C for 5 minutes before loading to the gel. Gels were run at 145 V under constant voltage condition for approximately 1.5 hours. For analysis purposes, protein bands were visualised by staining the gel with Coomassie Brilliant Blue (Sigma) for 1 to 2 hours at room-temperature. The molecular weight of the separated proteins was estimated by reference to dual colour protein markers (10 – 250 kDa) (Bio-Rad, UK). The gels were recorded and archived using a Gel Doc imaging system (Bio-Rad, UK).

Compositions	9%	10%	12%	15%	20%
ddH <sub>2</sub> O (ml)	6.9	6.3	5.3	3.7	1
1.5 M Tris-HCl pH8.8 (ml)	4	4	4	4	4
10% SDS(μl)	150	150	150	150	150
10% Ammonium persulphate (μl)	150	150	150	150	150
30% Acrylamide (ml)	4.8	5.4	6.4	8	10.7
TEMED (μl)	10	10	10	10	10

**Table 2.3 Composition of separation gels**

Compositions	4%	6%
ddH <sub>2</sub> O (ml)	3	2.65
1.5 M Tris-HCl pH8.8 (ml)	1.25	1.25
10% SDS(μl)	50	50
10% Ammonium persulphate (μl)	670	1000
30% Acrylamide (ml)	100	100
TEMED (μl)	5	5

**Table 2.4 Composition of stacking gels**

### 2.2.3 Liquid Chromatography Mass Spectrometry (LCMS)

The LCMS experiments were kindly conducted by Dr. Jason Crack (School of Chemistry, UEA). The LCMS experiments were mainly used to further confirm the presence of a mutation generated in the purified proteins or to confirm the presence of a modification on an amino acid residue. The samples for LCMS measurement were at a range of concentration between 20  $\mu\text{M}$  to 50  $\mu\text{M}$  diluted directly from the stock protein solution in a volume of 200  $\mu\text{l}$ . The samples were normally snap frozen in liquid nitrogen and were thawed and mixed with 2% acetonitrile in water and 0.1% formic acid prior to the experiments.

### 2.2.4 Analytical Gel Filtration

Analytical gel filtration is a technique to determine the size and the molecular weight of a protein of interest by comparing its elution volume ( $V_e$ ), or elution time with reference to protein standards with known molecular weight. The experiments were done using a Superdex 75 10/30 gel high performance gel filtration column (Amersham Bioscience, UK) which attached to an AKTA FPLC system (GE healthcare). The column was equilibrated with 5 column volumes (C.V.) of buffer (20 mM Tris-HCl, 150mM NaCl, pH 8.0) prior to injection of protein standards. After the column was equilibrated, 100  $\mu\text{l}$  of the following standard protein solutions: Blue Dextran (200 kDa), BSA (68 kDa, 1mg  $\text{ml}^{-1}$ ), Ovalbumin (45 kDa, 1mg  $\text{ml}^{-1}$ ), Myoglobin (17 kDa, 1mg  $\text{ml}^{-1}$ ) and Aprotinin (6.5 kDa, 1mg  $\text{ml}^{-1}$ ) were injected sequentially with the elution volume recorded at the point where peak absorption at  $A_{280}$  is observed.

To construct a protein standard curve for molecular weight determination, the partition coefficient ( $K_{av}$ ) of each of the protein standards were calculated using the following formula:  $K_{av} = (V_e \text{ of protein standard} - V_0) / (V_t - V_0)$  in which  $V_0$  was usually referred to the  $V_e$  of Blue Dextran. A linear plot of the  $K_{av}$  against

logarithms of the molecular weights of the protein standards was constructed. The  $K_{av}$  value of the unknown protein was determined by the experiment, and the molecular weight was determined by the standard curve.

## **2.3 General Molecular Biology Techniques**

### **2.3.1 Plasmid DNA Extractions**

Extraction of plasmid DNA for cloning and sequencing was done by using a commercial DNA extraction kit (Mini prep, Qiagen UK) strictly following the manufacturer's protocols. Generally, *E.coli* DH5 $\alpha$  was chosen to propagate the plasmid DNA. 5  $\mu$ l glycerol stock of *E. coli* DH5 $\alpha$  carrying the plasmid DNA of interest was inoculated into 5 ml LB culture and allowed to grow overnight at 37°C with shaking (180 rpm). The bacteria from the overnight culture were harvested and lysed under alkaline conditions. The cell lysate was neutralized in high salt buffer to allow the precipitation of denatured protein and chromosomal DNA. The lysate was centrifuged at ~17,900 g for 10 minutes to get rid of the cell debris and precipitated protein after the cell lysis. The supernatant was applied to the silica membrane column, which is specific for binding of plasmid DNA, provided in the kit. The column was centrifuged at ~17,900 g for 1 minute to get rid of the high salt buffer and then further washed with buffer containing 80% ethanol to remove any contaminants. Finally, the plasmid DNA was eluted with 30 to 50  $\mu$ l of molecular grade water and stored at -20 °C until required.

### **2.3.2 Preparation of Competent *E.coli* Cells**

5  $\mu$ l of *E.coli* cells from glycerol stock was inoculated into 5 ml LB culture and allowed to grow overnight at 37 °C with shaking (180 rpm). 2 ml of the overnight culture was inoculated in 100 ml LB medium and were grown until the O.D.  $A_{590}$  reaching ~ 0.4 to 0.5. The cells were centrifuged at 10,000 g for 20 minutes at 4 °C. The cell pellet was re-suspended in 30 ml of

ice-cold 100 mM calcium chloride solution and incubated on ice for 30 minutes. The cell suspension was centrifuged again at 10,000 g for 20 minutes. The supernatant was discarded. The cell pellet was re-suspended again in 2 ml of ice-cold 100 mM calcium chloride solution and incubated on ice for further 2 hours. Treatment of bacterial cells with ice-cold calcium chloride solution allows the cell wall to become permeable in order to take up exogenous DNA plasmids. After the incubation, the E.coli cells are said to be competent. The competent cells were pipetted into 200 µl aliquots ready for transformation.

### **2.3.3 Plasmid Transformations**

1 to 5 µg of plasmid DNA was added into the 200 µl aliquots of competent cells and incubated on ice for 30 minutes to allow plasmid DNA to stick to the cell surface. After incubation, the cells were heat shocked at 42 °C for 90 seconds to allow the uptake of plasmid DNA. The transformed cells were further incubated on ice for 2 minutes. 800 µl of LB medium was added into the transformed cells with gentle mixing. The transformants were grown at 37 °C for 45 minutes with shaking (180 rpm). Following the incubation, the transformants were plated onto a solid LB medium in the presence of appropriate antibiotics. The plates were incubated overnight at 37 °C. Positive and negative control experiments of transformation were carried out using plain expression vector pET24d and water to inoculate the competent cells. The cells were plated onto solid LB medium in the presence of appropriate antibiotics.

### **2.3.4 Restriction Digestions**

Restriction enzymes were mainly used for cloning of synthetic DNA fragments into existing expression vectors. Generally, 1 µg of plasmid DNA was digested in each reaction containing 1 µl of 10x enzyme-specific reaction buffer, 1 µl of restriction enzyme and X µl of plasmid DNA made up with appropriate volume of molecular grade water to a total volume of 10 or 20 µl. All restriction enzymes were purchased from the same company (New England Biolabs). When a double digestion using two different restriction enzymes was needed, a suitable buffer for both enzymes was chosen according to a buffer compatibility table provided by the company. The restriction digestion was normally incubated at 37 °C in a water bath for at least 1 hour. After the incubation, the digested DNA was mixed with DNA loading dye and analyzed on agarose gel described in 2.3.6. A negative control experiment was carried out in the absence of restriction enzyme.

### **2.3.5 Site-directed Mutagenesis**

Mutation involving a substitution of a single amino acid residue in a protein is achieved by site-directed mutagenesis. Mutation was created by a pair of short synthetic oligonucleotide primers (typically 25 bp) carrying the mutation(s) in a temperature-controlled PCR reaction using a thermo-cycler (Techne, Bibby Scientifics, UK). Typically, a PCR reaction mix was prepared as shown in table 2.5. The PCR reactions were initiated 2 minutes at 95 °C, followed by 30 cycles of denaturation for 30 seconds at 95 °C, annealing for 30 seconds at the appropriate temperature for the primers (normally, a temperature gradient  $\pm 6$  °C of suggested temperature was employed) and extension at 72 °C (2 min/1 kb). After the final cycle, a further extension for 10 minutes at 72 °C was included to ensure complete polymerization of the PCR products. Samples of the PCR product were analysed by agarose gel electrophoresis described in 2.3.6. If the amplicants were confirmed, the PCR products were treated with Dpn1

for 1 to 2 hours at 37 °C to digest the plasmid DNA template. After the digestion, the restriction enzyme was inactivated by heat-kill at 65 °C for 15 minutes. The amplicants were transformed into the competent *E.coli* DH5α cells as described in 2.3.3 or stored at -20 °C until required.

Compositions	Amount
Plasmid DNA template	~ 100ng
Forward primer	1 µl (~100pmol )
Reverse primer	1 µl (~100pmol )
10x reaction buffer	5 µl
dNTP mix	1 µl (0.2 mM)
DNA polymerase	1 µl
Molecular grade water	X µl up to a total volume of 50 µl

**Table 2.5 Sample preparation for PCR reactions in site-directed mutagenesis**

### 2.3.6 Agarose Gel Electrophoresis

Plasmid DNA from site-directed mutagenesis or DNA fragments from restriction digestions were analysed by agarose gel in the presence of ethidium bromide. Appropriate amount of agarose (typically 0.8% to 1.5% (w/v) depending on the size of the DNA samples) was dissolved in 1x TAE buffer (40 mM Tris-HCl, 20 mM acetic acid, 1 mM EDTA, pH 8.0) and boiled at 100% until the agarose was completely dissolved. The agarose solution was cast and allowed to set in a ventilated fume hood until required. DNA samples were mixed with 6x DNA loading buffer (10 mM Tris-HCl, 50 mM EDTA, 10% Ficoll 400, 0.4% Orange G, pH 7.5) in a 6:1 ratio. The agarose gel was run in a gel tank containing 1x TAE buffer under constant current at 120 mA for 1.5 hours. DNA ladders (1Kb, Bionline) were run adjacent to the DNA samples. The DNA fragments were visualised under UV light using Gel Doc imaging system (Bio-Rad).

## 2.4 Expression Vectors of Recombinant Globins

### 2.4.1 Expression Vectors of Recombinant Human Cytoglobin

All expression vectors of recombinant human cytoglobin used in this study and their relevant characteristics are shown in table 2.6.

Vectors	Description	Source or reference
pET24d	Expression vector under control of T7 promoter with kanamycin resistance	Novagen
pET24dCgb	pET24d containing wild-type full-length human <i>CYGB</i> gene	A kind gift of Dr. Eve Royal
pET24dCgb $\Delta$ C	pET24d containing wild-type human <i>CYGB</i> gene lacking the last 18 amino acid residues of the C-terminus	A kind gift of Dr. Eve Royal
pET24dCgbC38S	pET24d containing full-length human <i>CYGB</i> gene with the Cysteine at position 38 substituted by serine	In this work
pET24dCgbC83S	pET24d containing full-length human <i>CYGB</i> gene with the Cysteine at position 83 substituted by serine	In this work
pET24dCgbH81F	pET24d containing full-length human <i>CYGB</i> gene with the Histidine at position 81 substituted by Phenylalanine	In this work
pET24dCgbH81M	pET24d containing full-length human <i>CYGB</i> gene with the Histidine at position 81 substituted by Methionine	In this work
pET24dStrep-Cgb	pET24d containing an additional N-	In this work

	terminal Strep(II)tag sequence (TGGAGCCACCCGCAGTTCG-AAAAG) to the wild-type full-length human <i>CYGB</i> gene	
pET24dStrep-Cgb	pET24d containing an additional N- terminal Strep(II)tag sequence (TGGAGCCACCCGCAGTTCG-AAAAG) to wild-type human <i>CYGB</i> gene lacking the last 18 amino acid residues of the C- terminus	In this work

**Table 2.6 List of expression vectors of recombinant human cytoglobin used in this study**

## 2.4.2 Expression Vectors of Recombinant Sperm Whale Myoglobin

All expression vectors of recombinant sperm whale myoglobin used in this study and their relevant characteristics are shown in table 2.7.

Vectors	Description	Source or reference
pMb413	pUC19 containing a synthetic sperm whale Myoglobin gene	A kind gift from Prof. J. Olson
pMbH93K	pUC19 containing a synthetic sperm whale Myoglobin gene with the Histidine at position 93 substituted by Lysine	In this work

**Table 2.7 List of expression vectors of recombinant sperm whale myoglobin used in this study**

## 2.4.3 Construction of Expression Vectors for the Cys38 and Cys83 Variants of Cytoglobin

To examine the role of the disulphide bond in cytoglobin, two variant forms of cytoglobin in which one of the two cysteine (Cys) residues was replaced by a serine residue (Ser) to prevent formation of the disulphide bond were generated.

Substitution of the cysteine at position 38 with serine was achieved by site-directed mutagenesis as described in 2.3.5 using a pair of complementary synthetic primers (25 bp each) synthesised and purchased from Eurofins MWG Operon. About 100ng of each forward primer (5'-CTCTATGCCAACAGCGAGGACGTGG-3') and reverse primer (3'-CCACGTCCT-CGCTIGTTGGCATAGAG-3') was mixed with 100ng of pET24dCgb as template in a

temperature controlled PCR reaction. The PCR reaction conditions were optimized using a range of different annealing temperature (+/- 6 °C) selected according to the calculated melting temperature of the primers provided by the manufacturer. DMSO (5-10% (v/v)) was added due to high GC content of the primers. A sample of the resultant PCR product was checked on 1% agarose gel to confirm the presence of amplicants and remainder of the product was treated with DpnI (New England Biolabs) to digest the original DNA template. The PCR product containing the mutation (pET24dCgbC38S) was transformed into *E.coli* DH5 $\alpha$  strain and transformants selected on the basis of resistance to kanamycin (50  $\mu\text{g ml}^{-1}$ ). Colonies were randomly selected and propagated in 5 ml of LB in the presence of the same concentration of kanamycin. The plasmid DNA was extracted from the bacteria using commercial purification kits (Miniprep, Qiagen) as described in 2.3.1 and sequenced to confirm the presence of the mutation.

Substitution of the cysteine at position 83 with serine was achieved by replacing a fragment delineated by an internal BamHI site and an EcoRI site in the 3' flanking region of the *CYGB* gene cloned in pET24dCgb plasmid with a piece of synthetic DNA that encodes the Cys to Ser substitution. The mutation bearing DNA fragment was synthesized by GenScript (New Jersey, USA and is shown in figure 2.1).

The fragment was excised by restriction digestion of pET24dCgb with BamHI/EcoRI and the cut plasmid was isolated by agarose gel electrophoresis and subsequent gel purification using commercial kits (gel extraction, Qiagen). Ligation of the cut plasmid DNA and the synthetic fragment was achieved by incubating them in the presence of 1  $\mu\text{l}$  of T4 DNA ligase (New England Biolabs) overnight at 4 °C. The ligation product (pET24dCgbC83S) was transformed into *E.coli* DH5 $\alpha$  strain and transformants selected on the basis of resistance to kanamycin (50  $\mu\text{g ml}^{-1}$ ). Colonies were randomly selected and propagated in 5 ml of LB in the

presence of kanamycin ( $50 \mu\text{g ml}^{-1}$ ). The plasmid DNA was extracted from the bacteria as described in 2.3.1 and sequenced to confirm the presence of the mutation

#### **2.4.4 Construction of Expression Vectors for the His81 Variants of Cytooglobin**

To examine the effect of replacing the distal histidine in cytooglobin with different amino acids to mimic different heme pocket environments in other globins, variants of pET24dCgb which expressed variants of cytooglobin in which the histidine at position 81 was substituted with methionine (pET24dCgbH81M), tyrosine (pET24dCgbH81Y) or phenylalanine (pET24dCgbH81F) were generated by replacing the BamH1/EcoR1 fragment of the plasmid with a fragment of synthetic DNA (GenScript, New Jersey, USA) carrying the required as described in 2.2.3. The synthetic DNA sequences are shown in the figure 2.2.

#### **2.4.5 Construction of Expression Vectors for the Strep-tagged Cytooglobin**

The Strep-tagged versions of recombinant human cytooglobin the variant lacking the C-terminus required were generated by a variation of the method described in 2.2.3. In this case a fragment delineated by the 5' Nco1 and the internal BamH1 site was replaced by a synthetic DNA fragment that is identical except for the presence of additional sequence at the 5' end encoding a strep(II)-tag sequence (5'-TGGAGCCACCC-GCAGTTCGAAAAG-3'). An additional restriction site for SacI was introduced through a silent mutation to allow screening for the presence of the synthetic DNA fragment in the expression plasmid. The resultant plasmids designated pET24dStrep-Cgb and pET24dStrep-Cgb $\Delta$ C respectively.

**BamHI**  
gag**ggatcc**tctggagatggagcggagccctcagctgcggaagcacgcca**agc**gcggtcatg  
E D P L E M E R S P Q L R K H A **S** R V M  
ggggccctcaacactgtcgtggagaacctgcatgaccagacaaggtgtcctctgtgctc  
G A L N T V V E N L H D P D K V S S V L  
gcccttgtggggaaagcccacgcccctcaagcacaaggtggaaccggtgtacttcaagatc  
A L V G K A H A L K H K V E P V Y F K I  
ctctctgggggtcattctggaggtggcgcgaggaatttgccagtgacttcccacctgag  
L S G V I L E V V A E E F A S D F P P E  
acgcagcgtgcctgggccaagctgcgtggcctcatctacagccacgtgaccgctgcctac  
T Q R A W A K L R G L I Y S H V T A A Y  
aaggaagtgggctgggtgcagcaggtccctaacgccaccacccaccggccacactgcct  
K E V G W V Q Q V P N A T T P P A T L P  
tcttcggggccgtag**gaattc**  
S S G P - E F  
**EcoRI**

**Figure 2.1 DNA sequence of synthetic DNA fragment for cloning of cytoglobin C83S variant.** Original codon TGC which encodes a cysteine residue was replaced with AGC which encodes a serine highlighted in yellow. The synthetic DNA was cloned into the pET24dCgb expression plasmid using BamHI (cyan) and EcoRI (red).

**BamHI**  
gag**ggatcc**tctggagatggagcggagccctcagctgcggaag**ttt**gcctgccggtcatg  
E D P L E M E R S P Q L R K **F** A C R V M  
ggggccctcaacactgtcgtggagaacctgcatgaccagacaaggtgtcctctgtgctc  
G A L N T V V E N L H D P D K V S S V L  
gcccttgtggggaaagcccacgcccctcaagcacaaggtggaaccggtgtacttcaagatc  
A L V G K A H A L K H K V E P V Y F K I  
ctctctgggggtcattctggaggtggcgcgaggaatttgccagtgacttcccacctgag  
L S G V I L E V V A E E F A S D F P P E  
acgcagcgtgcctgggccaagctgcgtggcctcatctacagccacgtgaccgctgcctac  
T Q R A W A K L R G L I Y S H V T A A Y  
aaggaagtgggctgggtgcagcaggtccctaacgccaccacccaccggccacactgcct  
K E V G W V Q Q V P N A T T P P A T L P  
tcttcggggccgtag**gaattc**  
S S G P - E F  
**EcoRI**

**BamHI**

```

gagggatcctctggagatggagcggagccctcagctgcggaagatggcctgccgcgcatg
E D P L E M E R S P Q L R K M A C R V M
ggggccctcaacactgtcgtggagaacctgcatgacctcagacaaggtgtcctctgtgctc
G A L N T V V E N L H D P D K V S S V L
gcccttgtggggaaagcccacgccctcaagcacaaggtggaaccggtgtacttcaagatc
A L V G K A H A L K H K V E P V Y F K I
ctctctgggggtcattctggaggtgggtcgccgaggaatttgccagtgacttcccacctgag
L S G V I L E V V A E E F A S D F P P E
acgcagcgtgcctgggccaagctgcgtggcctcatctacagccacgtgaccgctgcctac
T Q R A W A K L R G L I Y S H V T A A Y
aaggaagtgggctgggtgcagcaggtccctaacgccaccacccaccggccacactgcct
K E V G W V Q Q V P N A T T P P A T L P
tcttcggggccgtagaagctt
S S G P - K L
HindIII

```

**BamHI**

```

gagggatcctctggagatggagcggagccctcagctgcggaagtacgcctgccgcgcatg
E D P L E M E R S P Q L R K Y A C R V M
ggggccctcaacactgtcgtggagaacctgcatgacctcagacaaggtgtcctctgtgctc
G A L N T V V E N L H D P D K V S S V L
gcccttgtggggaaagcccacgccctcaagcacaaggtggaaccggtgtacttcaagatc
A L V G K A H A L K H K V E P V Y F K I
ctctctgggggtcattctggaggtgggtcgccgaggaatttgccagtgacttcccacctgag
L S G V I L E V V A E E F A S D F P P E
acgcagcgtgcctgggccaagctgcgtggcctcatctacagccacgtgaccgctgcctac
T Q R A W A K L R G L I Y S H V T A A Y
aaggaagtgggctgggtgcagcaggtccctaacgccaccacccaccggccacactgcct
K E V G W V Q Q V P N A T T P P A T L P
tcttcggggccgtaggaattc
S S G P - E F
EcoRI

```

**Figure 2.2 DNA sequence of synthetic DNA fragment for cloning of cytoglobin H81F, H81M and H81Y variants.** Original codon CAC which encodes a histidine was replaced with TTT, ATG and TAC which encode a phenylalanine, a methionine and a tyrosine, respectively. The mutation sites are highlighted in yellow. The synthetic DNA was cloned into pET24dCgb expression plasmid using BamHI (cyan) and EcoRI/HindIII (red/green)

CAGG **CCATGG** CAAGCTGGAGCCACCCGCAGTTCGAAAAGGTGCCAGGCGAGATGGAGATCGAG  
 Q A M A S **W S H P Q F E K** V P G E M E I E  
 CGCCGTGAGCGGAGCGAG **GAGCTC** TCCGAGGCGGAGCGCAAGGCGGTGCAGGCTATGTGGGCC  
 R R E R S E E L S E A E R K A V Q A M W A  
 CGGCTCTATGCCAACTGCGAGGACGTGGGGGTGGCCATCCTGGTGC GTTTCTTTGTGAACTTC  
 R L Y A N C E D V G V A I L V R F F V N F  
 CCGTCGGCCAAGCAGTACTTCAGCCAGTTCAAGCACATGGAG **GGATCC** TCTGGAG  
 P S A K Q Y F S Q F K H M E D P L E

**Figure 2.3 DNA sequence of synthetic DNA fragment for cloning of cytoglobin Cloning strategy of strep-tagged cytoglobin.** A strep(II)-tag sequence (WSHPQFEK highlighted in red) was introduced to the 5' end of the *CYGB* DNA sequence to encode a strep-tag at n-terminus of cytoglobin. The synthetic DNA fragment was cloned into the pET24dCgb expression plasmid using NcoI (yellow) and BamHI (blue). A special restriction site of SacI (grey) was created by a silent mutation (GAGCTG → C) in the synthetic DNA to confirm successful insertion of the synthetic DNA fragment into the expression plasmid.

## 2.4.6 Construction of Expression Vectors for the H93K Variant of Sperm Whale

### Myoglobin

To examine the effect of changing proximal heme ligands on nitrite reductase activity of myoglobin, a variant form of myoglobin in which the proximal histidine (His93) residues was replaced by a lysine residue (Lys) which is commonly found in bacterial nitrite reductase.

Substitution of the histidine at position 93 with lysine was done by site-directed mutagenesis as described in 2.3.5 using a pair of complementary synthetic primers (26bp each) synthesised by Eurofins MWG Operon. About 100ng of each forward primer (5'-GCTTGCGCAATCGAAAGCTACTAAAC-3') and reverse primer (3'-GTTTAGTAGCTTTTCGATTGCGCAAGC-3') was mixed with 100ng of pMB413 expression plasmid as template in a temperature controlled PCR reaction. The PCR reaction conditions were optimized using a range of different annealing temperature (+/- 6 °C) selected according to the calculated melting temperature of the primers provided by the manufacturer.

A small amount of the resultant PCR product was checked on 1.5% agarose gel to confirm the presence of amplicants and remainder of the product was treated with DpnI (New England Biolabs) to digest the original DNA template. The PCR product containing the mutation (pMBH93K) was transformed into *E.coli* DH5 $\alpha$  strain and transformants selected on the basis of resistance to ampicillin (100  $\mu\text{g ml}^{-1}$ ) and streptomycin (50  $\mu\text{g ml}^{-1}$ ). Colonies were randomly selected and propagated in 5 ml of LB in the presence of the same concentration of ampicillin and streptomycin. The plasmid DNA was extracted from the bacteria using commercial purification kits (Miniprep, Qiagen) as described in 2.3.1 and sequenced to confirm the presence of the mutation.

## **2.5 Expression and Purification of Human Recombinant Cytoglobin and Variants**

### **2.5.1 Expression of Recombinant Human Cytoglobin in *E.coli***

Human recombinant *CYGB* gene cloned into pET24d expression vectors (pET24dCgb) was transformed into *E.coli* BL21 (DE3) strain and plated on the solid LB medium in the presence of 50 µg ml<sup>-1</sup> kanamycin. Transformed bacterial colonies were subjected to an expression trial in 100 ml LB before a scale-up expression in 6 L LB. Bacterial colonies were selected randomly from the LB plate and inoculated into a 5 ml LB starting culture supplemented with 50 µg ml<sup>-1</sup> kanamycin. The culture was incubated overnight at 37 °C with shaking (180 rpm). The overnight culture was used to inoculate a 50ml LB supplemented with the same concentration of kanamycin and incubated at 37 °C with shaking (180 rpm) until O.D. A<sub>590</sub> reaching to 0.8 which is said to be ready for induction of protein expression. The Induction of expression of recombinant cytoglobin was achieved by adding a final concentration of 1mM of Isopropyl β-D-1-thiogalactopyranoside (IPTG) into the cultures. The cultures were allowed to further incubate for 4 hours at 24 °C with shaking (180 rpm). A small sample of culture (500 µl) was taken out before and after the induction for an expression check by SDS-PAGE.

### **2.5.2 Extraction of Recombinant Human Cytoglobin**

A large scale expression of recombinant cytoglobin was performed in 6 x 1L LB cultures in the presence of 50 µg ml<sup>-1</sup> kanamycin. Incubation and induction protein of expression were done under the same conditions as described in 2.3.1. All cultures were collected in 1L centrifuge flasks and centrifuged at 9,000 g for 20 minutes (Beckman Avanti J-20, rotor JLA 8.1000). The pellets were collected and re-suspended in a minimal volume of resuspension buffer (50 mM Tris-HCl, 1 mM EDTA, pH 8.0). The re-suspended pellets were snap frozen in liquid nitrogen and then stored at -80 °C until required.

The re-suspended pellets were thawed and passed through twice in a French Press cell disruptor at high pressure (12000 psi). The cell homogenate was kept on ice throughout the process to minimise proteolysis. Two to three protease inhibitors (EDTA-free) tablet (Roche, UK) and small amount ( $1 \text{ mg ml}^{-1}$ ) of DNase 1 (Sigma-aldrich, UK) was added into the cell homogenate. The homogenate was centrifuged at  $\sim 10,000 \text{ g}$  (Philip Harris Sigma3k30 centrifuge, rotor 19776-H) for 30 minutes at  $4 \text{ }^{\circ}\text{C}$ . The supernatant was separated from the pellet and further centrifuged at  $\sim 164,600 \text{ g}$  (Beckman Optima XL-100K Ultracentrifuge, rotor 70Ti) for 1 hour to get rid of the cell membrane. The supernatant which contains the soluble form of recombinant cytoglobin was collected and transferred into a 50 ml centrifuge tube until required.

### **2.5.3 Heme Reconstitution of Apo-cytoglobin Protein in the Cell Lysate**

In order to determine the amount of heme cofactor required to reconstitute the folded recombinant protein in the cell lysate, a sample (typically  $600 \text{ }\mu\text{l}$ ) of cell lysate was removed and diluted 5-fold with resuspension buffer in a 3 ml quartz cuvette. The UV/vis absorption spectrum ( $750 \text{ nm}$  to  $250 \text{ nm}$ ) of the dilute cell lysate was recorded to assess the basal level of holo-protein. A concentrated stock solution ( $1\text{-}2 \text{ mM}$ ) of hemin was prepared by dissolving hemin chloride (Sigma Aldrich, UK) in 50% (v/v) ethanol with an addition of NaOH at a final concentration of  $5 \text{ mM}$ . Sequential additions of 2 to  $5 \text{ }\mu\text{l}$  of the concentrated hemin solution were made to the dilute cell lysate and the UV/vis spectrum re-recorded after each addition until the apo-cytoglobin appeared to be saturated with hemin (holo-cytoglobin) when the increase in the absorbance of free hemin at  $385 \text{ nm}$  became more prominent than the absorbance of the solet peak at  $427 \text{ nm}$  ( $\Delta 385 \text{ nm} > \Delta 427 \text{ nm}$ ). The amount of stock hemin solution needed to fully reconstitute the apo-cytoglobin in the cell lysate was calculated from the volume of the cell lysate and an appropriate amount of hemin solution was added into the

cell lysate drop-wise and the solution left stirring at 4 °C overnight.

#### **2.5.4 Refolding and Reconstitution of Recombinant Cytoglobin from Inclusion Bodies**

Recombinant cytoglobin produced by *E.coli* in this study was found mainly in the cell lysate as a soluble, folded apo-protein. However, some recombinant cytoglobin was also found in inclusion bodies in a missfolded or unfolded form. In order to recover recombinant cytoglobin the inclusion bodies must first be solubilised. This was achieved by washing the inclusion bodies 3 to 4 times with resuspension cell lysis buffer (50 mM Tris-HCl, 1mM EDTA, 1% (w/v) Triton X-100, pH 7.5) followed by repelleting them by centrifugation at 10,000 g for 20 minutes. The supernatant was discarded after each wash. After the final wash the pellet was dissolved in a minimal volume of solubilization buffer (50 mM Tris-HCl, 6 M Guanidium Hydrochloride, 1% (v/v)  $\beta$ -mercaptoethanol, pH 7.5) before reconstitution with hemin using a method described by Vinck and co-workers for the purification of neuroglobin with minor modifications (Vinck et. al. 2001). The protein concentration and the purity of the protein in the solubilised inclusion bodies were first determined using Bradford assay and SDS-PAGE, respectively. Once the purity and the concentration were determined, the apo-cytoglobin was mixed with 1.4 times molar excess hemin solution and followed by dialysis against 20 mM Tris-HCl pH 8.0 at 4 °C overnight to allow refolding of the recombinant cytoglobin.

#### **2.5.5 Purification of Recombinant Cytoglobin from Cell Lysate**

Ammonium sulphate (194 g of solid  $(\text{NH}_4)_2\text{SO}_4 \text{ L}^{-1}$ ) was added to the cell lysate containing reconstituted holo-cytoglobin was subjected to precipitation at 35% saturation and allowed to stir for at least an hour at 4 °C. The mixture was centrifuged at 15,000 g for 30 minutes (Philip Harris Sigma3k30 centrifuge, rotor 19776-H) and the pellet discarded. The supernatant was treated with a further addition of ammonium sulphate (164 g of solid  $(\text{NH}_4)_2\text{SO}_4 \text{ L}^{-1}$ ) as

described above to bring the concentration to 60% (saturation and allowed to stir overnight at 4 °C. The mixture was centrifuged at 48,400 g for 30 minutes (Beckman Avanti J-20, rotor JA 25.50) the following day. The supernatant was discarded, and the pellet was re-suspended in a minimum volume of 20 mM Tris-HCl pH 8.0.

The re-suspended protein solution was adjusted to 25% saturated ammonium sulphate and loaded onto a hydrophobic interaction (phenyl sepharose) column equilibrated with equilibration buffer (20 mM Tris-HCl, 30 % ammonium sulphate, pH 8.0) at a flow rate of 0.5 ml min<sup>-1</sup> using a AKTA prime Liquid chromatography system (GE healthcare). The protein was eluted by running a reverse gradient over 8 column volume (C.V.) from 30% saturated ammonium sulphate to 0 % ammonium sulphate in the elution buffer (20 mM Tris-HCl, pH 8.0) at a flow rate of 0.5 ml min<sup>-1</sup> collecting 10ml fractions. The fractions containing the recombinant cytoglobin were analysed by a combination of UV/vis spectroscopy and SDS-PAGE.

The protein fractions containing the cytoglobin were collected and concentrated down to around 50 ml using a stirred ultrafiltration cells (Amicon) fitted with a 75mm YM10 membrane (Millipore) and then dialyzed against dialysis buffer (20 mM Tris-HCl pH 8.0) to remove the residual ammonium sulphate. The dialysed protein was loaded on to a DEAE sepharose fast-flow column equilibrated in the same buffer. The bound protein was eluted by running a gradient over 8 C.V. from 0 mM to 150 mM NaCl at a flow rate of 1.0 ml min<sup>-1</sup> collecting 3 ml fractions. Fractions were analysed and selected as described above.

The protein fractions containing semi-pure cytoglobin ( $A_{416}/A_{280}$  or Rz value~ above 2.0) were pooled and further concentrated into small volume using a centrifugal concentrator (Vivaspin 500 MWCO 10k, Viva Science). The pooled protein was loaded onto a gel filtration column (Superdex75 16/600 prep grade, GE) equilibrated in the buffer (20 mM Tris-HCl,

150mM NaCl, pH 8.0) for the final polishing step. The sample volume (typically 2 to 5 ml) and the flow rate ( $0.1 \text{ ml min}^{-1}$ ) were minimized as possible to get the best resolution for the separation of the impurities from the pure cytoglobin protein. The fractions were analysed and selected as described above. Fractions containing pure recombinant cytoglobin protein ( $R_z$  value  $\sim 2.80$ ) were concentrated and desalted using the centrifugal concentrator and then stored at  $-80 \text{ }^\circ\text{C}$  until used.

### **2.5.6 Purification of Recombinant Cytoglobin from Inclusion Bodies**

The reconstituted protein was adjusted to 25% saturated ammonium sulphate and loaded to a phenyl sepharose column equilibrated with equilibration Buffer (20 mM Tris-HCl, 30 % ammonium sulphate, pH 8.0) at a flow rate of  $1 \text{ ml min}^{-1}$ . The column was developed by running a reverse gradient over 8 C.V. from 30% saturated ammonium sulphate to 0% ammonium sulphate in elution buffer (20 mM Tris-HCl pH 8.0) at a flow rate of  $1 \text{ ml min}^{-1}$ . Fractions containing recombinant cytoglobin were analysed and selected by a combination of UV spectroscopy and SDS-PAGE.

The pooled protein fractions were collected and concentrated using a stirred ultrafiltration cell (Amicon) fitted with a 25 mm PLBC membrane (Millipore). The concentrated protein was treated with 10 mM DTT on ice and stored at  $4 \text{ }^\circ\text{C}$  overnight in order to remove any undesired adduct formed between the free thiol groups and the  $\beta$ -mercaptoethanol during reconstitution.

The protein samples were further concentrated down to 5 ml by a ultrafiltration cell (Amicon) before loading onto a gel filtration column (Hiload 16/60 superdex75 prep grade, Pharmacia) equilibrated in the buffer (20 mM Tris-HCl, 100 mM NaCl, pH 7.5) at a flow rate of  $0.5 \text{ ml min}^{-1}$ . The column was run at a minimum flow rate ( $0.1 \text{ ml min}^{-1}$ ) to get the best

resolution for the separation of the impurities from the pure cytoglobin protein. The fractions containing pure cytoglobin were analyzed by a combination of UV spectroscopy and SDS-PAGE. The fractions containing pure cytoglobin (Rz value ~ 2.80) were pooled, concentrated and desalted using a centrifugal concentrator (Vivaspin 500 MWCO 10k, Viva Science) and then stored at -80 °C until required.

### **2.5.7 Expression and Purification of Recombinant Cytoglobin Variants**

All other cytoglobin variants including Cgb $\Delta$ C, C38S, C83S, H81M, H81F, H81Y and strep-Cgb were expressed and purified from the soluble fractions of the *E.coli* BL21 (DE3) strain following the same procedures as described in 2.5.5

### **2.5.8 Expression and Purification of Strep-tagged Recombinant Cytoglobin**

Strep-tagged recombinant cytoglobin (strep-Cgb) was expressed in *E.coli* BL21 (DE3) transformed with plasmid and subsequently purified according to the procedures as described in 2.5.2 and 2.5.3 with some minor variations. The cell lysate was subjected to ammonium sulphate precipitation at 35% saturation and 60 % saturation as described above. The re-suspended protein solution was loaded in batches onto a Strep-tactin super-flow Plus cartridge column (Qiagen) which had been equilibrated with washing buffer (20 mM Sodium phosphate, 300mM NaCl, pH 8.0). After loading the protein solution, the column was washed with five column volumes of the same buffer to remove any unbound protein, and the  $A_{280}$  of the eluent was checked to ensure that it had returned to its baseline value. Elution of strep-cytoglobin from the column was achieved by washing the column with two C.V. of elution buffer (20 mM Sodium phosphate, 300 mM NaCl, 2.5 mM Desthiobiotin, pH 8.0) at a flow rate of 1 ml min<sup>-1</sup> collecting 1 ml fractions. The column was regenerated by washing with 5 C.V. of regeneration buffer (20 mM Sodium phosphate, 300 mM NaCl, 1 mM HABA (2-(4-Hydroxyphenylazo)

benzoic acid, pH 8.0) and followed by washing with 5 C.V. of 0.5 M NaOH to remove any residual HABA which may lower the binding capacity of the Strep-tactin column. After regeneration, the column was re-equilibrated with the washing buffer again ready for purification of the next batch of strep-Cgb.

Fractions containing strep-Cgb were analysed and selected by a combination of UV spectroscopy and SDS-PAGE. The fractions containing pure strep-Cgb were pooled together. The pooled protein was loaded onto the gel filtration column (Superdex75 16/600 prep grade, GE) equilibrated in the buffer (20 mM Tris-HCl, 150 mM NaCl, pH 8.0) at a flow rate of 0.1 ml min<sup>-1</sup> for the final polishing step. The sample volume and the flow rate were minimized as possible to get the best resolution for the separation of the impurities and the pure protein. The fractions were analysed and selected as described above. Fractions containing pure strep-Cgb protein was further concentrated and desalted using the centrifugal concentrator (Vivaspin 500 MWCO 10k, Viva Science) and then stored at -80 °C until used.

## **2.6 Expression and Purification of Sperm Whale Myoglobin and Variants**

### **2.6.1 Expression of Sperm Whale Myoglobin in *E.coli***

A 5  $\mu$ l of glycerol stocks of *E.coli* TB1 containing a pMb413 synthetic sperm whale myoglobin gene that has been cloned into pUC19 vectors was inoculated into a 10 ml LB culture containing ampicillin (100  $\mu$ g ml<sup>-1</sup>) and streptomycin (50  $\mu$ g ml<sup>-1</sup>). The bacterial culture was incubated overnight at 37 °C with shaking (180 rpm). 1ml of the overnight culture was inoculated into a 50 ml LB culture in the presence of the same concentration of ampicillin and streptomycin for further 7 hours. 2.5 ml of the bacterial culture was inoculated into 5 x 1.25L LB culture in the presence of the same concentration of ampicillin and streptomycin and allowed to grow overnight at 37 °C with shaking (180 rpm).

### **2.6.2 Extraction of Sperm Whale Myoglobin**

All cultures were collected in 1 L centrifuge flasks and centrifuged (Beckman Avanti J-20, rotor JLA 8.1000) at 9,000 g for 20 minutes. The bacterial cell pellets were collected and re-suspended in a minimal volume of the re-suspension buffer (50 mM Tris-HCl, 1 mM EDTA, pH 8.0). The re-suspended pellets were snap frozen in liquid nitrogen and stored at -80 °C until required.

The re-suspended pellets were thawed and broken by two passages through a French Press at 16000 psi. 1 ml of 5 mM DTT, 2 x EDTA-free protease inhibitors tablet (Roche, UK) and 1mg ml<sup>-1</sup> of DNase 1 (Sigma-aldrich, UK) were added into the cell homogenate. The homogenate was centrifuged at ~10,000 g (Philip Harris Sigma3k30 centrifuge, rotor 19776-H) for 30 minutes at 4 °C. Supernatant was taken out and further centrifuged at 186,000 g (Beckman Optima XL-100K Ultracentrifuge, rotor 45Ti) for 1 hour at 4 °C. Supernatant was collected and transferred into a 50 ml centrifuge tube.

For expression of myoglobin proximal histidine H93K variants, due to the fact that the proteins were expressed mainly as apo-protein in the cell lysate, reconstitution of hemein was performed to make holo-protein before subsequent column purification steps. The detail of the heme reconstitution follows the same procedures as described in 2.5.3 heme reconstitution for apo-cytoglobin. The protein solution that was saturated with hemein was allowed to incubate with stirring at 4 °C overnight.

### **2.6.3 Purification of Sperm Whale Myoglobin**

The cell lysate containing myoglobin was subjected to the first ammonium sulphate precipitation at 50% saturation (313.5 g of solid  $(\text{NH}_4)_2\text{SO}_4 \text{ L}^{-1}$ ) and allowed to stir for at least an hour at 4 °C. The mixture was centrifuged at 15,000 g for 30 minutes (Philip Harris Sigma3k30 centrifuge, rotor 19776-H). The pellet was discarded. The supernatant was subjected to a further ammonium sulphate precipitation at 90% saturation (302 g of solid  $(\text{NH}_4)_2\text{SO}_4 \text{ L}^{-1}$ ) and allowed to stir overnight at 4 °C. The mixture was centrifuged at 48,400 g for 30 minutes (Beckman Avanti J-20, rotor JA 25.50) the following day. The supernatant was discarded, while the pellet was re-suspended in a minimal volume of buffer (20 mM Tris-HCl, 1mM EDTA, pH 8.0). The re-suspended protein solution was dialysed against 4 L of dialysis buffer (20 mM Tris-HCl, 1mM EDTA, pH 8.0) overnight at 4 °C. After the dialysis, the protein solution was centrifuged at 15,000 g for 30 minutes (Philip Harris Sigma3k30 centrifuge, rotor 19776-H) to remove any precipitation.

The supernatant was loaded on to a DEAE sepharose fast-flow column equilibrated in the same buffer as above. Since only impurities are binding to the matrix, the column was further washed with the same buffer at a flow rate of  $1.0 \text{ ml min}^{-1}$  collecting 10 ml fractions until  $A_{280}$  return to baseline. Fractions containing myoglobin were analysed by a combination

of UV/vis spectroscopy and SDS-PAGE. The fractions were collected and concentrated to around 50 ml using stirred ultrafiltration cells (Amicon) fitted with a 75 mm YM10 membrane (Millipore). The resultant protein solution was adjusted to pH 6.0 by adding a few drops of 10% acetic acid and then centrifuged at 15,000 g for 30 minutes (Philip Harris Sigma3k30 centrifuge, rotor 19776-H) to remove any precipitation.

The supernatant was loaded on to a CM sepharose fast-flow column equilibrated with Sodium phosphate A (20 mM sodium phosphate pH6.0). The column was washed by the same buffer for a further 2 C.V. until the  $A_{280}$  return to baseline. The column was developed by running a gradient over 8 C.V. from 0% of Sodium phosphate A to 100% of Sodium phosphate B (50 mM sodium phosphate pH 9.0) at a flow rate of  $0.2 \text{ ml min}^{-1}$  overnight collecting 3 ml fractions. Fractions were analysed and selected as described above.

The protein fractions containing virtually pure myoglobin were pooled together and further concentrated into small volume using a centrifugal concentrator (Vivaspin 500 MWCO 10k, Viva Science). To ensure all protein is in oxidized state, a small amount of Potassium Ferricyanide was added into the protein. The pooled protein was loaded onto the gel filtration column (Superdex75 16/600 prep grade, GE) equilibrated with buffer (20 mM sodium phosphate pH 6.0) for the final polishing step. The sample volume and the flow rate were minimized as possible to get the best resolution for the separation of the impurities and the pure protein. The fractions were analyzed and selected as described above. Fractions containing pure recombinant sperm whale myoglobin protein were concentrated using the centrifugal concentrator and then stored at  $-80 \text{ }^{\circ}\text{C}$  until used.

## **2.7 Spectroscopic Characterisation of Globins**

### **2.7.1 Electronic Adsorption Spectroscopy**

Electronic adsorption (UV/vis) spectroscopy was routinely used in this study for a number of purposes. All the electronic adsorption spectra recorded in this study were obtained from a Cary4000 UV/Vis spectrophotometer or a Cary50 UV/vis spectrophotometer (Agilent technologies, UK).

For analysing protein fractions eluted from column chromatography during the purification, a 2 mm path-length quartz cuvette was used. Protein fractions were directly transferred to the cuvette and a full spectrum scan from 750 nm to 250 nm was performed.

For monitoring reduction of the heme iron and the disulphide bond in cytoglobin. The samples preparation method for specific reduction of heme iron and the disulphide bond is described in 2.8.1 and 2.8.2, respectively. Once the cytoglobin protein is in the appropriate redox state, the cuvette was sealed and wrapped with parafilm and transferred to the Cary4000 UV/Vis spectrophotometer. A full spectrum scan from 750 nm to 250 nm was recorded every 5 to 10 minutes using cycle mode until no further change of the spectrum was observed.

For monitoring static ligand binding to globins in the ferric state, such as fluoride binding to cytoglobin and nitrite binding to myoglobin, the binding of ligands was performed on the Cary4000 UV/Vis spectrophotometer scanning using a 10 mm path-length split cuvette which is divided into two identical chambers as shown in figure 2.4. Typically, 1 ml of  $x \mu\text{M}$  protein solution in an appropriate buffer was placed in one of the chambers, while 1 ml of the appropriate buffer was placed in another chamber acting as a blank. Spectrum of protein

solution was scanned from 750 nm to 250 nm (Figure 2.4A). Subsequently, the cuvette is cleaned and the chamber was filled with 1 ml of buffer containing x mM ligands of interest and the spectrum of the ligands was scanned (Figure 2.4B). After recording the individual spectrum of protein and ligands, the solution of 1 ml of x  $\mu$ M protein and 1 ml of x mM ligands was added into the separate chamber and the spectrum of the two solutions (before mixing) was recorded (Figure 2.4C). Finally, the cuvette was sealed parafilm. The two solutions were mixed by inverting the parafilm-sealed cuvette several times and allowed to stand for 2 minutes. The spectrum of the mixture of protein-ligand complex was recorded (Figure 2.4D). The spectra of the mixture of protein-ligand complex before and after mixing were overlaid to examine the changes in the spectrum.

For measuring the rate of nitrite reduction by myoglobin, samples of myoglobin protein were prepared anaerobically in an anaerobic chamber. The samples were diluted to approximately 5  $\mu$ M in 5 ml of 100 mM Sodium phosphate pH 7.0, and reduced in the presence of 30 mM sodium dithionite to prevent the formation of ferrous oxy complex. The protein samples were aliquot into the 1 ml quartz cuvettes which were sealed with air-tight suba-seal rubber septa and wrapped with parafilm. The reactions were monitored by a multiple-cycle scanning mode from 500 nm to 350 nm at 25 °C with a scan rate at 300 nm min<sup>-1</sup>. The nitrite reduction reactions were initiated by adding 10  $\mu$ l of anaerobic sodium nitrite stock solutions to yield a final concentration of nitrite at 0.5 mM. Nitrite concentration dependence experiments were done at various nitrite concentrations from 0.05 mM to 1 mM under the same conditions and set-up. The experiments were typically done in triplicate unless otherwise specified. The spectral changes during the nitrite reduction were recorded at a specific time interval. For measuring the rate of nitrite reduction by sperm whale myoglobin and the distal pocket variants, the absorbance at 419 nm was plotted as a function of time. The resultant scatter plot was analysed and fit into a single exponential curve to obtain the first order rate constant ( $k_{obs}$ ).

The bimolecular rate constant ( $k$ ) of the nitrite reduction by myoglobin was obtained from the plot of the first order rate constant at different nitrite concentrations from 0.05 mM to 1 mM.

### **2.7.2 Stopped-Flow Spectroscopy**

The stopped-flow spectroscopy was mainly used to monitor changes in absorbance in rapid mixing experiments. Typically, the experiments were performed on a Bio-Sequential DX.17MV stopped-flow spectrophotometer (Applied Photophysics, Surrey, UK) using a 1 cm path-length cell in a steady temperature condition at 25 °C.

For monitoring heme reduction in myoglobin by dithionite, 60 mM of sodium dithionite was prepared immediately before the experiment by dissolving dithionite powders in degassed buffer (100 mM sodium phosphate pH 7.0) in an anaerobic chamber under nitrogen atmosphere. Sperm whale myoglobin proteins were diluted to approximately 10  $\mu$ M in the same buffer. Solutions were transferred into 5 ml gas-tight Hamilton syringes and taken out from the anaerobic chamber. All sample chambers and tubing in the stopped-flow spectrophotometer were flushed with degassed buffer (100 mM sodium phosphate pH 7.0) before the experiment to ensure absolute no oxygen in the system. The myoglobin solution was mixed with the dithionite rapidly in the sample mixing chamber under a computer controlled manner. The reduction of myoglobin by dithionite was detected with a side window photomultiplier at a single wavelength at 420 nm. The rates of heme reduction of distal pocket variants were measured in the same manner as in wild-type myoglobin.

To determine the dissociation constant ( $k_d$ ) for nitrite binding to myoglobin in the ferric state. The kinetic measurements of nitrite binding were done by rapid mixing method described by Wanat and colleagues on the stopped-flow spectrophotometer using a 1 cm

pathlength cell. 10  $\mu\text{M}$  of ferric myoglobin and different concentrations (0.02 mM to 300 mM) of sodium nitrite were prepared in buffer (20 mM citric acid phosphate pH 7.0) and mixed together under pseudo first order conditions (concentration of nitrite is in excess). Detection at a single wavelength was with a side window photomultiplier. In this configuration a minimum of 1000 data points were collected per experiment. Experimental traces recorded at 407 nm were analysed as single exponential decay to derive pseudo-first order rate constant ( $k_{\text{obs}}$ ) and amplitude ( $\Delta\text{absorbance}$ ) for the reaction. Since, the pseudo first order rate constant for the nitrite binding is linear with increasing nitrite concentration, the  $k_{\text{obs}}$  can therefore be expressed as  $k_{\text{on}}[\text{NO}_2^-] + k_{\text{off}}$  (Wanat et al., 2002). Thus, the association ( $k_{\text{on}}$ ) and dissociation rate constant ( $k_{\text{off}}$ ) for nitrite binding was determined from the slope and y-intercept of the  $K_{\text{obs}}$  against nitrite concentration plot, respectively.

### **2.7.3 Magnetic Circular Dichroism (MCD) Spectroscopy**

Magnetic circular dichroism detects a differential absorption of left and right circular polarised light induced by passing through a molecule under a strong magnetic field. MCD spectroscopy is a useful technique to examine the electronic structure of metalloproteins, especially heme-containing enzymes (Cheesman et al., 1991). Briefly, the MCD signals in the UV-visible region between 300 and 600 nm provides information of the spin and oxidation state of the heme iron. Whilst in the near infra red (Near IR) region between 600 and 2500 nm, the nature of the axial ligands of the heme iron could be observed.

Room temperature magnetic circular dichroism (MCD) spectra were recorded in collaboration with Dr. Myles Cheesman (School of Chemistry, UEA) on a Jasco J-810 CD spectrophotometer (Tokyo, Japan) equipped with super conducting magnet (Oxford Instruments, Abingdon, UK). For the room-temperature MCD measurement, cytoglobin at

different redox states in the presence or absence of exogenous ligands was prepared according to the methods described in section 2.8. The sample concentration of cytoglobin was at approximately 100  $\mu\text{M}$ .

For the room temperature MCD measurement on the nitrite-bound myoglobin, the original buffer (20 mM sodium phosphate pH 6.0) in the wild-type sperm whale myoglobin and distal pocket variants was changed to 20 mM citric acid phosphate pH 7.0 using spin concentrators prior to the experiments. Stock solution of nitrite was prepared in the same buffer and added into the protein solution at a final concentration of 200  $\mu\text{M}$ . All the samples containing nitrite were allowed to incubate for at least 10 minutes at room temperature to ensure stable binding before being transferred into the cuvettes. The same samples containing nitrite-bound myoglobin were transferred into EPR tube for subsequent EPR measurement

#### **2.7.4 Electron Paramagnetic Resonance (EPR) spectroscopy**

EPR measurements were kindly conducted by Mr. Alexander Pak and Dr. Fraser Macmillan (School of Chemistry, UEA). All measurements were obtained from a Bruker ELEXSYS 500 spectrometer equipped with Super X system (Bruker, USA). Low temperature experiments were performed using a ESR-900 helium cryostat (Oxford Instruments, UK) and ITC3 temperature controller. For the low temperature x-band EPR measurement to characterise the heme pocket environment of the cytoglobin, the protein concentration of cytoglobin samples are at a region of 150  $\mu\text{M}$  to 250  $\mu\text{M}$  in the buffer of 20 mM Tris-HCl pH 8.0 or 20 mM sodium phosphate pH 7.0. All the cytoglobin samples were transferred to EPR tubes (Wilmad Glass) and snap frozen in liquid nitrogen and then stored in  $-80\text{ }^{\circ}\text{C}$  until ready for measurements.

For low-temperature EPR measurement to examine the effect of the state of the disulphide bond on the heme iron, wild-type cytoglobin, C38S and C83S variants were mixed with 50 mM of GSH in a 1:1 (v/v) in 20 mM Tris-HCl pH 8.0 and allowed to incubate at room temperature for 30 minutes to ensure completed reduction of the disulphide bond before being transferred to EPR tubes (Wilmad Glass). Anaerobic samples were prepared in the same way as the aerobic samples, except that it is done in an anaerobic chamber. The EPR tubes were frozen in liquid nitrogen and then stored in -80 °C until ready for measurements.

### **2.7.5 Data Handling**

Spectra were saved as and exported out as CSV files (.CSV). The spectra were re-plotted using data analysis and graphics software (Origin lab). Calculation of the pseudo-first order rate constant of nitrite reduction by myoglobin and the bimolecular rate constant of nitrite reduction were done by the built-in curve fitting function in the same software.

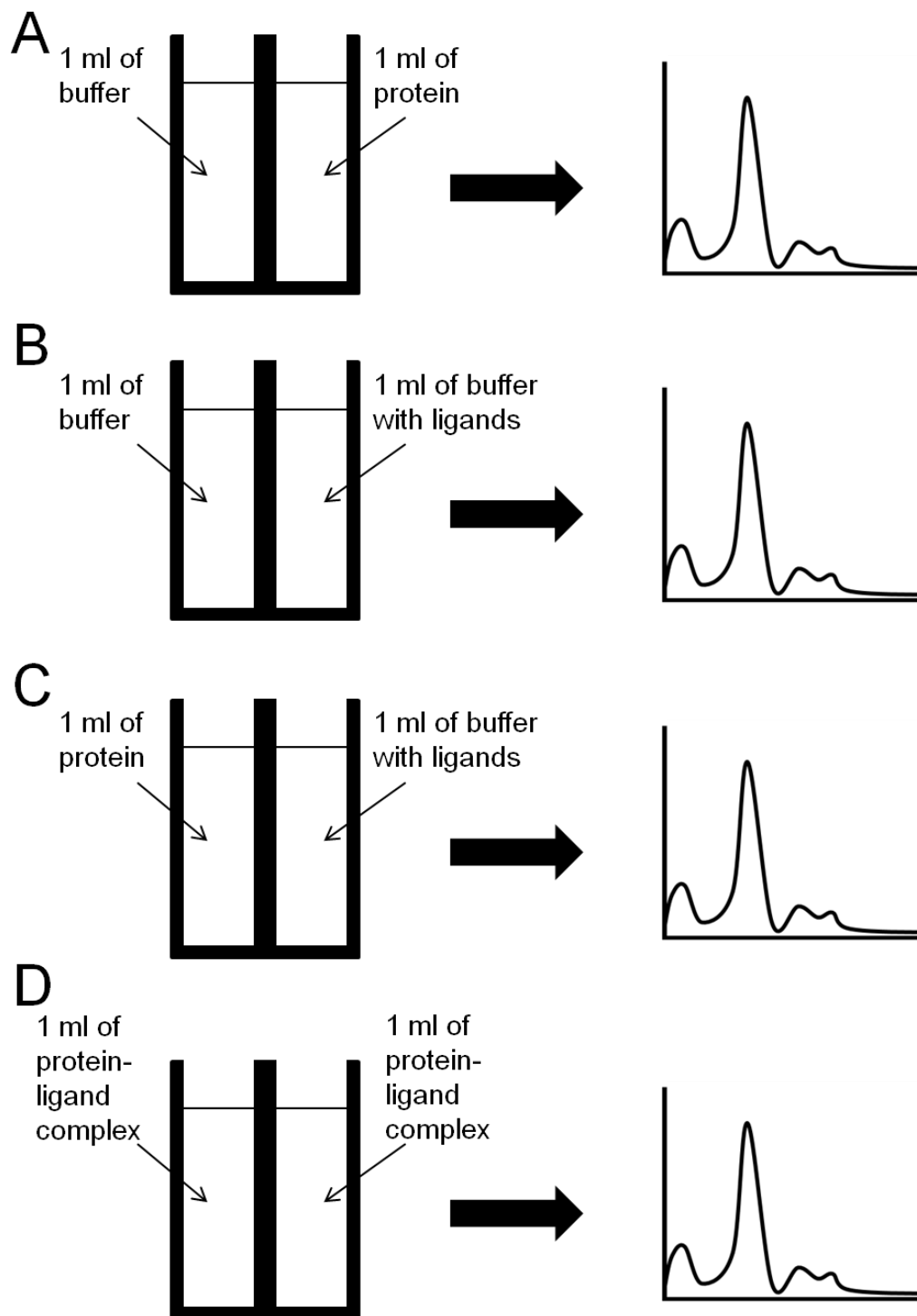


Figure 2.4 Diagram showing a workflow of studying static ligand binding on the spectrophotometer using a split cuvette.

## **2.8 Independent Reduction of Heme and Disulphide Bond in Cytochrome**

### **2.8.1. Reduction of Heme in Cytochrome**

As described in chapter 3 that interpretation of the ligand binding properties has been greatly hampered due to the misuse of reducing agents which reduce the heme iron and disulphide bond at the same time. Therefore, in order to facilitate the investigation of the ligand binding properties of cytochrome in this study without interfering with another redox site, a systematic way to control the redox state of the two redox sites is needed. Theoretically, four principle redox states could exist in cytochrome as shown in figure 2.5. The preparation methods are stated as below:

Redox state #1 was assigned to purified cytochrome as the heme iron and the disulphide bond is in the ferric and oxidized state before any treatments (Chapter 3.2.1). To generate cytochrome at redox state #2 at which the heme iron is reduced to ferrous state while the disulphide bond remains intact, cytochrome was first made anaerobic in an anaerobic chamber for at least 30 minutes prior to reduction. Enzymatic oxygen scrubbing system using Protocatechuate dioxygenase (PCD) and the substrate Protocatechuic acid (PCA) was employed to get rid of any residual oxygen in the buffer. Anaerobic protein solution was transferred into 1 ml quartz cuvette which was sealed with air-tight suba-seal rubber septa and wrapped with parafilm. Typically, the ferric spectrum of anaerobic cytochrome was recorded on the UV/vis spectrophotometer. Following the record of ferric spectrum, a final concentration of 1 to 2 mM of NADH was added to the protein solution in the presence of 1 to 10  $\mu$ M of PMS as a mediator to reduce the heme iron under anaerobic conditions. Such reduction system selectively reduces the heme iron but not the disulphide bond in cytochrome (Section 3.2.5). The cuvette was sealed again and the reduction of cytochrome was monitored by the spectrophotometer as described in section 2.7.1. At this point, exogenous gas ligands, such

as CO and NO solution can be injected into the anaerobic cytoglobin protein solution using a gastight Hamilton syringe to make ligand bound cytoglobin complex in the ferrous state.

### **2.8.2. Reduction of Disulphide Bond in Cytoglobin**

As described in chapter 3.2.4, the state of the disulphide bond is independent to the heme iron as the redox potential of the disulphide bond is reported to be at -280 mV. Prolonged incubation of cytoglobin with DTT and TCEP partially reduce the heme iron. Hence, to reduce the disulphide bond without affecting the oxidation state of the ferric heme iron (assigned as redox state #3), 10 mM of GSH was added in ferric cytoglobin in the appropriate buffer. The mixture was incubated for 30 minutes at room temperature to ensure completed reduction. The reduction of the disulphide bond can be checked by non-reducing SDS-PAGE described in section 2.2.2.

To generate the cytoglobin with both heme iron and disulphide bond being reduced (assigned as redox state #4), typically, the heme iron was reduced as described in 2.8.1 and following by adding an appropriate amount (~ 10 mM) of reducing agents to reduce the disulphide bond, such as DTT and TCEP. Reduction of the disulphide bond was confirmed by non-reducing SDS-PAGE (Section 2.2.2). Exogenous ligands, such as CO, NO can be injected into the protein solution by using a gastight Hamilton syringe to make ligand-bound ferrous cytoglobin in the absence of the disulphide bond.

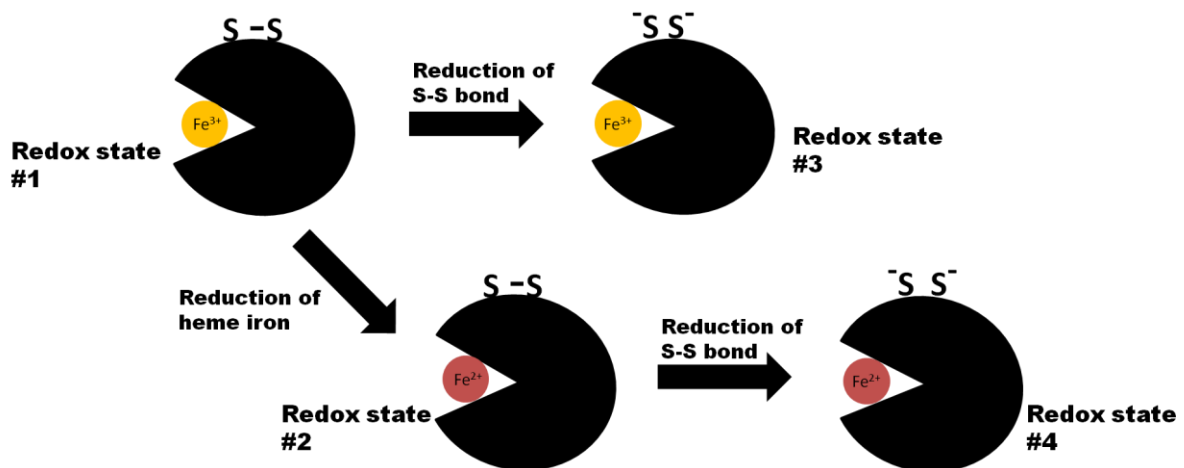


**Figure 2.5 Cartoon illustrations of four principal redox states in human cytoglobin.**

Redox state #1, the heme is in the ferric state and the disulphide bond is intact. Redox state #2, the heme is reduced to ferrous state while the disulphide bond remained intact. Redox state #3 the heme is in the ferric state, but the disulphide bond is reduced. Redox state #4, both heme and disulphide bond are reduced.

## 2.9 Verification of RCC4 cells

### 2.9.1 Cell Culture of RCC4 cells

RCC4 cells are VHL-deficient renal carcinoma cell line. Two sub cell lines were generated by stably transfection with vectors containing a full length HA-tagged VHL tumour suppressor protein (RCC4 WTHA4) and a control vector containing only the HA-tag (RCC4 VHA) which are selected by antibiotic resistance of G418 (Geneticin) (Sigma Aldrich). Both cell lines were grown in the DMEM media (GIBCO) supplemented with 10% fetal calf serum (GIBCO), 1 mg ml<sup>-1</sup> G418 (Sigma-Aldrich, UK), 100 units ml<sup>-1</sup> penicillin and 100 µg ml<sup>-1</sup> streptomycin and 2.5 mM L-glutamine at 37 °C and 5% CO<sub>2</sub>. The cells were subcultured twice a week at a dilution of 1:3 in T-25 tissue culture flasks (Nunc, Rockilde, Denmark) for general cell passaging.

### 2.9.2 MTT-Cell Viability Assay

A colorimetric cell viability assay was conducted to examine the cytotoxicity of demethylating drugs to the cells. RCC4 WTHA4 (+ *VHL*) cells and RCC4 VHA4 (*VHL* null) cells were seeded at a cell density at  $8 \times 10^4 \text{ ml}^{-1}$  in a separate 96-well plate. The demethylation drug, 5-aza-2'-deoxycytidine, was added to the cells at different concentration ranging from 1  $\mu\text{M}$  to 100  $\mu\text{M}$ . The cells were allowed to incubate with the drugs for 72 hours. On the second day of incubation, both the cell culture medium and the drugs were replenished. After the treatment of demethylation, the cell culture medium was removed following by adding 100  $\mu\text{l}$  of yellow tetrazolium compound MTT (3-[4, 5-dimethylthiazol-2-yl]-2, 5-diphenyltetrazolium bromide) dissolved in PBS at a concentration of 0.5  $\text{mg ml}^{-1}$ . The plate was incubated for an hour for the formation of purple formazan crystals. After incubation, 100  $\mu\text{l}$  of solubilization solution (10% *Triton-x* 100 in acidic isopropanol with 0.1 M HCl) was added into the plate to dissolve the purple crystals. Each well was gently mixed by pipetting up and down to ensure completed dissolution. The plate was taken to a plate reader (Omega). Absorbance of each well at 595 nm was measured with a reference wavelength of 655 nm. Triplicates were conducted in each concentration of 5-aza-2'-deoxycytidine.

### 2.9.3 Protein Quantification

Total protein concentration of cell lysate of RCC4 cells was determined using a standard Bradford assay which is described in 2.2.1 with minor modifications. Due to the smaller volume of the cell lysate, the Bradford assays were done on 96-well plates in which 10  $\mu\text{l}$  of BSA solution at each concentration was added to the wells in triplicates mixed with 200  $\mu\text{l}$  of pre-diluted Bradford reagent. Cell lysate with unknown protein concentration was diluted 10 times in 50 or 100  $\mu\text{l}$  of water prior to the detection. 10  $\mu\text{l}$  of the diluted cell lysate was added to the wells also in triplicates. The protein concentration of cell lysate was measured by absorbance

of the solution at 595 nm by a plate reader (Omega). The absorbance at 595 nm was recorded and plotted in Excel, and the protein concentration was determined as described in section 2.2.1.

#### **2.9.4 Western Blot**

RCC4 Cells lysate were prepared by adding 400 to 500  $\mu$ l of ice-cold RIPA buffer (50mM Tris-HCl, 150 mM NaCl, 1% Triton X-100, 0.5% Sodium deoxycholate and 0.1% Sodium dodecyl sulphate, pH 8.0, in the presence of 1x protease inhibitor cocktail tablet) to the cells followed by quick scraping using cell scrapers. The cell lysate was collected in Eppendorf tubes and further incubated on ice for 10 minutes. The cell lysate was centrifuged at 9,100 g for 10 minutes (Philip Harris Sigma3k30 centrifuge, rotor 12154-H) at 4 °C to remove any cell debris.

Protein concentration was determined by standard Bradford assay described in 2.9.3. 50  $\mu$ g of cell lysate was mixed with 4x SDS-PAGE sample loading buffer and loaded on to 12% Polyacrylamide gels. The resultant gel was transferred onto a PVDF membrane (GE healthcare) using sem-dry transfer methods. The membranes was blocked with 3% skimmed milk in PBST (1x PBS, 0.1% Tween 20) for an hour and then incubated with primary antibodies (1:250 to 1:500, mouse monoclonal anti-human cytoglobin; 1:5000, mouse monoclonal anti-human glucose transporter-1; 1:5000, mouse monoclonal anti-human  $\beta$ -actin, all purchased from Abcam UK. 1:1000, mouse monoclonal anti-human VHL, Novus Biologicals; 1:1000, mouse monoclonal anti-human HIF-1 $\alpha$ , BD Bioscience) overnight at 4 °C. The membranes were washed 3 times with PBST (0.1% Tween 20) and then incubated with sheep polyclonal anti-mouse IgG peroxidase-conjugated secondary antibody (1:5000, Sigma). Protein bands were detected using commercial chemiluminescent substrate, (Thermo Scientific) and

visualized by using X-ray film (Kodak, JP).

### **2.9.5 Quantitative Reverse Transcription Polymerase Chain Reaction (qRT-PCR)**

The measurement of the qRT-PCR was kindly done by Dr. Damon Bevan, (School of Biological Science, UEA) in collaboration with Dr. Jelena Garilovic. Total RNA was isolated from RCC4 cells using RNeasy® (Qiagen, Germany) following strictly manufacturer's instructions. 350 to 500 µl of buffer RLT (containing 1% beta-mercaptoethanol) was added to the cells and incubated on ice for 10 minutes. The cells were homogenized by direct pipette mixing and then transferred into new Eppendorf tubes and frozen until required. The cell lysate containing the RNA was transferred to spin columns and centrifuged at full speed for 2 minutes. 1 volume of 70% ethanol was applied to the flow-through and transferred to RNeasy spin column. The samples were centrifuged at 10,000 rpm for 30 seconds. 700 µl Buffer RW1 was added to the spin column and centrifuged at 10,000 rpm for 30 seconds to wash the spin column membrane. 2 x 500 µl Buffer RPE was added to the spin column and centrifuged at 10,000 rpm for 30 seconds to further wash the spin column membrane. The RNA was eluted from the spin column by adding 30 to 40 µl of RNA free water to the spin column and centrifuged at 10,000 rpm for 1 minute. The RNA concentration was determined by nano-drop.

The cDNA was synthesized by reverse transcription using M-MLV reverse transcriptase (Life technologies, Carlsbad, CA, USA). A total of 450 ng RNA was mixed with PCR reaction mixture (2 µl of random primers, 2 µl of dNTPs, 5 µl of 5x M-MLV buffer, 0.5 µl of M-MLV and 0.5 µl of water). Specific oligo-nucleotide primers for *CYGB*, *VHL*, *HIF-1α* and *Glut-1* (Table 2.8) for quantitative TaqMan Real time PCR were kindly designed by Dr. D. Bevan and synthesized by Primer design (Southampton, UK).

5  $\mu$ l of cDNA (ca 1 ng  $\mu$ l<sup>-1</sup>) was mixed with 15  $\mu$ l of Real time PCR reaction mixture (6.7  $\mu$ l of master mix solution containing Taq DNA polymerase, 1  $\mu$ l of sense primer, 1  $\mu$ l of anti-sense primer, 1  $\mu$ l TaqMan fluorescence probe and 6.8  $\mu$ l of water) in a 96-well plate. Reactions carried out in quadruplicate and the expression of each target genes was normalized to Eukaryotic 18s RNA. Fold change was presented as the expression level compared to untreated RCC4 cells. T-test was used to show the change in expression level is statistically significant ( $P$ -values  $\leq$  0.05).

<b>Gene</b>	<b>Sense Primer</b>	<b>Anti-sense Primer</b>
<i>CYGB</i>	5'-ATCCTCATCCTCATCTTCATCCT- 3'	5'-CTGGGTCTGGTTACAAACATCA- 3'
<i>VHL</i>	5'-AATTAGCATGGCGGCACAC-3'	5'-GCAGCCTCCAATTCCTAAACT-3'
<i>HIF-1<math>\alpha</math></i>	5'-TGCCACATCATCACCATATAGAG- 3'	5'-TGACTIONAAAGCGACAGATAACA- 3'
<i>GLUT-1</i>	5'-ACCTCACTCCTGTTACTTACCTA- 3'	5'-ACCCCACTTACTTCTGTCTCA-3'

**Table 2.8 Primers for TaqMan real time PCR reactions**

## **2.10 Identification of Putative Binding Partner(s) of Cytoglobin in RCC4 Cells**

### **2.10.1 Preparation of Cell Lysate**

RCC4 Cells from T-25 tissue culture flasks were transferred to T-75 tissue culture flasks (Nunc, Rockilde, Denmark) 3 days ahead of the experiments. Cells were checked again on the day of experiments and were considered as ready for subsequent pull down assays when they are at full confluence. Cell culture medium was discarded and the cells were washed in

ice-cold PBS twice to remove residual cell culture medium. 400 to 500  $\mu\text{L}$  of ice-cold cell lysis buffer (50 mM Tris-HCl, 150 mM NaCl, 0.5% Tween 20, 0.5% Triton X-100, 1 mM EDTA, pH 7.2, in the presence of 1x protease inhibitor cocktail tablet) was added to the cells immediately. The cell lysate was prepared by incubating the flasks on ice for 10 minutes followed by quick scraping using cell scrapers. The cell lysate was collected and transferred into Eppendorf tubes which were centrifuged at 9,100 g for 10 minutes (Philip Harris Sigma3k30 centrifuge, rotor 12154-H) at 4 °C to remove cell debris. Supernatants containing the clear cell lysate were transferred to new Eppendorf tubes and placed on ice until ready for pull down assay.

### **2.10.2 Pull Down Assay**

Procedures of pull down assays using MagStrep “Typer2HC” Beads (Iba, Germany) were followed by instructions provided by the manufacturer with some modifications. 40  $\mu\text{L}$  of 5% magnetic beads suspension (approx. 2 mg beads) was taken out and washed with wash buffer (50 mM Tris-HCl, 150 mM NaCl, pH 7.2) twice before use. Strep-tagged cytoglobin protein (both strep-Cgb and strep-Cgb $\Delta\text{C}$ ) was diluted in the same buffer to about 200 ng  $\mu\text{L}^{-1}$ . 2  $\mu\text{g}$  of Strep-tagged cytoglobin was added to the beads and incubated on ice for 15 minutes to allow the tagged cytoglobin to bind to the beads. Lastly, cell lysates of RCC4 cells were added to the beads and further incubated for 2 hours at 4 °C with mild agitation.

The beads containing the bound proteins were separated from supernatant (cell lysate) by using a magnetic separator. The supernatant was removed carefully by pipette. The magnetic beads were washed with 50  $\mu\text{L}$  of wash buffer twice with mild agitation and then put back on the magnetic separator. Wash buffer was removed carefully by pipette. Elution of the bound proteins was achieved by adding 40  $\mu\text{L}$  of elution buffer (50 mM Tris-HCl, 150 mM NaCl

and 2 mM d-biotin, pH 7.2) to the beads with mild agitation. Supernatants containing the eluted proteins were separated by the magnetic separator. The supernatants were collected and transferred to new Eppendorf tubes for subsequent analysis using non-reducing SDS-PAGE. Protein visualisation and detection was achieved by leaving the SDS-gel in coomassie brilliant blue solution for at least 2 hours.

## Chapter 3: Characterisation of Human Recombinant Cytoglobin

### 3.1 Introduction:

Since cytoglobin was identified as the fourth member of vertebrate globin family (Burmester et al., 2002; Trent and Hargrove, 2002), there has been intense interests in understanding its physiological role(s). The principal approach has been comparative structural analysis with other globins which have well characterised functions, in particular the myoglobin which is believed to originate from the same ancestral globin as cytoglobin (Burmester and Hankeln, 2014). From a structural perspective, the tertiary structure of cytoglobin resembles that of other vertebrate globins. This includes the canonical  $\alpha$ -helical globin scaffold and the presence of two conserved histidine residues which coordinate the heme cofactor (chapter 1.1.1). On the other hand, the quaternary structure of the vertebrate globins vary; haemoglobin is a hetero-tetramer composed of two  $\alpha$ - and  $\beta$ -subunits, myoglobin is a monomer and the physiologically relevant quaternary structure of cytoglobin is uncertain.

To date, all the reported X-ray structures of recombinant human cytoglobin in the ferric state are homo-dimers although dimerization interface and relative orientation of the subunits differs between structures (see also section 1.3.2; Table 1.2). For example, the X-ray structure of wild-type cytoglobin reported by Sugimoto and colleagues (PDB: 1V5H), shows a dimer forming at the AB-corner and E-helix via two intermolecular disulphide bonds formed between Cys38 residue of one subunit and Cys83 residue of another and vice versa. Heme cofactors are buried inside the dimerization interface. Beside linkage via disulphide bond, intermolecular forces and hydrogen bonds were shown to also contribute to the stable dimeric structure (Sugimoto et al., 2004).

On the contrary, in another structure reported by de Sanctis and colleagues, using a

variant form of cytoglobin in which both cysteine residues were substituted with serine (PDB: 1URV), a completely different dimeric interaction between the two subunits is described. In this structure, the two cytoglobin subunits are held together at the G-helix via interactions between hydrophobic amino acid residues in such a way that the heme groups of each subunit are exposed to solvent. In addition to the hydrophobic interactions, electrostatic interactions and hydrogen bonds also contribute to the stabilisation of the dimer interface (de Sanctis et al., 2004). Interestingly, in this structure, the cytoglobin dimer was found to be asymmetric. The distal heme pocket in one of the subunits (B subunit) displayed two alternative conformations. In one conformation the heme is hexa-coordinate whereas in the other it is penta-coordinate with the distal histidine ligand (His81) displaced away from the coordination site due to an upward shift of a part of the E-helix near the distal heme pocket. The ratio of the two conformations was reported to be close to 1:1 (de Sanctis et al., 2004). A similar dimeric interaction was described in a X-ray structure reported by Gabba and colleagues of a variant cytoglobin bearing triple mutations with the distal histidine (His81) substituted by glutamine and the two cysteine (Cys38 and Cys83) substituted by serine (PDB: 4B3W), although both distal heme pockets in the subunits display solely a penta-coordination.

Nonetheless, the X-ray structure of carbon-monoxide bound cytoglobin in the ferrous state reported by Makino and colleagues is described as a monomer (Makino et al., 2011; PDB: 3AG0). However, since the cytoglobin was crystallised in the presence of dithionite which interferes with the disulphide bond formation which is described in detail later in this chapter, presumably, all these observations from the X-ray crystallography studies highlight a formation of stable dimeric structure of cytoglobin under crystallisation conditions.

On the other hand, a mixture of oligomeric states of cytoglobin was reported in the solution studies of recombinant cytoglobin. For example, Hamdane and colleagues reported

that in their hands purified recombinant human cytoglobin was a stable homo-dimer even after treatment with DTT suggesting that the dimeric interaction is not mediated by intermolecular disulphide bonds (Hamdane, et al., 2003). Moreover, Lechauve and colleagues, using a combination of size exclusion chromatography and mass spectrometry, concluded that in dilute solution (< 20  $\mu$ M) cytoglobin is predominately a monomer with only ca 5% existing as dimers which are linked by intermolecular disulphide bonds (Lechauve et al., 2010). More recently, the mystery of the oligomeric state of cytoglobin was further complicated by studies reported from two other groups in which cytoglobin was purified predominately in dimeric form (Beckerson et al., 2015) or even higher oligomeric form, such as tetramer (Tsujino et al., 2014) linked by inter-molecular disulphide bond(s).

Hence, there is no consensus in the literature as to the oligomeric structure of recombinant human cytoglobin possibly due to variations between different sample preparation methods and different interpretations of the experimental data by different researchers. It is worth noting that some studies use recombinant human cytoglobin that has been refolded after purification from inclusion bodies whilst others use a His<sub>6</sub>-N-terminal tag to simplify the purification procedures without demonstrating if there is any effect caused by the additional amino acid sequences. Ideally, recombinant cytoglobin should be purified as naturally folded soluble protein free from any modification that influences the structure and redox properties of the protein.

In this chapter, I report the expression and purification of a naturally folded form of recombinant human cytoglobin from the soluble fraction of *E.coli* BL21 (DE3). The recombinant cytoglobin was characterised using a range of biochemical and biophysical methods in order to establish its oligomeric state in solution and the redox properties of both the disulphide bond and the heme iron.

## 3.2 Results

### 3.2.1 Purification of Human Recombinant Cytochrome b5

Human recombinant cytochrome b5 was expressed in and purified from the soluble fraction of *E.coli* BL21 (DE3) using the method described in chapter 2.5. During each stage of the purification, representative samples were analysed by a combination of SDS-PAGE and UV/vis spectroscopy to assess the purity of the recombinant protein. Figure 3.1 shows representative SDS-PAGE gels of fractions of partially pure and pure protein collected after ion exchange (upper panel) and size exclusion chromatography (lower panel), respectively. The protein band associated with recombinant human cytochrome b5 was found to migrate slightly less distance than the 20 kDa molecular marker on 15 % SDS-PAGE gels and was estimated to have a molecular weight of 21 kDa (Figure 3.1). The purified protein was confirmed by mass spectrometry (data not shown) and Western blot as being human cytochrome b5 using a monoclonal antibody raised against full-length human cytochrome b5 (Figure 3.2). The results are in agreement with the molecular weight of cytochrome b5 at 21,402 Da obtained by mass spectrometry previously reported by other groups (Hamdane et al, 2003, Lechauve et al, 2010).

The spin- and ligation- states of the heme iron in purified cytochrome b5 was examined using a combination of UV/vis, room temperature magnetic circular dichroism (MCD) and low temperature X-band electronic paramagnetic resonance (EPR) spectroscopies (Figure 3.3.) In the UV/vis absorption spectrum of cytochrome b5, it has the Soret absorption maximum at 416 nm and the  $\alpha$ - and  $\beta$ -band at 563 nm and 534 nm respectively. Besides, there are some weak but notable features at ~612 nm and ~675 nm (Figure 3.3A) which are usually not seen in the reported UV/vis spectrum from other groups as only the spectrum from 350 nm to 600 nm is shown in the literature. The UV/vis spectrum of the purified cytochrome b5 resembles that reported for the ferric form of other globins that have a hexa-coordinate heme, such as

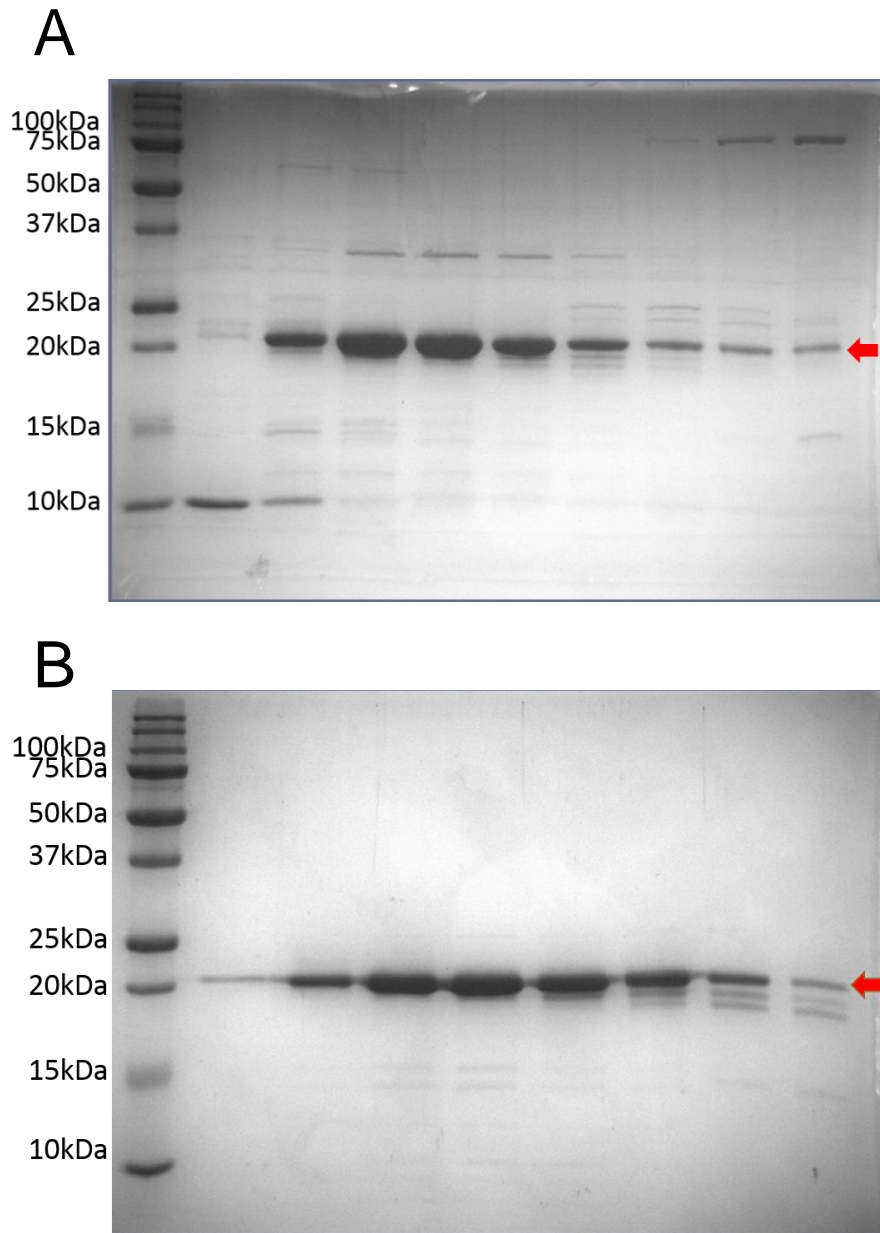
neuroglobin (Dewilde et al., 2001). Hence, this provides a good indication that the preparations of human cytoglobin reported here have a hexa-coordinate heme in the ferric state.

The RT-MCD spectrum between 300nm and 800nm is dominated in the Soret region by a derivative-shaped feature with an intensity (peak-trough) of approximately  $95 \text{ M}^{-1}\text{cm}^{-1}\text{T}^{-1}$  with a maximum at 407 nm and a minimum at 422 nm. In the visible region there is a second derivative shaped feature (*ca*  $10 \text{ M}^{-1}\text{cm}^{-1}\text{T}^{-1}$ ) with a minimum 572 nm at and a maximum 555 nm. Note that the MCD spectrum contains no features at wavelengths greater than 600 nm suggesting that the longer wavelength features (i.e. broad band at 612 nm and 675 nm) in the UV/vis spectrum do not arise from the heme (Figure 3.3B). The form and intensity are consistent with a single low-spin ferric heme. Confirmation of bis-histidine ligation comes from the NiR-MCD spectrum which contains a single band at 1622 nm (Data not shown) which is characteristic of this ligand set (Cheesman et. al, 1993).

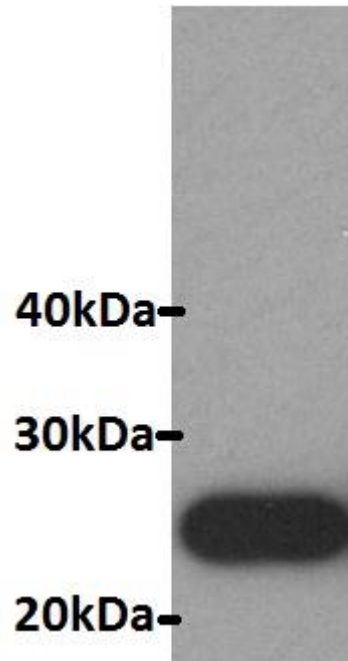
The low-temperature X-band EPR spectrum of recombinant cytoglobin is dominated by a rhombic trio ( $g = 3.21, 2.05$  and  $1.70$ ) which arises from a low-spin ferric heme. In addition there is a very small signal arising from a high-spin species ( $g = 5.95$ ) in the sample which suggests that a minor fraction ( $< 5\%$ ) of the heme in the sample exists in the penta-coordinate state (Figure 3.3C). Hence the results from the spectroscopies confirm that the heme iron in the purified recombinant cytoglobin is a low-spin heme with hexa-coordinate by two histidine ligands in the ferric state.

The R<sub>z</sub> value which is the absorbance of the Soret maximum divided by the absorbance at 280nm ( $A_{416}/A_{280}$ ) for pure recombinant cytoglobin was determined to be about 2.80 (Figure 3.3A). In addition pure recombinant cytoglobin eluted from the final gel filtration (Superdex 75) column with a retention volume that was consistent with it being a monomer (see also 3.2.3).

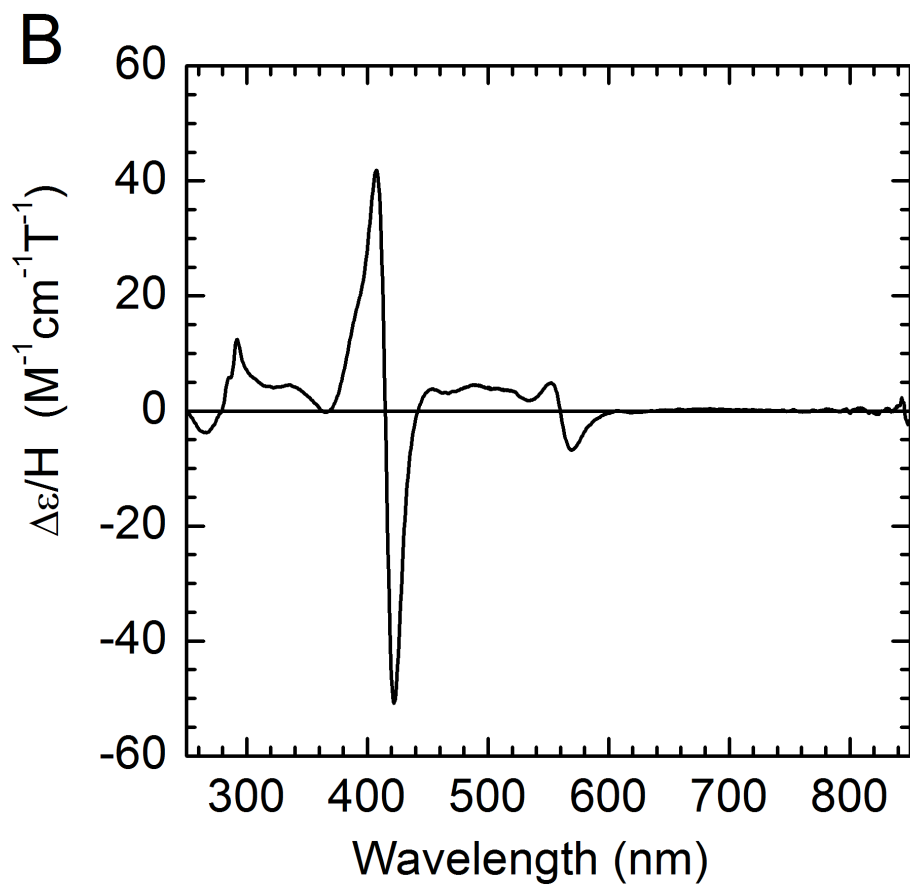
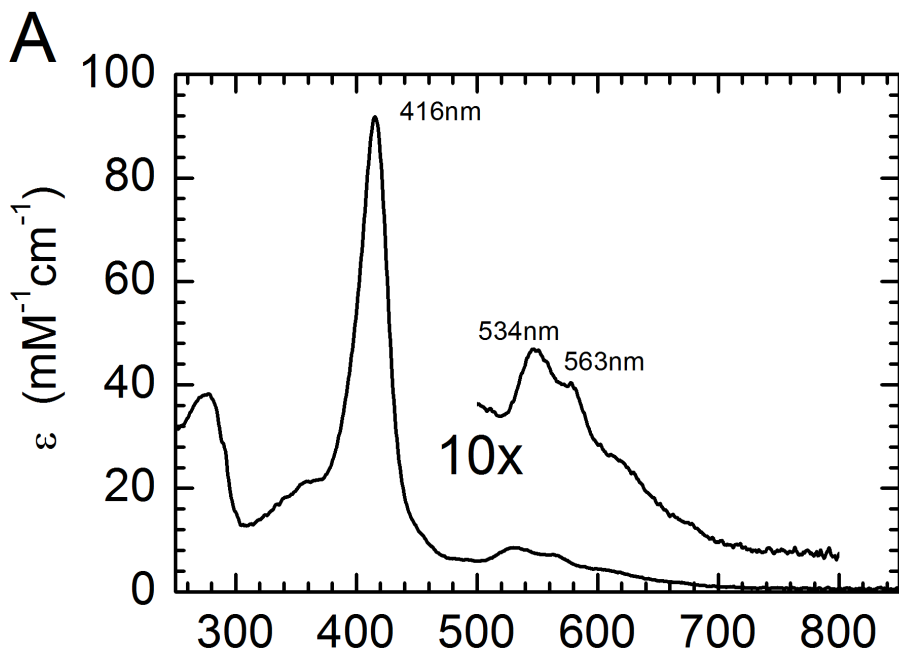
No dimeric or any higher oligomeric state was observed throughout the whole purification and only monomeric cytoglobin with  $R_z \geq 2.8$  was used in subsequent experiments.



**Figure 3.1 Representative SDS-PAGE gels showing human recombinant cytoglobin during purification. (A)** Fractions of semi-pure recombinant cytoglobin protein from DEAE anionic exchange chromatography. **(B)** Fraction of highly pure recombinant cytoglobin protein eluted from size exclusion chromatography. The red arrow indicates the protein bands of recombinant cytoglobin protein.



**Figure 3.2 Western blot of purified recombinant cytoglobin.** The purified protein was transferred onto a PVDF membrane and incubated a mouse monoclonal anti-human cytoglobin antibody at a dilution of 1:500 and a secondary HRP conjugated polyclonal anti-mouse IgG antibody at a dilution of 1:5000. The blot was detected by chemiluminescent substrate and visualized by using X-ray film as described in section 2.9.4.



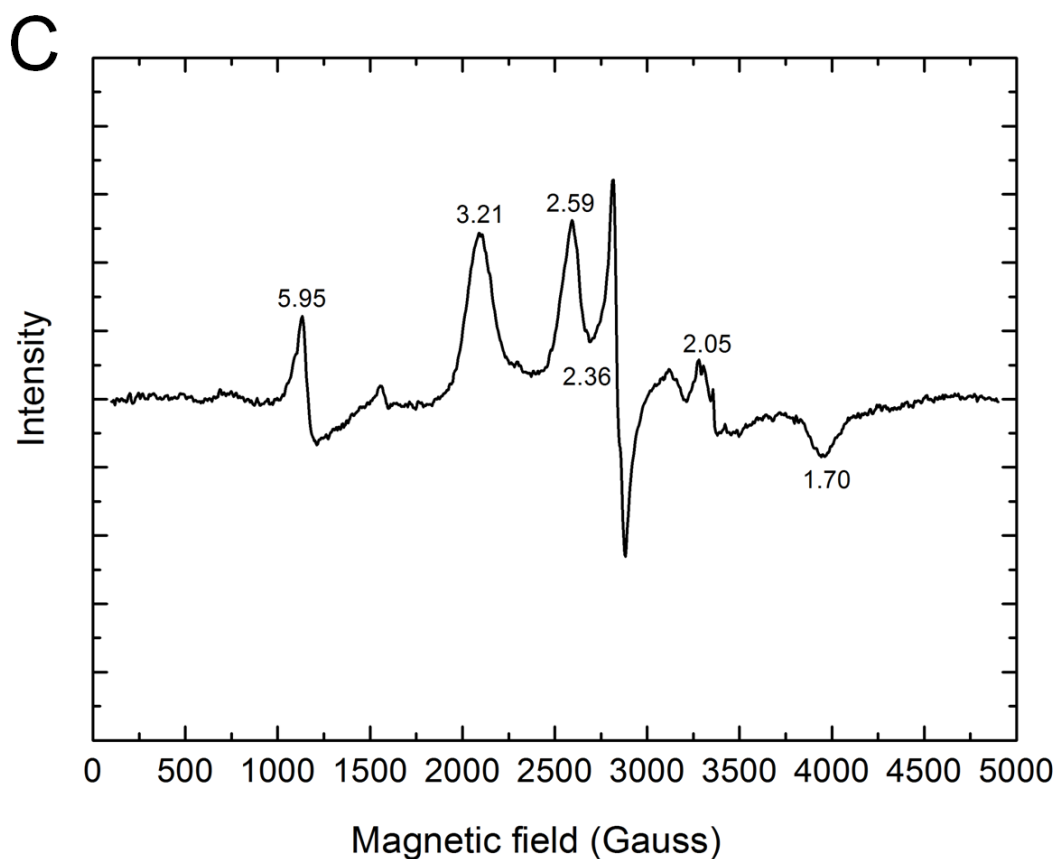


**Figure 3.3 Spectroscopic characterisation of purified recombinant cytoglobin in the ferric state (A)** UV/vis spectrum of ferric cytoglobin. The spectrum was recorded in a 2 mm path-length quartz cuvette with a concentrated sample of cytoglobin in 20 mM Tris-HCl pH 8.0. The numbers indicate the position of the Soret peak,  $\alpha$  and  $\beta$  bands in the spectrum. **(B)** Room temperature magnetic circular dichroism spectrum of cytoglobin in 20 mM Tris-HCl pH 8.0. The MCD signals indicate a low-spin heme in the ferric state with bis-histidyl ligation. **(C)** Low temperature X-band continuous-wave EPR spectrum of ferric cytoglobin taken at 11K. The numbers indicate the  $g$  values in the EPR spectrum. The  $g$  values indicate a low-spin heme in the ferric state and a presence of a minor fraction of high-spin species ( $g = 5.95$ ).

### 3.2.2 The State of the Disulphide Bond in Recombinant Cytoglobin

In order to determine whether the two surface cysteine residues could contribute to the formation of dimers purified recombinant cytoglobin protein was resolved using non-reducing SDS-PAGE from which  $\beta$ -mercaptoethanol was omitted from the sample loading buffer. In the absence of the  $\beta$ -mercaptoethanol, the cytoglobin protein was found to migrate slightly further than the 20 kDa molecular weight marker, with an apparent molecular weight of approximately 19 kDa (Figure 3.4, lane #1). This contrasts with its behaviour on a reducing SDS-PAGE gel where it behaves as a protein of MW = 21 kDa (Figure 3.1). Neither dimer nor any higher oligomeric state was observed on the non-reducing SDS-PAGE gel providing further evidence the recombinant cytoglobin purified in this study is monomeric.

When recombinant cytoglobin was pre-incubated with a range of other reducing agents to break the disulphide bond, including DTT, TCEP and GSH prior to analysis by non-reducing SDS-PAGE, the protein was found to migrate with an apparent MW = 21kDa (Figure 3.4, lane #2 - #4) as was observed in reducing SDS-PAGE (Figure 3.1). Similar behaviors on non-reducing SDS-PAGE gels was also demonstrated for two variant forms of cytoglobin, C38S (Figure 3.4, lane #5) and C83S (data not shown) in which one of the cysteine residues has been substituted with serine to mimic the case of a chemically reduced disulphide bond.

Taken together, the results from the non-reducing SDS-PAGE provide convincing evidence that the two cysteine residues form an intra-molecular disulphide bond in the purified cytoglobin. In the absence of reducing agents, the disulphide bond is oxidized (intact) and the protein has a higher mobility on non-reducing SDS-PAGE gels and hence a lower apparent molecular weight (19 kDa) is observed. On the other hand, in the presence of reducing agents which break the disulphide bond, the protein band of cytoglobin runs at a higher apparent molecular weight (21 kDa). Therefore, the difference in the mobility of the protein band of

cytoglobin is correlated with the integrity of the intra-molecular disulphide bond. The higher mobility of cytoglobin in the non-reducing SDS-PAGE is possibly due to a more compact structure maintained by the disulphide bond even after heat denaturation. Therefore, non-reducing SDS-PAGE can be used to assess the state of the disulphide bond of cytoglobin based on the difference in the apparent mobility

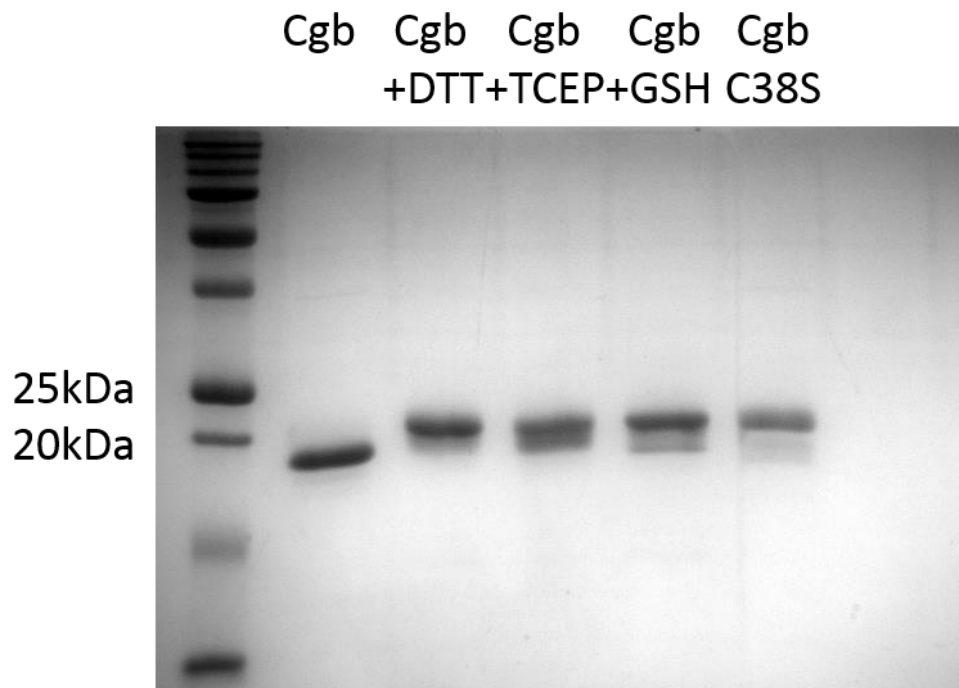


**Figure 3.4 A non-reducing SDS-PAGE gel showing the state of the disulphide bond in recombinant cytoglobin under different treatments.** Lane #1 = recombinant cytoglobin protein (250 ng). Lane # 2 = 250 ng of cytoglobin protein pre-incubated with 10 mM DTT. Lane # 3 = 250 ng of cytoglobin protein pre-incubated with 10 mM TCEP. Lane #4 = 250 ng of cytoglobin protein pre-incubated with 10 mM GSH. Lane #5 = A variant form of cytoglobin (C38S) that has a no intra-molecular disulphide bond. Cytoglobin protein was pre-incubated with reducing agents for 30 minutes before running non-reducing SDS-PAGE as described in 2.2.2.

### 3.2.3 Analytical Gel Filtration of Recombinant Cytoglobin

Further examination of the quaternary structure of recombinant cytoglobin in solution was achieved by using analytical gel filtration chromatography on a Superdex-75 gel filtration column. It is a chromatographic technique to measure molecular weight of a protein by determining its elution volume with reference to protein standards of known molecular weights (MW) as described in 2.2.4. The standard curve for molecular weight determination (Figure 3.5) was constructed using the following standard proteins; BSA (66 kDa), ovalbumin (45 kDa), myoglobin (17 kDa) and aprotinin (6.5 kDa).

The elution profile of recombinant cytoglobin analysed is presented in figure 3.6 and the elution volume ( $V_e$ ) of cytoglobin is determined to be 9.773 ml, which corresponds to a MW ~ 44 kDa which is about double that for cytoglobin (MW = 21.4 kDa). Thus the elution volume suggests that cytoglobin is a dimeric protein in the solution, however when the eluted proteins were analysed using non-reducing SDS-PAGE only a single band of apparent MW = 19 kDa was observed. On the other hand, a truncated cytoglobin (Cgb $\Delta$ C) in which the last 19 amino acid at the C-terminus was removed gives a  $V_e$  at ~10.14 ml, which corresponds to a MW = ca 38 kDa. The calculated MW is also about 2 times of the predicted MW for the truncated cytoglobin (MW = 19.5 kDa). The predominant protein band of the truncated cytoglobin appeared at MW = ca 17 kDa on the non-reducing gel, although a small amount of protein is found at ca 19 kDa which indicates that the disulphide bond was reduced in a fraction of the truncate cytoglobin (Figure 3.6A and C). Taken together, these data do not support the notion that the cytoglobin exists as homodimers that are linked via inter-molecular disulphide bonds. However, the results would be consistent with a homodimer in which each of the subunits contains an intact intra-molecular disulphide bond. An alternative explanation is that the extensions to the N- and C- termini increase the effective hydrodynamic radius of the protein causing it to behave anomalously in gel filtration experiments.

Having established the intra-molecular nature of the disulphide bond in cytoglobin, it was of interest to determine if changing the state of the disulphide bond has any impacts on the overall structure of the protein. This was achieved by comparing the  $V_e$  of cytoglobin with reduced disulphide bond with that having intact disulphide bond. The disulphide bond was reduced by pre-incubation of the cytoglobin with 10 mM TCEP before analysis on a gel filtration column which had been equilibrated with the same buffer used previously except for the addition of 1 mM of TCEP to prevent re-oxidation of the disulphide bond during the experiment. The  $V_e$  of the full-length cytoglobin and the truncated cytoglobin in the presence of 10 mM TCEP increased to 10.337 mL and 10.79 mL, respectively. Hence, the  $V_e$  corresponds to a MW = ca 34 kDa for the full-length cytoglobin and a MV = ca 29.5 kDa for the truncated cytoglobin with the disulphide bonds in both proteins being reduced. The state of the disulphide bond was confirmed by non-reducing SDS-PAGE that the disulphide bond was essentially reduced, although a small proportion intact disulphide bond was also observed (Figure 3.6B and D).

Interestingly, the  $V_e$  obtained for C38S variant of cytoglobin in which formation of intra-molecular bond is prevented is found to be about 10.456 mL which corresponds to a MW = 33.6 kDa. The calculated MW of the C38S variant is similar to that of full-length cytoglobin which has the disulphide bond reduced. Moreover, the changes in the apparent MW upon reduction of the disulphide bond in both full-length and truncated cytoglobin are consistent to be ca 10 kDa, although the apparent MW calculated for both proteins with reduced disulphide bonds do not correspond to either a dimer or a monomer. The shifts in the  $V_e$  after the treatment of TCEP indicate that reduction of the disulphide bond induces a massive conformational change which causes a reduction in the effective hydrodynamic radius, hence the apparent MW of the protein. Thus, this experiment appears to confirm that the preparations reported here do not form dimers via intermolecular disulphide bonds and the apparent dimer-

like interaction is maintained even when the C-terminus and the disulphide bond are absent. Since Lechauve and colleagues reported that cytoglobin with both N- and C- termini deleted behaves as a monomer (*ca* 17 kDa) in the gel filtration experiments (Lechauve et al., 2010), it is therefore speculated that the N-terminus could be responsible for the dimer formation in solution.

To validate the observations that the increases in the  $V_e$  were caused by the reduction of the disulphide bond by TCEP, the same experiments were repeated with the use of sperm whale myoglobin (*ca* 17 kDa) and the C38S variant (*ca* 21 kDa) as both of which have no disulphide bond formation in the structure. Surprisingly, a similar trend of an increase in the  $V_e$  was observed in the presence of TCEP, although differential values of  $V_e$  in the presence and absence of TCEP are not as significant (between 0.1 to 0.2 ml which corresponds to no more than 2 kDa difference in MW) as those observed for full-length and truncated cytoglobin. Hence, it is still possible to conclude a conformational change due to the reduction of the disulphide bond. However, repeated experiments with more data points are needed to improve reliability of the analytical gel filtration experiments.

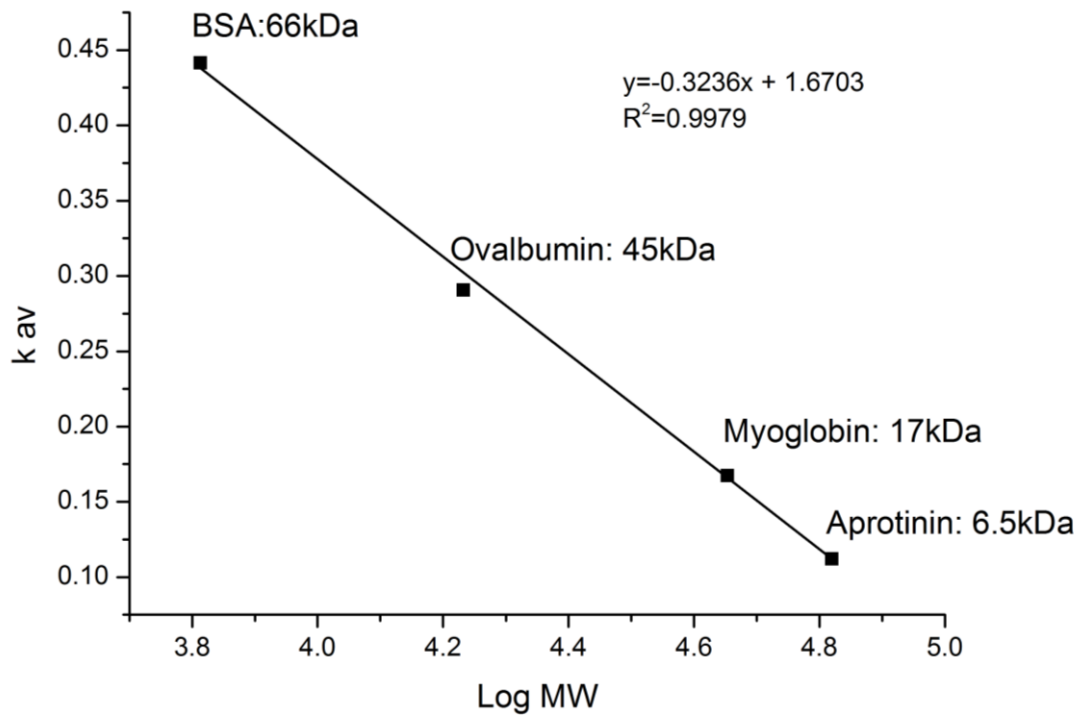


**Figure 3.5 Calibration curve of superdex 75 analytical gel filtration column.** 4 points calibration was done using Bovine Serum Albumin (66 kDa), Ovalbumin (45 kDa), Myoglobin (17 kDa) and Aprotinin (6.5 kDa). The equation of the line of best fit was constructed for the determination of the mass of cytoglobin protein as described in 2.2.4.

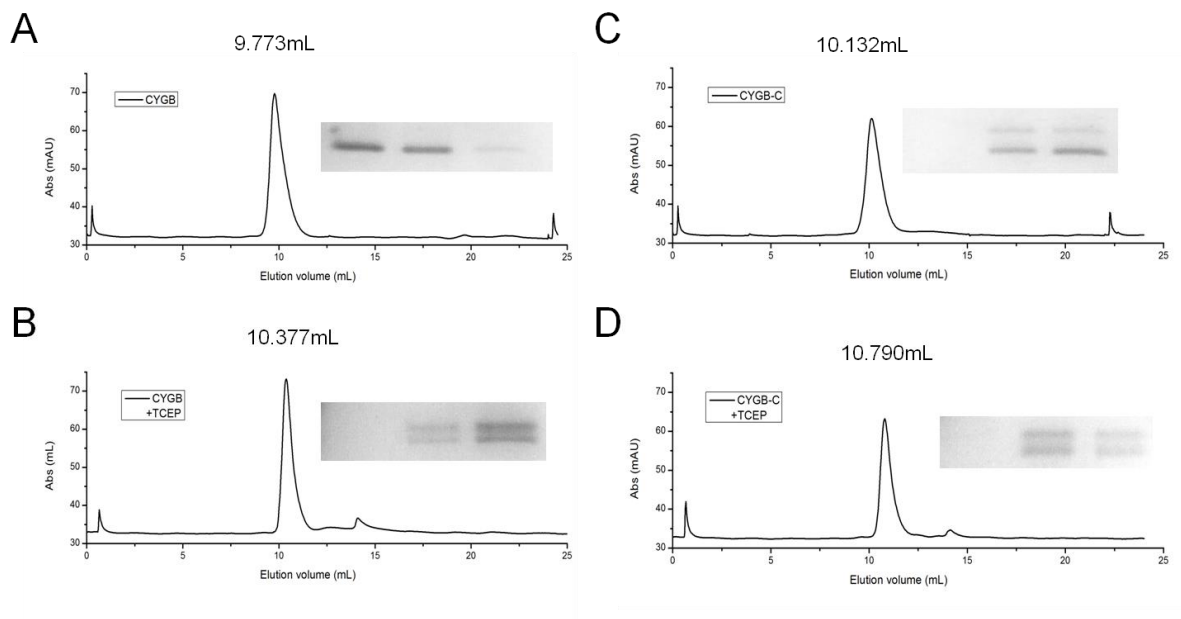


**Figure 3.6 Measuring molecular weight of cytoglobin in analytical gel filtration. (A)** A chromatograph shows elution volume of the wild-type recombinant cytoglobin in 20 mM Tris-HCl pH 8.0. **(B)** The chromatograph shows elution volume of the wild-type recombinant cytoglobin in 20 mM Tris-HCl pH 8.0 in the presence of 1 mM TCEP. Cytoglobin was pre-incubated with 10 mM TCEP before running through the column. **(C)** A chromatograph shows elution volume of truncated recombinant cytoglobin (Cgb $\Delta$ C) in 20 mM Tris-HCl pH 8.0. **(D)** The chromatograph shows elution volume of the truncated recombinant cytoglobin (Cgb $\Delta$ C) in 20 mM Tris-HCl pH 8.0 in the presence of 1 mM TCEP. The truncated cytoglobin was pre-incubated with 10 mM TCEP before running through the column. The state of the disulphide bond of the protein was checked by a 15% non-reducing SDS gel. The flow rate was kept constant throughout the experiments at 0.5 mL min<sup>-1</sup>.

### 3.2.4 Mid-point Potential of Disulphide Bond

The presence of a disulphide bond is not a common feature in cytoplasmic proteins, cytoglobin has been predicted to be a cytoplasmic protein (Burmester et al., 2002) which could translocate to the nucleus (Geuens et al., 2003; Singh et al., 2014). The intra-molecular disulphide bond of cytoglobin forms between two cysteine residues (Cys38 and Cys83), one of which (Cys83) lies on the same helix as the distal heme ligand (His81) (refer to chapter 1.3; Figure 1.3). Therefore, it would be conceivable to suggest that the disulphide bond in cytoglobin could play a role in maintaining the heme environment to modulate any heme mediated physiological functions. As a first step to understand the role of disulphide bond, reduction potential of the disulphide bond was measured by a gel shift assay in which the cytoglobin was poised in buffers with a wide range of solution potentials at pH 7.0.

Dithiothreitol (DTT) reduces the disulphide bonds in proteins by a mechanism involved thio/disulphide exchange which is a two-step event to transfer the disulphide bond from the protein to itself that a ring structure containing an internal disulphide bond is formed within the DTT molecules (oxDTT). According to the Nernst equation, the ratio of the oxidized and reduced forms of any redox active molecule are determined by its standard redox potential and the solution potential under standard conditions. A range of solution potentials were established using defined mixtures of dithiothreitol (DTT) which has a standard reduction potential at -330 mV, and its oxidized form, trans-4,5-Dihydroxy-1,2-dithiane (ox DTT), at pH 7.0 (Table 3.1). Hence, in principle, the ratio of oxidised (disulphide) and reduced (free thiols) forms of the intra-molecular disulphide bond found in cytoglobin should respond to the change in the solution potentials according to the Nernst equation. The solution potential at which 50% of the disulphide bond of cytoglobin is in the reduced state is therefore regarded as mid-point potential of the disulphide bond.

Cytoglobin was poised in different solution potentials that had been set by mixing different ratios of DTT/oxDTT in 20 mM Tris-HCl pH 7.0. The state of the disulphide bond was examined by non-reducing SDS-PAGE as previously described in section 3.2.2. Two forms of cytoglobin with different mobilities which reflect the states of disulphide bond were observed. Based on the gel shift assay, the measured mid-point potential was shown to be in a region of -271 mV to -292 mV (Figure 3.7A). Densitometry analysis was attempted to semi-quantify the distribution of the two protein bands. However, since separation of the two protein bands were not satisfactory, results from the analysis could not give reliable values. Hence, a mathematical approach using the Nernst equation was used. Theoretical distribution of the oxidised and reduced disulphide bond is plotted in Figure 3.7B using an estimated value ca -280 mV, the ratios of the oxidised and reduced disulphide were consistent with those observed in the gel shift assay. Therefore, it is concluded that the disulphide bond in cytoglobin is redox active and estimated to have a mid-point potential ca -280 mV (Figure 3.7).

Treatments	[oxDTT]	[DTT]	Em (V)
Solution potential #1	10mM	1uM	-0.212
Solution potential #2	10mM	5uM	-0.232
Solution potential #3	10mM	10uM	-0.241
Solution potential #4	10mM	50uM	-0.262
Solution potential #5	10mM	100uM	-0.271
Solution potential #6	9.6mM	500uM	-0.292
Solution potential #7	9.0mM	1.0mM	-0.302
Solution potential #8	5.0mM	5.0mM	-0.330
Solution potential #9	0.5mM	9.5mM	-0.368

**Table 3.1 List of solution potentials poised by different concentrations of DTT and oxDTT in 20 mM Tris-HCl pH 7.0.**

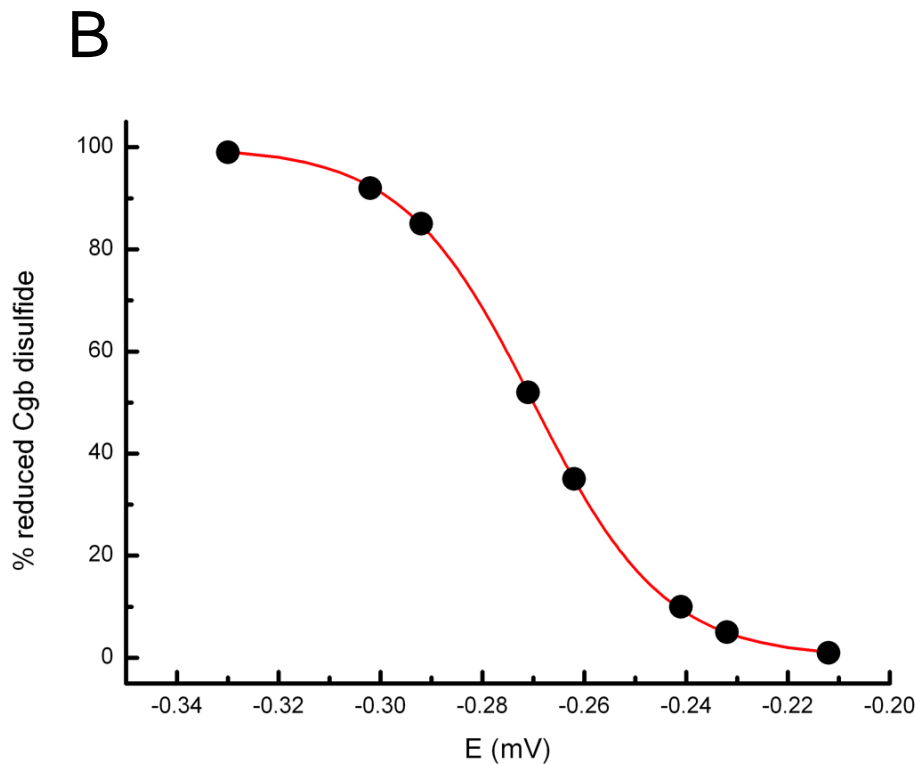
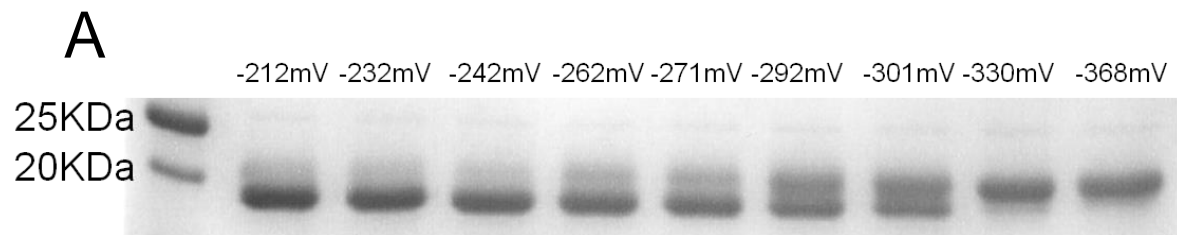


**Figure 3.7 Measuring the mid-point potential of the disulphide bond in cytoglobin.** The solution potentials were set up in 20 mM Tris-HCl pH 7.0 using various concentrations of DTT and oxDTT as shown in table 3.1. **(A)** A representative non-reducing SDS-PAGE gel shows a distribution of the disulphide bond and free thiols in cytoglobin under different solution potentials poised by DTT and oxDTT at pH 7.0. Approximately 250 ng of cytoglobin in 20 mM Tris-HCl pH 7.0 was mixed 1:1 with the same buffer containing various concentrations of DTT and oxDTT and incubated at room temperature for at least 30 minutes prior to gel electrophoresis. **(B)** Theoretical distribution of the disulphide bond and free thiols at different solution potentials at pH 7.0 calculated based on the Nernst equation.

### 3.2.5 Principal Redox States of Cytochrome c

Cytochrome c has two apparently independent redox active sites; an intramolecular disulphide bond ( $E_m = ca -280$  mV) (Chapter 3.2.4) and a *b*-type heme ( $E_m = +20$  mV) (Sawai et al., 2003). Consequently before any spectroscopic or functional investigation of the protein, it is important to establish control over the redox state of both sites. In principle, cytochrome c can exist in four different redox states. Details of methods and experimental set-up to selectively control the redox states of the two redox active sites are described in section 2.8. Typically, after purification, both the heme iron and the disulphide bond in the cytochrome c are oxidized; the heme iron is in the ferric state and the disulphide bond intact. Hence, this is designated as redox state #1.

In order to understand role of the disulphide bond in modulating the biological functions of cytochrome c the disulphide bond it is necessary to control its redox state independently of the heme iron. It was established in section 3.2.2 that the disulphide bond can be reduced by treating cytochrome c with various reducing agents including DTT and TCEP agents but these experiments did not assess the state of the heme iron. Hence the form of cytochrome c in which the disulphide bond is reduced (broken) while the heme iron remains in the ferric state is assigned as redox state #3.

Both DTT and TCEP have both been previously shown to effectively reduce the disulphide bond (Figure 3.4). However, when the reduction of the disulphide bond by 5 mM TCEP was monitored spectroscopically over a period of time, some changes in the heme iron were observed. Specifically a red shift of the Soret peak and an emergence of two bands at 539 nm and 578 nm are observed, respectively. These spectral changes were completed by the addition of a small amount of ascorbate. Through comparison with myoglobin (Antonini and Brunori, 1971) the changes are interpreted in terms of TCEP partially reducing the heme

iron which then reacts with atmospheric oxygen to form an oxy-ferrous species (Figure 3.8A). When sperm whale myoglobin was treated with the same concentration of TCEP, no change in the spectrum was observed (Figure 3.8B).

The same experiment was repeated under anaerobic conditions in two different buffer systems (20 mM Tris-HCl pH 8.0 and 20 mM sodium phosphate pH 7.2) to exclude the possibility that electron donor originates from the buffer itself. Instead of formation of the oxy-ferrous species, the heme iron was partially reduced and further heme reduction was achieved by an addition of ascorbate under different buffer systems (Figure 3.8C & D). These data are consistent with confirming the observation in the aerobic condition when cytoglobin was treated with TCEP. Such partial reduction of the heme iron was also observed when using DTT (data not shown).

Interestingly, when the disulphide bond was reduced by 10 mM glutathione (GSH) – a natural thiol reductant in human cells, no formation of oxy-ferrous species was observed under aerobic conditions suggesting no reduction of the heme iron. However, a small decrease in the absorption of the Soret peak and a minor shift in the visible region was observed which may imply that reduction of the disulphide bond perturbs the heme distal pocket (Figure 3.9). Further analyses of these changes at the heme distal pocket due to reduction of the disulphide bond by GSH are considered in Chapter 4.

Since the reported redox potential of the heme iron in cytoglobin is at +20 mV (Sawai et al., 2003), it is believed that the heme iron should be in the ferrous state in cytoplasm. Moreover, majority of the functions found in globin, such as carrying gaseous ligands including oxygen (O<sub>2</sub>), carbon monoxide (CO) and nitric oxide (NO) are only happen when the heme iron is in the ferrous state. Therefore, examining cytoglobin in a physiological relevant redox

state in cytoglobin is of paramount importance to reveal the effect of the reduction or formation of the disulphide bond. Sodium dithionite is a very strong reducing agent ( $E_m = -660$  mV) (Mayhew, 1978) which is often used in studies of heme proteins in the ferrous state, such as cytoglobin (Trent and Hargrove, 2002; Li et al., 2012; Astudilo et al., 2013; Beckerson et al., 2015). However, in the case of cytoglobin, although treatment with dithionite can completely reduce the heme iron in cytoglobin (Figure 3.10A), it also causes a partial reduction to the disulphide bond (3.10D lane 5) which would lead to a major problem when examining the influence of the disulphide bond on the gaseous ligand binding.

To tackle this problem, an alternative reduction system was sought. These experiments explored the use of either ascorbate ( $E_m = -60$  mV) or NADH ( $E_m = -320$  mV) as the primary reductant, in the presence of trace amounts of Phenazine Methosulfate (PMS) as a mediator. The heme iron of cytoglobin is progressively reduced to completion by NADH/PMS under anaerobic conditions (Figure 3.10B). By comparison when ascorbate/PMS was used, incomplete reduction of the heme is observed (Figure 3.10C). The state of the disulphide bond after reduction of the heme by both ascorbate/PMS and NADH/PMS was checked by non-reducing SDS (Figure 3.10D). It is clear that the disulphide bond remains intact after reduction of the heme iron (Figure 3.10D, lane 1 to lane 3) but the use of NADH/PMS was preferred as it reduced the heme iron to the same extent as dithionite. The NADH/PMS reduction system was also used with the C38S variant of cytoglobin to establish if it could reduce the heme in a form of the protein with no disulphide bond. The results are consistent with reduction of the heme iron being independent of the presence of a disulphide bond (Figure 3.11).

These experiments established that the use of NADH/PMS as a reducing system yielded a form of cytoglobin in which the heme iron is fully reduced and the disulphide bond remains oxidised (intact). Hence, this is assigned to redox state #2. Finally, to obtain a form of

cytoglobin in which both heme and disulphide bond are reduced (which I assign as redox state #4) the reduced protein was simply incubated with 5 to 10 mM of TCEP or DTT under anaerobic conditions (Figure 3.10D lane 4).

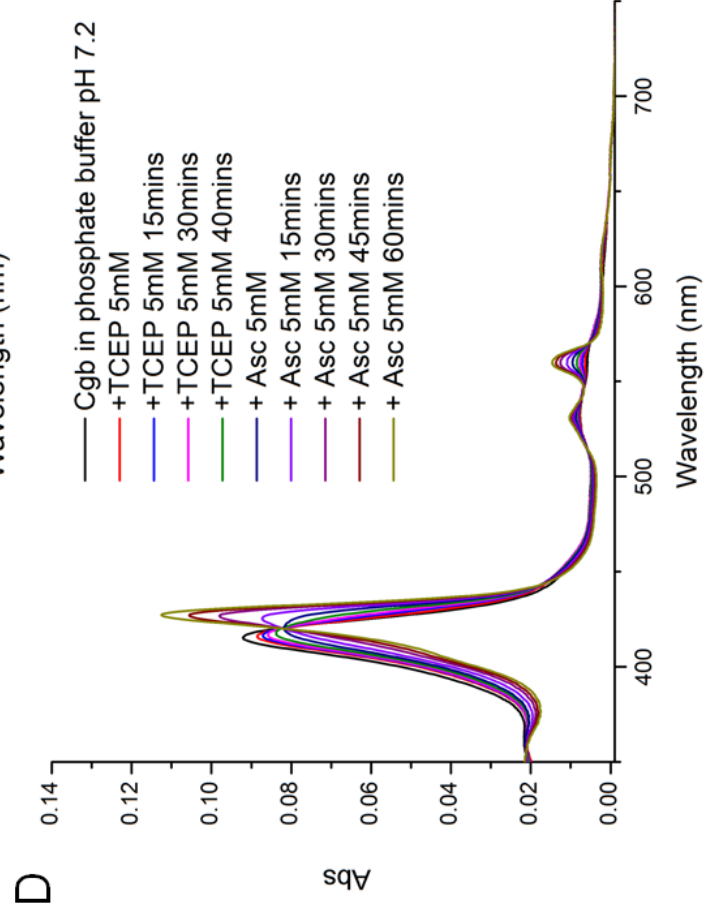
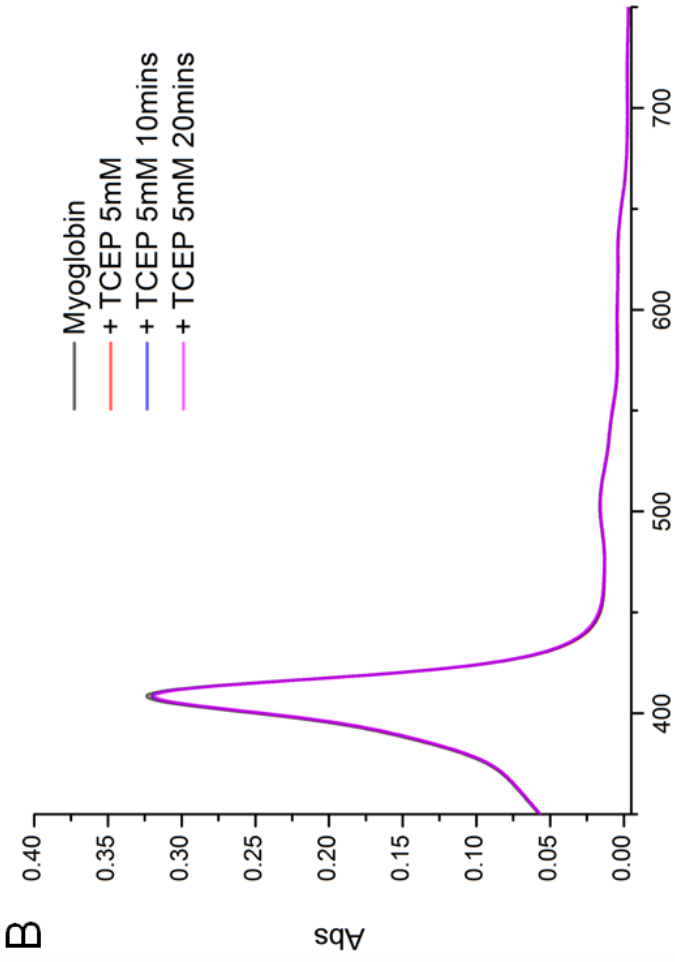
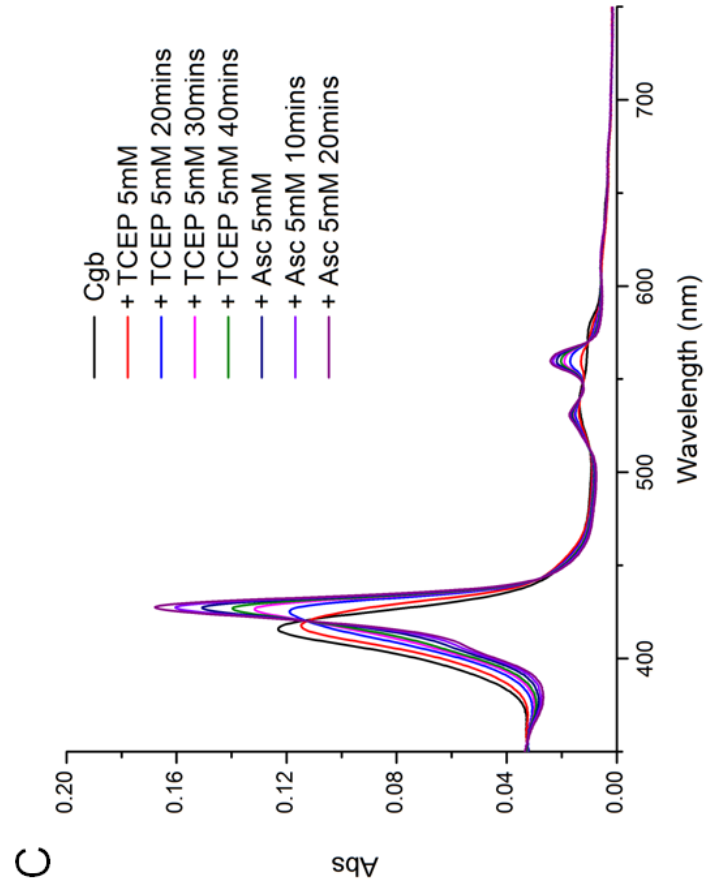
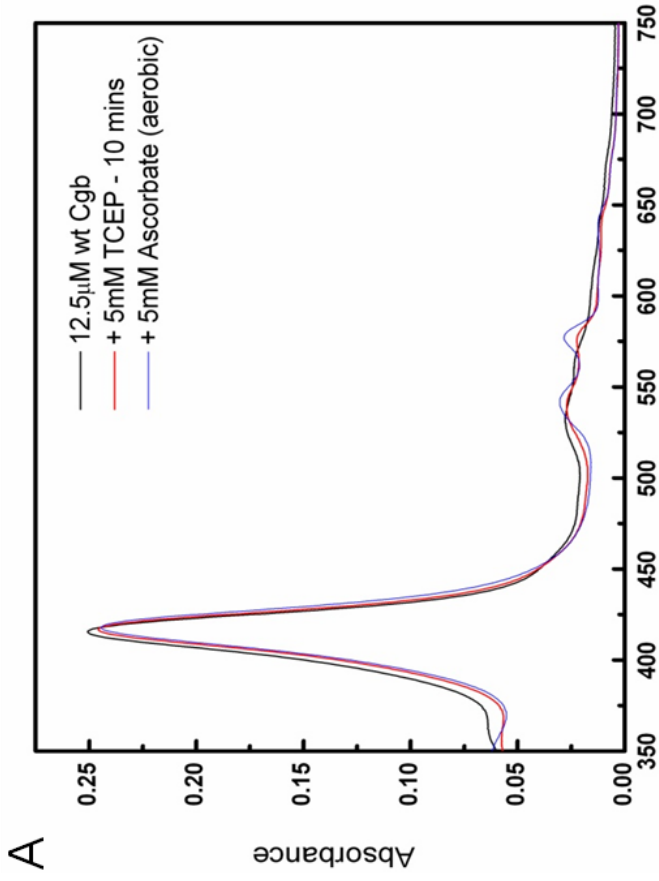


**Figure 3.8 Partial reduction of the heme iron in cytoglobin by TCEP. (A)** Cytoglobin was incubated with 5 mM TCEP under aerobic condition. Formation of ferrous-oxy species was observed due to a partial reduction of the heme iron by TCEP and the addition of 5 mM ascorbate completed the formation of ferrous-oxy species. **(B)** Sperm whale myoglobin was incubated with 5 mM TCEP under aerobic condition. No reduction of the heme was observed. **(C)** Cytoglobin was incubated with 5mM TCEP in 20 mM Tris-HCl pH 8.0 under anaerobic conditions. 5 mM ascorbate was added to cytoglobin after incubation with TCEP for 40 minutes. **(D)** Cytoglobin was incubated with 5mM TCEP in phosphate buffer pH 7.2 under anaerobic conditions to examine the source of electrons for the reduction of the heme iron of cytoglobin.

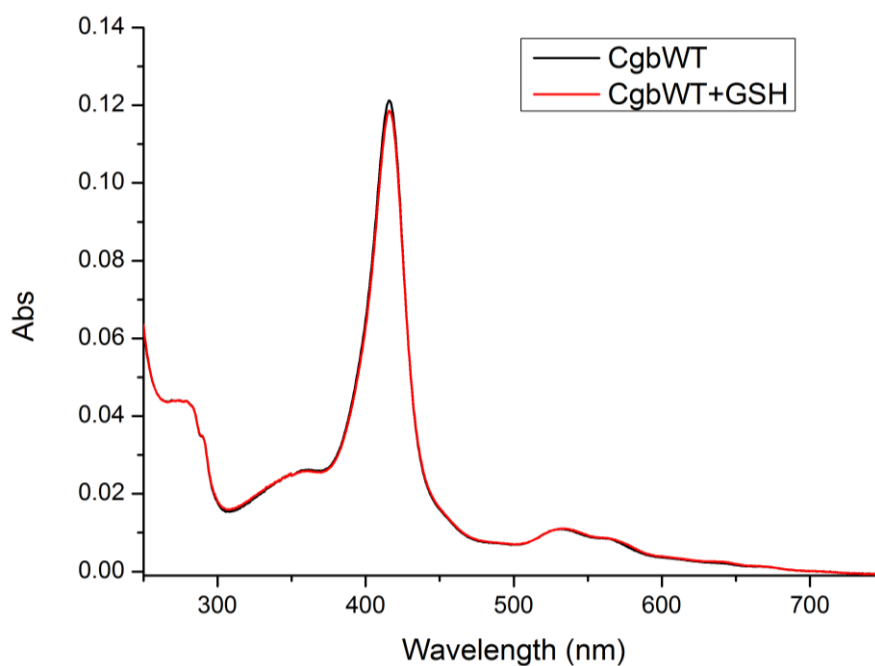


**Figure 3.9 UV/vis spectrum of cytoglobin treated with GSH in the ferric state.** Approximately 6  $\mu$ M of cytoglobin in the ferric state was mixed with a final concentration of 5 mM GSH in 20 mM Tris-HCl pH 7.0 in a 2 mm path-length quartz cuvette. Spectrum was recorded before (black trace) and after (red trace) addition of GSH.

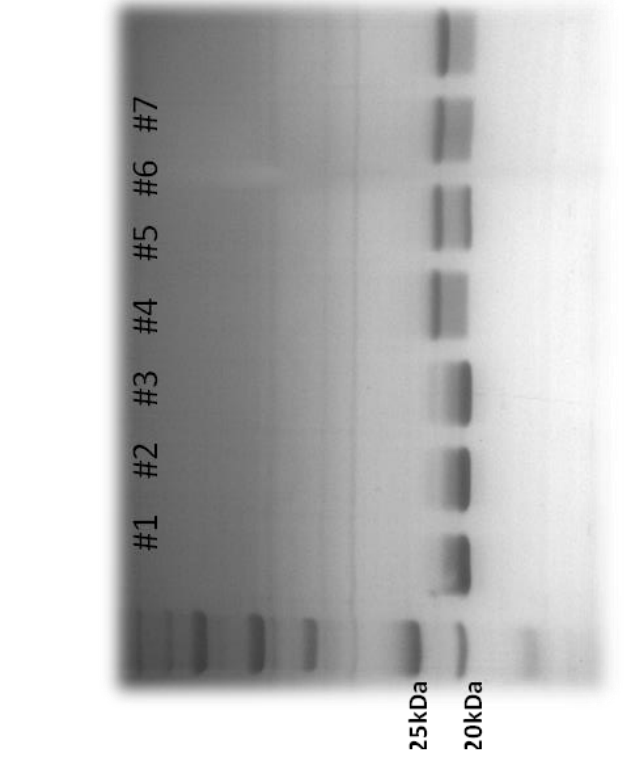
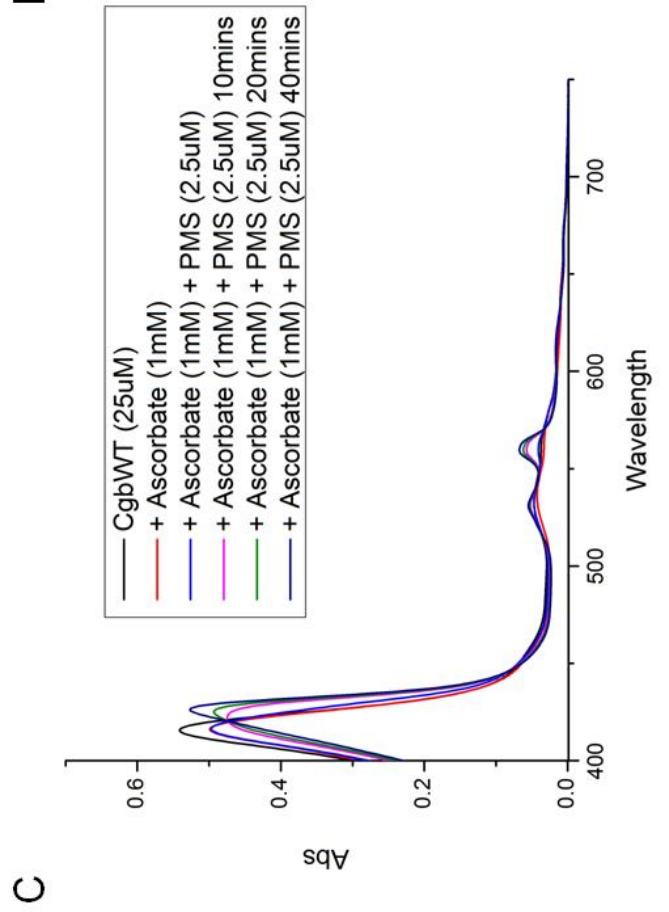
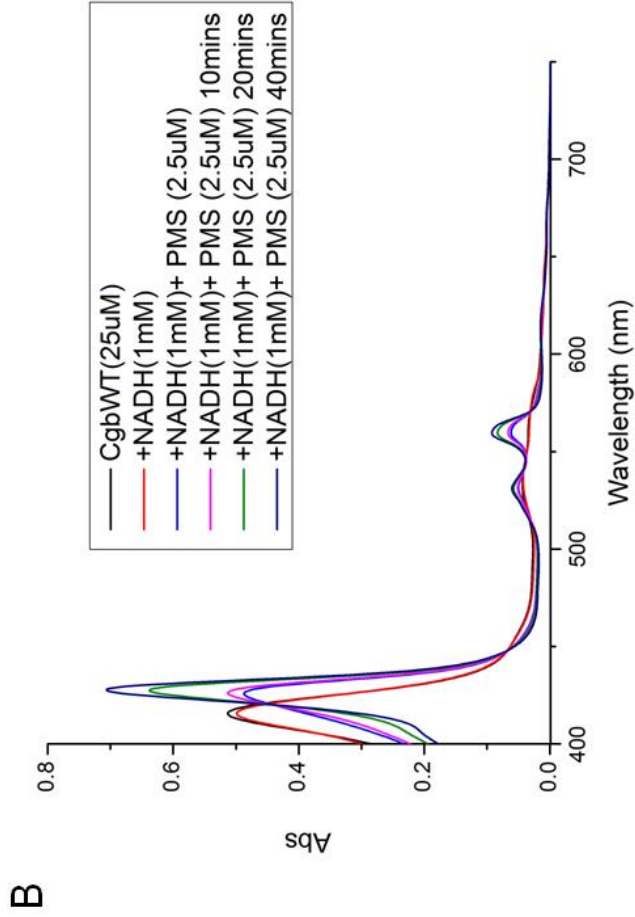
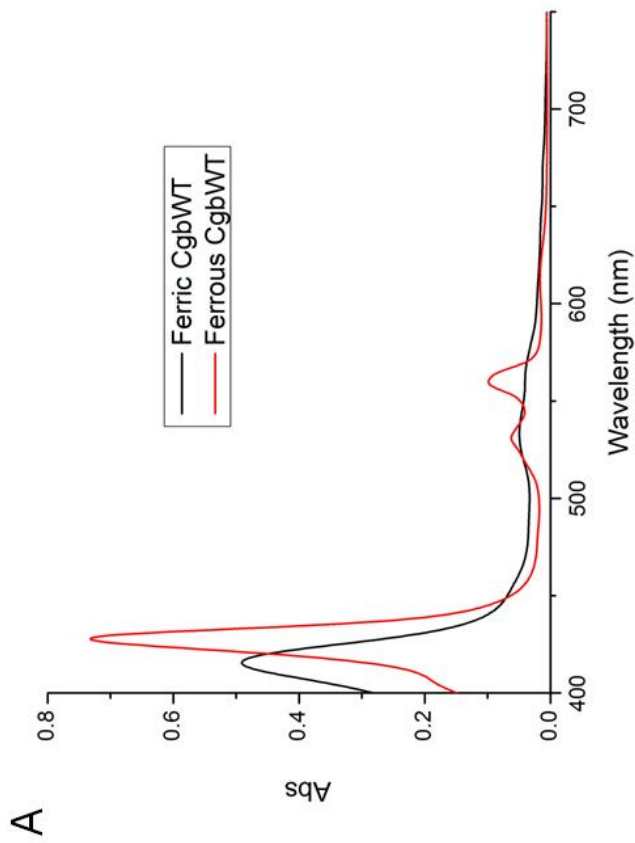


**Figure 3.10 Reduction of heme iron in cytoglobin by ascorbate/PMS and NADH/PMS under anaerobic conditions.** **(A)** UV/vis spectra of cytoglobin in ferric and ferrous states. Reduction of cytoglobin was achieved by treating cytoglobin with small amount of solid sodium dithionite under anaerobic condition. **(B)** Reduction of heme iron using NADH and PMS monitored spectroscopically. Reduction of cytoglobin was achieved by treating 25  $\mu$ M cytoglobin with 1 mM NADH and 2.5  $\mu$ M PMS under anaerobic condition for 40 minutes. **(C)** Reduction of heme iron using ascorbate and PMS monitored spectroscopically. Reduction of cytoglobin was achieved by treating 25 $\mu$ M Cytoglobin with 1mM Ascorbate and 2.5  $\mu$ M PMS under anaerobic condition for 40 minutes. **(D)** The state of the disulphide bond at different stages of reduction shown on a non-reducing gel: #1 = Cytoglobin, #2 = Cytoglobin + NADH, #3 = Cytoglobin + NADH + PMS, #4 = Cytoglobin + NADH + PMS + TCEP, #5 = Cytoglobin + Na<sub>2</sub>S<sub>2</sub>O<sub>4</sub>, #6 = Cytoglobin + TCEP, #7 = Cytoglobin + DTT.

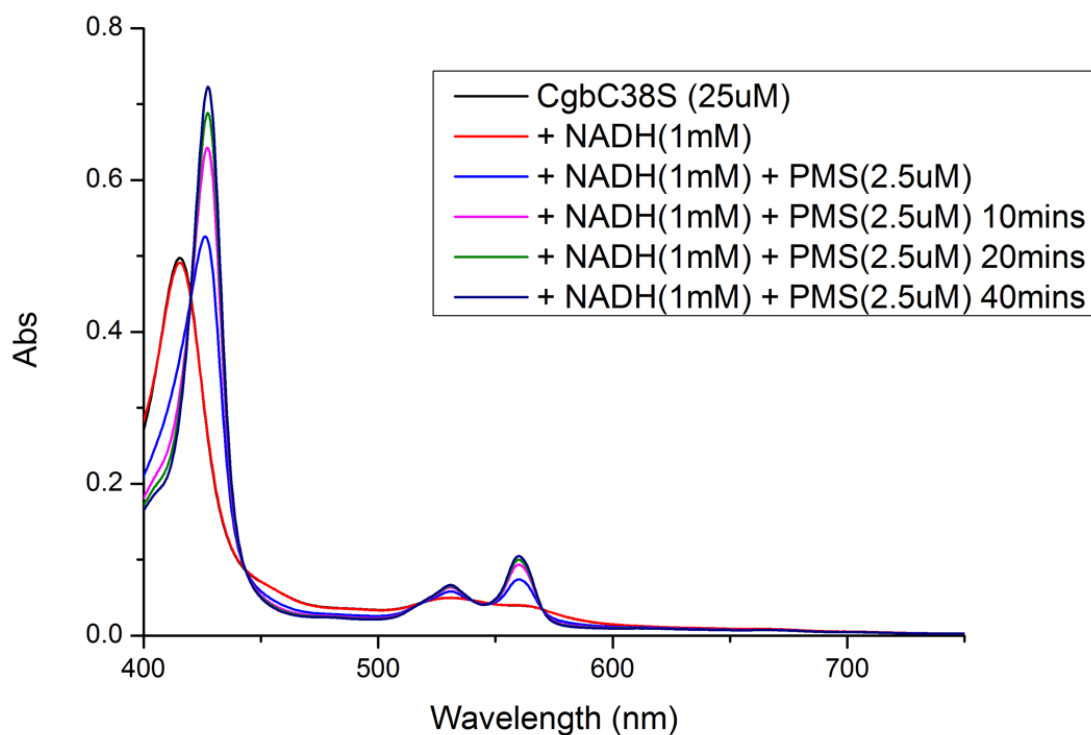


**Figure 3.11 Reduction of heme iron in C38S variant by NADH/PMS under anaerobic conditions.** 25  $\mu$ M of C38S variant was reduced with 1 mM NADH and 2.5  $\mu$ M in 20mM Tris-HCl pH 8.0 for 40 minutes under anaerobic conditions. The reduction of heme iron was monitored every 10 minutes on the UV/vis spectrophotometer.

### 3.3 Discussion

The results presented in this chapter laid the foundation for the studies of spectroscopic and biochemical properties of cytoglobin in those redox states that are likely to occur in cells. Unlike previous reports which used either refolded recombinant protein purified from inclusion bodies or a tagged version of the protein, the protocol for expression and purification of recombinant cytoglobin in this study was optimised to only purify the naturally folded recombinant cytoglobin from the soluble fraction of *E. coli* BL21 (DE3). This is critically important to eliminate any undesirable effect on the structure of cytoglobin either as a result of the *in vitro* refolding process or because of the presence of a non-benign tag, although no evidence is available in the literature to suggest any critical differences between refolded protein and protein purified from soluble fractions.

During the course of this study, I have purified recombinant cytoglobin from both sources and spotted some variations between the two preparation methods. For instance, in the refolded cytoglobin, various oligomeric states were observed in the protein fractions eluted from gel filtration column (Figure 3.12A), while the naturally folded cytoglobin exists only as one single form as shown in figure 3.4. Moreover, a comparison of the UV/vis spectrum clearly showed some subtle differences in spectral features in the UV/vis spectrum, especially between the region of 600 nm to 700 nm (Figure 3.12B) which suggest that different preparation methods could affect the qualities and the properties of the recombinant protein. When comparing the EPR spectrum of cytoglobin prepared in this study (Figure 3.3C) with the EPR spectra of His-tagged cytoglobin (Beckerson et al., 2015) and the cytoglobin prepared from refolded protein (Vinck et al., 2003) some subtle differences in terms of the heme local environments although all of which are generally in agreement with a predominant ferric low-spin species in the cytoglobin. Although to what extent that properties of refolded cytoglobin differs from the naturally folded cytoglobin is not a subject of this study, it is still strongly

advised that recombinant cytoglobin should be purified as naturally folded soluble protein free from any modification which may hamper interpretations of the properties of the protein.

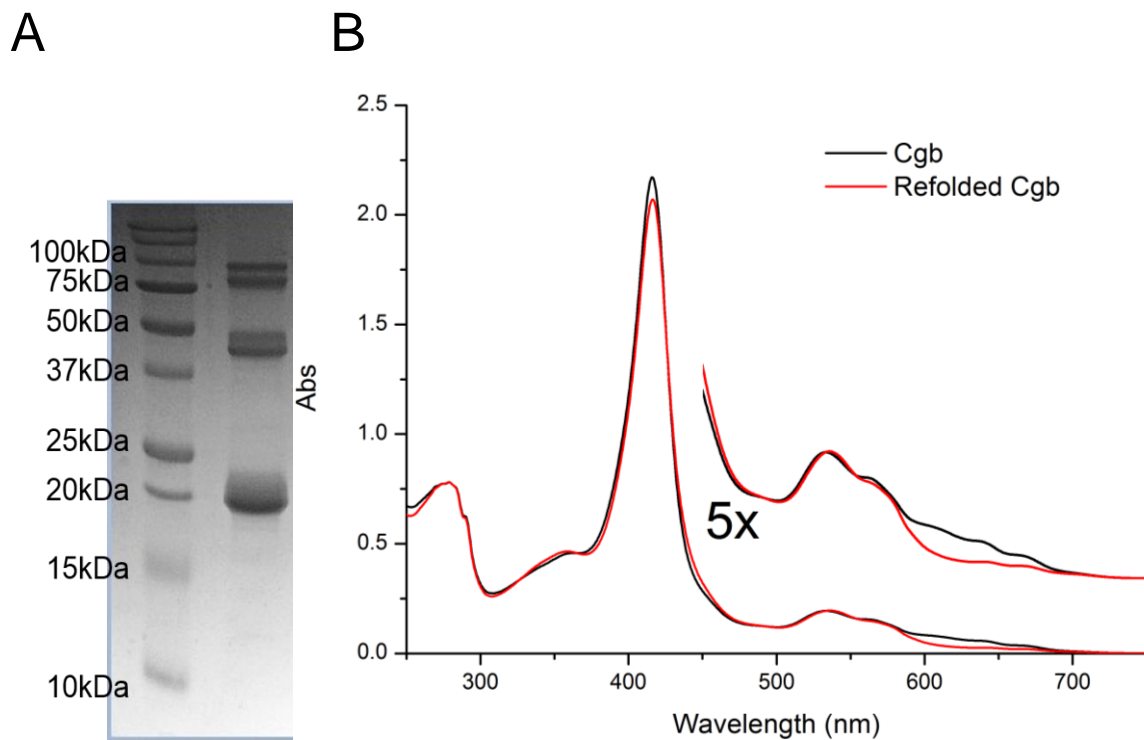


**Figure 3.12 Comparison of recombinant cytoglobin purified from different sources.** The recombinant cytoglobin was purified from cell lysate using method described in section 2.5.5. While the refolded cytoglobin was purified from inclusion body using method described in chapter 2.5.4. **(A)** A non-reducing SDS-PAGE gel showing refolded cytoglobin at different oligomeric states. **(B)** Adsorption spectra of recombinant cytoglobin purified from different sources. The spectra were recorded in a 2 mm path length cuvette with highly pure protein eluted from the gel filtration column in 20 mM Tris-HCl, 150 mM NaCl, pH 8.0.

To date, the physiological oligomeric state of cytoglobin is still controversial. One of the X-ray structures of cytoglobin suggests that it is a homo-dimer linked via two intermolecular disulphide bonds (Sugimoto et al., 2004) whilst another one suggests a homo-dimer with different interaction interface when the formation of disulphide bond is prevented by substitution of cysteines with serine (de Sanctis et al., 2004). However, those structures could possibly be just an artefact created during the process of crystallography because an exceptionally high concentration of protein may force unwanted interaction between proteins which may not be of physiological relevant.

The purified recombinant cytoglobin prepared in this study is shown to be purely monomeric (~21 kDa) in the non-reducing SDS-PAGE. However, in our studies of cytoglobin protein in solution using analytical gel filtration chromatography, it is clear that cytoglobin has a dimer-like molecular weight in solution (~44 kDa) which could be either due to the presence of a dimeric quaternary structure or protein running with an abnormal hydrodynamic radius which is possible due to the extension at N- and C- termini. In fact, it is clearly that cytoglobin does not form dimer involving inter-molecular bonds in the solution that was described in the X-ray structure by Sugimoto and colleagues. Moreover, the results also indicate that the dimer of cytoglobin in solution is unlikely to link via the C-termini as the dimeric property is also observed in the truncated protein (Cgb $\Delta$ C). Interestingly, according to the study done by Lechauve and colleagues using the same chromatographic technique, a cytoglobin which is without both N- and C- termini has an apparent MW similar to a monomer (Lechauve et al., 2010). Hence, if the dimeric interaction does exist in the physiological conditions, the dimeric interaction should be similar to what is described in the X-ray structure by de Sanctis and colleagues but with an intra-molecular bond in each subunit depending on the redox state in the environment. Alternatively, the dimeric interface could be at the N-terminus, although this is just a speculation as no related X-ray structure is available.

It is known that changing the state of the disulphide bond changes the position of the E-helix in both neuroglobin and cytoglobin (Hamdane et al., 2003). It would be tempting to see if such an effect could be examined by analytical gel filtration. Eluting the cytoglobin in the presence of TCEP resulted in a significant decrease in the effective hydrodynamic radius and hence a decrease in the apparent molecular weight (ca 10 kDa), the resultant apparent molecular weight of cytoglobin in the presence of TCEP (ca 34 kDa) is in agreement with cytoglobin C38S variant in the absence of TCEP (ca 33.6 kDa) suggesting a significant conformational change upon reduction of the disulphide bond. However, when the same treatment was applied to proteins without disulphide bonds (i.e. myoglobin and cytoglobin C38S variant), a similar decrease in the apparent molecular weight, but to a less extent (ca 1 to 2 kDa), was also observed. One could say that the extent of reduction of hydrodynamic radius is more significant in cytoglobin compared to the negative controls suggesting that there is a measurable conformational change. However, there is not enough evidence to conclude that the disulphide bond could control the hydrodynamic radius in this case. Obviously, more data points will be needed in order to draw a statistically significant conclusion. Alternatively, other experimental approaches, such as nuclear magnetic resonance (NMR), that are more sensitive and accurate to detect changes in the position of amino acid residues within a three dimension structure should be employed in order to effectively assess the effect of reduction or formation of disulphide bond on the overall structure of cytoglobin.

A few studies have shown that the purified cytoglobin exists as dimers that are linked by inter-molecular disulphide bonds in non-reducing SDS-PAGE (Beckerson et al., 2015; Tsujino et al., 2014). However, no dimeric nor any higher oligomeric states was present in the purified cytoglobin protein from the soluble fractions in this study. The purified cytoglobin appears as monomeric based on the fact that there only a single protein band was observed in the non-reducing SDS-PAGE in the absence of any reducing agents for disulphide bond. Although

results obtained from analytical gel filtration predicted that the cytoglobin is a dimer which is shown in section 3.2.3, It is clearly that the dimer-like behaviour is not due to via inter-molecular disulphide bond. The only exception for the dimerisation via inter-molecular disulphide bond is observed during the purification of the C38S variant in which the inter-molecular disulphide bond is linked between the cysteine residues at position 83 (Cys83) from two sub-units.

Under normal circumstances, the two cysteine residues – Cys38 and Cys83 in the purified cytoglobin form an intra-molecular disulphide rather than inter-molecular disulphide bonds. Additionally, formation of the intra-molecular disulphide bond causes a difference in the mobility of cytoglobin in non-reducing SDS-PAGE as shown in figure 3.4 because the difference in the “apparent” molecular weight of the cytoglobin under different treatments is dependent to the state of the disulphide bond. Therefore, when the disulphide bond is intact, the protein band will migrate further down and show a lower apparent molecular weight due to its compact in shape whilst when the disulphide is reduced the protein band will run at a higher apparent molecular weight.

Since the state of the disulphide bond is reversible and the position of the disulphide bond is at proximity to His81 – the endogenous axial ligand of the heme iron in cytoglobin, many studies have suggested that changes in the state of the disulphide bond would affect the local environment of the heme active site (Hamdane et al 2003, Vinck et al 2004, Lechauve et al, 2010, Tsujino et al, 2014). In this study I demonstrate that the redox state of the disulphide bond responds to the change over a range of solution potentials set by the DTT/oxDTT couple and these changes can be accounted for by a reduction potential of disulphide bond which was estimated to be at -280 mV. The redox potential of the heme iron of cytoglobin was reported to be +20 mV by Sawai and colleagues. Thus, it is believed that the heme iron should

be readily reduced inside the cells and the disulphide bond could offer an extra regulation to the ligand accessibility to heme active site which is described in more details in chapter 4 and 5. In other words, cytoglobin is a redox sensitive protein due to the presence of a pair of redox active cysteine residues which could act as a redox switch responding to the changes in the redox potential in the environment by changing the state of the disulphide bond.

To be able to elucidate the changes in the properties of the heme active site caused by the change in the state of the disulphide bond, one has to be able to control the redox state of each redox site independently. The data presented in this chapter clearly demonstrate that conventional approaches based on using DTT and TCEP to reduce the disulphide bond and dithionite to reduce the heme iron of cytoglobin cause reduction in the second redox active site. Therefore, I developed a method to systematically and independently control the two redox active sites in the cytoglobin so as to facilitate the examination of the biochemical properties of cytoglobin at different redox states. Instead of using DTT and TCEP which were shown to cause partial reduction in the heme iron, the disulphide bond in the ferric cytoglobin was reduced with GSH – a natural reductant in eukaryotic cells. The disulphide bond was reduced effectively while no reduction in the heme iron was observed. On the other hand, to avoid partial reduction of the disulphide bond by dithionite while reducing the heme iron, an anaerobic method using NADH as the primary reductant in the presence of tPMS as a mediator was employed. This system was shown to selectively reduce the heme iron to its ferrous state while keeping the disulphide bond intact until DTT or TCEP was added to reduce the disulphide bond. Taken together, these methods opened a possibility to investigate the effects caused by the change in the state of the disulphide bond in cytoglobin protein at both ferric and ferrous state using various advanced spectroscopic techniques later in this study.

## Chapter 4: Redox Linked Ligand Accessibility of Cytochrome c

### 4.1 Introduction

The best understood physiological role of the globins is to carry gaseous ligands such as diatomic oxygen, which bind reversibly to the reduced heme cofactor. In the case of cytochrome c, the heme coordination is described as being hexa-coordinate. That is to say that the heme iron is bound with four pyrrole nitrogen atoms at the same plane of the porphyrin ring and two other nitrogen atoms provided by the imidazole rings of the histidine residues (His81 and His113) at the opposite axial positions (His/His ligation) in both oxidation states (Sawai et al., 2003; Trent and Hargrove, 2002), although direct evidence of His/His ligation in the ferrous state is rather limited. In myoglobin, because the axial ligand (His64) on the distal side of the heme pocket is not directly coordinated to the heme iron, the heme is said to be penta-coordinate. However, a water molecule is usually found coordinated to the heme iron in the ferric state (Quilin et al., 1993). Therefore, it is believed that the mechanism and kinetics of ligand binding to the hexa-coordinate cytochrome c and the penta-coordinate myoglobin should be very different from each other. However the details of ligand binding to cytochrome c may not be completely delineated due to the fact that interpretation of ligand binding experiments are complicated by the use of either dithionite to reduce the heme iron or DTT to reduce the disulphide bond which interferes with another redox active site as shown in chapter 3.2.5

In the case of a simple bimolecular ligand binding reaction to a penta-coordinate heme in myoglobin, exogenous ligands do not need to compete with the distal histidine residue (His64) to bind to the open face of the heme iron. However for exogenous ligands to bind to the hexa-coordinate heme in cytochrome c, the distal histidine residue (His81) must be displaced from its axial position. Therefore, cytochrome c is believed to follow a general three-state mechanism for binding of exogenous ligands that was first described in nonsymbiotic

hemoglobins in plants to account for data obtained in flash photolysis experiments (Trent et al., 2001). In this model, a bound exogenous ligand, carbon monoxide, is dissociated from its axial position on the reduced heme by photolysis leaving the distal heme pocket temporarily empty. Following the formation of the intermediate penta-coordinate species, the unbound exogenous ligand competes with the distal histidine residue for rebinding to the vacant coordination site on the distal site of the heme. Once the exogenous ligand binds back to the heme iron, the distal histidine is displaced from the distal heme pocket again. However, the model described by Trent and colleagues was only a simplified view of the binding of exogenous ligands to the hexa-coordinate heme because in physiological conditions the protein should exist in equilibrium between hexa-coordinate and penta-coordinate forms rather than solely the penta-coordinate intermediates in the photolysis experiment (Trent et al., 2001). Moreover, structural comparisons between ferric cytoglobin and carbonmonoxy-ferrous cytoglobin revealed that the actual structural changes coupled with the binding of exogenous ligand involve an upward movement of a part of the E-helix together with a re-arrangement of the CD loop regions rather than just a simple outward movement of the distal His81 residue alone due to a steric hindrance caused by nearby residues (Makino et al., 2011).

Furthermore, the presence of an intra-molecular disulphide bond near the distal histidine ligand was reported to influence the ligand binding properties in cytoglobin, as well as neuroglobin, in a similar fashion despite of a difference in the position of the disulphide bond. Lechavue and colleagues reported that the disulphide bond may regulate exogenous ligand binding by adjusting the final position of the E-helix which subsequently modulates the affinity of the distal histidine ligand to the heme iron. Early EPR studies on the ferric cytoglobin with an intact intramolecular disulphide bond showed that the proteins contain a sub-population of high-spin heme species, which represent loosely coordinated or off position of the distal His81 residue, while they were not present in variant form of cytoglobin (C38S, C83S) in which

disulphide bonds cannot be formed (Vinck et al, 2004).

Taken together, a number of reports suggested that the ligand binding properties of cytoglobin are regulated by the state of the disulphide bond, as suggested by the redox potential of the disulphide bond reported in chapter 3.2.4, which could respond to changes in intracellular redox state. However, interpretations of these experiments are severely hampered by the use of inappropriate methods to control the oxidation states of the heme iron and the disulphide bond. Therefore, as a prelude to understanding the ligand binding properties of cytoglobin it is necessary to carefully design experiments to understand how the ligation state of the heme iron is influenced by the redox state of both the heme and the disulphide bond and consider any potential effects on the physiological function(s) of cytoglobin.

In this chapter, I used the methods developed in section 3.2.5 to explore the binding of ligands to cytoglobin in its four principal redox states with three specific aims. Firstly, the ligation state of cytoglobin in the ferrous state is examined by room-temperature MCD with the use of exogenous ligand probe carbon monoxide. Secondly, the influence on the local environment of the distal heme pocket by changing the state of the disulphide bond was characterised by a combination of advanced spectroscopic analyses and protein engineering that each of the two cysteine residues (C38S and C83S) was substituted by a serine residue to mimic the situations where the intra-molecular disulphide bond is reduced. Finally, the heme accessibility for exogenous ligand in cytoglobin is explored.

## 4.2 Results

### 4.2.1 Spectroscopic Characterisation of Cytochrome c in the Ferrous State

The ligation state of heme in human cytochrome c in the ferric state has been characterised by a combination of EPR and MCD (Chapter 3). This work showed that the axial ligands of the heme iron are two histidine ligands (His81 and His113). Information about the ligation state of the heme in the ferrous state is limited due to a lack of a relevant X-ray structure. However it is generally accepted that the ferrous heme iron of human cytochrome c retains the two axial histidine ligands. Hence, having established the biochemical methods to selectively reduce the two redox active sites – the heme and the disulphide bond, in cytochrome c described in the previous chapter, I wished to examine the ligation state in the ferrous cytochrome c and the effect of changing the state of the disulphide bond on the heme ligation spectroscopically. Since the reduced heme iron is diamagnetic and therefore EPR silent, the characterisation of the ferrous cytochrome c is done using a combination UV/vis and room temperature MCD spectroscopies.

Generation of deoxy-ferrous cytochrome c (redox state #2) was achieved by using NADH/PMS under anaerobic conditions as previously (section 2.8.1). The UV/vis spectrum, of deoxy-ferrous cytochrome c has a Soret absorption maximum at 427 nm and the  $\alpha$ - and  $\beta$ -bands are at 530 nm and 560 nm, respectively. In addition, a weak feature at 612 nm is observed (Figure 4.1 A; black trace). The RT-MCD spectrum between 300nm and 800nm is dominated in the visible region by a derivative-shaped feature with an intensity (peak-to-trough) of approximately  $200 \text{ M}^{-1}\text{cm}^{-1}\text{T}^{-1}$  with a maximum at 554 nm and a minimum at 561 nm. While in the Soret region, there is a derivative shaped feature ( $\text{ca } 15 \text{ M}^{-1}\text{cm}^{-1}\text{T}^{-1}$ ) with a maximum at 430 nm and a minimum at 415 nm. In common with the RT-MCD spectrum of cytochrome c in the ferric state as shown in the section 3.2.1 (Figure 3.3B) that no features at wavelengths greater than 600 nm is observed which again suggests that the broad weak feature at 612 nm

seen in the UV/vis spectrum does not arise from the heme. The form and intensity these features are consistent with a single low-spin ferrous heme (Figure 4.1 B; black trace).

Unlike the room temperature MCD of a heme protein in the ferric state there is no ligand to metal CT band in the near-IR region of the MCD spectrum of a ferrous heme protein to provide information on the ligation set of the heme iron. Instead carbon monoxide (CO) was used to probe the ligation state of the cytoglobin as it has been shown previously that ferrous cytoglobin binds CO presumably by displacing the distal His 81 ligand (Trent and Hargrove, 2002; Sawai et al., 2003; Makino et al., 2011; Tsujino et al., 2014; Beckerson et al., 2015).

Upon addition of CO, a blue shift of the Soret peak to 421 nm, together with a red shift of the  $\alpha$ - and  $\beta$ -bands and 570 nm and 540 nm and a change in intensity of the  $\alpha$ -band are observed in the UV/vis spectrum suggesting the formation of CO-cytoglobin complex (Figure 4.1 A; red trace). The RT-MCD spectrum, the CO-bound ferrous cytoglobin exhibits a number changes arising from ligand binding. The previously weak derivative signal in the Soret region changes sign (maximum at 514 nm and a minimum at 525 nm) and intensifies to approximately  $85 \text{ M}^{-1}\text{cm}^{-1}\text{T}^{-1}$  and a narrow intense derivative-shaped feature in the visible region is replaced by a broader derivative with an intensity of about  $45 \text{ M}^{-1}\text{cm}^{-1}\text{T}^{-1}$  and a maximum at 561 nm and a minimum at 575 nm. The spectral features of the MCD spectrum are consistent a low-spin ferrous heme with CO/histidine ligation (Figure 4.1 B; red trace) (Dhawan et al., 1999). Note also, upon binding of the CO, the weak feature at 612 nm is also red shifted to 628 nm in the UV/vis spectrum but again, no corresponding MCD band is detected.

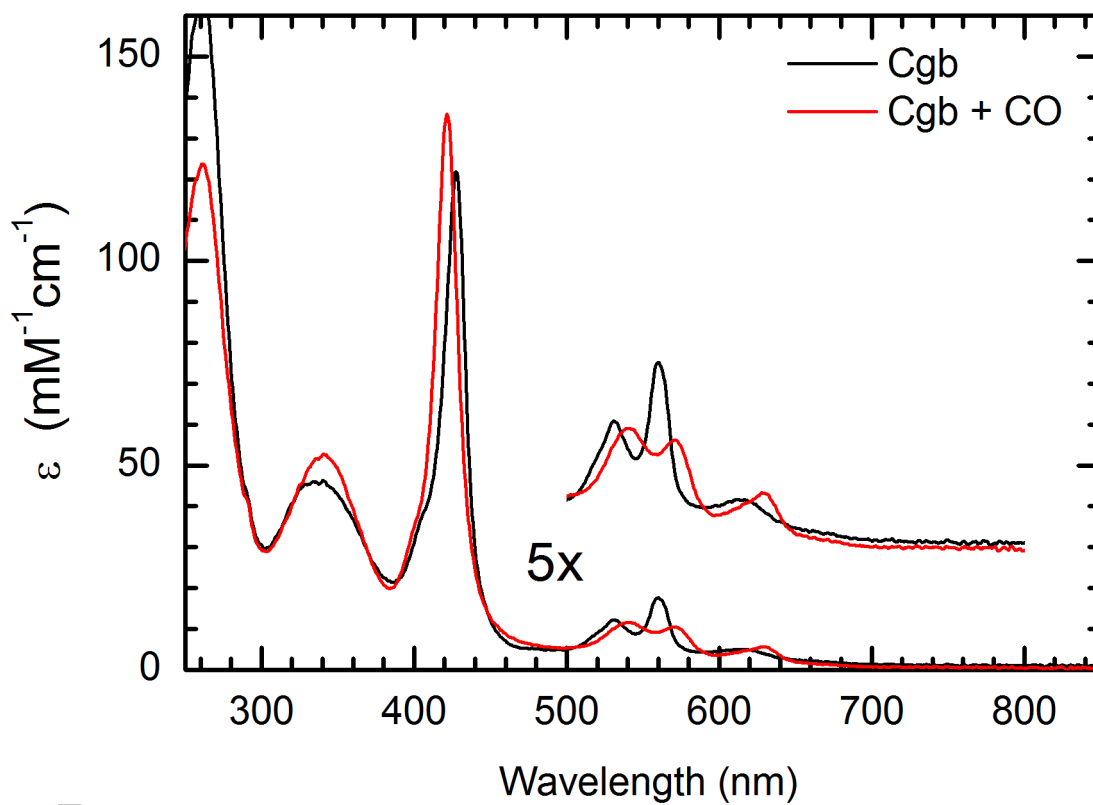
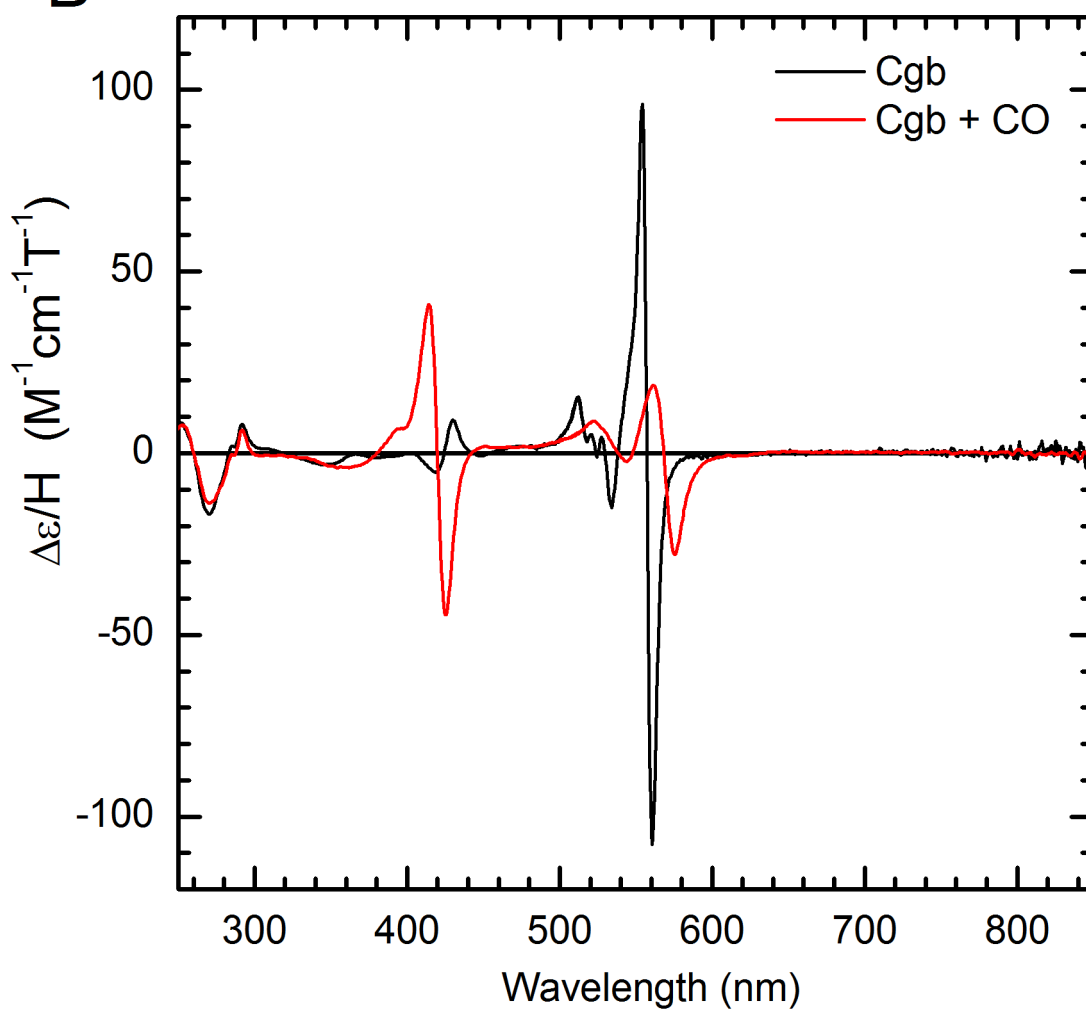
Taken together, these data can be interpreted as follows. In redox state #2 in which the disulphide bond remains oxidized (intact) cytoglobin displays a MCD spectrum typical of low-spin ferrous heme. Binding of carbon monoxide induces a new set of MCD features which are

consistent with CO/His ligation. The heme axial ligand set of cytoglobin in the low-spin ferric state was clearly demonstrated to His/His by the MCD experiment described in chapter 3. Since the ferrous heme is shown to be low-spin and the RT-MCD spectrum after CO binding is consistent with a His/CO ligated heme then it is highly likely that the axial ligand set remains His/His in the reduced heme with the distal histidine (His81) being displaced by CO as observed in the x-ray structure (Makino et al., 2011).

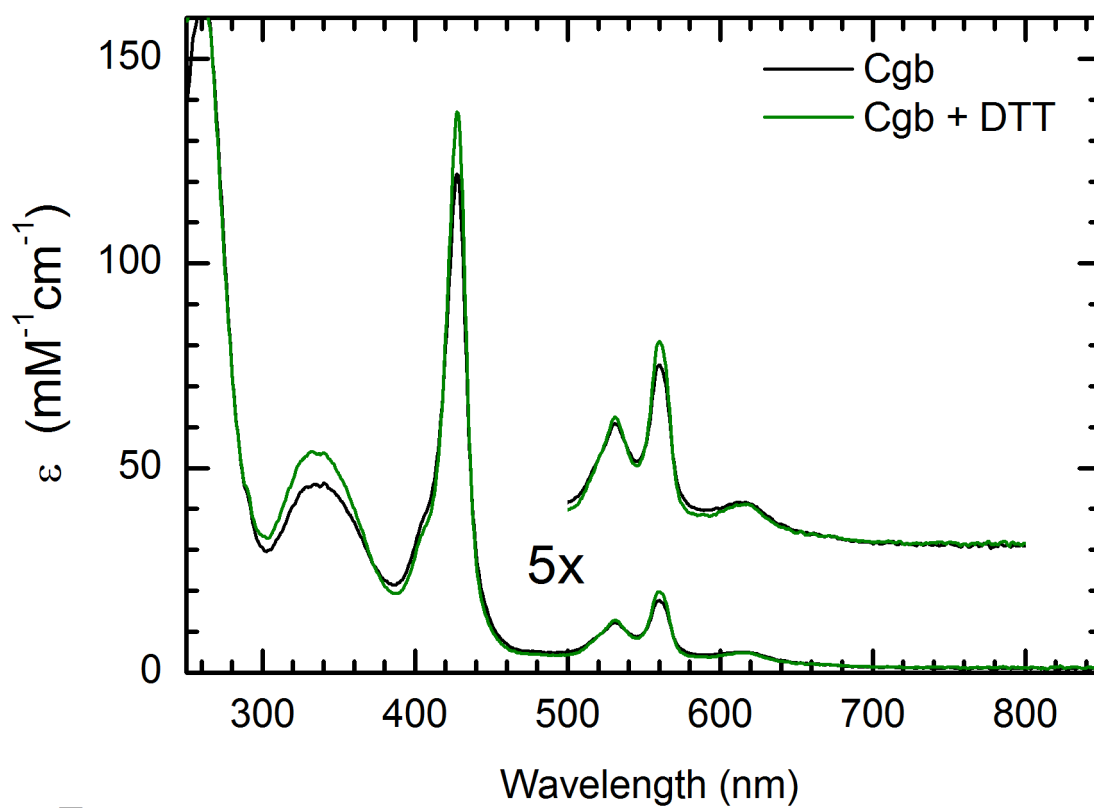
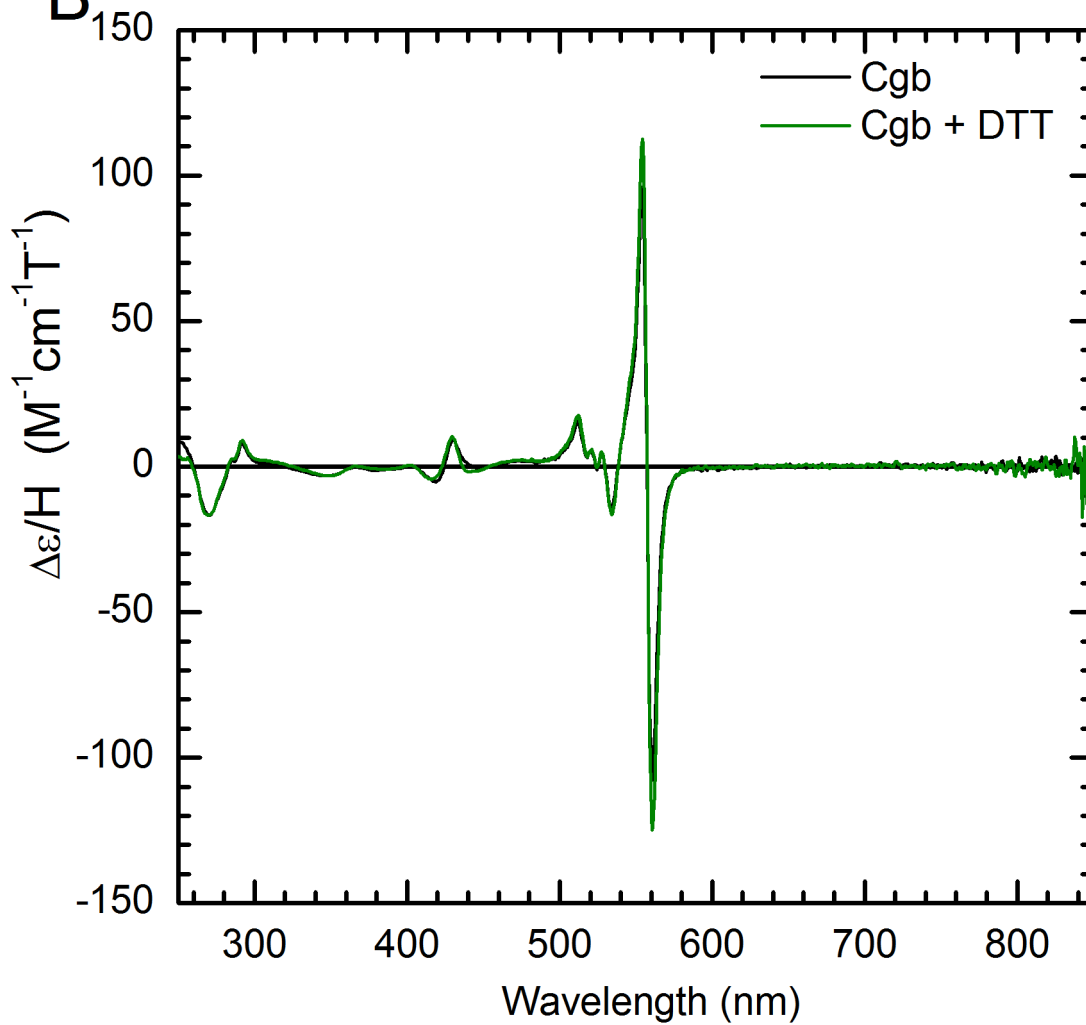
Having established the likely axial heme ligand set in ferrous cytoglobin, the next question was whether changing the state of the disulphide bond would cause this to change. Therefore, a sample of ferrous cytoglobin with a reduced disulphide bond (redox state #4) was prepared and compared with a sample of ferrous cytoglobin with an intact disulphide bond (redox state #2 - above). The UV/vis spectrum of ferrous cytoglobin before and after reduction of the disulphide bond looks identical in terms of the positions of the Soret peak and the bands in the visible region. However, a small but notable increase in the absorption maxima of Soret peak ( $\sim 15 \text{ mM}^{-1} \text{ cm}^{-1}$ ) and the  $\alpha$ - and  $\beta$ -bands are observed (Figure 4.2A). In the RT-MCD spectrum, a similar pattern of changes is observed. Reduction of the disulphide bond does not change the positions of the derivative shaped bands in either the Soret or visible regions. However the intensity of the derivative bands in the visible region is increased by  $35 \text{ M}^{-1} \text{ cm}^{-1} \text{ T}^{-1}$  ( $\sim 235 \text{ M}^{-1} \text{ cm}^{-1} \text{ T}^{-1}$ ) compared with the ferrous cytoglobin with intact disulphide bond (Figure 4.2B). Therefore, the spectra suggest that the reduction of the disulphide bond does not change the dominant oxidation or ligation state of the heme iron compared to redox state #2 as the MCD spectrum is still dominated by a low-spin ferrous species with His/His ligation as previously described. However the increase in intensity in both UV/vis and MCD spectra needs to be accounted for. One possibility is that it could be due to a complete reduction of any residual ferric heme iron in the samples by DTT. Alternatively, as indicated in the EPR spectrum of wild-type cytoglobin in the ferric state that a sub-population (*ca* 15%) of high-spin

penta-coordinate species is present when the disulphide bond is intact (Chapter 3.2.1), reduction of the disulphide bond may actually promote the complete formation of low-spin hexa-coordination in those penta-coordinate species which is reflected in the MCD spectrum as an increase in the intensity of low-spin ferrous spectrum.

Changing the state of the disulphide bond does not seem to significantly alter the spin or ligation state of the ferrous heme iron. However the consequence of changing the state of the disulphide bond on the binding of an exogenous ligand was further explored with the use of CO as a ligand probe. Interestingly, although the form of CO-bound ferrous cytoglobin complex is the same regardless of the state of the disulphide bond as this is reflected by the position of those spectral features in both UV/vis and MCD which are identical indicating the same CO/His ligation as previously described, the intensity of these spectral features is decreased when the disulphide bond is reduced by DTT. Specifically in the UV/vis spectrum there is a decrease in the Soret peak of (*ca*  $25 \text{ mM}^{-1} \text{ cm}^{-1}$ ) which is reflected in the RT-MCD spectrum in which the intensity of the feature in the Soret region is reduced by *ca*  $20 \text{ M}^{-1} \text{ cm}^{-1} \text{ T}^{-1}$ . There is no obvious emergence of any new spectral feature that suggests a different spin- or ligation-state of the heme iron accompanying the reduction of the intensity of CO/His ligation bands is observed. Hence, the ferrous cytoglobin is still saturated with CO in the distal heme pocket when the disulphide bond is reduced. The change in the intensity of MCD spectrum could result from a subtle difference in the polarity or hydrogen bonding interaction in the CO-bound form (Dhawan et al., 1999) caused by the reduction of the disulphide bond which leads to a rearrangement of E-helix at the distal heme pocket as suggested by the X-ray structure (Makino et al., 2011).

**A****B**

**Figure 4.1 Spectroscopic characterisation of cytoglobin in the ferrous state (A)** UV/vis spectra of 200  $\mu\text{M}$  of ferrous cytoglobin in 20 mM Tris-HCl pH 8.0 (Black trace) and 100  $\mu\text{M}$  of CO-bound cytoglobin in 20 mM Tris-HCl pH 8.0 (Red trace). The preparation of CO samples is described in section 2.7.3. The absorbance is adjusted and plotted as molar extinction coefficient verse wavelength for comparison **(B)** Room-temperature MCD spectra of 200  $\mu\text{M}$  ferrous cytoglobin in 20 mM Tris-HCl pH 8.0 and 100  $\mu\text{M}$  of CO-bound cytoglobin in 20 mM Tris-HCl pH 8.0 (Red trace). MCD conditions: 298 K, 6 T

**A****B**

**Figure 4.2 Spectroscopic characterisation of ferrous cytoglobin with a different state of disulphide bond (A)** UV/vis spectra of 200  $\mu$ M ferrous cytoglobin in 20 mM Tris-HCl pH 8.0 (Black solid trace) and in the presence of 10 mM DTT (Olive green solid trace) **(B)** Room temperature MCD spectra of 200  $\mu$ M ferrous cytoglobin in 20 mM Tris-HCl pH 8.0 (Black solid trace) and in the presence of 10 mM DTT (Olive green solid trace). MCD conditions: 298 K, 6 T.

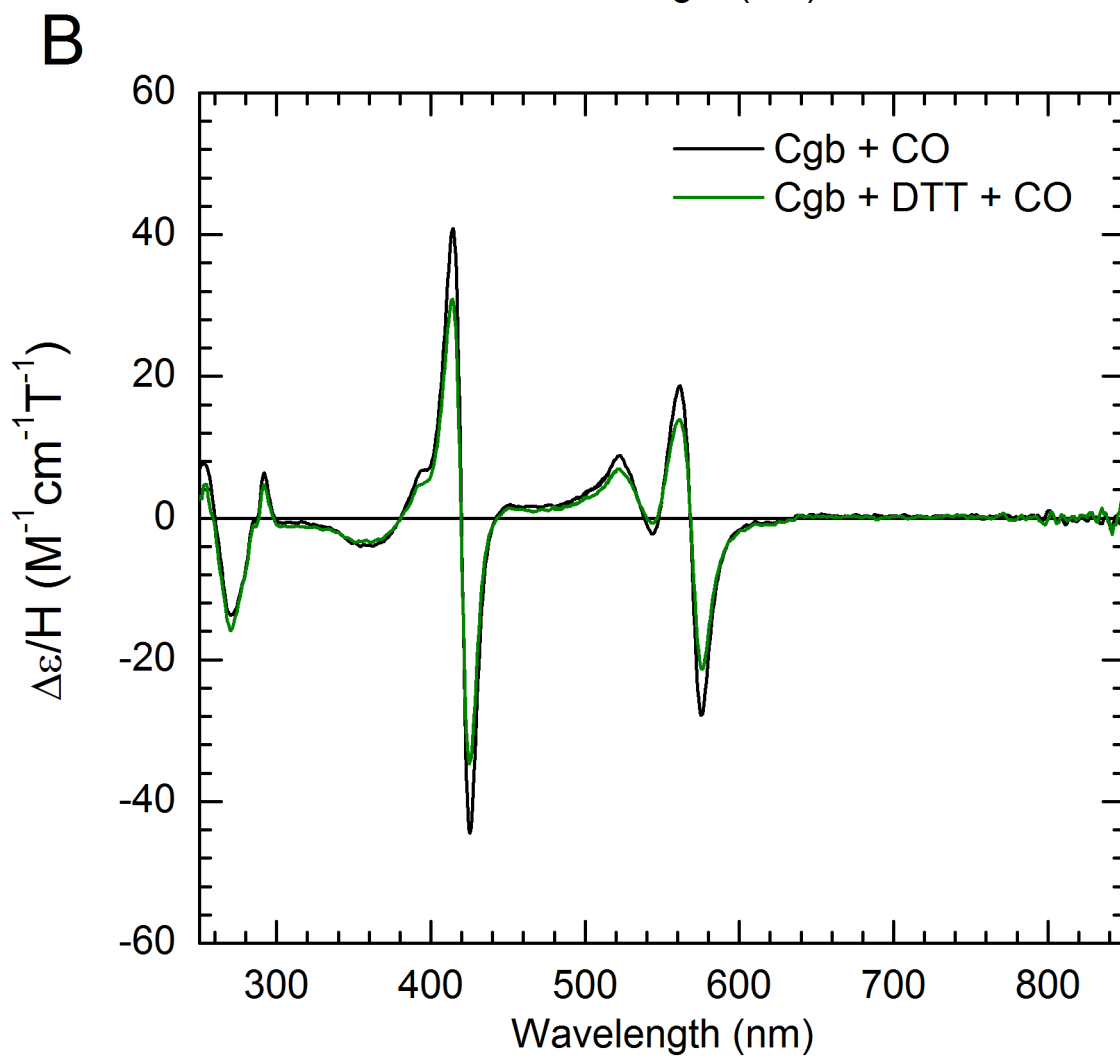
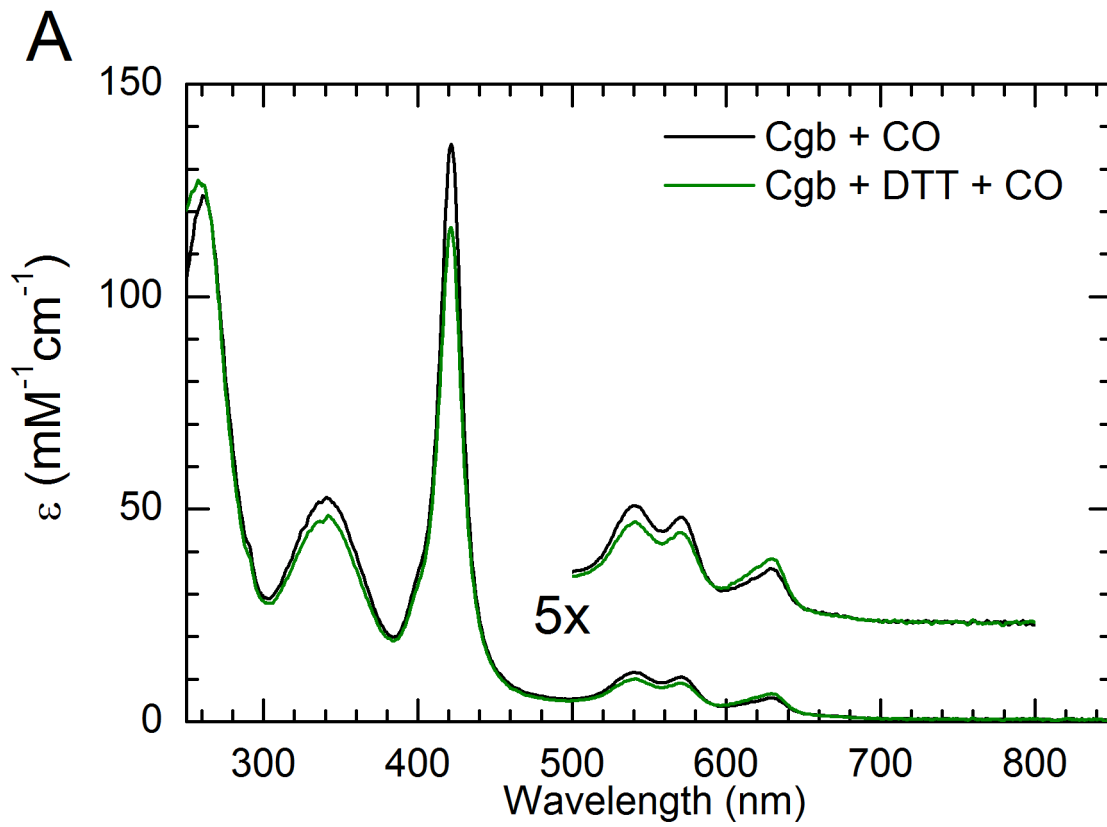


**Figure 4.3 Spectroscopic characterisation of CO-bound ferrous cytoglobin under different state of disulphide bond** (A) UV/vis spectra of 100  $\mu$ M CO-bound cytoglobin in 20 mM Tris-HCl pH 8.0 (Black solid trace) and in the presence of 10 mM DTT (Olive green solid trace) (B) Room temperature MCD spectra of 100  $\mu$ M CO-bound cytoglobin in 20 mM Tris-HCl pH 8.0 (Black solid trace) and in the presence of 10 mM DTT (Olive green solid trace). MCD conditions: 298 K, 6 T.

## 4.2.2 Spectroscopic Characterisation of Cytooglobin C38S and C83S variants in the Ferric State

To further investigate how the local environment of the heme is changed by breaking the intra-molecular disulphide bond, constructs encoding two cytooglobin variants, C38S and C83S, each of which bearing a single cysteine to serine substitution, were generated as described in section 2.4.3. The variant proteins were expressed and purified in order to study cytooglobin that cannot form a disulphide bond. The purified C38S and C83S variants were initially characterised in the ferric state by a combination of UV/vis, room-temperature MCD and low-temperature EPR spectroscopies to allow comparison with the wild-type cytooglobin.

In the ferric state, both C38S and C83S variants, despite the absence of a disulphide bond, have a similar UV/vis spectrum to the wild-type cytooglobin. The Soret peak,  $\alpha$ - and  $\beta$ -bands are at 416 nm, 563 nm and 534 nm, respectively. These spectral features suggest that like the wild-type cytooglobin the heme iron in both variants is hexa-coordinate with His/His ligation. Note, however, the absorption maxima of the Soret peaks and the  $\alpha$ - and  $\beta$ -bands in both cysteine variants are slightly higher than that in the wild-type cytooglobin. Moreover, some differences are found in the visible region between 600nm to 700nm where two bands at 612nm and 670nm appear more intense in the C83S variant compared to wild-type cytooglobin. Interestingly, both of these bands are absent in the C38S variant (Figure 4.4A).

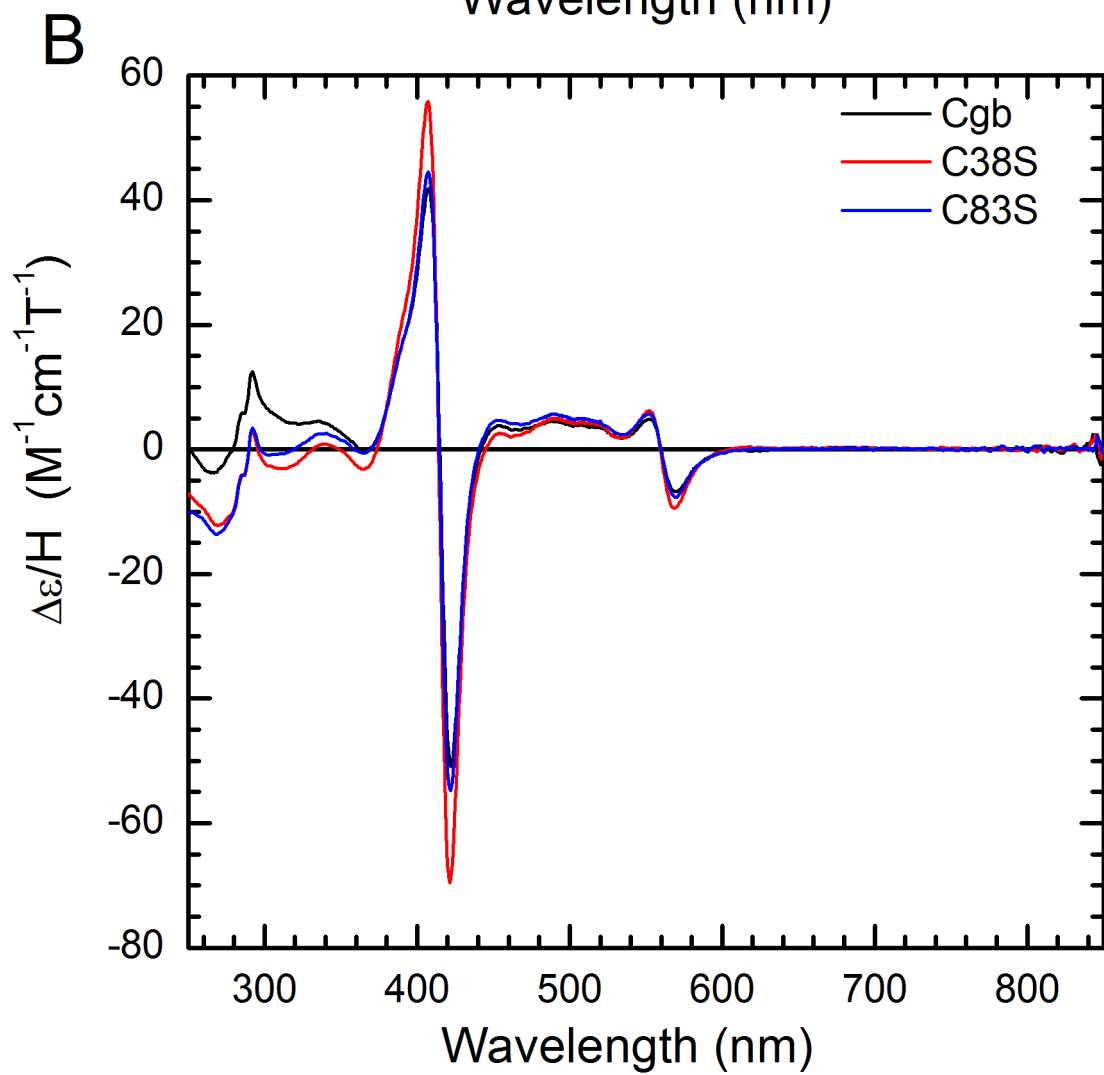
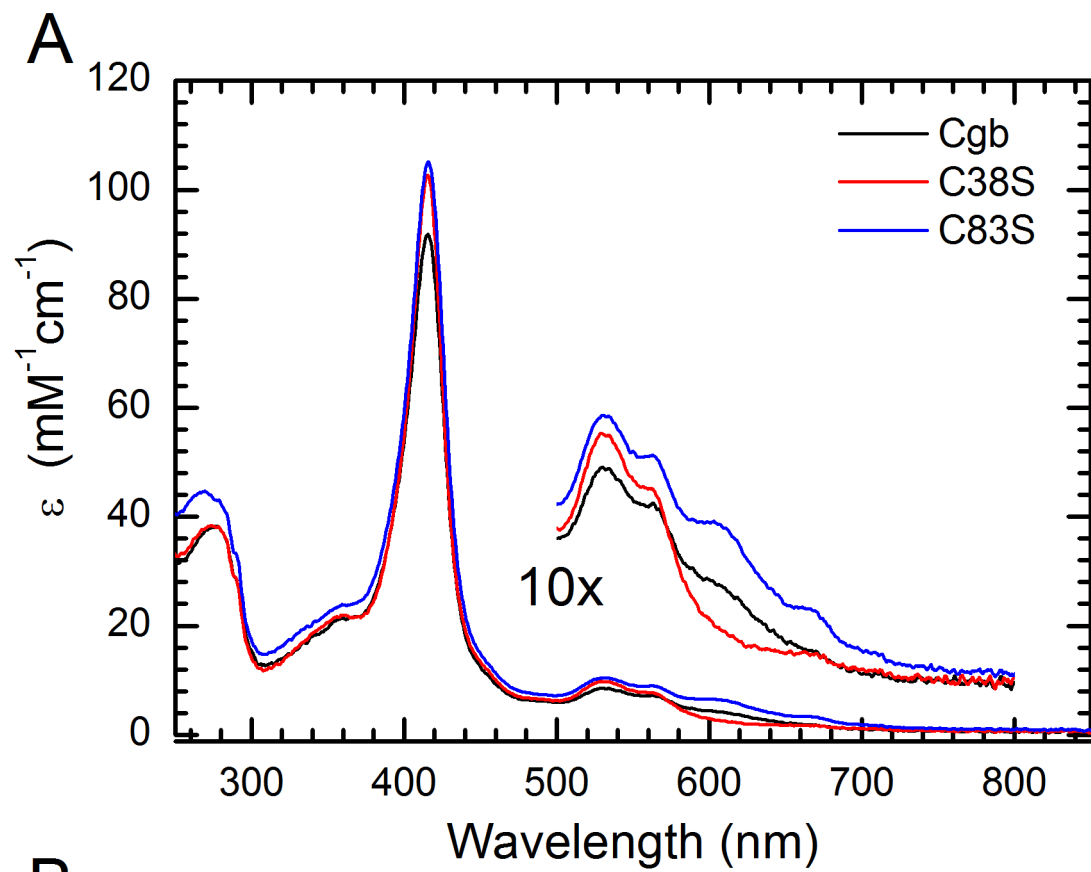
The spin and ligation states of the heme iron in the two cysteine variants were subjected to further analysis by a combination of RT-MCD and low-temperature EPR spectroscopies. The RT-MCD spectra of the two cysteine variants are shown in figure 4.4B. Briefly, both C38S and C83S variants display a typical low-spin ferric heme RT-MCD spectrum with an intense derivative-shaped feature in the Soret region that has a maximum at 407 nm and a minimum at 422 nm. This is broadly similar to the same feature observed in wild-type cytooglobin, but

with a slight difference in the intensity. In the C38S variant, the intensity of the derivative feature in the Soret region is approximately  $125 \text{ M}^{-1}\text{cm}^{-1}\text{T}^{-1}$  while it is about  $100 \text{ M}^{-1}\text{cm}^{-1}\text{T}^{-1}$  in the C83S variant. Both derivative signals appear to be greater than in the case of the wild-type cytoglobin ( $\sim 95 \text{ M}^{-1}\text{cm}^{-1}\text{T}^{-1}$ ). In the visible region, not much difference is observed in the intensity of the second derivative shaped feature ( $\sim 2 \text{ M}^{-1}\text{cm}^{-1}\text{T}^{-1}$ ) (Figure 4.4B). Hence, the general increase in the intensity of the MCD bands seems to correlate with the same observation in the UV/vis spectra which may suggest that the low-spin species is enhanced in the absence of disulphide bond which is reflected by the two variants.

In the low-temperature X-Band EPR spectrum of wild-type cytoglobin, the principle EPR signals are shown to be at  $g = 3.21, 2.05$  and  $1.70$ , and a small population of high-spin signal at  $g = 5.95$  as shown in chapter 3 (Section 3.2.1). These signals indicate that the majority of the heme iron in cytoglobin is in the low-spin state. Whereas in the EPR spectra of the two cysteine variants, the patterns of the EPR signals are consistent with those observed in the wild-type cytoglobin with very similar  $g$  values which further confirm that the two cysteine variants exhibit the similar spin-state as well as the ligation state as the wild-type cytoglobin. It is of note that the  $g$  value at  $5.95$  in wild-type cytoglobin which represents the high-spin fraction is diminished in both of the cysteine variants indicating that when the intra-molecular disulphide bond is not present in the cytoglobin, virtually all the heme iron is in low-spin hexa-coordinate state (Figure 4.3).

Interestingly, the EPR signals ( $g = 2.36$  and  $2.59$ ) in the C83S variant appear to have intensified relative to the EPR spectrum of the wild-type cytoglobin. Whereas in the C38S variant, these signals appear absent. The RT-MCD spectrum does not support any reduction of or decrease in the amount of the low-spin ferric heme. The position and intensity of the  $g = 3.21$  feature is unchanged, thus an alternative explanation must be sought for these

observations. However, taken together, no significant change in the spin state and the oxidation state of the heme iron is observed in the two cysteine variant. Moreover, removal of the intra-molecular disulphide bond does not seem to affect the ligation state of the heme in the ferric state as the EPR and MCD spectrum indicate a low-spin ferric spectrum similar to wild-type cytoglobin, hence the ligation is very likely to be His/His ligation.



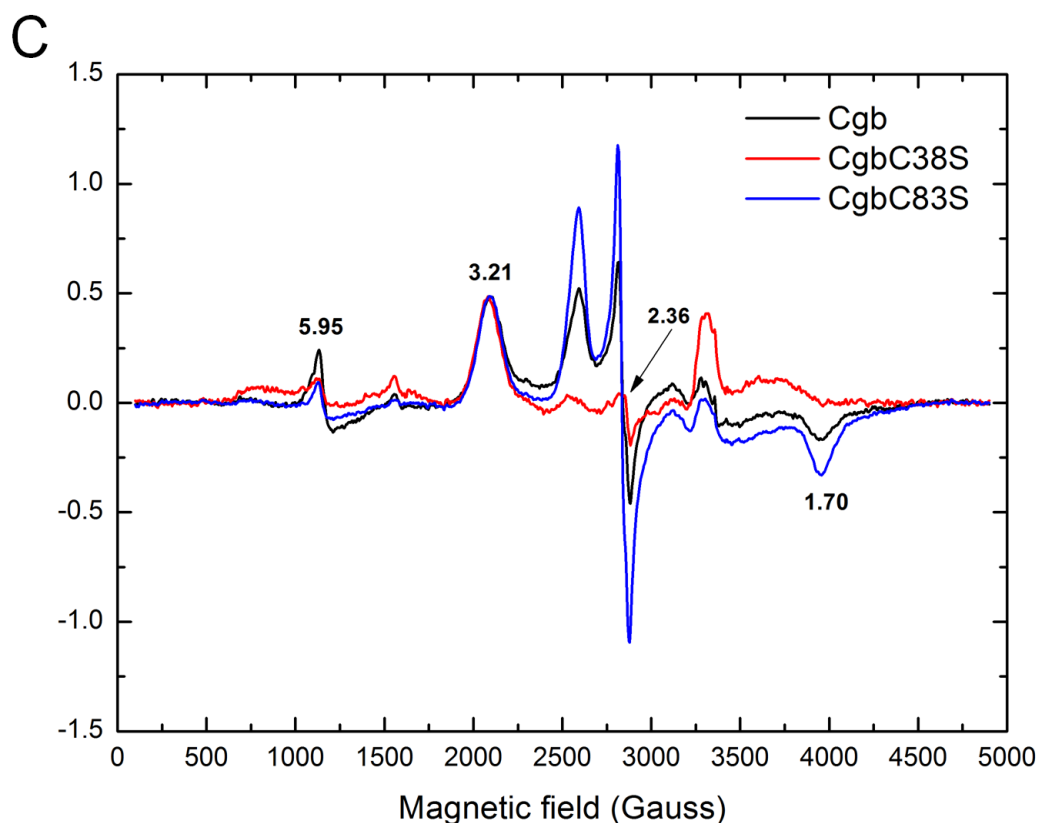


**Figure 4.4 Spectroscopic analyses of cytoglobin cysteine variants in the ferric state. (A)**

UV/vis spectra of 250 $\mu$ M wild-type cytoglobin (Black trace), C38S variant (Red trace) and C83S variant (Blue trace) in 20 mM Tris-HCl pH 8.0. **(B)** Room temperature MCD spectra of the same amount of wild-type cytoglobin (Black trace), C38S variant (Red trace) and C83S (blue trace) variant in 20 mM Tris-HCl pH 8.0. MCD conditions: 295 K 6 T. **(C)** Low-temperature EPR spectra of 150  $\mu$ M of wild-type cytoglobin (Black trace), C38S variant (Red trace) and the C83S (Blue trace) in 20 mM Tris-HCl pH 8.0. EPR conditions: microwave frequency 9.35 GHz; microwave power 2 mW; temperature 11 k; modulation amplitude 10 G. The intra-molecular disulphide bond is intact in the wild-type cytoglobin. Whereas in C38S and C83S, the disulphide bond formation is prevented leaving the free cysteine residue available. In the C38S variant, the Cys83 which is next to the distal histidine (His81) residue is free. Whilst in C83S variant, the Cys38 on the B-helix is free.

### 4.2.3 Spectroscopic Characterisation of Ferrous Cytochrome b5 with Different States of Disulphide Bond

The effect of the absence of the disulphide bond on the heme iron of human cytochrome b5 was further examined in the ferrous state. In the UV/vis spectra, the spectra of both cysteine variants display an identical spectral characteristics with the wild-type cytochrome b5 that the position of the Soret absorption maxima in the ferrous state is at 427 nm, while the  $\alpha$ - and  $\beta$ -bands are at 530 nm and 560 nm, respectively. The key difference between the three proteins, however, is between the regions of 600 nm to 650 nm that the broad single band at 612 nm, which is also observed in the ferric spectra described in section 4.2.2. The 612 band is consistently intensified in the C83S variant, and diminished in the C38S variant (Figure 4.5A). Interestingly, when the disulphide bond of the wild-type cytochrome b5 was reduced by DTT, an increase in the intensity of both Soret peak and  $\alpha\beta$  bands is observed. Such increase is in agreement with a generally higher intensity in the Soret and  $\alpha\beta$  region found in the two cysteine variants where the disulphide is removed.

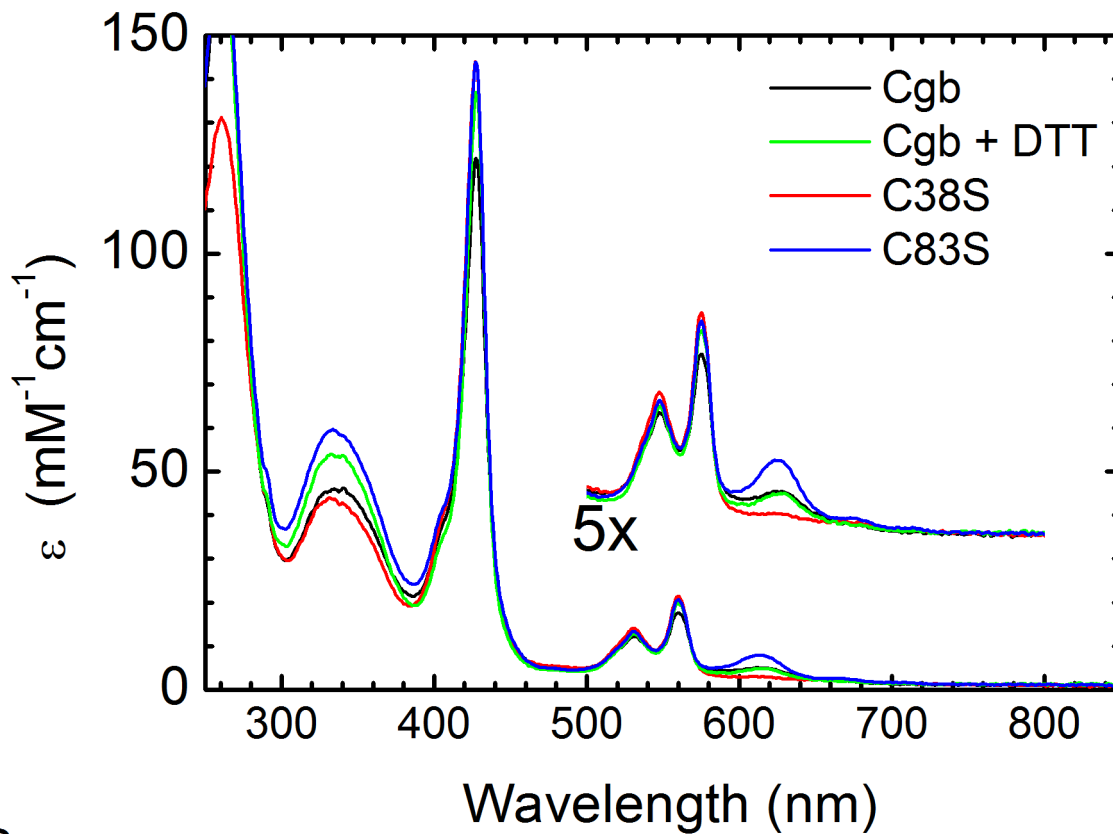
The RT-MCD spectra, all the three cytochrome b5 protein shows the distinctive feature between 550 nm to 560 nm indicating the presence of ferrous low-spin species that is consistent with cytochrome b5 maintaining the His/His ligation in the ferrous state. Comparing the C38S and C83S variants with wild-type cytochrome b5, it is clear that the C38S variant shows a subtle difference in the MCD pattern, including a small variation at the region of 420 nm and a higher MCD intensity at 550 nm and 560 nm ( $\sim 230 \text{ M}^{-1}\text{cm}^{-1}\text{T}^{-1}$ ) perhaps suggesting an minor perturbation of the heme environment by the free Cys83 residue. On the other hand the RT-MCD spectrum of C83S closely resembles that of wild-type cytochrome b5. Nevertheless, when the disulphide bond was reduced in the wild-type cytochrome b5 by DTT, a similar phenomenon in the cysteine variant where the intensity of MCD signal is intensified is observed suggesting it

is due to a complete formation of low-spin species (Figure 4.5B).

Since the intra-molecular disulphide bond cannot form in the two cysteine variants, treating the reduced forms with either DTT or TCEP should not induce any further spectral changes. In order to determine whether the increase in the intensity of the heme signals observed in the wild-type cytoglobin in both UV/vis absorption and MCD spectra is a consequence of reducing the disulphide bond or due to some other effect of DTT, the reduced form of each variant was treated with DTT. Surprisingly, a similar increase in the intensity of the both UV/vis spectrum and RT-MCD spectrum was observed when the cysteine variants were treated with DTT, although the changes are small compared to wild-type cytoglobin. The results suggest that the enhancement in the intensity of the heme signals in the UV/vis region may not be due only to reduction of the disulphide bond (Figure 4.6). Explanation of the enhanced signals in the spectrum is needed to be sought.

Taken together, the spectroscopic data further confirm that the spin and ligation state of the cysteine variants in the ferrous state is the same as in the wild-type cytoglobin, although the intensity of the MCD band is slightly higher in the cysteine variants, especially the C38S, than the wild-type cytoglobin. In other words, these observations are consistent with the those reported in the section 4.2.1 that show reduction of the disulphide bond by DTT in wild-type ferrous cytoglobin to form redox state #4 does not change the spin and/or ligation state of the heme. Similarly, removal of the disulphide bond in the two cysteine variants also does not change the spin- and/or ligation- state of the ferrous heme compared to wild-type cytoglobin.

A



B

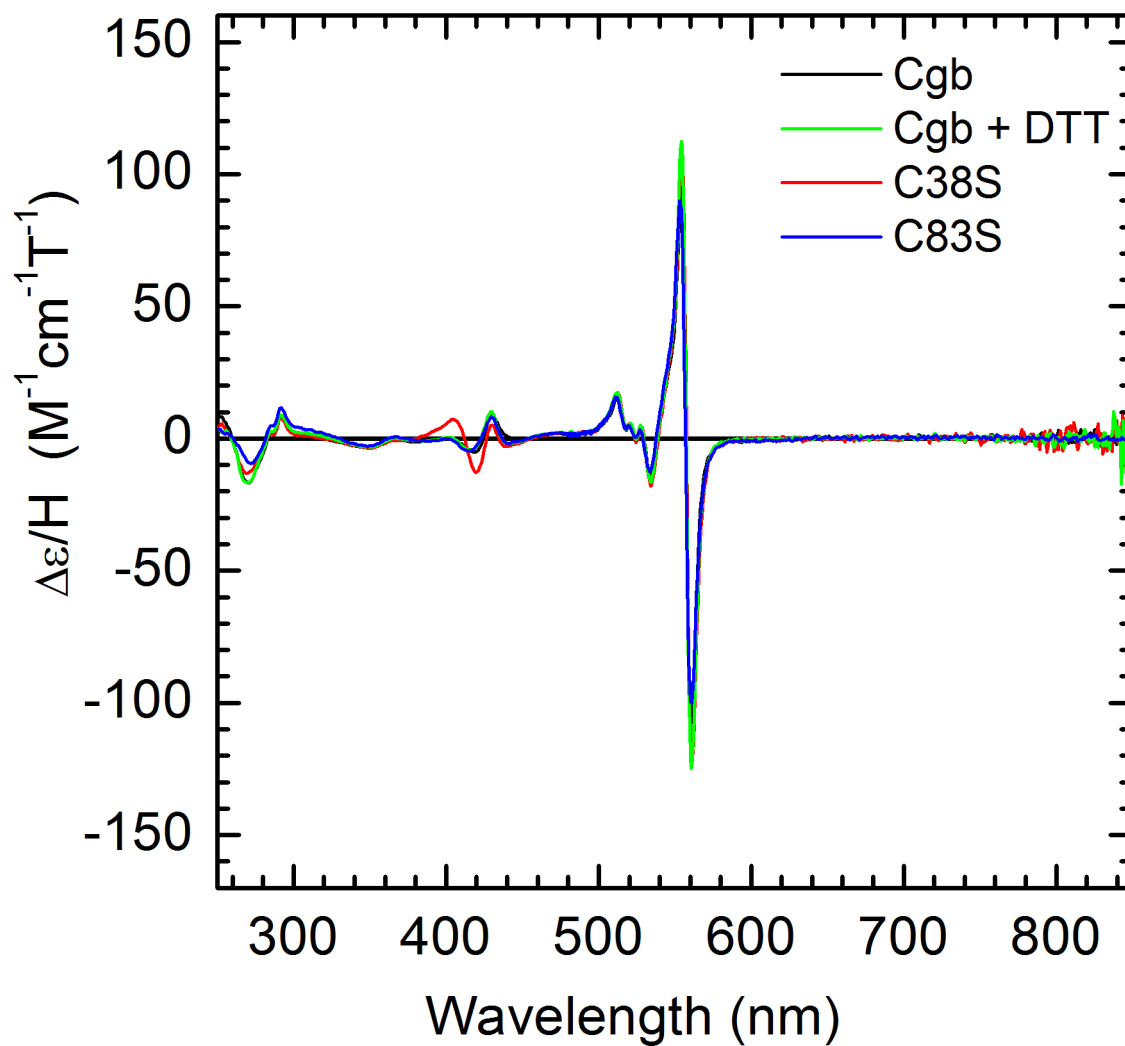
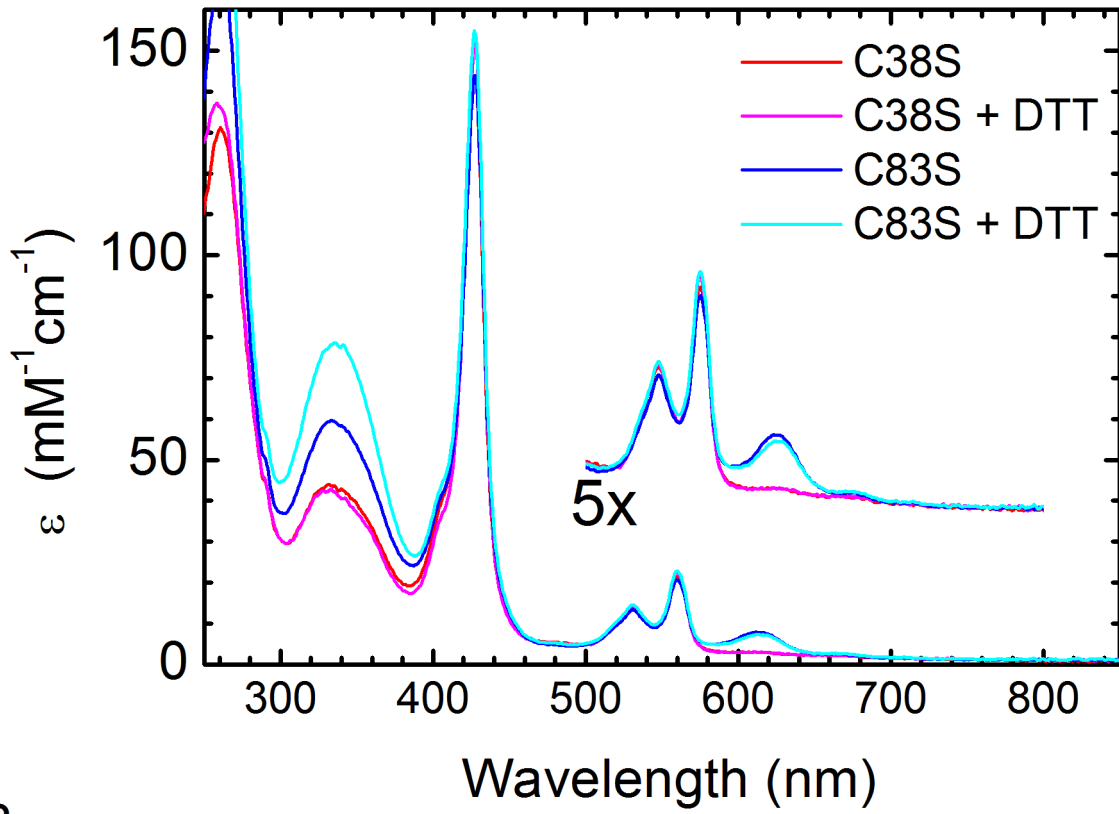


**Figure 4.5 Spectroscopic analyses of ferrous cytoglobin and Cys variants.** The reduction of the heme iron was achieved by following the methods described in 2.8.1 under anaerobic conditions. Reduction of the disulphide bond of cytoglobin was achieved by adding 10 mM DTT to the cytoglobin in the ferrous state **(A)** UV/vis spectra of ferrous cytoglobin variants in 20 mM Tris-HCl pH 8.0. **(B)** Room temperature MCD spectra of the same cytoglobin samples in 20 mM Tris-HCl pH 8.0.

A



B

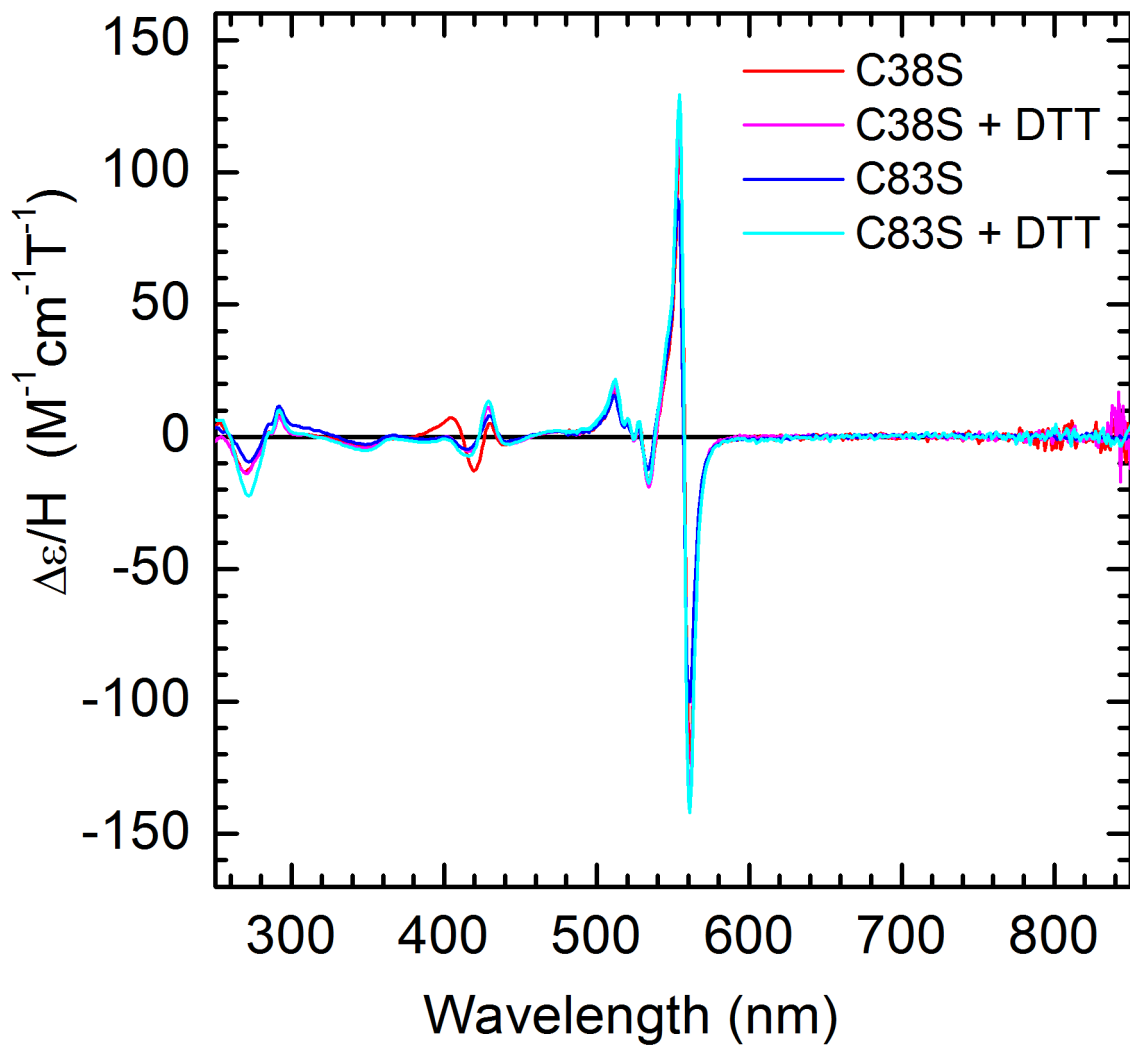


**Figure 4.6 Spectroscopic analyses of cysteine variants in the presence of DTT.** The reduction of the heme iron was achieved by following the methods described in chapter 2.8.1 under anaerobic conditions. After completed reduction, 10 mM of DTT was added to the reduced samples for both UV/vis and MCD measurement. **(A)** Electronic adsorption spectra of ferrous cysteine variants in 20 mM Tris-HCl pH 8.0 with and without adding DTT **(B)** Room temperature MCD spectra of the same cysteine samples in 20 mM Tris-HCl pH 8.0.

#### 4.2.4 Spectroscopic Characterisation of Carbmonoxy Cytoglobin and Cysteine

##### Variants

It was shown in the previous section that the spin and ligation state of the ferrous heme in the two cysteine variants are the same as wild-type cytoglobin in which the disulphide bond has been reduced by DTT. It is believed that CO can bind to the cysteine variants in the same fashion of the wild-type cytoglobin as described in section 4.2.1. Hence, the CO-bound complexes of both cysteine variants are examined spectroscopically.

As anticipated, upon addition of CO, the UV/vis spectrum of both cysteine variants show features that closely resemble the CO-bound wild-type cytoglobin with the Soret peak at 421 nm together with the  $\alpha$ - and  $\beta$ -bands and 570 nm and 540 nm suggesting the formation of the same CO-bound complex reported in section 4.2.1 (Figure 4.7A). However, the intensity of the Soret peak in the CO-bound C83S complex appears to be approximately  $50 \text{ mM}^{-1}\text{cm}^{-1}$  (Figure 4.7A; blue trace) greater than that of the C38S variant (Figure 4.7A; red trace). In the RT-MCD spectrum, the CO-bound cytoglobin exhibits a low-spin ferrous spectrum that is dominated by a derivative-shaped feature in the Soret region with an intensity of approximately  $95 \text{ M}^{-1}\text{cm}^{-1}\text{T}^{-1}$  with a maximum at 514 nm and a minimum at 525 nm. A second derivative-shaped feature in the visible region has an intensity of approximately  $50 \text{ M}^{-1}\text{cm}^{-1}\text{T}^{-1}$  with a maximum at 561 nm and a minimum at 575 nm. The spectral features observed in the MCD spectrum of cysteine variants are consistent with the presence of the same species of low-spin ferrous heme with CO/histidine ligation described for the CO-bound wild-type cytoglobin (Figure 4.7B).

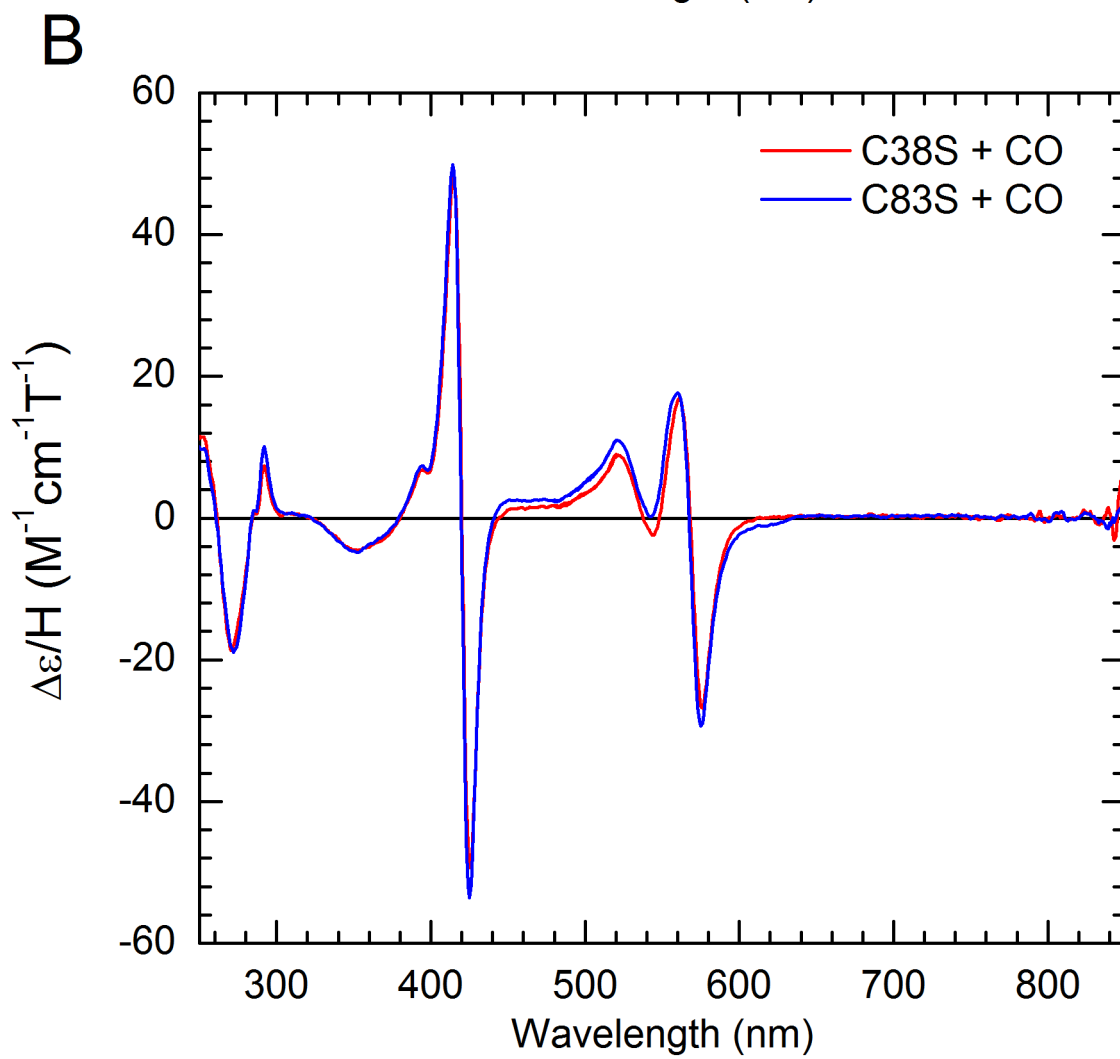
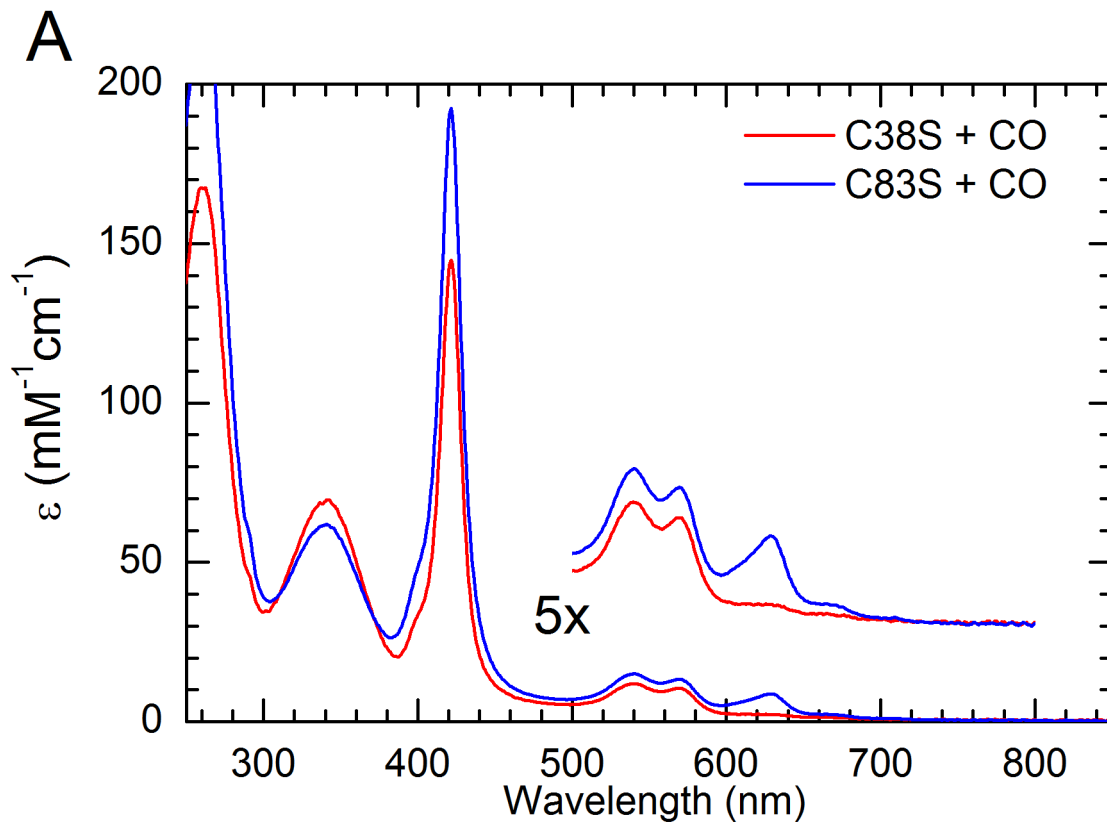


**Figure 4.7 Spectroscopic characterisation of CO-bound ferrous C38S and C83S variants (A)** UV/vis spectra of 100  $\mu$ M CO-bound C38S (Red trace) and CO-bound C83S (Blue trace) in 20 mM Tris-HCl pH 8.0 **(B)** Room temperature MCD spectra of 100  $\mu$ M CO-bound C38S (Red trace) and CO-bound C83S (Blue trace) in 20 mM Tris-HCl pH 8.0. MCD conditions: 298 K, 6 T.

#### 4.2.5 Heme Accessibility for Exogenous Ligands in Ferric Cytochrome b5

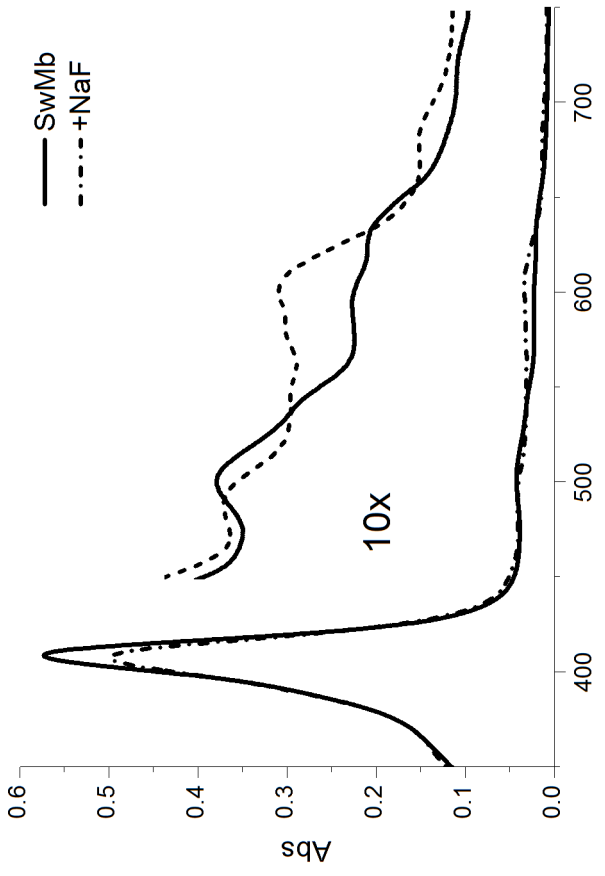
The binding of exogenous ligand to cytochrome b5 in the ferric state was examined using fluoride as a ligand probe. Fluoride was chosen because, as a weak field ligand, the binding of fluoride ions to the ferric heme iron will form a high-spin ferric complex. One of the advantages of using fluoride as a ligand probe is that it gives a clean and distinctive signal in the absorption spectrum which is characterized by a small blue shift in the Soret peak and a charge transfer band at about 605nm as shown in the case of fluoride-bound myoglobin (Figure 4.8A) which is well resolved from the CT bands associated with His/H<sub>2</sub>O and His/-ligand sets and a characteristic EPR spectrum in which the  $g \perp$  feature is split by influence of the <sup>19</sup>F nucleus.

Binding of fluoride ions to cytochrome b5 causes some spectral changes in the absorption spectrum, especially the emergence of the band at ~625 nm and the reduction in the intensity of the  $\alpha$ - and  $\beta$ -band which suggest a formation of high-spin species. However, the spectral changes due to the binding of fluoride are less significant than those observed in myoglobin (Figure 4.8B). This suggests that only a small population of cytochrome b5 is fluoride-bound which is confirmed by the EPR in which the high-spin signal at  $g = 6$  increases slightly upon binding with fluoride (ca 5%), but the spectrum is still dominated by the low-spin signals ( $g = 3.21$ , 2.05 and 1.70) (Figure 4.9). The results imply that ligand accessibility to the heme iron in cytochrome b5 is complicated by the presence of the distal His81 residue as an internal heme ligand.

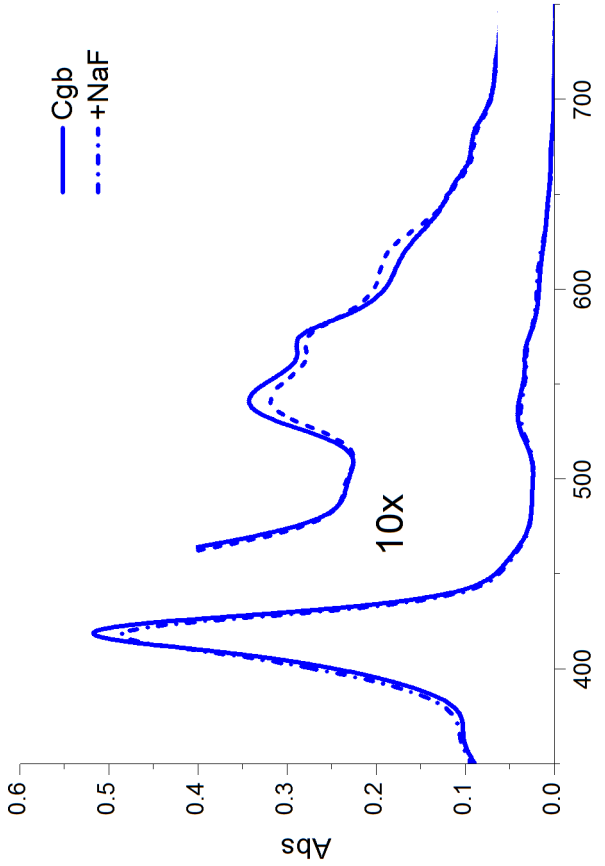
On the other hand, the absence of the intra-molecular disulphide bond seems to have a negative impact on the ligand accessibility. Binding of fluoride ions to the two cysteine variants are found to be trivial compared to that in the wild-type cytochrome b5 under the same conditions (Figure 4.8C and D). These results suggest that ligand accessibility to the heme iron in the

absence of disulphide bond is impaired in the case of anionic ligand. Such a phenomenon may possibly be correlated to the fact that the original equilibrium of high-spin (penta-coordinate) and low-spin species (hexa-coordinate) in the cytoglobin, as indicated in both MCD and EPR spectra, is shifted to favour the formation of low-spin species when the disulphide bond is not present (Chapter 4.2.1 & 4.2.2) which subsequently restricts the binding of the exogenous ligands due to all the coordinate site being occupied by the distal His81 residue.

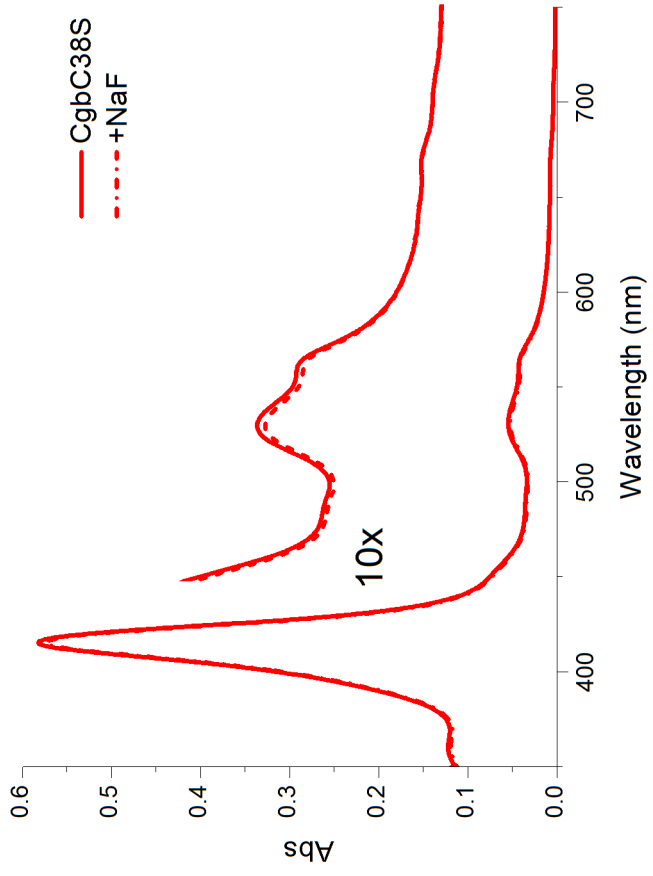
**A**



**B**



**C**



**D**

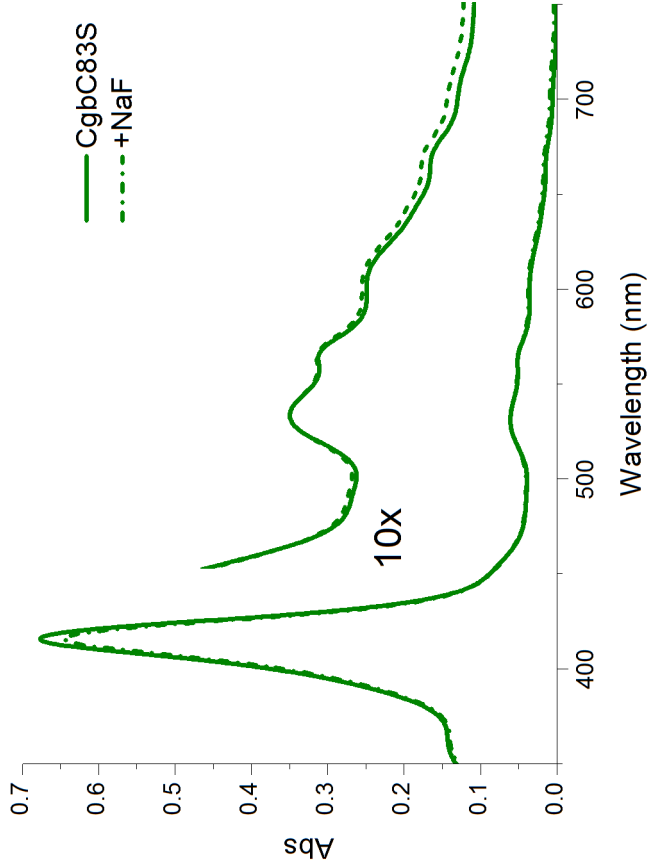


**Figure 4.8 Static fluoride binding to myoglobin and cytoglobin.** Approximately 5  $\mu\text{M}$  of protein; (A) Sperm whale myoglobin; (B) Cytoglobin; (C) C38S; (D) C83S, was mixed with a final concentration of 50 mM sodium fluoride in 20 mM sodium phosphate pH 7.0 in a 1 cm path-length quartz split cuvette. The spectra were recorded before (solid trace) and two minutes after mixing (dash trace).

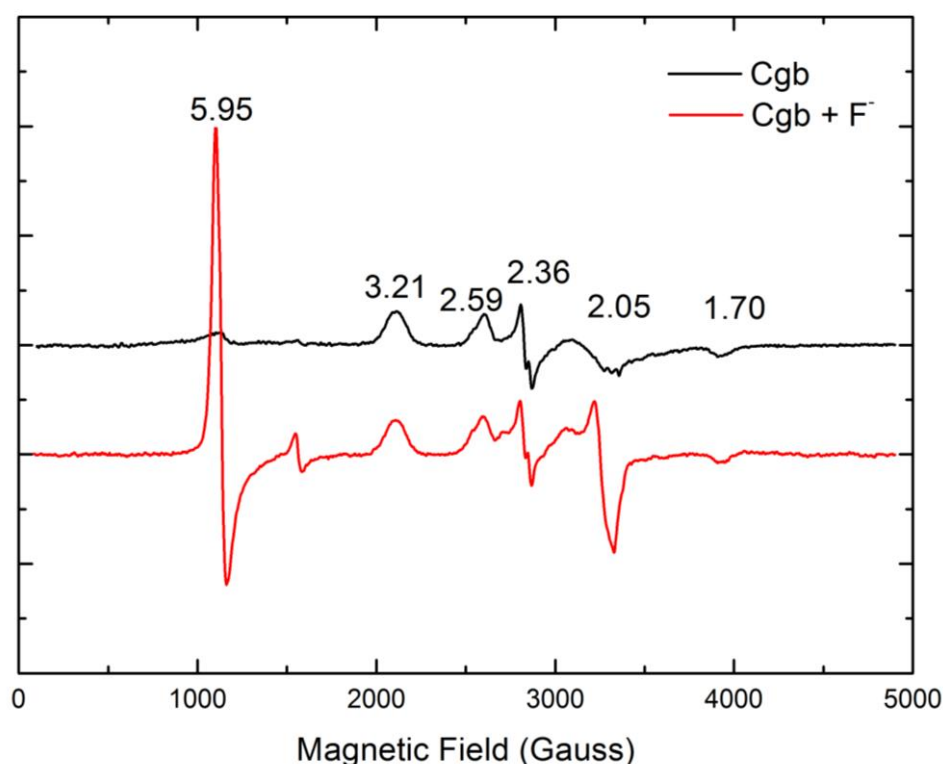


**Figure 4.9 Low-temperature X-band EPR spectrum of fluoride-bound ferric cytoglobin.** 200 mM of sodium fluoride was mixed with approximately 80  $\mu\text{M}$  of cytoglobin in 20 mM sodium phosphate pH 7.0. The numbers indicate the  $g$  values in the EPR spectrum. The  $g$  values trio (1.70, 2.59, 3.21) indicate a low-spin heme with a rhombic symmetry in the ferric state. An emergence of ( $g = 5.95$ ) indicate formation of a high-spin species upon binding of fluoride. EPR conditions: microwave frequency 9.5 GHz; microwave power 0.5 mW; temperature 15 k; modulation amplitude 10 G

#### 4.2.6 Effect of GSH on the Heme Accessibility in Cytoglobin

In order to discriminate between the lack of access by fluoride to the distal heme pocket of human cytoglobin and the inability of the ligand to displace presence of the axial ligand (His81), a new variant form of cytoglobin (H81F) was created in which His81 was substituted with phenylalanine as described in chapter 2.4.4. This cytoglobin variant should contain a heme which by analogy to myoglobin will be penta-coordinate (i.e. His/- ligation) with no water molecule occupying the sixth coordination site due to the size and hydrophobicity of the phenylalanine residue. It is important to note that the disulphide bond in the H81F variant remains intact and functional as tested in the non-reducing gel (data not shown).

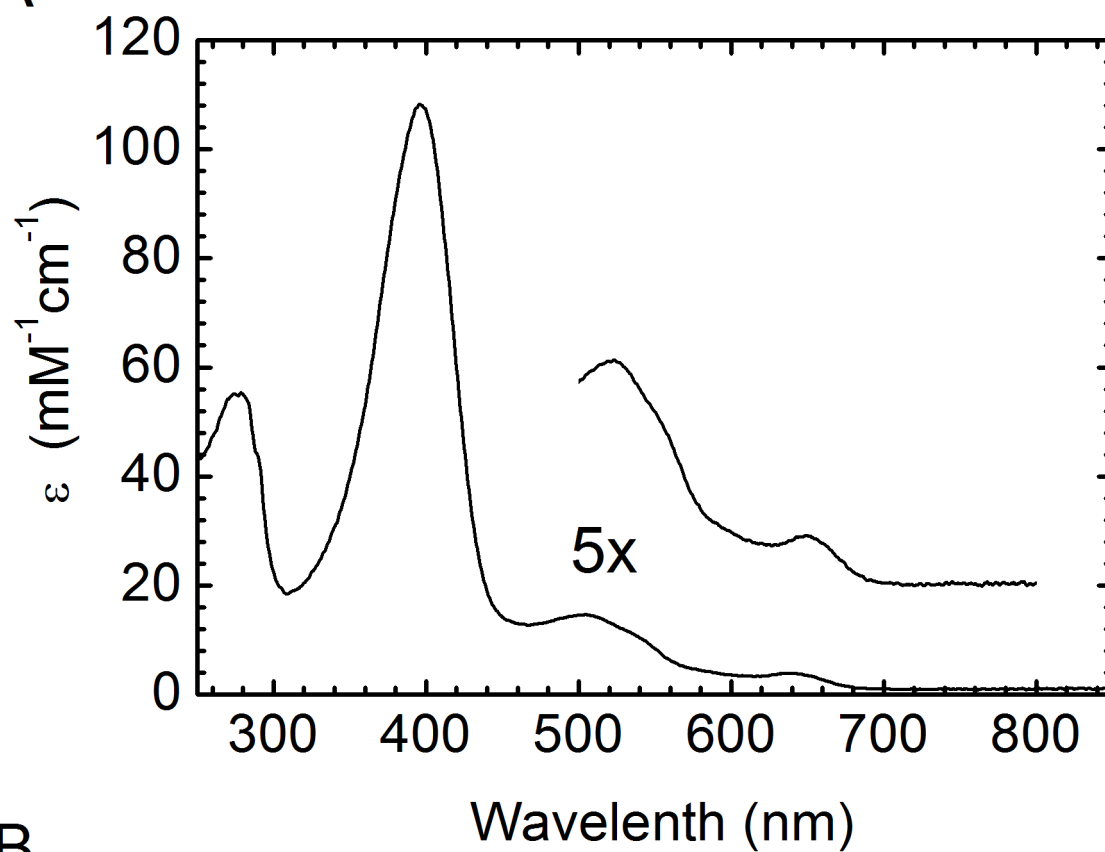
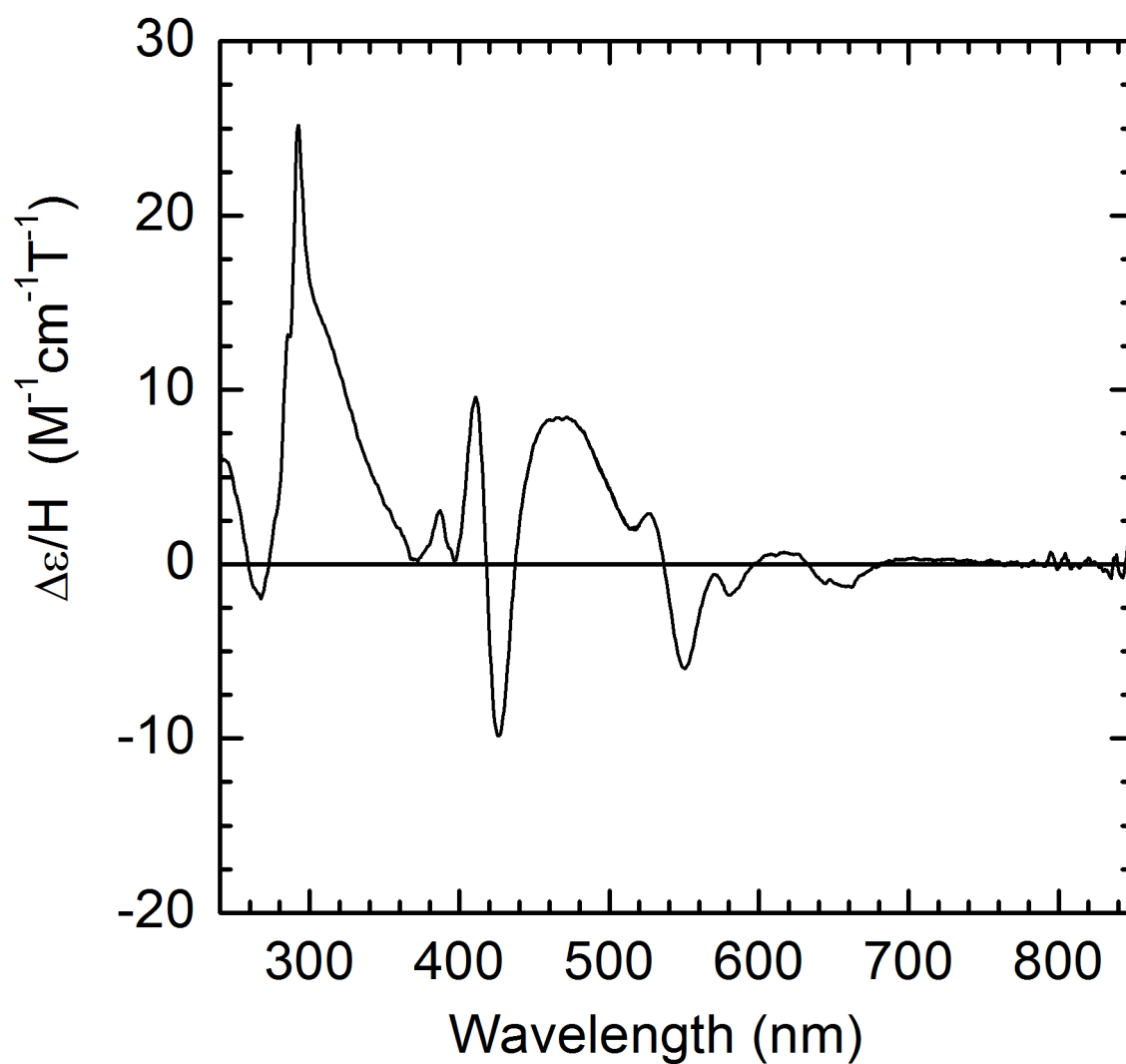
Replacing the distal histidine with phenylalanine causes a dramatic change in the UV/vis spectrum, including a blue shift and broadening of the Soret peak with a new absorption maximum at 398 nm which is consistent with a five coordinate high-spin heme. There is a related change in the visible regions with a broadening of the  $\alpha$ - and  $\beta$ - band which also indicates that the bis-histidine ligated heme in wild-type cytoglobin is replaced by a new penta-coordinate (His/-). Subsequent analyses confirmed that the resultant H81F variant has a ferric heme that is high-spin and penta-coordinate. This is indicated by the presence of a distinctive CT-2 band at the visible region between 620 nm to 660 nm in the RT-MCD spectrum and the EPR spectrum being dominated by a signal with principle  $g$  values at 6.0, 5.8x 2.05 that are consistent with a high spin ferric heme with rhombic symmetry (Figure 4.10 B and C).

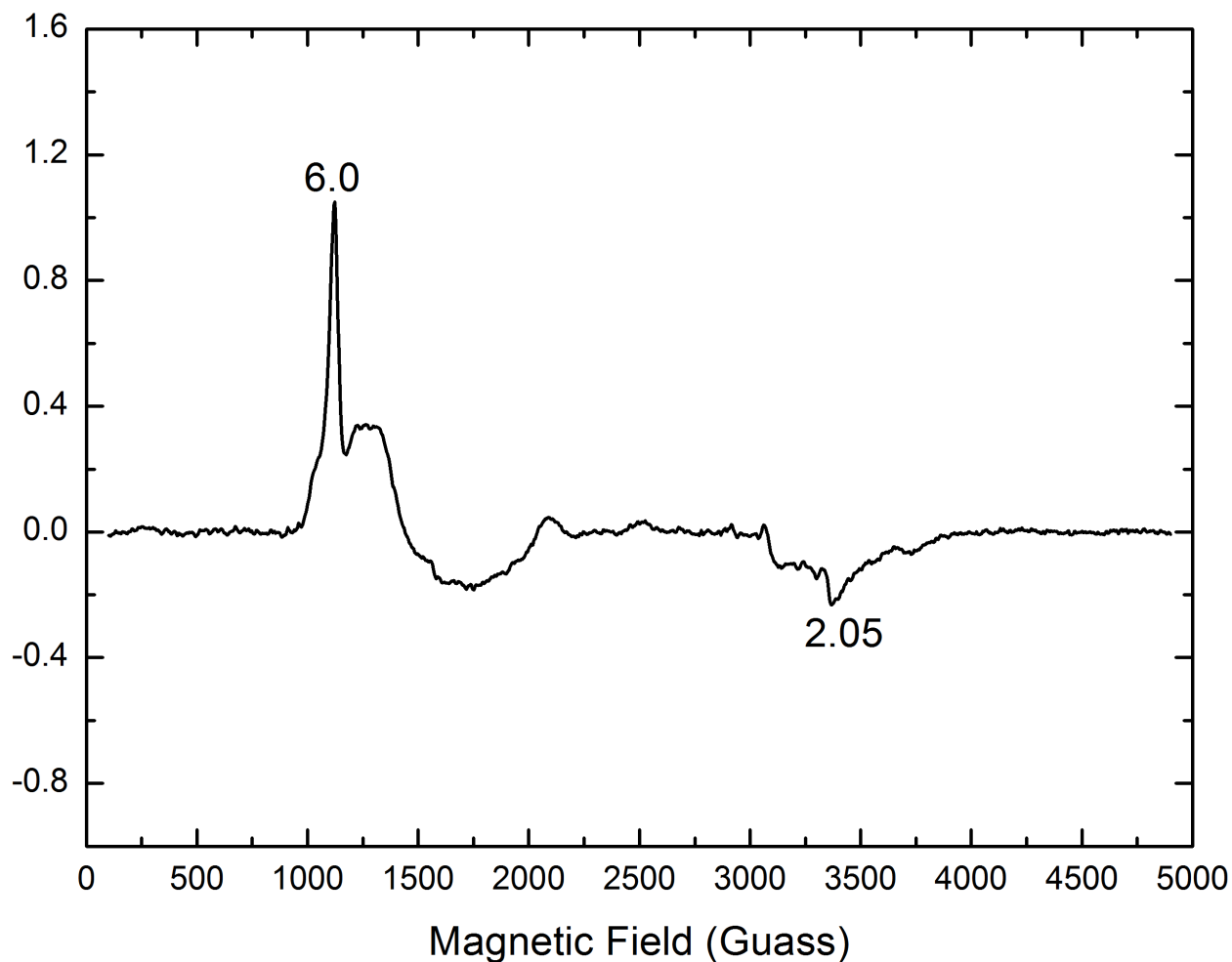
The accessibility of fluoride ions to the distal pocket was investigated using the penta-coordinate H81F. Surprisingly, the results show that even though the distal histidine ligand had been substituted with phenylalanine which cannot bind to the heme iron, the accessibility of the fluoride ions remains poor as the formation of the fluoride bound cytoglobin is still insignificant (Figure 4.11; black solid and dot traces). Thus, based on this observation, we

could probably suggest that the coordination state is not a determinant for the ligand accessibility in cytoglobin as both hexa-coordinate and penta-coordinate hemes in cytoglobin show very limited fluoride binding.

Interestingly, the extent of ligand binding is much greater after incubation of the H81F cytoglobin with GSH to reduce the disulphide bond. Treatment of H81F variant with 50 mM GSH causes a spectral change in which there is a blue shift of the Soret peak to ~ 378 nm and a concomitant reduction in its intensity together with some changes in features in the visible region (Figure 4.11; red solid trace). Similar changes in the spectrum are also observed in both wild-type cytoglobin and C38S variants upon treatment with high concentration of GSH and may be due to oxidative damage of the heme (see Chapter 7).

As shown in Figure 4.11 (red dash-and-dot trace), binding of fluoride ions to this GSH treated cytoglobin was greatly enhanced as compared with the treatment without GSH. The change in the spectrum is more significant than that observed when the disulphide bond is still intact, especially the CT band at 605 nm which is the signature of fluoride binding, although a shoulder peak appears at 370nm suggesting that fluoride binding is not 100% (Figure 4.11; red dash-and-dot trace). To summarise, the heme accessibility for exogenous ligand is inefficient in cytoglobin. However, neither changing of ligation state (His/His to His/-) nor the nature of the distal ligand could improve the heme accessibility. Apparently, treatment with GSH seems to have a positive impact on the accessibility of ligand. However, damage of the heme cofactor is also observed. Further characterisation of GSH treatment is needed in order to conclude the effect.

**A****B**

**C**

**Figure 4.10 Spectroscopic characterisations of H81F variant of cytoglobin. (A)** Electronic absorption spectrum of CgbH81F in 20 mM Tris-HCl pH 8.0 **(B)** Room temperature MCD of 200  $\mu$ M CgbH81F in 20 mM Tris-HCl /D<sub>2</sub>O pH 8.0\* MCD conditions: 295K 6T **(C)** Low-temperature X-band EPR of 200  $\mu$ M CgbH81F in 20mM Tris-HCl/D<sub>2</sub>O pH 8.0\*. EPR conditions: microwave frequency 9.35 GHz; microwave power 2 mW; temperature 11 k; modulation amplitude 10 G.

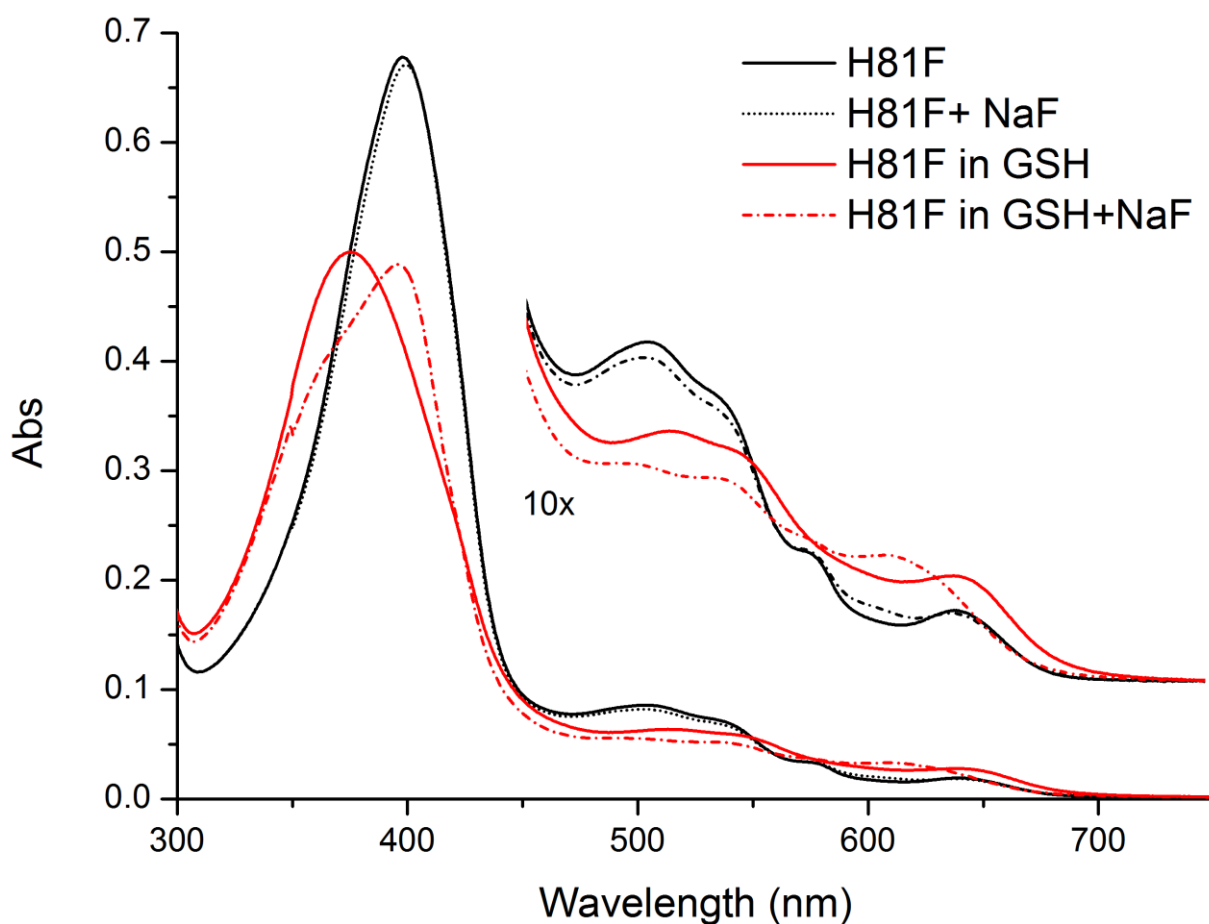


**Figure 4.11 UV/vis spectra of static fluoride binding to H81F variant.** (Black solid trace) 5  $\mu\text{M}$  of Ferric CgbH81F was mixed with a final concentration of 50mM sodium fluoride in 20 mM sodium phosphate pH 7.0 (Black dot trace) in a 1cm path length split quartz cuvette (Red solid trace). 5  $\mu\text{M}$  of CgbH81F was incubated with a final concentration of 50 mM GSH in 20 mM sodium phosphate pH 7.0 (Red dash-and-dot trace) for 10 minutes. GSH treated CgbH81F was mixed with a final concentration of 50 mM sodium fluoride in the same buffer..

### 4.3 Discussion

The earlier part of this chapter provided spectroscopic evidence for the heme ligation of cytoglobin in the ferrous state in the presence or absence of CO. Investigation of the ligation state by room-temperature MCD indicates that the heme iron is His/His ligated in the ferrous cytoglobin in which the distal histidine can be displaced by CO to form a CO/His ligation that gives a distinctive MCD spectrum as shown in section 4.2.1. Changing of the state disulphide bond did not seem to change the binding mode of CO to the ferrous cytoglobin as suggested by the MCD spectra. However, how the state of the disulphide bond may affect the kinetics of the binding of CO or other gaseous ligands to the cytoglobin will be subjected to further investigation using the same method to generate the cytoglobin at different redox state.

This study provides more information for investigations of the effect of the disulphide bond on ligand binding to cytoglobin with the use of two single cysteine variants (C38S and C83S), both of which lack the ability to form the intra-molecular disulphide bond, thus effectively mimicking the situation where the disulphide bond is chemically reduced in cytoglobin. Characterisation of the heme pocket environment by advanced spectroscopies indicated that both of the cysteine variants displayed predominately a low-spin signal in both ferric and ferrous state which is in agreement to the observation of wild-type cytoglobin when the disulphide bond is chemically reduced.

However, detailed examination of the two cysteine variants revealed that there are some subtle differences in their spectroscopic properties which could be due to the single free cysteine. For example, a band at 612 nm is consistently found in the UV/vis spectra of cytoglobin in both ferric and ferrous states, but no MCD band is detected at that region suggesting that the band does not arise from electronic transition at the heme porphyrin. Interestingly, the 612 nm band observed in the wild-type cytoglobin is intensified in the C83S

variant, but it was not seen in the C38S variant. The origin of the band at 612 nm is not known as the band cannot be detected by the room temperature MCD in the visible region, which means that the signal did not come from the ligation and the oxidation state of the heme iron. However, the intensity of the 612 nm band appears to reflect the state of the free Cys38 residues, and its position shifts to 628 nm upon binding of CO in the ferrous state suggesting that it may report the state of ligand binding.

Early studies on the effect of changing the state of the disulphide bond on the heme environment has concluded that the disruption of the disulphide bond results in a disappearance of the minor population of the high-spin species in the EPR spectra (Vinck et al., 2004; Van Doorslaer et al., 2004; Beckerson et al., 2015) which is believed to cause a decrease in the dissociation rate constant of the distal histidine residue, hence cause a lower affinity to the exogenous ligands (Hamdane et al., 2003; Tsujino et al., 2014; Beckerson et al., 2015). In this study, a slightly different approach from the literature was taken. We demonstrated that the ligand accessibility for fluoride ions is limited in ferric cytoglobin due to the presence of the distal histidine and the heme accessibility is controlled by the disulphide bond in cytoglobin. The heme accessibility for fluoride ions is hampered in the absence of the disulphide bond in the ferric state as shown in the two cysteine variants. However, when the protein is incubated with GSH, a dramatic change in the Soret peak to ~378 nm suggest a drastic change in the heme environment which is believed to be due to an oxidative damage of the heme. Interestingly, the fraction of cytoglobin which has heme intact clearly shows improved ligand accessibility for fluoride ions.

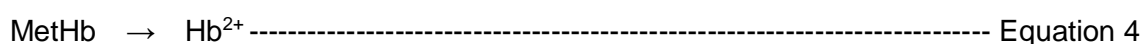
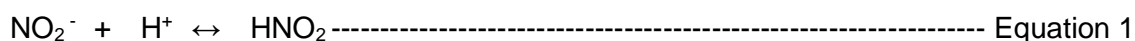
The increase in ligand accessibility in GSH-treated cytoglobin prompted us to speculate a potential modification on the cysteine residue by GSH (i.e. S-glutathionylation). Cysteine is a reactive amino acid residue due to the presence of the thiol side chain which is able to exist

in different oxidation states in response to the change in the redox state in the environment. It has been well documented that some proteins which bear cysteine residues could undergo chemical modification by GSH to modify their structures and functions as well as the stability of the protein (Grek et al., 2013). There is a lot of evidence in the literature suggesting that S-glutathionylation could alter the structure of a protein and subsequently change the function. For instance, S-glutathionylation of endothelial nitric oxide synthase (e-NOS) could regulate the production of nitric oxide (Chen et al., 2010), whereas S-glutathionylation of Rac-2 could activate the binding of GTP (Kil et al., 2012). Whether or not S-glutathionylation of cytoglobin could happen in the cells remain to be clarified. However, if it does happen, the most interesting question here would be what the effects of the S-glutathionylation on the two cysteine residues in cytoglobin, in particular the Cys83 residues due to its close proximity to the distal heme pocket. Some preliminary data on the potential S-glutathionylated cytoglobin is discussed in chapter 7.

## Chapter 5: Nitrite Reductase Activity of Globins

### 5.1 Introduction

Nitrite ( $\text{NO}_2^-$ ) has long been thought as an important nutrient that contributes to the regulation of blood pressure in the human circulatory system. A number of studies have confirmed that the physiological pathway of nitrite metabolism involves its reduction to a gaseous molecule, nitric oxide (NO), which can act upon a number of downstream NO-dependent signalling pathway (reviewed in Kim-Shapiro and Gladwin, 2014). The best characterised nitrite reduction reaction is that mediated by heme-iron that has been reported in a number of heme-proteins, including cytochrome *c* and globins. The detailed mechanism of nitrite reduction in globins was first described in haemoglobin by Doyle and colleagues which can be summarised as follows. Nitrite ions are first protonated in solution to form nitrous acid (Equation 1) which binds to deoxy-ferrous haemoglobin ( $\text{Hb}^{2+}$ ) to form met-haemoglobin ( $\text{Hb}^{3+}$ ) and nitric oxide (Equation 2). Since nitric oxide has high affinity to the deoxy-ferrous heme, the nitric oxide in the solution could bind to any free deoxy-ferrous haemoglobin in the solution to form nitrosyl-haemoglobin which inhibits further nitrite reduction (Equation 3) (Doyle et al, 1981). In the presence of suitable reducing agents, deoxy-ferrous haemoglobin could be regenerated (Equation 4), and the catalytic reaction continues until all the heme cofactor are occupied by nitric oxide (Equation 1-3). Since then, other members of the vertebrate globin family including myoglobin (Shiva, et al., 2007), neuroglobin (Tiso, et al., 2011) and cytoglobin (Li et al., 2012) have been shown to catalyse the same reaction in the absence of oxygen.



Nitric oxide generated from myoglobin-mediated nitrite reduction under hypoxic conditions has been demonstrated to inhibit respiration *in vitro* in both isolated mitochondria and cardiomyocytes (Shiva et al., 2007) and cause vasodilation *in vivo* by activating the soluble guanylate cyclase/cGMP pathway in vascular tissues (Totzeck et al., 2012) which are believed to be a countermeasure of tissue hypoxia as described in section 1.7. The rate of this reaction depends upon the concentration of both nitrite and myoglobin, and has a reported bimolecular rate constant of  $12 \text{ M}^{-1} \text{ s}^{-1}$  at  $37 \text{ }^\circ\text{C}$  which is significantly faster than that of haemoglobin ( $0.35 \text{ M}^{-1} \text{ s}^{-1}$ ). Although the lower heme redox potential of myoglobin (*ca* +59 mV) than haemoglobin (*ca* +150 mV) which tends to favour the reduction of nitrite has been put forward to account for the faster reaction rate (Haung et al., 2005; Shiva et al., 2007), such explanation cannot be applied to other vertebrate globins, such as neuroglobin and cytoglobin, which have a more negative heme redox potentials than myoglobin, but appear to have a much slower rate of nitrite reduction (Tiso, et al., 2011; Li et al., 2012). Therefore, a more comprehensive understanding of the biochemical basis of the reaction mechanism is needed.

This chapter describes an investigation of the detailed mechanism of nitrite reduction by myoglobin using sperm whale myoglobin variants carrying site-specific mutations at the distal or proximal histidine residues. The rate of nitrite reduction and the mode of binding of nitrite in these myoglobin variants were examined in details in order to elucidate the roles of the distal and proximal histidine residues in nitrite reduction. The outcomes of this study led to consideration of the accessibility of nitrite to the ferric heme iron in cytoglobin and the effect of changing the state of the disulphide bond.

## 5.2 Results

### 5.2.1 Nitrite Reduction by Sperm Whale Myoglobin

The influence of the distal histidine (His64) on nitrite reductase activity was examined by comparing the rate of nitrite reduction in wild-type myoglobin with a number of variants in which the distal His64 residue had been substituted with a range of apolar residues. 10  $\mu\text{M}$  of myoglobin in 100 mM sodium phosphate at pH 7.0 was reduced anaerobically by a treatment with 30 mM sodium dithionite as described in chapter 2.7.2. Under these conditions the observed rate constant for reduction of the heme iron by dithionite is  $14.5 \text{ s}^{-1}$  (Cox and Hollaway, 1977), hence all metmyoglobin will be re-reduced back rapidly to deoxy-ferrous myoglobin by dithionite to continue the reaction cycle (Equation 4), and auto-oxidation of deoxy-ferrous myoglobin is also prevented. The reaction initiated by an addition of 0.5 mM sodium nitrite. The addition of nitrite to deoxy-ferrous myoglobin in the presence 30 mM sodium dithionite led to a rapid decrease in absorbance at 434 nm and a concomitant increase in absorbance at 419 nm (Figure 5.1A). This shift in the Soret maximum is consistent with the formation of nitrosyl-ferrous complex. The progress of the reaction monitored at 419 nm (the wavelength at which there is the greatest change in the absorbance during the reaction) was plotted as a function of time and was fitted into a single exponential curve ( $Y = A \cdot \exp(k \cdot t) + C$ ), where  $k$  is the pseudo first order rate constant at a given time ( $k_{\text{obs}}$ ) (Figure 5.1B). Therefore, the resultant  $k_{\text{obs}}$  of nitrite reductase activity of wild-type myoglobin is calculated to be  $0.53 \text{ min}^{-1}$ . The  $k_{\text{obs}}$  obtained here could be regarded as a direct measure of how efficient the reduction of nitrite by myoglobin, in other words the  $k_{\text{cat}}$ . However, it is of note that conventional method using linear fit of initial rates is not compatible here as a difference of absorbance against time plot which has units of absorbance per second is required, hence simple comparison of  $k_{\text{obs}}$  is impossible.

Subsequently, the apparent bimolecular rate constant of the nitrite reduction was determined by obtaining the  $k_{\text{obs}}$  of nitrite reduction by myoglobin with a range of concentrations of nitrite (0.05 mM to 1 mM) under the same conditions. Decreasing or increasing the nitrite concentration changes the  $k_{\text{obs}}$  of such reactions which show a clear dependence on substrate concentration. The bimolecular rate constant for the nitrite reduction by wild-type myoglobin at pH 7.0, 25 °C was found to be  $14.4 \text{ M}^{-1} \text{ s}^{-1}$  (Figure 5.2).

The rate of reaction was also measured in four distal pocket variants (H64A, H64F, H64T and H64V), previously generated by site-directed mutagenesis, that introduce structural differences in the microenvironment at the distal heme pocket. As a prelude to using the same method to determine the rate of nitrite reduction of distal pocket variants, the effect of the substitution of His64 on the rate of heme reduction by 30 mM dithionite was established using a stopped-flow spectrometer as described in section 2.7.2. Since the rates of heme reduction are comparable with wild-type myoglobin (data not shown), it is concluded that no significant effect on the rate of heme reduction is caused by substitution of His64, and hence the nitrite reductase activities of distal pocket variants can be determined using the same method.

Interestingly, although the distal pocket variants at the reduced state look identical to the wild-type myoglobin, the apparent rates of nitrite reduction are much slower compared to wild-type myoglobin which highlights the importance of distal histidine in the nitrite reduction. For examples, in the H64A variant where the positively charged distal histidine (His64) was replaced with a small nonpolar alanine residue, the  $k_{\text{obs}}$  is found to be  $0.191 \text{ min}^{-1}$ , which is about 3 times slower than that in the wild-type myoglobin (Figure 5.3). The first order rate constants and the relative rates of reaction of all the distal pocket variants (H64A, H64F, H64T and H64V) and wild-type myoglobin are summarised in Table 5.1. All the distal pocket variants tested show substantially reduced rates of nitrite reduction, but those variants in which a water

molecule remains in the active site (i.e. H64A and H64T) and are His/H<sub>2</sub>O coordinated in the ferric state are less affected than those which exclude water from the active site and are five coordinate in the ferric state (i.e. H64V and H64F). Therefore the results indicate that the nitrite reduction efficiency in myoglobin is impaired when the distal histidine was replaced by other amino acid residues as the histidine residue is important for stabilising the water molecule at the distal active site where its role may be to donate one of the protons required for nitrite reduction.

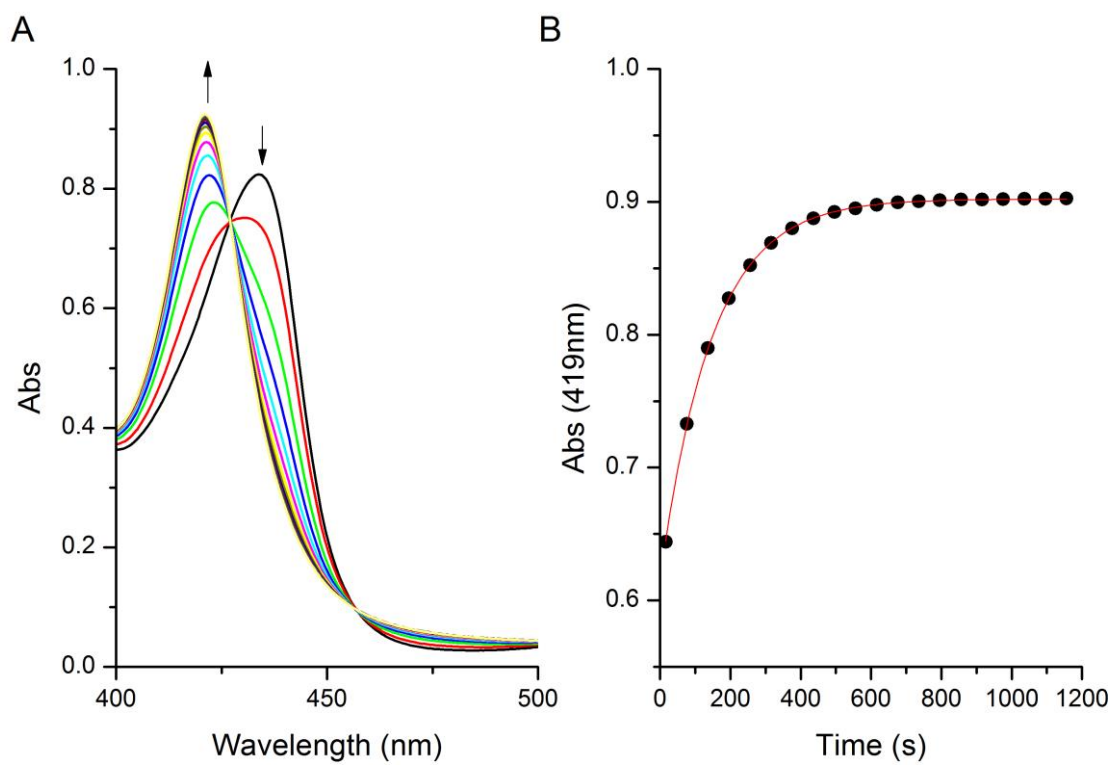


**Figure 5.1 Nitrite reduction by wild-type sperm whale myoglobin.** Deoxy-ferrous myoglobin was transferred to a sealed-cuvette, placed in the thermostated cuvette holder (25 °C) of a UV/vis spectrophotometer and the reaction was monitored by multiple-cycle scanning mode from 500 nm to 350 nm at a scan rate = 300 nm min<sup>-1</sup> at done in 100 mM sodium phosphate pH 7.0. **(A)** The absorption spectra showing the spectral changes during the nitrite reduction reaction by mixing 0.5 mM nitrite with deoxy-ferrous myoglobin in the presence of 30 mM sodium dithionite. **(B)** The absorbance changes at 419 nm during the reaction in the time course of 20 minutes. The data points were fit into a single exponential equation, indicated by the red line, in order to determine the observed first order rate constant ( $k_{\text{obs}}$ ).

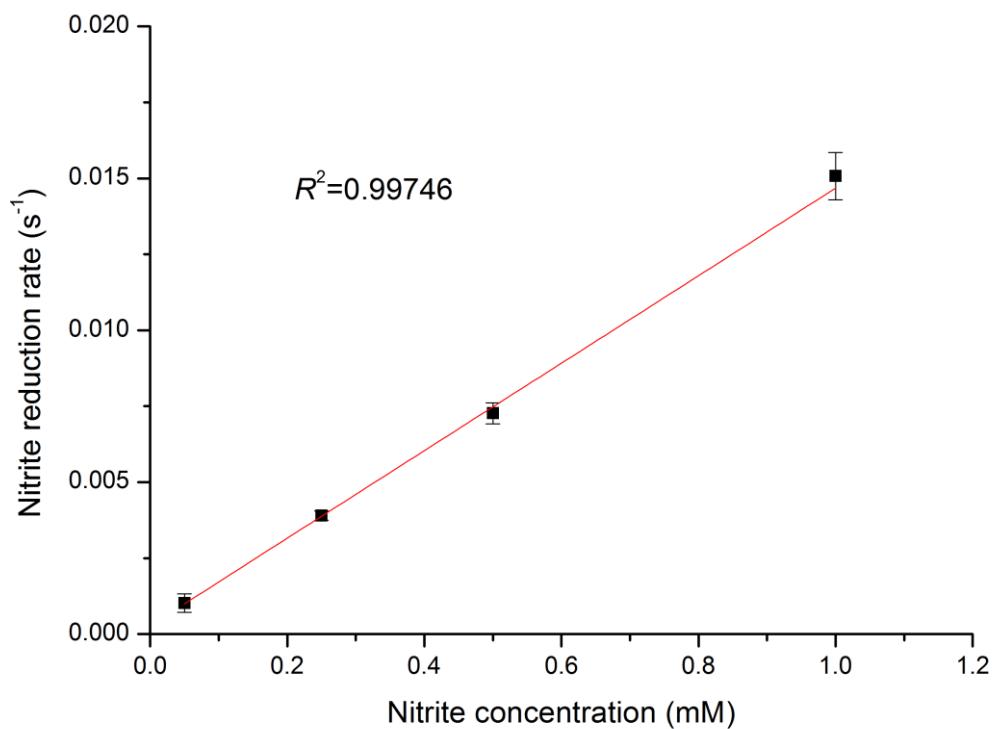


**Figure 5.2 Nitrite concentration dependence of nitrite reductase activity of myoglobin.**

Nitrite reduction reactions were carried out at different concentrations of sodium nitrite (0.05 mM, 0.25 mM, 0.5 mM and 1 mM) and were monitored by multiple-cycle scanning mode from 500 nm to 350 nm at a scan rate = 300 nm min<sup>-1</sup> at 25 °C done in 100 mM phosphate buffer pH 7.0. The average rate of nitrite reduction at each nitrite concentration was calculated from triplicate or quadruplicate. Error bars represent the standard error of the reaction rate obtained at each nitrite concentration.

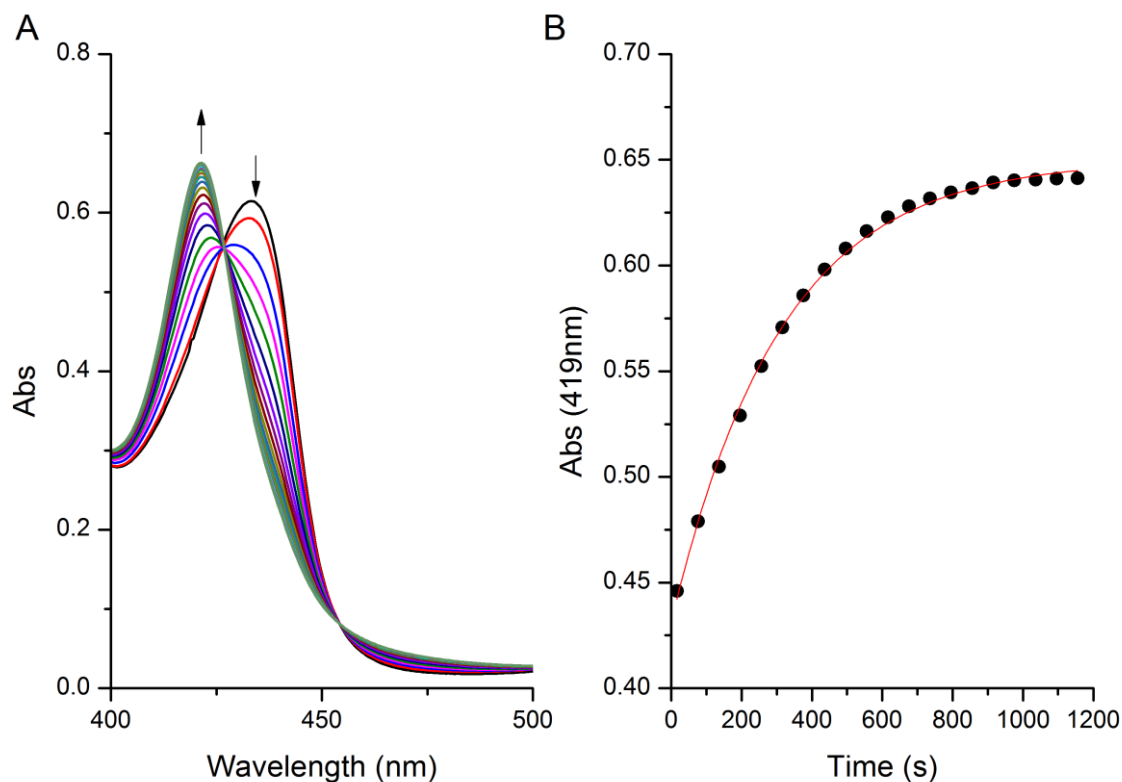


**Figure 5.3 Nitrite reduction by H64A variant.** The reaction was monitored by multiple-cycle scanning mode from 500 nm to 350 nm at a scan rate = 300 nm min<sup>-1</sup> at 25 °C done in 100mM phosphate buffer pH 7.0. **(A)** The absorption spectra showing the spectral changes during the nitrite reduction reaction by mixing 0.5 mM nitrite with deoxy-ferrous myoglobin H64A variant in the presence of 30 mM sodium dithionite. **(B)** The absorbance changes at 419 nm during the reaction in the time course of 20 minutes. The data points were fit into a single exponential equation, indicated by the red line, in order to determine the first order rate constant.

	<b>WT</b>	<b>H64A</b>	<b>H64F</b>	<b>H64T</b>	<b>H64V</b>
Wavelength for monitoring turnover (nm)	419	419	419	419	438
Rate constant (min <sup>-1</sup> )	0.53 ±	0.191 ±	0.019 ±	0.169 ±	0.046 ±
Relative activity (%)	100	36.2	3.5	32	8.6

**Table 5.1 Nitrite reductase activities of distal pocket variants of myoglobin**

### 5.2.2 Nitrite Binding to Ferric Myoglobin

To gain further insights into the mechanism of nitrite reduction by myoglobin, the distal His64 on the binding of nitrite to myoglobin was investigated. The experimental approach was to examine the static binding of nitrite to myoglobin in the ferric state using a 10 mm path-length quartz split cuvette on a UV/vis spectrophotometer as described in section 2.7.1 (refer to figure 2.4). The spectral changes of binding of nitrite to myoglobin are shown in figure 5.4. Upon mixing with nitrite, a red shift of the Soret peak from 409 nm to 411 nm and a concomitant decrease in the absorbance are observed. While in the visible region, small, yet notable changes in the spectral features including a decrease in the absorbance at 504 nm an emergence of a feature at 571 nm and a small blue shift of a band at 642 nm are also observed. Notably, the absorbance of nitrite at 354 nm did not change throughout the experiment, hence the spectral changes observed in the UV/vis spectrum must be due to the formation of nitrite-bound complex of myoglobin in the ferric state (Figure 5.4).

The reduced rate of nitrite reductase activity of the distal pocket variants compared to wild-type myoglobin, suggests an important role for the distal His64 in the nitrite reduction reaction. The two most likely roles are promoting correct orientation of the nitrite to the heme (Yi et al., 2009) or serving as a source of protons for the reaction. Since numerous studies have failed to detect the transient nitrite-ferrous heme intermediate, I examined the pH dependence of nitrite binding to wild-type ferric sperm whale myoglobin using an approach based on rapid mixing of protein with nitrite under pseudo-first order conditions previously described for horse heart myoglobin (Wanat et al., 2002). Solutions of myoglobin (10  $\mu$ M) and sodium nitrite (400  $\mu$ M – 2 mM) were mixed in a stopped-flow spectrometer as described in section 2.7.2 and the progress of the reaction monitored via the decrease in absorbance at 407 nm. The progress of each reaction was fitted to a single exponential (Figure 5.5A) to determine the observed first order rate constant ( $k_{\text{obs}}$ ) and the amplitude of the reaction. The

amplitude (Figure 5.5B) and  $k_{obs}$  (Figure 5.5C) of the reaction were plotted as a function of nitrite concentrations in order to determine the association rate constant ( $k_{on}$ ), the dissociation rate constant ( $k_{off}$ ) and the dissociation constant ( $K_d$ ) for nitrite binding.

The amplitude of the reaction shows a hyperbolic dependence on nitrite concentration (Figure 5.5B) suggesting that at lower nitrite concentrations binding is incomplete, but that the binding site is saturated at higher nitrite concentration. The data were fitted using a simple binding curve for a single site (Equation 5) which yielded an estimate for the  $K_d$  of 8.93 mM. The observed rate constant was fitted according to the pseudo-first order assumption (Equation 6) in figure 5.5C. Thus the slope and the intercept of the plot represent the  $k_{on}$  and  $k_{off}$  for nitrite binding, respectively. The  $k_{on}$  is found to be  $0.35 \text{ mM}^{-1} \text{ s}^{-1}$  and the  $k_{off}$  is found to be  $1 \text{ s}^{-1}$  which together give an equilibrium binding constant ( $K_d$ )= 2.68 mM. When the same experiment was repeated at pH 6.0, the binding is almost complete at lower nitrite concentration and the data from the simple binding curve yields an estimate for the  $K_d$  of 4.66 mM (Figure 5.5D). Fitting the observed rate constant for nitrite binding at pH 6.0 with the same equation yields a  $k_{on} = 4.86 \text{ mM}^{-1} \text{ s}^{-1}$  and  $k_{off} = 2.56 \text{ s}^{-1}$  which together give an  $K_d = 0.5 \text{ mM}$ . Therefore, comparing the calculated  $K_d$  at two pH, it is found to be more than 5 times at pH 6.0 than that at pH 7.0. According to this observation, the active species to bind to the myoglobin must be free nitrous acid since lowering pH promotes formation of free nitric acid.

$$A_{obs} = (A_{max} \times [NO_2^-]) / (K_d + [NO_2^-]) \text{ ----- Equation 5}$$

$$k_{obs} = (k_{on} \times [NO_2^-]) + k_{off} \text{ ----- Equation 6}$$

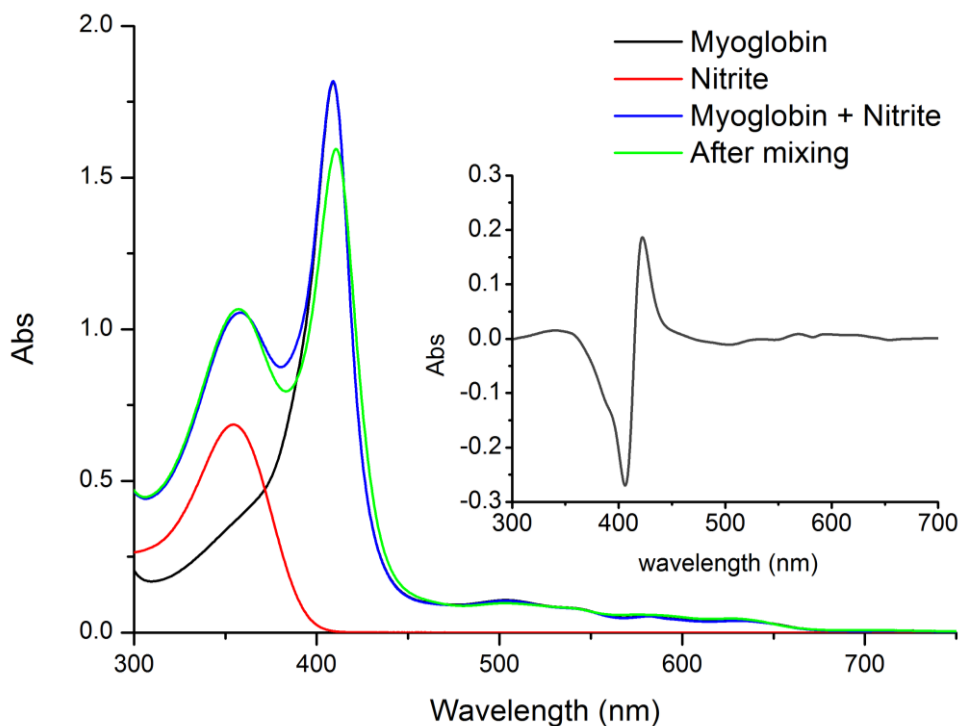


**Figure 5.4 Nitrite binding to ferric sperm whale myoglobin.** The experiment was done in a UV/vis spectrometer with a 10 mm path-length quartz cuvette that is divided into two chambers (each holding 1.6 ml with a 5mm path-length). The following combinations of solutions were added into two chambers: Spectrum of approx. 10  $\mu$ M ferric myoglobin / 20 mM citric acid phosphate pH 7.0 (black trace), 80 mM nitrite/ buffer (red trace), and 10  $\mu$ M ferric myoglobin/ 80 mM nitrite (blue trace) before mixing was recorded sequentially. Finally, the top of the cuvette was sealed and nitrite and myoglobin solutions mixed and the spectrum re-recorded (green trace). Myoglobin remained at ferric state throughout the experiment, while Nitrite was not consumed either. The binding of nitrite can be observed by subtracting the nitrite-bound myoglobin from the nitrite-free myoglobin (inset: dark grey trace)

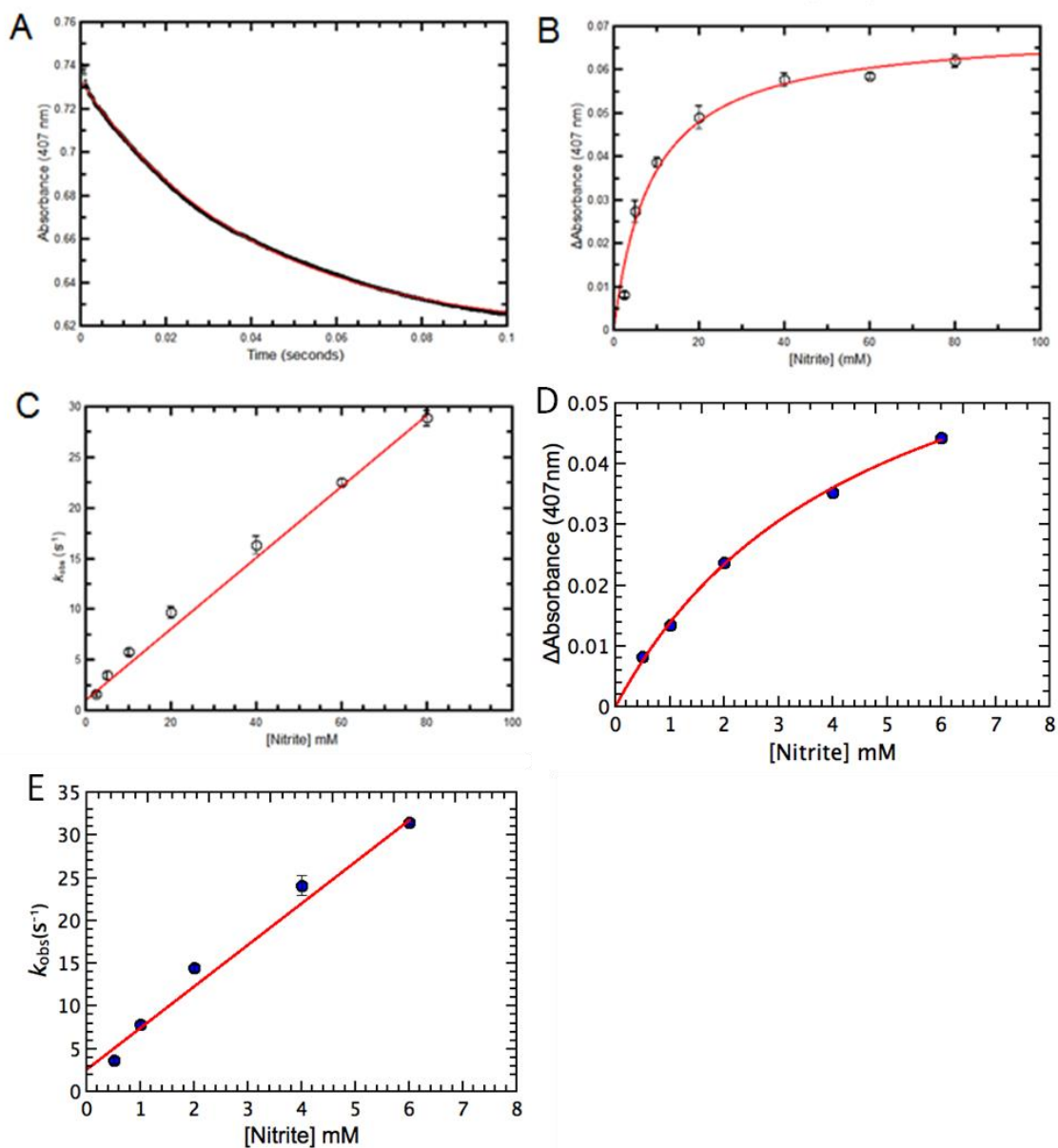


**Figure 5.5 pH dependence of nitrite binding to ferric sperm whale myoglobin.** Approx. 10  $\mu$ M of myoglobin and various concentration of sodium nitrite were prepared in 20 mM citric acid phosphate pH 7.0 and mixed in a stopped-flow spectrometer 25°C. **(A)** Changes of absorbance at 407 nm upon nitrite binding to myoglobin. **(B)** Amplitude of the nitrite binding to myoglobin. **(C)** Observed rate constant of nitrite binding to myoglobin as a function of nitrite concentration. **(D)** Amplitude of the nitrite binding to myoglobin at pH 6.0 as a function of nitrite concentration. **(E)** Observed rate constant of nitrite binding to myoglobin at pH 6.0.

### 5.2.3 Spectroscopic Analysis of Nitrite Binding to Wild-type Sperm Whale Myoglobin

In order to understand the nature of the ferric-heme-nitrite complex formed in solution, the product of the reaction was further investigated using a combination of room-temperature MCD and low-temperature X-band EPR spectroscopies. The purpose of these experiments was to determine whether nitrite was bound to the heme iron in the nitrito-orientation, as predicted by the X-ray structure of the horse heart myoglobin-nitrite complex (Yi et al., 2009) or in the alternative nitro-orientation.

The positions and intensities of the bands in the room-temperature MCD spectrum (Figure 5.6A; black trace) of the wild-type protein prior to the addition of nitrite are consistent with a high-spin His/H<sub>2</sub>O coordinated ferric heme (Cheesman et al., 1994). Specifically the charge transfer band known as CT<sub>2</sub> (Cheesman et al., 1991) seen observed as a shoulder at 635 nm in the UV/Vis spectrum is represented by a trough at 642 nm and the intensity (peak-to-trough) of the derivative-shaped band in the Soret region is about 20 M<sup>-1</sup> cm<sup>-1</sup> T<sup>-1</sup> (Cheesman et al., 1994). This is consistent with the low temperature (10K) CW-X-band EPR spectrum which shows a single purely high-spin ( $g = 6, 6, 2$ ) heme species (Figure 5.6B; black trace).

After addition of 200 mM nitrite, all of the bands in the room-temperature MCD spectrum remain consistent with a single ferric heme species. In other words, the addition of nitrite does not cause any fraction of the heme to become reduced. However the increase in the intensity (peak-to-trough) of the derivative feature in the Soret region to about 40 M<sup>-1</sup> cm<sup>-1</sup> T<sup>-1</sup> indicates some conversion from high-spin to low-spin ferric heme. However this is not sufficient to account for 100% conversion.

In principle, this observation could be accounted for by incomplete binding of nitrite, or free nitrous acid, to form a sub-stoichiometric amount of a purely low-spin form. However, such an interpretation would not be consistent with the apparent saturation observed in the kinetic titration (Figure 5.5B), nor with the observed change in position of the MCD CT<sub>2</sub> band, which moves from 642 nm to 637 nm (the shift in this band is also observed in the UV/vis spectrum (Figure 5.4). Note that although the position of the CT<sub>2</sub> band shifts there is no increase in the width of the band and the 642 nm has completely disappeared. This is best interpreted in terms of the new feature at 637 nm arising from a His/RO<sup>-</sup> ligated ferric heme, which is tentatively assigned to a nitrito species, with negligible amounts of the original His/H<sub>2</sub>O ferric heme remaining.

The low-temperature (10K) CW-X-band EPR spectrum (Figure 5.6B; red trace) of the same sample provides additional information. It contains a new broad feature with  $g_z \sim 3.00$  which might be considered to arise from a single low-spin ferric heme. However the  $g_z$  component is asymmetric and not in the direction that would be associated with " $g$ -strain". Accurate simulation of the feature (Figure 5.6B; blue trace) requires two principle species  $g_z = 3.06$  (58% of total heme) and  $g_z = 2.96$  (33%) plus a minor third  $g_z = 3.01$  7% (Dr M.R. Cheesman personal communication). The remaining 2% of the heme is accounted for the high-spin signal at  $g \sim 6$ . Interestingly the  $g \sim 6$  signal in the nitrite-bound sample is a different shape to that of the as-prepared wild-type myoglobin and must arise from a different high-spin species.

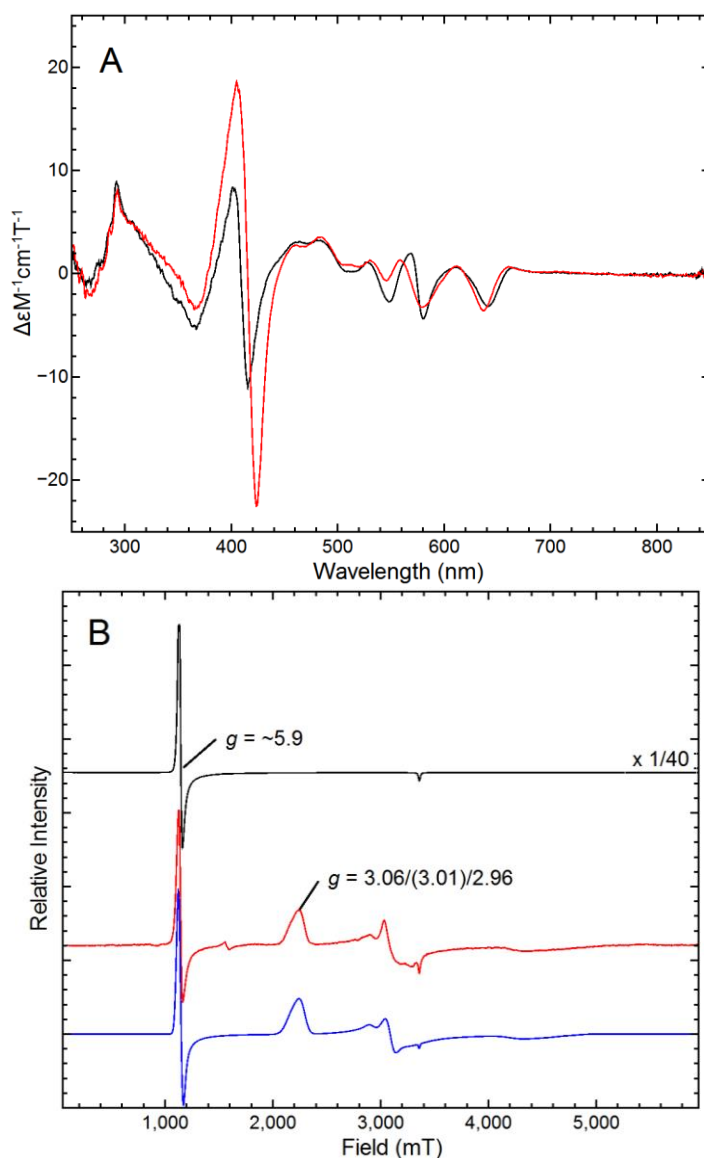


**Figure 5.6 Spectroscopic analyses of nitrite binding to wild-type myoglobin. (A)** Room-temperature MCD spectra show the binding of nitrite to wild-type myoglobin in 20 mM citric acid phosphate pH 7.0. Approximately 200  $\mu\text{M}$  of myoglobin (black trace) was mixed with 200 mM of nitrite solution in the same buffer (red trace). MCD conditions: 295 K; 8 T. **(B)** Low temperature CW-X-band EPR spectra show the binding of nitrite to wild-type myoglobin in the same samples. Wild-type myoglobin (black trace), nitrite-bound myoglobin (red trace) and stimulated EPR spectrum of nitrite bound myoglobin (blue trace). EPR conditions: microwave frequency 9.56 GHz; microwave power 2 mW; Temperature 10 K; modulation amplitude 10 G.

## 5.2.4 Spectroscopic Analysis of the Nitrite-bound Forms of Representative Distal Pocket Variants (H64V and H64A) of Sperm Whale Myoglobin

In section 5.2.1, the nitrite reductase activities in His64 variants are shown to be impaired, despite an increase in the heme pocket size which prompted us to hypothesise that one of the roles of distal histidine in nitrite reduction in globins is to stabilise the water molecule which is apparently missing in the His64 variants. Surprisingly, the H64A variant is an exception to this and shows the least effect in the nitrite reduction as the Soret peak at 408 nm suggests a presence of a bound water molecule in the ferric state. On the contrary, the H64V exhibits a vacant distal pocket (Figure 5.9A; Quillin et al., 1993). Interestingly, the orientation of the nitrite in the X-ray structure of nitrite-H64V complex shows a completely different orientation from the wild-type horse heart myoglobin (Yi et al., 2009). However, corresponding evidence in solution from spectroscopic studies is missing. Therefore, to investigate the influence of the His/H<sub>2</sub>O ligation on the binding of nitrite, the H64A and H64V which represents the presence and the absence of a bound water ligand at the distal coordination site in ferric state respectively were chosen.

The effect of nitrite binding on the UV/vis spectrum of the ferric forms of the H64A and H64V variants was determined using a split cuvette as described in section 2.7.1. Before the addition of nitrite to the H64V variant, the Soret maximum in the UV/vis spectrum at 395 nm (Figure 5.7A; red trace) which together with the broad CT-band at 657 nm is typical of His ligated ferric heme with an unoccupied sixth coordination site (His/-) (Springer et al., 1994). The room-temperature MCD spectrum is represented by just a few very weak features and the trough defining CT<sub>2</sub> is at 657 nm (Figure 5.7B, red trace). The low-temperature CW-X-band EPR spectrum contains a single purely high-spin ( $g = 6, 6, 2$ ) heme species (Figure 5.7C; red trace) arising from the His/- heme.

Upon addition of 200 mM nitrite, the MCD CT<sub>2</sub> trough at 657 nm of the H64V variant does not move, but the intensity diminishes by ~25% suggesting only a fraction of the heme has nitrite bound. This is interesting because at pH 7.0 200 mM potassium nitrite contains approximately 50 μM free nitrous acid – which represents about 25% of the H64V myoglobin concentration. In parallel the intensity (peak to trough) of the Soret increases to ~20 M<sup>-1</sup> cm<sup>-1</sup> T<sup>-1</sup> which suggests that the fraction (25%) of the heme that does have nitrite co-ordinated to it is a low-spin species. This implies that with 100% occupancy the Soret intensity (peak to trough) would be in the order of 80 M<sup>-1</sup> cm<sup>-1</sup> T<sup>-1</sup> which would be unusually weak for a low-spin species (although one that has not been described previously) but still much higher than anything reported for high-spin heme. Whilst ~75% of the ferric heme remains in the high-spin state after treatment with 200 mM nitrite at room temperature, but this is not the case when the sample is cooled to 10K. Although (after treatment with 200 mM nitrite) there is a signal ( $g = 6, 6, 2$ ) in the EPR spectrum arising from a high-spin species, it accounts for just ~ 1% of the total heme content. Instead the EPR spectrum is dominated by two new signals ( $g_z = 3.16$  and 2.93) both arising from low-spin ferric species (Figure 5.7C, blue trace). This observation is interesting for two reasons. First of all, cooling appears to cause nitrite that is bound to the protein, but too distant to ligate the heme iron and influence the UV/vis or RT-MCD spectra, to change position and become a heme ligand. Secondly, simulation of the spectrum suggests the  $g_z = 3.16$  species, which does not correspond to the nitrito species observed in the EPR spectrum of the wild-type protein, accounts for 90% of heme; the  $g_z = 2.93$  accounting for the remaining 10%,

In comparison the UV/vis spectrum of the ferric form of the H64A variant before the addition of nitrite has a Soret maximum at 408 nm and the charge transfer band is a 645 nm. Although the Soret band intensity in the RT-MCD is only 9.6 M<sup>-1</sup> cm<sup>-1</sup> T<sup>-1</sup> this is still more than

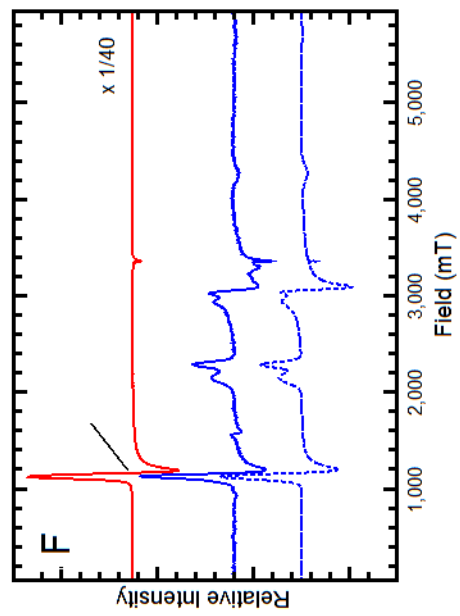
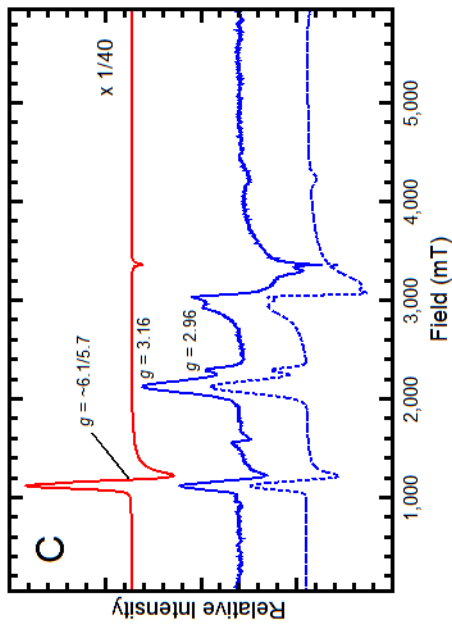
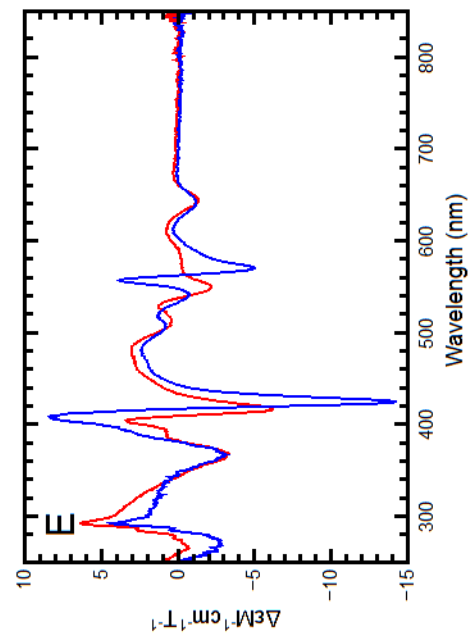
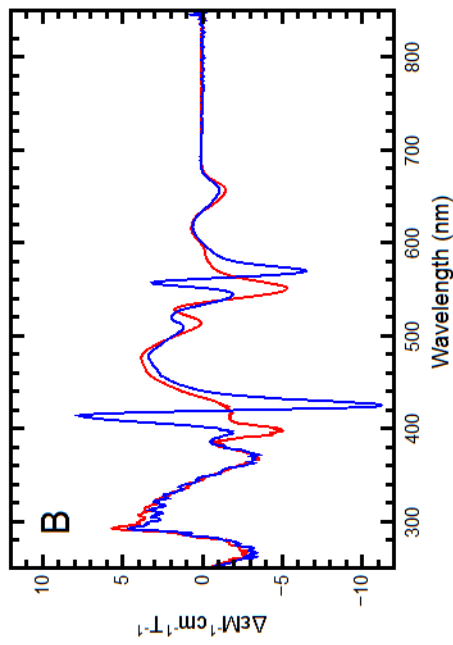
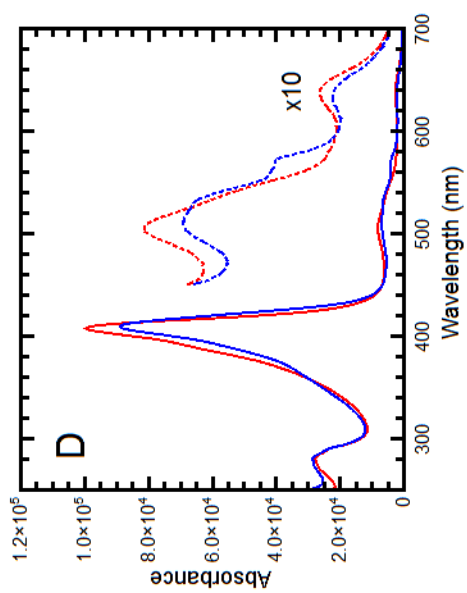
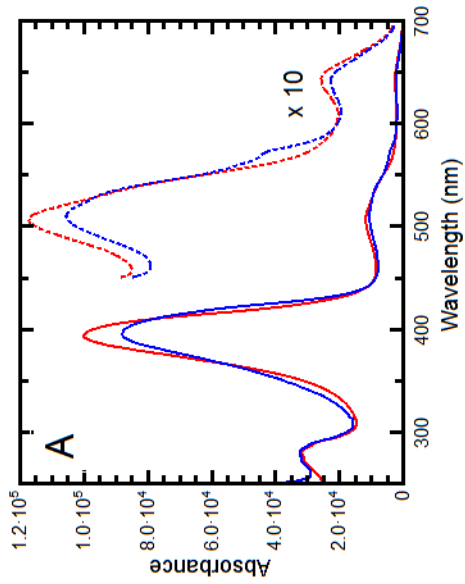
is usual for ferric heme with a His/- ligand set and the CT<sub>2</sub> trough has moved back to 645 nm a position which is indicative of His/H<sub>2</sub>O coordination (Figure 5.7D, blue trace). Again the low-temperature X-band EPR spectrum contains a single purely high-spin ( $g = 6, 6, 2$ ) heme species (Figure 5.7F, red trace) arising from the His/H<sub>2</sub>O coordinated heme.

After the addition of 200 mM nitrite, a red shift of the Soret peak from 408 nm to 411 nm together with an emergence of a feature at 576 nm and a small blue shift of a band at 645 nm which are similar to the spectral changes observed in wild-type myoglobin shown in figure 5.4 are observed (figure 5.7D, blue trace). In addition the shape of the Soret band in the RT-MCD spectrum changes in a way that suggests a narrow low-spin feature has become superimposed on the initial high-spin form. The level of this low-spin component is very similar to that in nitrite bound H64V i.e. ~25%. There is also a slight movement in the MCD CT<sub>2</sub> band showing the presence of a nitrite-induced low-spin species, possibly a trace of the same nitrito form provisionally identified in the RT-MCD spectrum of the nitrite complex of the wild-type protein.

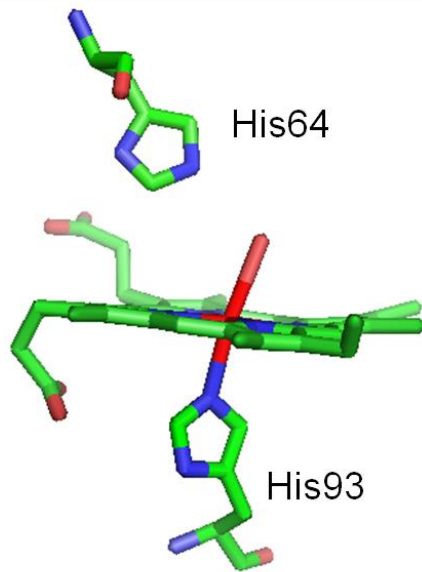
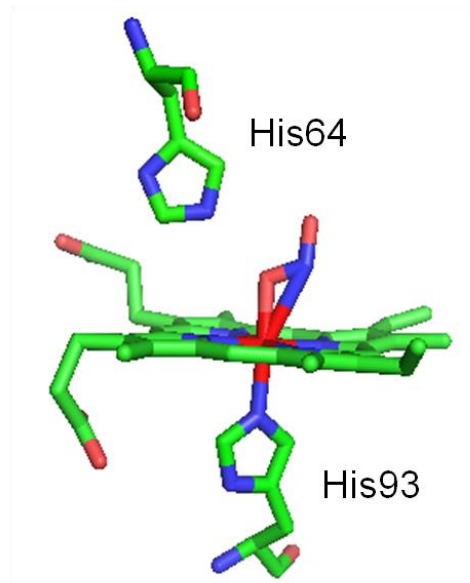
The low-temperature EPR spectrum of the nitrite complex of H64A variant, like that of H64V nitrite complex, contains two low-spin EPR species. The  $g_z$ -values are very similar; 3.12/2.94 (H64A) and 3.16/2.93 (H64V). Simulation of the EPR spectra suggests the presence of two low-spin species and both distal pockets lack the H-bonding residue so one possibility is to assign 3.16 & 3.12 to nitro and 2.93 & 2.94 to nitrito. Interestingly, in the H64A variant, with more space in the distal pocket, the nitro form is the majority species: 3.12 (56%), 2.94 (41%). This may be related to the higher proportion at 10 K of nitrito as estimated from the EPR: 41% as compared to 10% in the nitrite-H64V complex.

A number of X-ray crystallographic studies of myoglobin have suggested an important functional role of His64 in the stabilising exogenous ligand bound to the heme iron in both oxidation states such as oxygen (Quillin et al., 1993). The reported X-ray structures of ferric sperm wild-type whale and horse heart myoglobins are consistent with the solution spectroscopy reported in section 5.2.3 that they clearly show a water molecule ligated to the heme iron and stabilised by the distal histidine residue (His64) at a close distance that could involve hydrogen bonding (Figure 5.8A). However in the X-ray structure of the nitrite-bound form of wild-type ferric horse heart myoglobin, the distal water is replaced by nitrite which is in the nitrito- (O-bound) orientation stabilised by the His64 residue which may again via hydrogen bonding (Figure 5.8B; Copeland et al., 2006; Yi et al., 2009).

In contrast to wild-type myoglobin, the reported X-ray structure of the ferric forms of the H64V variant of sperm whale myoglobin(s) clearly lack a water molecule bound to the heme iron (Figure 5.9A). It is presumed that in the absence of any stabilizing influence water molecules are excluded from the distal pocket by the bulky hydrophobic side-chain of valine. However the X-ray structure of ferric nitrite-bound form of H64V variant of horse heart myoglobin reveals the nitrite to be in the nitro- (N-bound) orientation, rather than the nitrito-form reported for wild-type myoglobin (Figure 5.9B).



**Figure 5.7 Spectroscopic analyses of nitrite binding to H64V and H64A variants. (A)** UV/vis spectra of H64V variant (Red trace) and mixed with a 200 mM nitrite in 20 mM citric acid phosphate pH 7.0 (Blue trace). **(B)** Room-temperature MCD spectra of H64V variant (Red trace) and its nitrite-bound form (Blue trace). MCD conditions: 295 K; 8 T. **(C)** Low temperature CW-X-band EPR spectra of H64V variant (Red trace), its nitrite-bound form (red trace) and the stimulation of the nitrite-bound spectrum (blue dotted trace). EPR conditions: microwave frequency 9.56 GHz; microwave power 2 mW; Temperature 10 K; modulation amplitude 10 G. **(D)** UV/vis spectra of H64A variant (Red trace) and mixed with 200 mM nitrite in 20 mM citric acid phosphate pH 7.0 (Blue trace). **(E)** Room-temperature MCD spectra of H64A variant (Red trace) and its nitrite-bound form (Blue trace). MCD conditions: 295 K; 8 T. **(F)** Low temperature CW-X-band EPR spectra of H64A variant (Red trace), its nitrite-bound form (red trace) and the stimulation of the nitrite-bound spectrum (blue dotted trace). EPR conditions: microwave frequency 9.56 GHz; microwave power 2 mW; Temperature 10 K; modulation amplitude 10 G.

**A****B**

**Figure 5.8 X-ray structure of nitrite-bound wild-type myoglobin. (A)** nitrite-free sperm whale myoglobin in which a water molecule is ligated to the ferric heme iron (redrawn from PDB file IDUK using Pymol v1.3). **(B)** Nitrite-bound horse heart myoglobin in which the nitrite orientation is shown to be nitrito form (O-bound form) (redrawn from PDB file 3LR7 using Pymol v1.3).

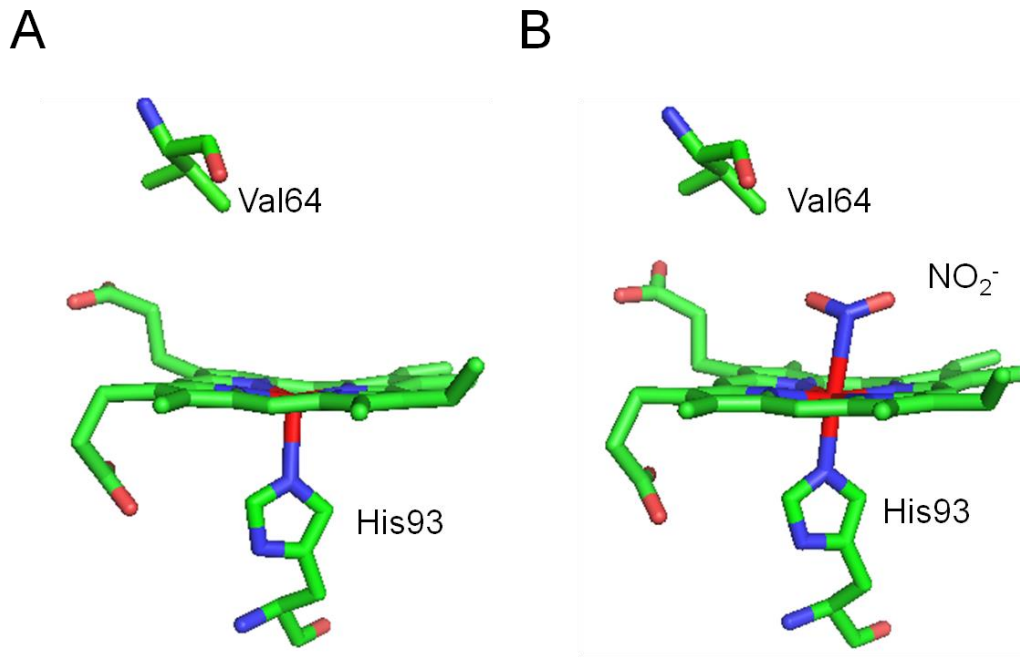


**Figure 5.9 X-ray structure of nitrite-bound myoglobin H64V variant. (A)** nitrite-free sperm whale myoglobin H64V variant (redrawn from PDB file 2MGJ using Pymol v1.3). **(B)** Nitrite-bound horse heart myoglobin in which the nitrite orientation is shown to be nitro form (N-bound form) (redrawn from PDB file 3HEP using Pymol v1.3).

### 5.2.5 Summary of Nitrite Binding to Myoglobin and H64 variants

The spectroscopic analyses of wild-type sperm whale myoglobin at both room-temperature (UV/vis and MCD) and low-temperature (X-band EPR) reported in 5.2.3 can be interpreted in terms of the bound water molecule in the distal pocket being replaced by nitrite which is coordinated to the heme iron in the nitrito- (O-bound) orientation. Both ligands, water and nitrite, are apparently stabilised in a specific orientation by the conserved distal histidine residue which has been shown by X-ray crystallography to be in hydrogen bonding distance of the ligands (Figure 5.8; Copeland et al., 2006; Yi et al., 2009).

In the case of the H64V variant the data from UV/vis, RT-MCD and EPR spectroscopies are consistent with water being excluded from the distal pocket. The extent of nitrite binding increases at low temperature and evidence from EPR spectroscopy suggests that the dominant nitrite-bound species ( $g_z = 3.16$ ) is different to that observed in the wild-type myoglobin. Based on the X-ray crystallography data (Figure 5.9B; Yi et al., 2009) this species can provisionally be assigned to the nitro- (N-bound) form.

In the case of the H64A variant no X-ray structures are currently available. The RT-MCD spectrum is however consistent with a water molecule being coordinated to the heme iron. And like wild-type myoglobin, this water molecule can be replaced by nitrite. As in the case of the H64V variant the extent of nitrite binding at room temperature is only 25%. Again lowering the temperature promotes full occupancy but here simulation of the EPR spectrum suggests approximately equal amounts of the nitro- and nitrito- bound.

### 5.2.6 Nitrite Reduction by Myoglobin H93K Variant

To further explore the role of the distal histidine residue in heme-iron mediated nitrite reduction it would be useful to understand the consequences of changing the proximal heme iron ligand. To that end I expressed a novel variant of sperm whale myoglobin in which the conserved proximal histidine at position 93 was substituted with lysine described in section 2.4.6 and 2.6.2. Lysine was chosen as the replacement ligand as there is a good precedent in nature. The bacterial cytochrome *c* nitrite reductases found in *E.coli* of proteobacteria which catalyse the six electron reduction of nitrite to ammonium generally have a lysine as a proximal ligand (Einsle et al., 1999).

Since the H93K variant of sperm whale myoglobin has not previously been described there was no available structural or spectroscopic information. Therefore, before studying the nitrite reduction reaction it was necessary to complete a preliminary UV/vis spectroscopic characterization of the protein in both ferric and ferrous states in the presence and absence of NO. Reduction was achieved using a minimal amount of dithionite (10 mM) and nitrosyl complexes of both ferric and ferrous forms were generated by incubating protein with excess NO released in solution from PROLI NONOate in a sealed and anaerobic cuvettes. The principle spectroscopic features of the H93K variant in its different oxidation states as well as the corresponding nitrosyl complexes are summarised in the table 5.2.

The UV/vis spectrum of the H93K variant in the ferric state resembles that of wild-type myoglobin with a Soret maximum at 408 nm (figure 5.10A), but there are also clear differences in the visible region. Specifically the weak feature at 720 nm found in the wild-type myoglobin is absent and the charge-transfer band, which corresponds to the MCD CT<sub>2</sub> band, has moved from 635 nm (wild-type) to 625 nm (H93K) (Figure 5.10A). A number of other weak features in the visible region are also blue-shifted by *ca* 10 to 20 nm (Figure 5.10A; Table 5.2). The most

reasonable interpretation of these spectral changes is that they arise from the substitution of H93 with lysine and a water molecule in the distal pocket coordinated between the distal histidine (H64) and the heme iron persist in this form. Evidence for this interpretation comes from a pH titration between pH 6 and pH 11 which shows the pKa for the spectroscopically monitored spin-state change known as the “alkaline transition” due to deprotonation of the distal water ligand shifts from pKa = 8.89 (wild-type) to 7.8 in H93K variant (Dr. M. R. Cheesman, personal communication).

In the deoxy-ferrous form, the H93K variant exhibit a smaller extent of red shift of Soret peak to 427 nm than that of wild-type myoglobin (Figure 5.10B; red trace). The nitrosyl-species of H93K variant are also similar to that of wild-type myoglobin, especially the nitrosyl-species in the ferrous state in which the H93K variant has a Soret peak and  $\alpha\beta$  bands at 419 nm, 576 nm and 545 nm, respectively (Table 5.2).

Since the spectra of the deoxy-ferrous and nitrosyl-ferrous forms of H93K variant closely resemble that of the equivalent forms of wild-type myoglobin, the nitrite reductase activity of H93K variant could be measured using exactly the same experimental methods described in 2.7.1. Surprisingly, the nitrite reduction of deoxy-ferrous H93K variant in the presence of 0.5 mM nitrite was found to be too fast to measure using the standard experimental conditions. Therefore, the nitrite concentration was reduced 10-fold to 50  $\mu\text{M}$ , which is still maintains pseudo-first order conditions, in order to obtain reaction progress curve. The first order rate constant of the nitrite reduction by H93K variant was determined to be  $0.358 \text{ min}^{-1}$  which is about six-times faster than wild-type myoglobin at the same nitrite concentration (Figure 5.11). The results strongly suggest that replacing the proximal histidine ligand with a lysine residue facilitates the nitrite reduction reaction although it is not clear if this is a direct consequence of the substitution or occurs indirectly through the change in the pKa of the proximal Lys/H<sub>2</sub>O

complex.

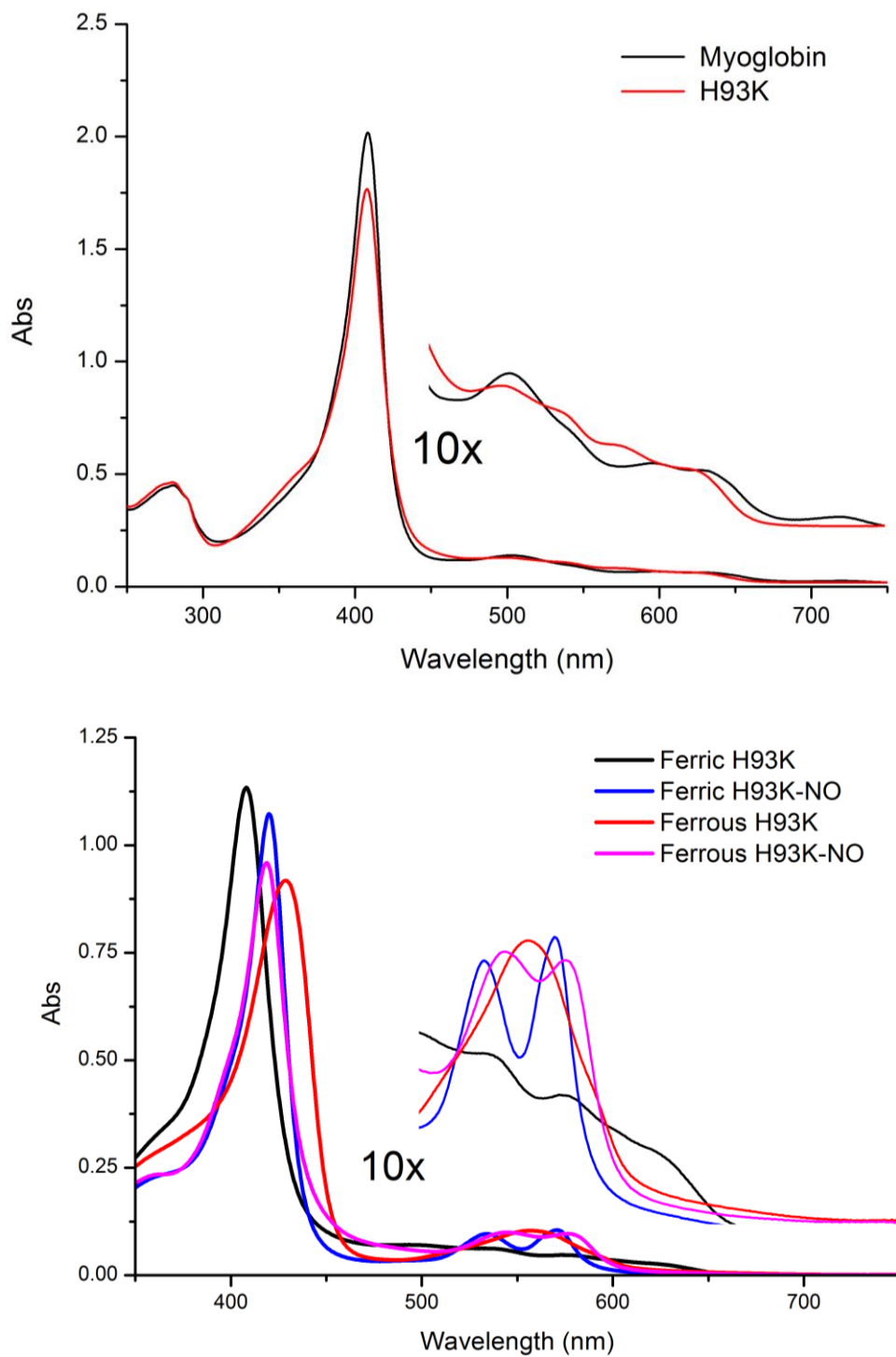


**Figure 5.10 Spectroscopic examination of myoglobin H93K variant in the ferric state.**

**(A)** Comparison of the absorption spectra of wild-type myoglobin with H93K variant in the ferric

state in 20 mM sodium phosphate pH 7.0. **(B)** Absorption spectra of nitrosyl species of H93K variants in ferric and ferrous state. Approximately 10  $\mu$ M of H93K variant at ferric state in sodium phosphate pH7.0 (black solid line), was reduced by 1 mM sodium dithionite to deoxy-ferrous state under anaerobic conditions (red solid line). A small amount (10  $\mu$ L) of stock solution of PROLI NONOate at 8 mM in 1 mM sodium hydroxide was added into the ferric H93K (blue solid line) and deoxy-ferrous (magenta solid line) until no further spectral change was observed.

<b>H93K Myoglobin</b>	<b>Soret peak (nm)</b>	<b>Other features (nm)</b>	<b>Wild-type Myoglobin</b>	<b>Soret peak (nm)</b>	<b>Other features (nm)</b>
<b>Ferric</b>	408	498, 542, 575, 625 (all broad & weak features)	<b>Ferric</b>	409	503, 596, 635, 720 (All broad & weak features)
<b>Nitrosyl-ferric</b>	420	570, 534	<b>Nitrosyl-ferric</b>	420	574, 535
<b>Ferrous</b>	429	565	<b>Ferrous</b>	434	557
<b>Nitrosyl-ferrous</b>	419	576, 545	<b>Nitrosyl-ferrous</b>	421	581, 549

**Table 5.2 Spectroscopic features of nitrosyl-species in H93K and wild-type myoglobin in ferric and ferrous states**

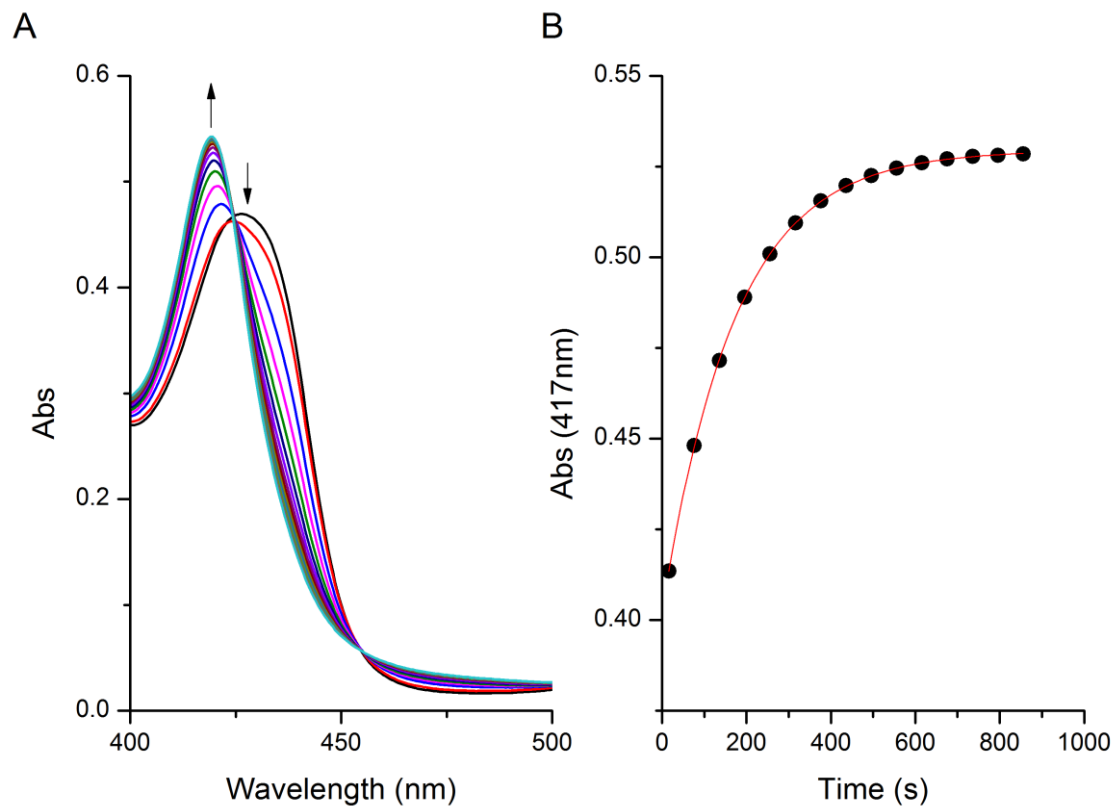


**Figure 5.11 Nitrite reduction by H93K variant.** The reaction was monitored by multiple-cycle scanning mode from 500 nm to 350 nm at a scan rate =  $300\text{nm min}^{-1}$  at  $25\text{ }^{\circ}\text{C}$  done in 100 mM phosphate buffer pH 7.0. **(A)** The absorption spectra showing the spectral changes during the nitrite reduction reaction by mixing 0.05 mM nitrite with deoxy-ferrous myoglobin H93K variant in the presence of 30 mM sodium dithionite. **(B)** The absorbance changes at 417 nm during the reaction in the time course of 20 minutes. The data points were fit into a single exponential equation, indicated by the red line, in order to determine the first order rate constant.

### 5.2.7 Spectroscopic Analysis of Nitrite Binding to Ferric H93K Variant

The observation that H93K variant exhibited a greater nitrite reductase activity than wild-type myoglobin is interesting as it implicates a functional advantage of having a lysine residue ligated to the heme iron at the proximal site which is commonly found in the active site of cytochrome *c* nitrite reductases in *E.coli*. Thus, characterisation of H93K variant will provide useful information for understanding the function role of the proximal lysine ligation in nitrite reduction in bacteria. The first step would be to look at the binding of nitrite to the H93K variant in the ferric state.

Binding of nitrite to ferric H93K causes a significant change in the UV/vis spectrum as shown in the figure.5.12A. Upon addition of 200 mM nitrite, a red shift of Soret peak from 408 nm to 415 nm is observed, together with arising of two bands at about 541 nm and 575 nm and a decrease in the shoulder peak signal at 625 nm which may tentatively indicate a formation of nitrite-bound complex. Binding of nitrite at lower pH (i.e. pH 6.0) shows no further increases in the absorbance in the difference spectrum (data not shown) suggesting that the binding of nitrite with 200 mM nitrite is complete at pH 7.0.

The binding kinetic of nitrite to ferric H93K was examined on the stopped-flow spectrometer as described for wild-type myoglobin in section 2.7.2, and progress of the reaction was monitored via the decrease in absorbance at 406 nm. The amplitude of the reaction also shows a hyperbolic dependence on nitrite concentration (Figure 5.12 B) similar with the wild-type myoglobin but with a much smaller estimated  $K_d = 1.92$  mM. When the observed rate constant was fitted according to the pseudo-first order in figure 5.12C, the  $k_{on}$  and  $k_{off}$  for nitrite binding is found to be  $0.33 \text{ mM}^{-1} \text{ s}^{-1}$  and the  $k_{off}$  is found to be  $0.61 \text{ s}^{-1}$ , respectively. The ratio of  $K_{off}/K_{on}$  gives an equilibrium binding constant ( $K_d$ )= 1.84 mM which is slightly smaller than that of wild type myoglobin (2.68 mM) at the same pH. Hence, the results

suggest that substitution of proximal histidine with a lysine has only small effects on the binding kinetic of nitrite.

The nitrite binding to H93K variant was further examined by EPR spectroscopy to confirm the presence of nitrite-bound species. As expected, in the nitrite-free met-H93K, the EPR spectrum displays a pure high-spin spectrum ( $g = 6, 6, 2$ ) similar to myoglobin (Figure 5.13, red trace). Since the distal His64 is present in this variant, it is conceivable that a water-molecule should be present at the distal site in the met-H93K. Further characterisation using room-temperature MCD and crystallography will be needed to confirm the Lys/H<sub>2</sub>O ligation in ferric state. Upon addition of 200 mM of nitrite, a decrease in the high-spin signal at  $g \sim 6$  and a concomitant emergence of low-spin signals at  $g = 2.93$  and  $g = 2.78$  strongly indicate the formation of nitrite-bound low-spin complex as indicated in the UV/vis spectrum (Figure 5.13, blue trace). In term of the orientation of the bound nitrite, the indicated  $g$ -values fall into a similar region of those assigned as nitro and nitrito signals in myoglobin which might imply a co-existent of the two species, although the X-ray structure of nitrite-complex of cytochrome c nitrite reductase in *Wolinella succinogenes* exhibits a n-bound nitro-orientation (Einsle, et al., 2002). Further characterisation of the lysine-ligated heme in myoglobin system will be needed to conclude the binding mode of nitrite in this system.

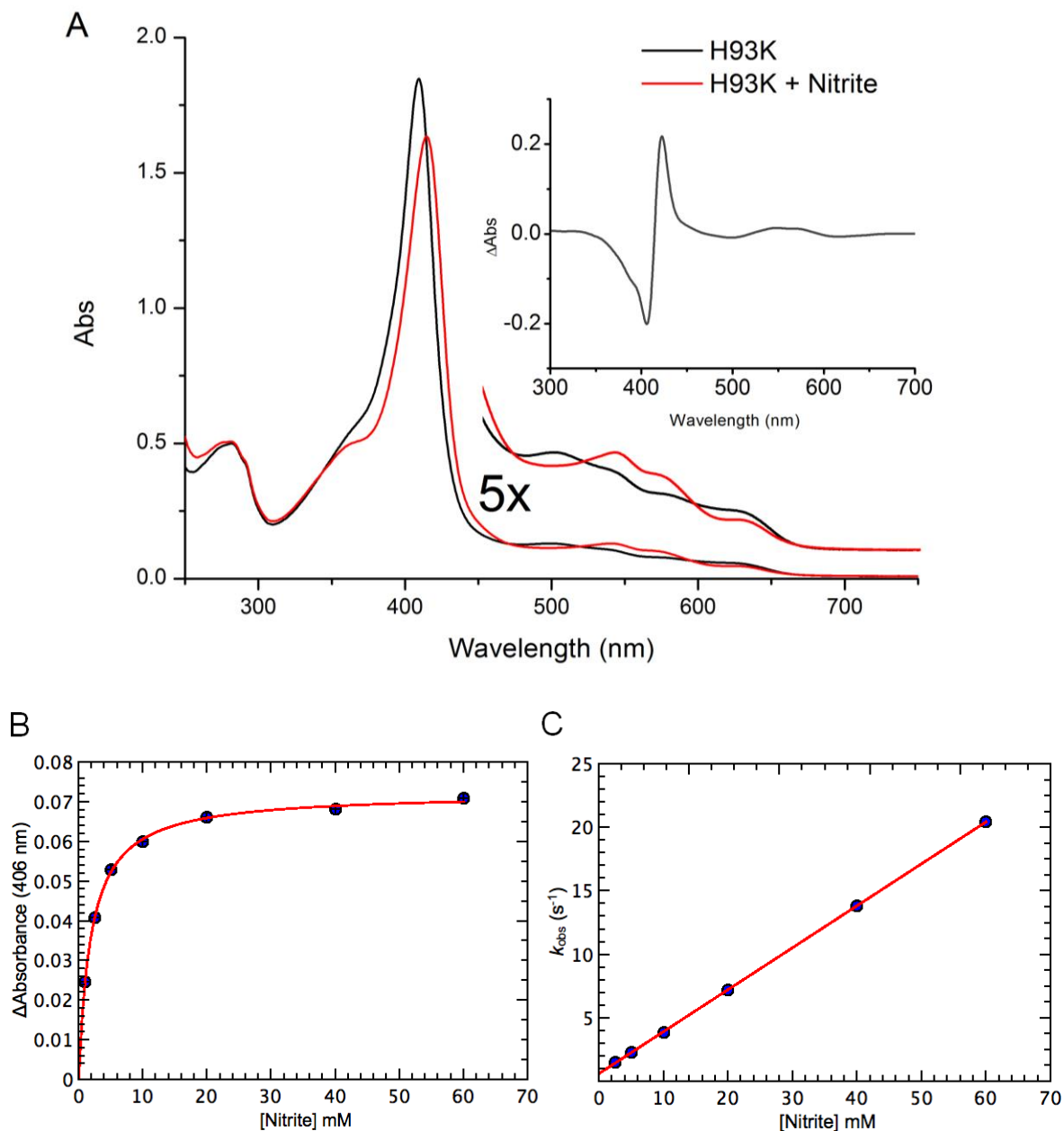


**Figure 5.12 Nitrite binding to ferric H93K variant. (A)** UV/vis spectrum of nitrite-bound H93K variant. 10  $\mu\text{M}$  of myoglobin proximal pocket H93K variants was mixed before (black solid line) and after (red solid line) with 200 mM sodium nitrite at 20 mM citric acid phosphate pH 7.0. Kinetic binding of nitrite to myoglobin proximal pocket H93K variants was done on a stopped-flow spectrometer as described in section 2.7.2. **(B)** Amplitude of the nitrite binding to H93K variant at pH 7.0 as a function of nitrite concentration. **(C)** Observed rate constant of nitrite binding to H93K variant at pH 7.0.

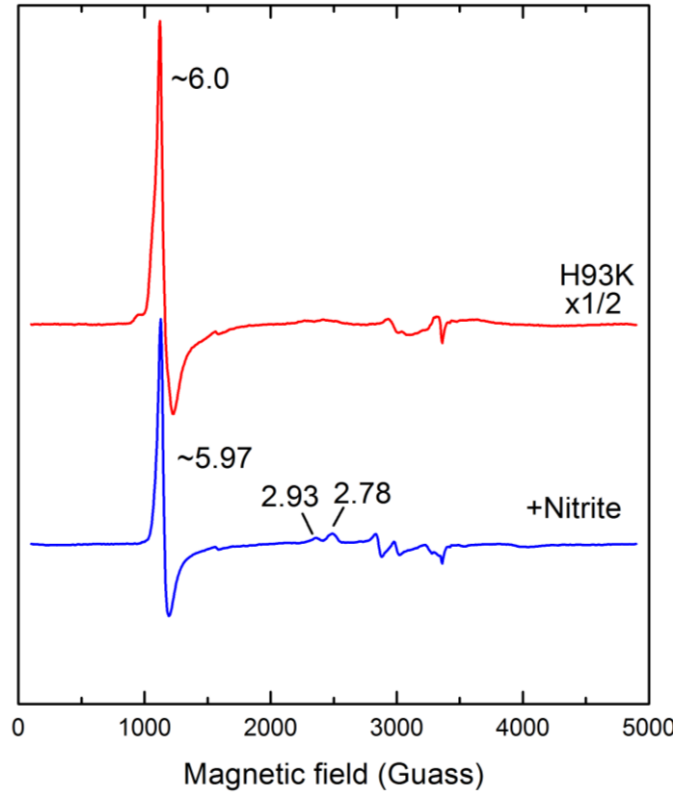


**Figure 5.13 EPR spectrum of nitrite-bound H93K variant.** A concentrated Myoglobin H93K variant approximately at 200  $\mu\text{M}$  (red line) was mixed 1:1 with 150 mM sodium nitrite (blue line) in 20 mM citric acid phosphate buffer pH 7.0. The spectra show a high spin species ( $g = 6, 6, 2$ ) in the H93K variant and an emerging of nitrite bound form ( $g = 2.93, g = 2.78$ ) upon binding to nitrite. EPR conditions: microwave frequency 9.68 GHz; microwave power 2 mW; temperature 15 K; modulation amplitude 10 G

The results obtained from the spectroscopic and kinetics studies on wild-type myoglobin and variants of myoglobin which show different local environments in the heme pocket provide valuable information for a detailed biochemical basis of the nitrite reductase activity in globins, especially the role of His64 residue in nitrite reduction by myoglobin. To summarise our findings, the ability to efficiently reduce nitrite to nitric oxide in heme-containing proteins is mainly governed by the presence of a histidine residue in the distal heme pocket and may be further enhanced by a lysine residue in the proximal site. The importance of the His64 in the distal pocket has been demonstrated in various aspects supported by evidence given by a combination of kinetic, spectroscopic and structural analyses. First of all, the His64 residue is important to the binding of nitrite to heme iron. Binding of nitrite to wild-type myoglobin is pH-dependent which strongly indicates the active species is the free nitrous acid rather than the nitrite ion as shown in the kinetic titration described in section 5.2.2. The binding of nitrite is completed in room-temperature only in the presence of the distal His64 residue, but not in H64 variants as indicated in the UV/vis and MCD spectroscopies in section 5.2.3 and 5.2.4.

Besides facilitating the binding of nitrite, the His64 residue is responsible for directing the specific orientation of nitrite in the heme distal pocket. In the case of wild-type myoglobin, consistent with the reported X-ray structures of nitrite-bound myoglobin complex, the nitrite is ligated to the heme iron via the oxygen atom, or “O-bound”, in a nitrito conformation (Figure 5.6; Figure 5.8B). Whilst, in the absence of the His64 residue, the predominant orientation of nitrite is via the nitrogen atom, thus “N-bound”, in a nitro conformation which is well described in H64V variants (Figure 5.7; Figure 5.9 B). Based on a calculation from the X-ray structure, the distance between the nitrite and the heme iron in the nitrito conformation (2.1 Å) is much closer than that in the nitro conformation (2.6 Å) (data not shown). In other words, the bound nitrite in the nitro conformation is loosely bound, whereas the binding of nitrite is tightened in the nitrito conformation which is stabilised by the His64. Nevertheless, it is not clear if there is

a real correlation between the orientations of the bound nitrite and the rate of nitrite reduction. Interestingly, it has been proposed that the difference in the orientations of the bound nitrite could determine the reaction products that bind to the heme iron when the nitrite is reduced to nitric oxide (Perissionotti et al., 2008).

Although the reaction mechanism described by Doyle and colleagues (see section 5.1 Equation 2) shows that when nitrite is reduced, the end products are nitric oxide and hydroxide ions which leave the heme pocket, it is conceivable that the presence of the His64 residue could provide a second proton which facilitates the conversion of hydroxyl ions to water molecules that helps directing the nitrite in the right orientation in a multiple turning over of nitrite in the presence of excess reductants.

The efficiency of nitrite reduction is significantly enhanced when the proximal histidine (His93) ligand is replaced by a lysine residue as shown in section 5.2.6. In such H93K system, the distal pocket environment is maintained as in the wild-type myoglobin suggested by the UV/vis spectrum (Figure 5.10), but the pKa of the distal water is shifted to 8.89 which suggests that the Lys/H<sub>2</sub>O ligation is less likely to be deprotonated compared to the His/H<sub>2</sub>O ligation in the neutral pH. It has been shown to be approximately 6 times faster than the wild-type myoglobin although the idea that the change in the pKa of the proximal His/H<sub>2</sub>O ligation indirectly facilitates the nitrite reduction is not completely understood.

### 5.2.8 Nitrite Reductase Activity of Cytoglobin

The bimolecular rate constant of nitrite reduction by cytoglobin has been reported by Li and colleagues to be about  $0.14 \text{ M}^{-1} \text{ s}^{-1}$  which is similar to that of another hexa-coordinate neuroglobin ( $0.12 \text{ M}^{-1} \text{ s}^{-1}$ ) reported by Tiso and colleagues. When compared with the bimolecular rate constant of cytoglobin with myoglobin, it is about 100x times slower than sperm whale myoglobin calculated in this study. The heme coordination of cytoglobin is hexa-coordinate, while it is penta-coordinate in sperm whale myoglobin. Hence it is conceivable to suggest that the slow nitrite reduction by cytoglobin could be due to the much lower heme accessibility which is demonstrated in chapter 4.

### 5.2.9 Nitrite Binding to Ferric Cytoglobin

In chapter 4 (Section 4.2.5), the heme accessibility for anionic fluoride ligand was shown to be inefficient in cytoglobin regardless of the coordination of the heme iron which implied other factors are controlling the heme accessibility such as the polarity of the heme pocket. On the other hand, as it has been demonstrated in the myoglobin that binding of nitrite requires a displacement of the coordinated water molecule to get the access to active site for nitrite reduction to produce nitric oxide. Therefore, the heme accessibility of nitrite in cytoglobin could be impaired due to the predominant His/His ligation. To gain more insights into the mechanism of nitrite reduction by cytoglobin, binding of nitrite to cytoglobin in the ferric state under the control of disulphide bond was also examined so as to investigate the impact of the position of the distal His81 residue to the binding of nitrite.

As expected, the binding of nitrite is also found to be trivial in the wild-type cytoglobin even incubated with nitrite in a concentration 10,000x times in excess than the protein. The spectral change in the UV/vis spectrum is subtle which suggests only a small fraction of

cytoglobin is nitrite bound (Figure 5.14A). We speculated that the nitrite could only bind to the small population of high-spin species in the cytoglobin which has a loosely coordinated distal His81. The binding of nitrite was then examined in the cysteine variants to assess the impact of the absence of disulphide on the accessibility for nitrite. In consistent with binding of fluoride ions in section 4.2.5, there is virtually no binding of nitrite to the two cysteine variants since no change in the absorption spectra is observed (Figure 5.14B & C). Hence, these results strongly indicate that nitrite binding is restricted by the presence of the distal His81 in cytoglobin. Nitrite can only bind to a trivial population of high-spin penta-coordinate cytoglobin which is found when the intra-molecular disulphide bond is intact, but not in any of the cysteine variants as the absence of the disulphide bond promotes the formation of complete hexa-coordinate species observed in EPR spectrum in section 4.2.2.

To further examine the effect of the distal His81 residue on heme accessibility for nitrite, the nitrite binding experiment was repeated in H81M and H81F variants of cytoglobin where the heme iron were described in high-spin penta-coordinate state. Interestingly, a significant binding of nitrite to the both distal His81 variants is observed compared to the wild-type counterpart. Both of them display distinctive spectral changes with a massive red shift of Soret peak to 421 nm and an emergence of two broad bands in the visible region that resembles the nitrite-bound complex in myoglobin (Figure 5.15). Since both methionine and phenylalanine are non-polar and hydrophobic, replacement of the positively charge histidine with the two residues would certainly change the hydrophobicity of the distal heme pocket which may facilitate the binding of nitrite in the form of nitrous acid. Also, the abolished His/His ligation may also promote the binding of nitrite as the coordination site became available in the case of the two His81 variants.

Notably, the nitrite-bound form of the H81F variant is unstable. Further spectral changes

are observed immediately after formation of the nitrite-bound complex. The changes in the spectrum are gradually monitored over a period of two hours and are shown in figure 5.15B. Interestingly, the changes are accompanying with a change in the colour of the solution from red to green (data not shown) which could be due to a modification by nitrite at one of the vinyl groups of the heme porphyrin ring (Yi et al., 2012).

As described in section 4.2.5 that ligand accessibility to the heme iron increases after the treatment of GSH which is speculated to be due to a modification effect at the cysteine residue. However, it is of note that examining the nitrite binding to the GSH treated cytoglobin in this experimental set up was proved to be problematic as the GSH which is supposed to reduce the disulphide bond in the cytoglobin also caused reduction of nitrite to nitric oxide. The nitric oxide was then scavenged by the excessive GSH in the buffer to form S-nitrosoglutathione (GSNO) with a massive absorbance at about 390 nm with a pink coloured solution. Formation of nitrosyl-ferrous cytoglobin is also observed and confirmed by EPR (data not shown).

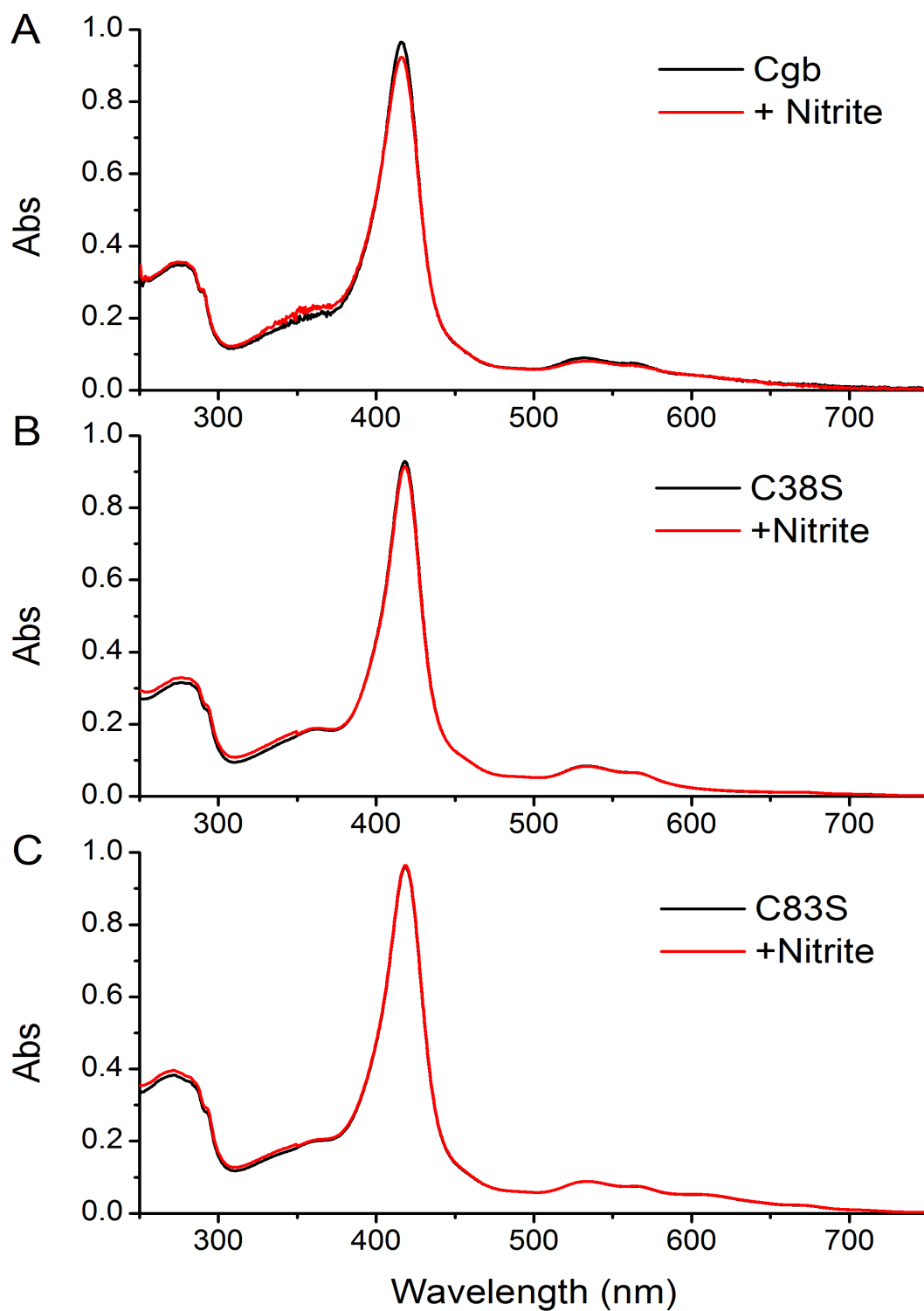


**Figure 5.14 Nitrite binding to ferric cytoglobin and cysteine variants.** 10  $\mu$ M of **(A)** wild-type cytoglobin, **(B)** C38S and **(C)** C83S was mixed with 100 mM nitrite in 20 mM citric acid phosphate pH 7.0. Spectrum was recorded before (black solid trace) and after the mixing (red solid trace).

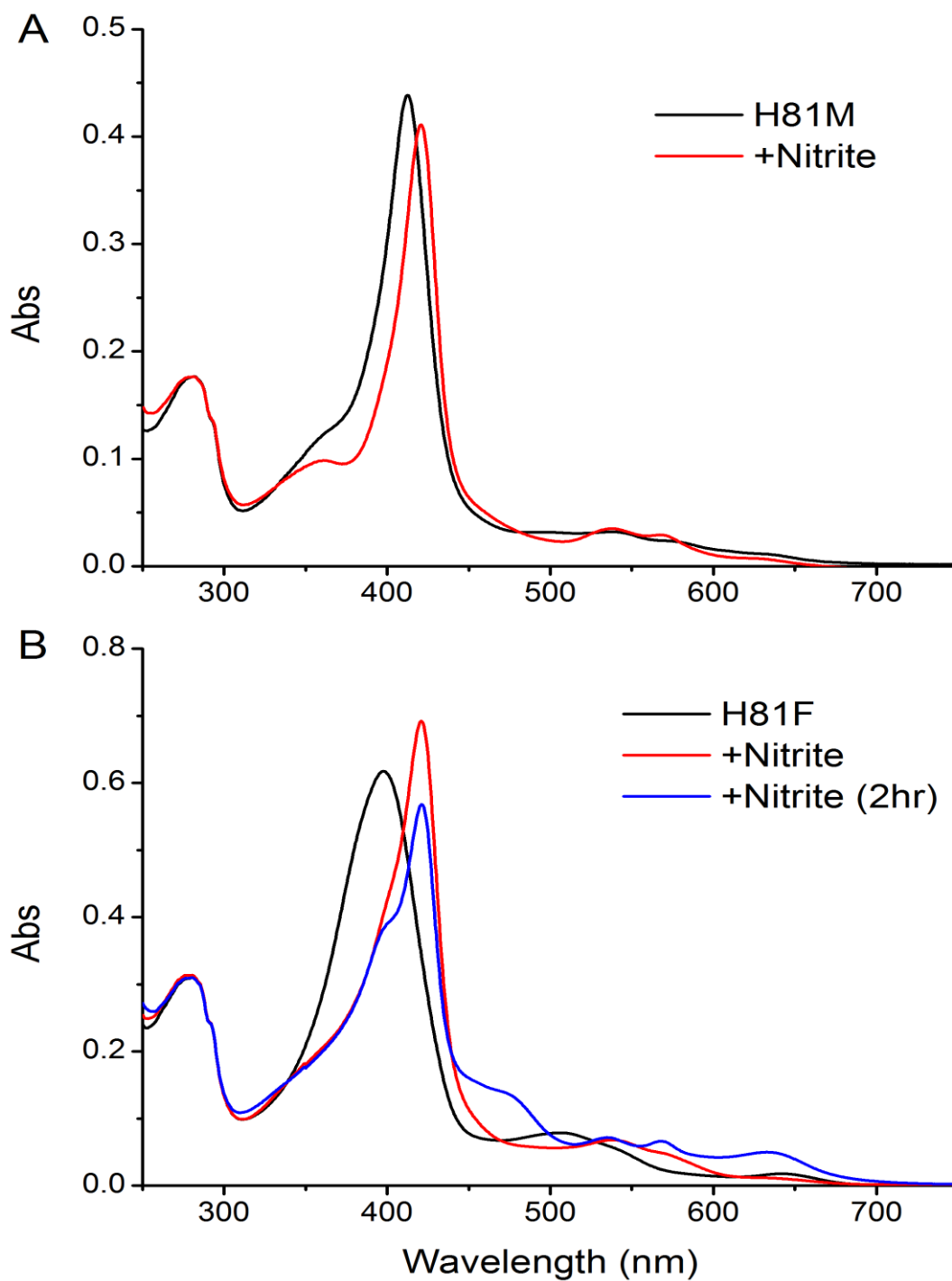


**Figure 5.15 Nitrite binding to Cytoglobin distal His81 variants.** 10  $\mu$ M of cytoglobin distal pocket variant (A) H81M and (B) H81F was mixed with 100 mM nitrite in 20 mM citric acid phosphate pH7.0, respectively. Spectrum was recorded before mixing (black trace), immediately after mixing (red trace) and after 2 hours for H81F variant (blue trace).

### 5.3 Discussion

The majority of work presented in this chapter highlights the detailed biochemical basis of the nitrite reductase activity in myoglobin which is of physiological significance since it may have therapeutic potential in ischemia-reperfusion injury in stroke and myocardial infarction. However, whether there is a similar physiological role in cytoglobin is still yet to be proved.

Like myoglobin, cytoglobin has also been detected in cardiovascular tissue including cardiomyocytes (Signh et al., 2009), smooth muscle cells and some other parts of the cardiovascular system (Halligan et al., 2009). It has been proposed that cytoglobin could play a similar role to that of myoglobin in the vasculature in nitric oxide metabolism, for example detoxifying nitric oxide via the dioxygenation reaction (Halligan et al., 2009; Gardner et al., 2010; Liu et al., 2012; Liu et al., 2013) and generating nitric oxide via nitrite reduction during hypoxia (Li et al., 2012). It would be tempting to postulate that nitric oxide metabolism could be modulated by cytoglobin especially in pathological conditions, such as cardiovascular diseases and cancer. On the other hand, unlike myoglobin, expression of cytoglobin is oxygen-dependent being up-regulated by hypoxia under the control of HIF signalling pathway (Emara et al. 2010; Gorr et al., 2011; Shaw et al., 2009). Augmented expression of cytoglobin under normoxia has been shown to reduce cell migration and invasion, but opposite effects were observed under hypoxia which suggested cytoglobin may have an unexplained bimodal role in cancer cells depending on the oxygen level (Oleksiewicz et al., 2013). Thus, there might be a possibility that the nitrite reductase activity of cytoglobin could also be of physiological significance.

The bimolecular rate constant of nitrite reduction in cytoglobin has been reported by Li and colleagues to be  $0.14 \text{ M}^{-1} \text{ s}^{-1}$  at pH 7.0 which is about a hundred times slower than wild-type myoglobin calculated in this study. The role of distal His64 in determining the nitrite

reductase activity of penta-coordinate myoglobin has been clearly demonstrated early in this chapter, while the role of the distal histidine in nitrite reduction by hexa-coordinate globins is not clear and has been shown to be elusive. Reported results of the bimolecular rate constants of nitrite reduction in globins so far are summarised in table 5.4 show that the rates of nitrite reduction in hexa-coordinate globins can vary to a great extent. The difference between the most efficient nitrite reductase found in the rice nonsymbiotic hemoglobin and the least found in neuroglobin could be about 700 times. Apparently, there is another determinant for the nitrite reductase activity in hexa-coordinate globins.

In an attempt to delineate the mechanism of nitrite reduction by neuroglobin, Tejero and colleagues have suggested that one of the possible determinants for nitrite reductase activity in neuroglobin could be the heme accessibility as the rate of nitrite reduction seems to correlate well with the volume of active site at the distal heme pocket. Dramatic increases in the rate of nitrite reduction were reported when the distal His64 residue in neuroglobin was replaced by other residues in which His/His ligation are abolished (Table 5.4). In contrast to the H64A variant in myoglobin which shows a significantly reduced rate of nitrite reduction compared to the wild-type myoglobin, the H64A variant in neuroglobin shows a huge increase in the rate of nitrite reduction and in fact the fastest nitrite reduction rate reported ever (Tejero et al., 2014).

The rate of nitrite reduction in cytoglobin is equally slow as that of neuroglobin (Li et al., 2013; table 5.4). Studies of the heme iron accessibility for nitrite ligand in cytoglobin (Section 5.2.9) clearly show that the accessibility to the sixth coordination site is limited by the presence of the distal His81 ligand in the wild-type cytoglobin. Although the affinity of the distal histidine has been shown to be relatively weak among hexa-coordinate globins (Hamdane et al., 2003; Tejero et al., 2014), the nitrite does not seem to be able to displace the distal His81 ligand

from the coordination site. Moreover, the heme accessibility for nitrite ligand is found to be further impaired in the absence of the disulphide bond as demonstrated by the two cysteine variants which may imply that the rate of nitrite reduction would be even slower when the disulphide bond is absent. However, a substitution of the distal His81 residue to apolar amino acid residues (i.e. methionine and phenylalanine) which turn the bis-histidyl low-spin species into his/- high spin species exhibits a dramatic increase in the heme accessibility for the nitrite ligand compared to the wild-type cytoglobin. Hence, the results suggested that heme accessibility for nitrite ligand is indeed impaired by the His81 residue as well as the disulphide bond in cytoglobin. However, whether these factors truly determine the rate of nitrite reduction in cytoglobin required more careful measurements. Li and colleagues suggested that cytoglobin could play a role in cytoprotection under hypoxia by generating nitric oxide from nitrite. Although the rate of nitrite reduction may be slow compared to myoglobin due to a rate limiting step in nitrite binding to the heme iron, the nitric oxide produced might be able to diffuse to a longer distance to trigger downstream signalling targets as the ligand affinity of nitric oxide cytoglobin might be effectively lowered by the distal histidine. Detailed biochemical basis of the nitrite reduction has to be further examined in order to support the physiological significance of such function.

	Heme coordination	Reported Bimolecular rate constant ( $M^{-1} s^{-1}$ )	References
Hemoglobin	T state (Penta & Hexa) R state (Hexa)	T state: 0.12 R state: 6.0	Huang et al., 2005
Myoglobin	Penta	12.4 (pH7.4, 37 °C)	Shiva et al., 2007
Neuroglobin	Hexa (Bishistidyl ligation)	S-S: 0.12 SH: 0.06 C46A/C55A: 0.06 (pH7.4, 25°C)	Tiso et al, 2011
Neuroglobin H64 variants	Penta	H64L: 259 H64Q: 285 H64W: 7.6 H64A:1120	Tiso et al, 2011 & Tejero et al., 2015
Cytoglobin	Hexa (bishistidyl ligation)	Mixed S-S/SH: 0.14 (pH7.0, 37°C)	Li et al., 2012
Plant Nonsymbiotic Hemoglobin ( <i>Arabidopsis thaliana</i> )	Hexa	AHb1: 19.8 AHb2: 4.9 (pH7.4, 25°C)	Tiso et al., 2012
Rice nonsymbiotic Hemoglobin	Hexa (bishistidyl ligation)	Class 1 Rice nsHb: 83 (pH7.0)	Sturms et al., 2011
Cyanobacterial Hemoglobin	Hexa (bishistidyl ligation)	SynHb: 68 (pH7.0)	Sturms et al., 2011

**Table 5.3 Reported bimolecular rate constants of nitrite reduction by different globins in the literature**

## Chapter 6: Putative Binding Partner(s) of Cytoglobin in Cancer Cells

### 6.1 Introduction

Cytoglobin has drawn enormous attention from cancer biologists since it was first identified as a biomarker in cancer cells which is associated with oesophageal cancer (McRonalD et al., 2006). Subsequently, Shivapurkar and colleagues (2008) discovered that the *CYGB* gene is a candidate tumour suppressor gene (TSG) which regulates cell growth and proliferation in cultured lung and breast cancer cell lines. Although detailed mechanisms of such tumour suppressor gene (TSG) activity of the *CYGB* gene are far from fully delineated, several downstream genes were identified in response to transient *CYGB* gene expression which suggests a possible role for cytoglobin in a novel cell signalling event, in particular to regulate the gene expression of its downstream targets, such as type-1 collagen (*Col1A1*) and uncoupling protein-2 (*UCP2*), DNA methyltransferase 1 (*DNMT1*) (Shivapurkar et al., 2008).

The idea of cytoglobin involving in a novel signalling event which may regulate downstream gene expression came from studies on subcellular localization of the cytoglobin that it localises in both cytoplasm (Schmidt et al., 2004; Shigematsu et al., 2008) and nucleus (Geuens et al., 2003; Hodges et al., 2008), and a nuclear translocation mechanism may be essentially related to certain structurally important amino acid residues (Singh et al., 2014). Therefore, it would be conceivable to suggest that such cell signalling cascade of cytoglobin may involve one or more cellular binding partners which are not only able to facilitate translocation of cytoglobin from the cytoplasm to the nucleus, but also binding to DNA sequence to regulate gene expression.

Cell signalling can be mediated by a series of protein-protein interactions. Recently, a novel binding mechanism, called “fly-casting”, which is a coupled folding and binding between intrinsically disordered or unstructured domains of proteins has been discovered (Sugase et al., 2007). In cytoglobin, as described by X-ray structure shown in figure 1.3B, the C-terminal extension is an unstructured loop region which could be a potential site for protein-protein interactions with novel binding partner(s). In this study, a tagged version of recombinant cytoglobin with an N-terminal Strep-tag, designated “strep-Cgb”, was expressed and purified from *E.coli*. Such strep-tagged cytoglobin was used as a bait protein in the “pull down assays” using two renal cell carcinoma cell lines in an attempt to identify any cognate cellular partners of cytoglobin under different cellular conditions. Moreover, a truncated form of the strep-tagged cytoglobin with the unstructured C-terminus deleted from the DNA sequence, designated “strep-Cgb $\Delta$ C”, was generated to test the hypothesis that such protein-protein interaction is mediated via the unstructured C-terminal domain.

## 6.2 Results

### 6.2.1 Verification of RCC4 Cells

Human renal clear cell carcinoma (RCC) arises from the epithelial cells in the proximal tubule of the kidney. In RCC4 cells, mutation in the *VHL* gene, a tumour suppressor gene, results in loss of function of VHL protein (pVHL). In this particular cell line, the mutation on pVHL is found on the serine residue at position 64 which is substituted by a tryptophan. Such mutation affects the stability of the pVHL protein which in turn fails to degrade the hydroxylated HIF- $\alpha$  subunits under normoxic conditions, hence up-regulation of downstream hypoxia inducible genes due to ectopic accumulation of HIF- $\alpha$  subunits in the cells as a result (Maxwell et al., 1999; Prof. Eamonn Maher, Personal communication). Re-introduction of wild-type *VHL* gene through stable transfection in RCC4 cells restores the ability to regulate oxygen-dependent proteolysis of HIF- $\alpha$  subunits by ubiquitin proteasome and prevent up-regulation of hypoxia inducible genes under normoxic conditions as described in 1.7.3 (figure 1.7).

Therefore, to verify the two RCC4 cell lines used in this study, protein expression of the pVHL, HIF-1 $\alpha$ , and glucose transporter 1 (Glut-1) – a known marker of hypoxia – were examined by western blots. pVHL is only detected in RCC4 WTHA4 cells carrying a transfected wild-type *VHL* gene, designated “+*VHL* cells”, but not in the RCC4 VHA4 cells which just carry an empty vector, designated “*VHL* null cells”. Thus, the expression of HIF-1 $\alpha$  and its downstream target Glut-1 in the RCC4 +*VHL* cells are both down-regulated due to the restoration of the functional pVHL (Figure 6.1). Expression of cytoglobin was also examined. However, no basal cytoglobin expression is detected in both cell lines with the monoclonal antibody used in this experiment. Taken together, the results of western blots confirmed that the functions of pVHL is restored by the stable transfection in the RCC4 WTHA4 cells (+*VHL* cells), but not in RCC4 VHA cells (*VHL* null cells). Therefore, the two RCC4 cell lines can be

used subsequently in the pull down assays which is to mimic normoxic and pseudo-hypoxic conditions, respectively.

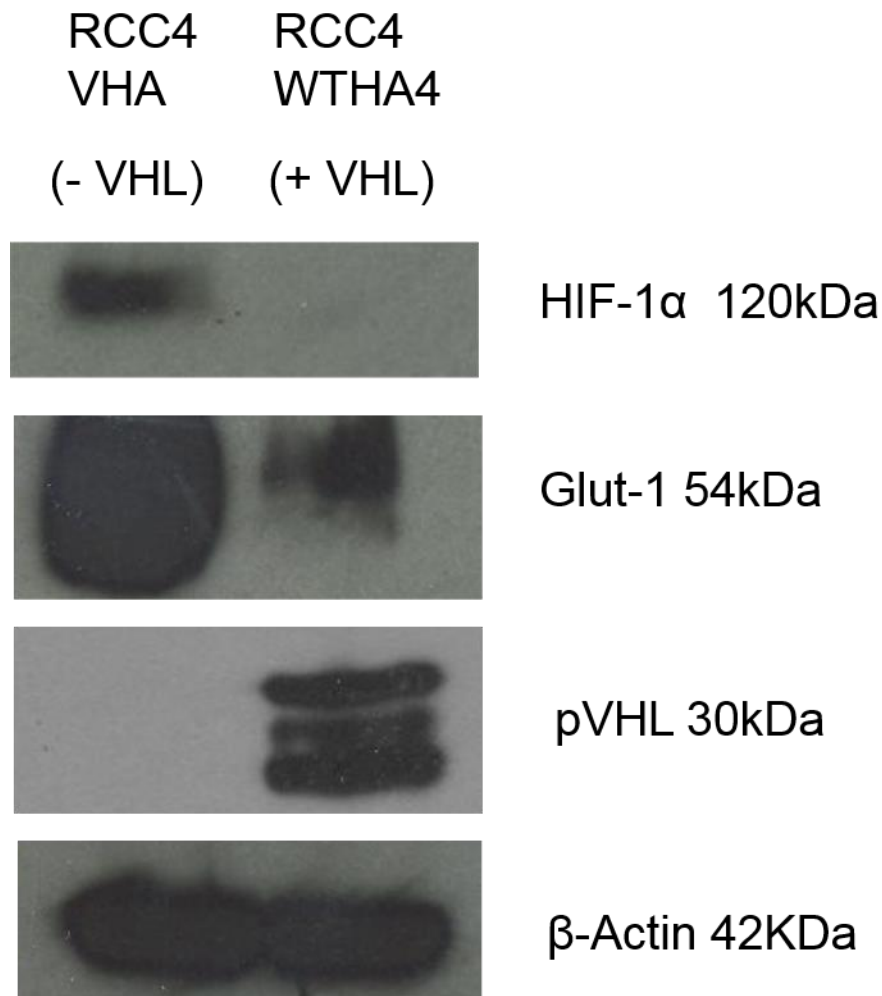


**Figure 6.1 Validation of RCC4 cell lines by detecting VHL protein re-expression and downstream HIF-1α signalling target.** 50 µg of cell lysate of each RCC4 cell line was detected by mouse monoclonal anti-human pVHL, mouse anti-human monoclonal glucose transporter-1, and mouse monoclonal anti-human HIF-1α antibodies. β-actin was used as a loading control to ensure equal loading between each sample, and was detected by mouse monoclonal anti-human β-actin antibody.

### 6.2.2 Restoration of *CYGB* gene Expression in RCC4 Cells by 5-aza-2'-deoxycytidine

*CYGB* gene was shown to be epigenetically down-regulated by hyper-methylation at its promoter region in a number of malignant cells that correlates with its suggested tumour suppressor role (McRonalD et al., 2006; Shivapurkar et al., 2008; Shaw et al, 2009; Oleksiewicz et al., 2013). Epigenetic down-regulation of TSGs, including cytoglobin, due to promoter hyper-methylation can be reversed by treatment with 5-aza-2'-deoxycytidine which inhibits the action of DNA methyltransferases (reviewed in Christman, 2002).

A suggested working concentration of the 5-aza-2'-deoxycytidine by the manufacturer is 5  $\mu$ M. To test whether the administration of the drug has any adverse effect on cell growth and proliferation, A MTT-cell viability assay was performed at the end of the drug treatment. Various concentrations of 5-aza-2'-deoxycytidine from 1  $\mu$ M to 100  $\mu$ M were added to the cells for 72 hours. No significant reduction of the cell viability after drug treatment was observed in both RCC4 sub lines even under high dosage (20 times more than suggested concentration) compared to their non drug-treated controls. This result indicates that the administration of 5-aza-2'-deoxycytidine at these levels had no adverse effect on the growth and proliferation of RCC4 cells (Figure 6.2). 5  $\mu$ M of 5-aza-2'-deoxycytidine was used in all the subsequent experiments unless otherwise stated.

The effects of de-methylation treatment on the steady state mRNA levels of several target genes of interest were examined at the transcriptome and proteome level by quantitative real-time RT-PCR (in collaboration with Dr. Damon Bevan) and western blot, respectively. In the presence of the de-methylating drugs, the mRNA level of *CYGB* is significantly elevated approximately 5-fold compared to their non-drug treated controls regardless of the pVHL status (Figure 6.3A; Ct values are provided in Appendix). Such increase in the gene expression level after the de-methylation treatment by 5-aza-2'-deoxycytidine is in an

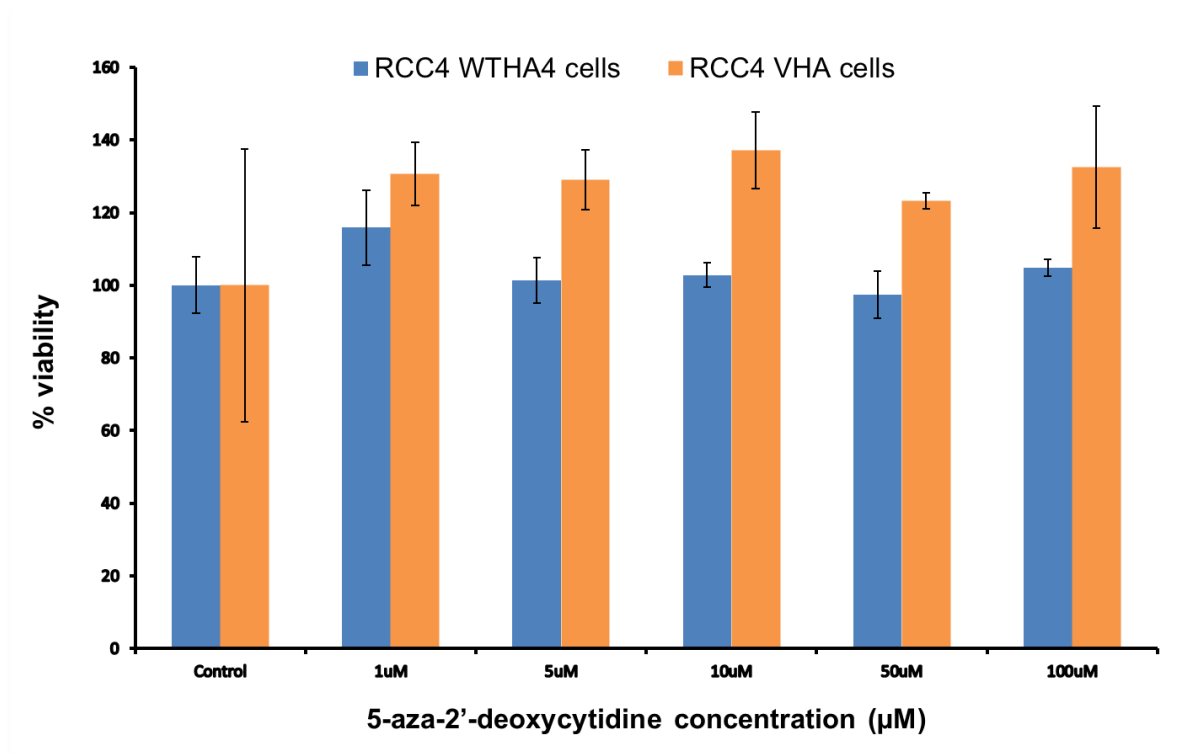
agreement with previous reports in other malignant cells (Shivapurkar et al., 2008; Shaw et al, 2009; Oleksiewicz et al., 2013) which support the idea that *CYGB* gene is a tumour suppressor gene which is down-regulated in cancer cells due to methylation at its promoter region. Notably, the demethylation treatment also causes a slight, but significant, increase in the expression of the *VHL* and *GLUT-1* genes. However, the increase in the mRNA level of *VHL* is only observed in the RCC4 +*VHL* cells, but not in the *VHL* null cells, whereas the increase in the mRNA level of *GLUT-1* gene is observed in both cell lines independent to the pVHL status just as the *CYGB* gene. Demethylation treatment has no effect on *HIF-1 $\alpha$*  gene expression at the transcriptome level.

Initial western blot experiments using a monoclonal anti human cytoglobin antibody which attempted to look at the basal expression of cytoglobin protein failed to detect any cytoglobin in both RCC4 cell lines where the *CYGB* gene is down-regulated due to DNA methylation as shown in the results of qRT-PCR. Although treatments with de-methylating drug caused a significant increase in the level of *CYGB* mRNA, no cellular cytoglobin was detected in both RCC4 cell lines in the western blot experiments on de-methylating drug treated samples, while only recombinant cytoglobin in control sample was detected (Figure 6.4A). Since poor immunoreactivity between antibody and antigen may be explanation, an alternative polyclonal antibody raised against human cytoglobin was used in the western blot experiments with the same set-up. However, in this case, the recombinant cytoglobin was not detected. Instead, a number of protein bands at high molecular region were observed in both cell lines, while no protein was detected as the expected molecular weight region of cytoglobin (~21 kDa) (Figure 6.4B).

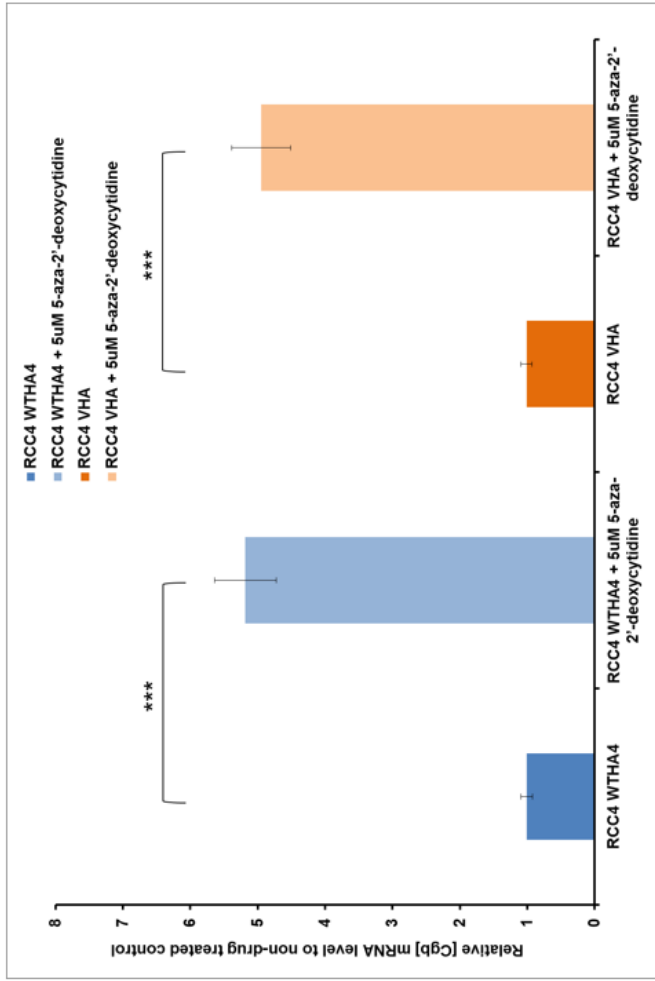
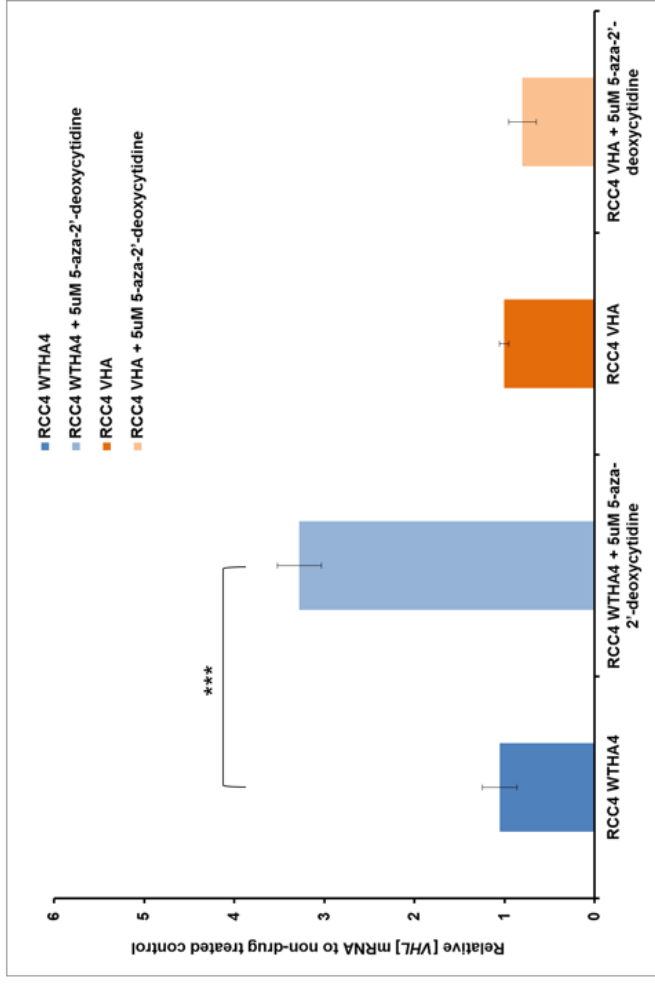
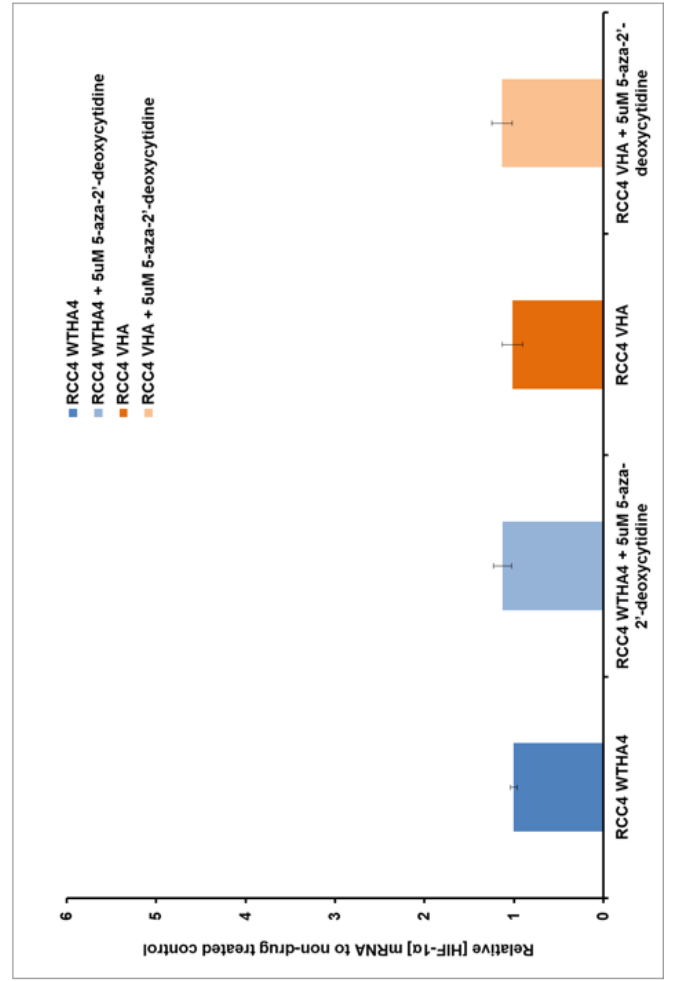
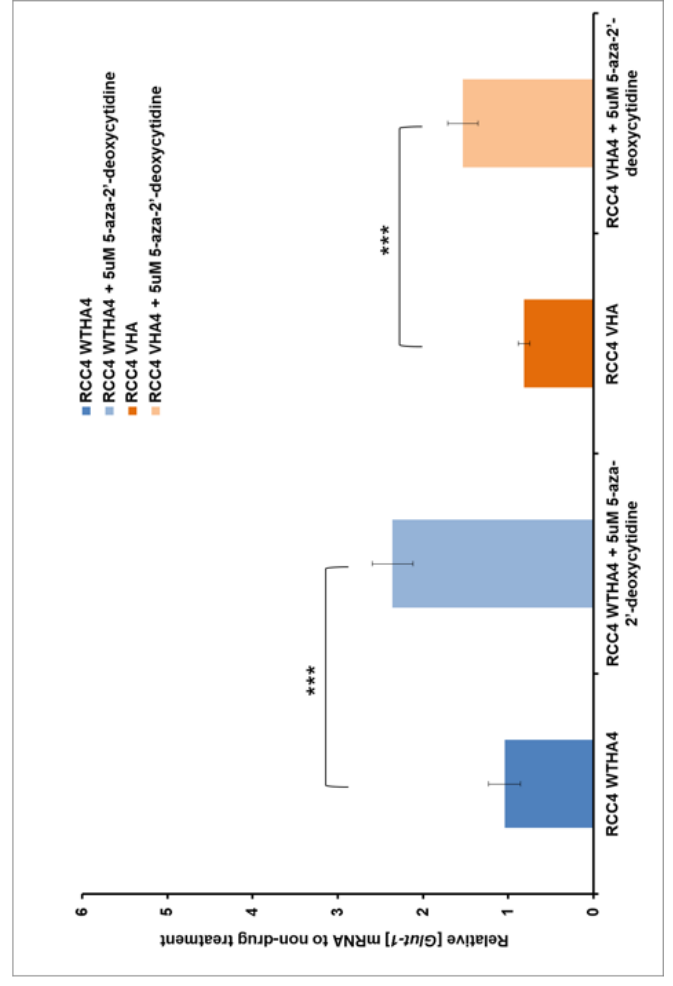
In order to determine whether the cytoglobin protein was masked in the cell lysates, a small amount (50 ng) of recombinant cytoglobin protein was added equally to the cell lysates

of both RCC4 cell lines. Surprisingly, the spiked recombinant cytoglobin in the cell lysate of *VHL* null cells disappeared and could merely be detected, while it remained detectable in the cell lysate of +*VHL* cells (Figure 6.4C). The same experiment was repeated under identical conditions and identical results obtained (data not shown). A possible explanation for these observations could be attributed to protein degradation in the *VHL* null cells as close examination of the lysis buffer used transpired that the lysis buffer contained a broad spectrum of proteinase inhibitors for most of the proteinases except for metalloproteinases. It is known that *VHL* null cells express higher levels of several metalloproteinases, including matrix metalloproteinases - 9 (Dr. Jelena Gavrilovic, personal communication) and thus it is possible that cytoglobin could be an unknown substrate of the metalloproteinases and subjected to degradation in the *VHL* null cells.

To block any undesirable metalloproteinases activities, 1 mM of EDTA was added to the lysis buffer in addition to the proteinase inhibitors. After addition of EDTA, the spiked recombinant cytoglobin could be detected in both RCC4 cell lines suggesting a protective effect (Figure 6.4D). However, since a control experiment in the absence of EDTA was not done in parallel and a repeated experiment failed to reproduce the same results (data not shown), it is not able to conclude the degradation of recombinant cytoglobin by matrix metalloproteinases. Since the cell lines had reached a higher passage by this time, the detection of cytoglobin protein was further explored in newly-thawed *VHL* null cells using cell lysates prepared in the presence or absence of EDTA. Moreover, cell lysates were incubated at different temperatures to test for a temperature-dependent enzymatic degradation. However, in this experiment, no degradation of cytoglobin was detected in the samples regardless of the presence or absence of EDTA and the temperatures (Figure 6.4E).



**Figure 6.2 MTT cell viability assays on de-methylation treatments by 5-aza-2'-deoxycytidine.** Both RCC4 WTHA4 (+VHL) and VHA4 (VHL null) cells were treated with demethylating drug, 5-aza-2'-deoxycytidine, for 72 hours at different concentrations within the range of 1 to 100 µM. Mean (n = 3, ± SEM) viability was normalized to control.

**A****B****C****D**

**Figure 6.3 Quantitative real-time RT-PCR measuring the steady state mRNA levels of of (A) CYGB, (B) VHL, (C) HIF-1 $\alpha$  and (D) Glut-1 in RCC4 cells, normalised to 18s levels in response to de-methylation (5-aza-2'-deoxycytidine) treatments.** Both RCC4 WTHA4 (+VHL) and VHA (VHL null) cells were treated with 5  $\mu$ M of de-methylating agent (5-aza-2'-deoxycytidine) for 72 hrs. Each bar represents mean  $\pm$  SEM (n=4) e. Fold change of mRNA level of were calculated using  $2^{-\Delta(\Delta CT)}$  method and presented as mRNA level relative to non-drug treated control cells. Statistical significance was calculated by two-tailed *t*-test. \*\*\* *P* < 0.01.

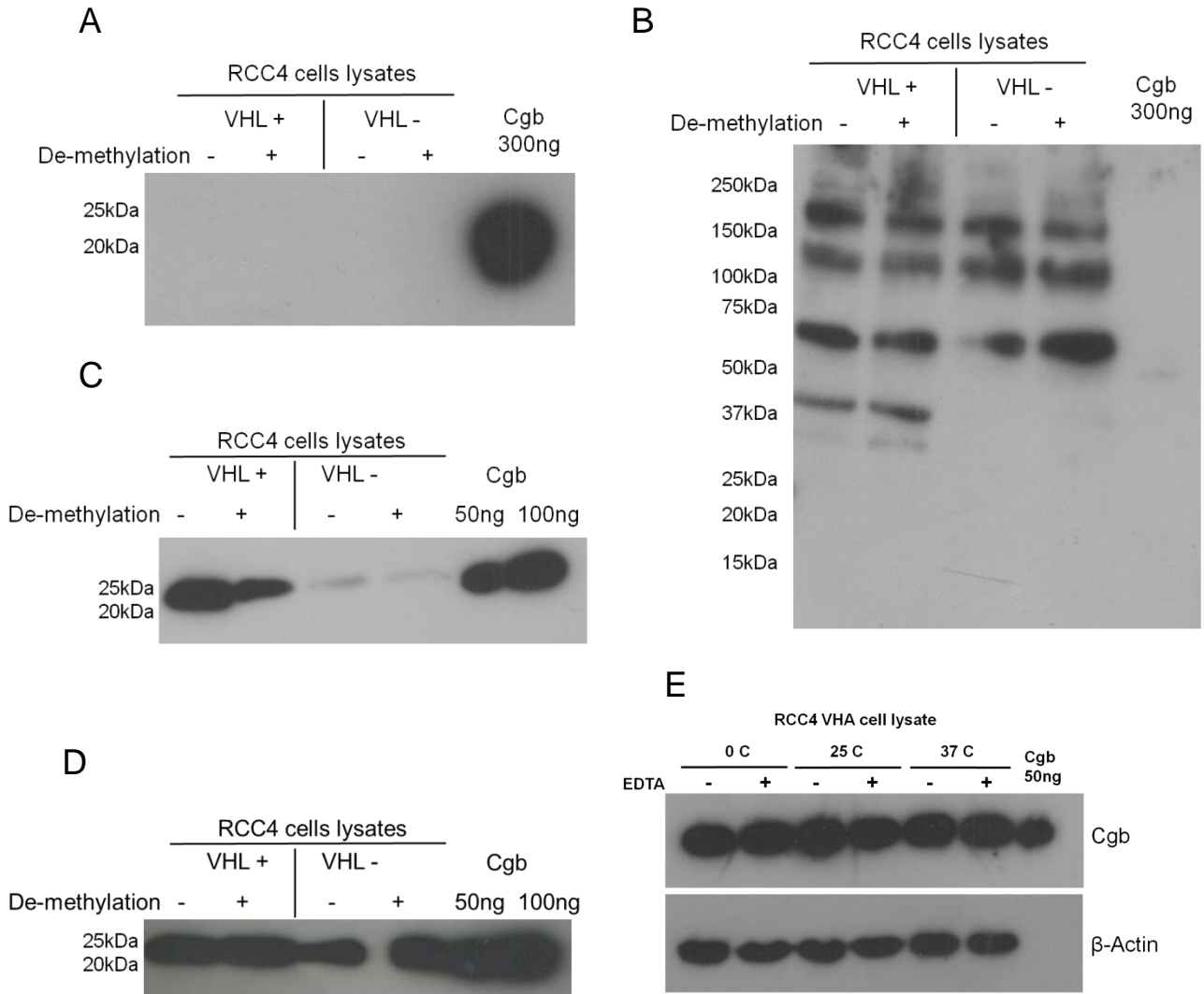


**Figure 6.4 Western blots measuring cytoglobin expression in RCC4 cells in response to de-methylation (5-aza-2'-deoxycytidine) treatments.** Both RCC4 WTHA4 (+VHL) and VHA4 (VHL null) cells were treated with 5  $\mu$ M of de-methylation agent (5-aza-2'-deoxycytidine) every 24 hours in a period of 72 hours. **(A)** 50  $\mu$ g of RCC4 cell lysate loaded, as indicated. 300 ng of recombinant cytoglobin protein was a positive control. Cytoglobin was detected by mouse monoclonal anti-human cytoglobin. **(B)** Blot incubated with mouse polyclonal anti-human cytoglobin. **(C)** 50 ng of recombinant cytoglobin protein was added each RCC4 cell lysate before loading to the gel. 50 ng and 100 ng of recombinant cytoglobin protein serve as positive controls for cytoglobin detection. Cytoglobin was detected by mouse monoclonal anti-human cytoglobin. **(D)** RCC4 cell lysates were prepared on lysis buffer in the presence of 1mM

EDTA. 50 ng of recombinant cytoglobin protein was added to each cell lysate sample before loading to the gel. 50 ng and 100 ng of recombinant cytoglobin protein serve as positive controls. Cytoglobin was examined under the same conditions as (C). (E) RCC4 VHA cell lysates prepared by lysis buffer with or without 1 mM EDTA. 50 ng of recombinant cytoglobin protein was added to each cell lysate sample and incubated at indicated temperatures (0 °C, 25 °C and 37 °C) for 5 min before loading on the gel. 50 ng of recombinant cytoglobin protein serves as a positive control. Cytoglobin was detected under the same conditions as (C) and  $\beta$ -actin was used as loading control.

### 6.2.3 Validation of Strep-tagged Cytoglobin

Cloning of strep-tagged cytoglobin expression plasmids has been described in 2.2.4 in which a piece of synthetic DNA fragment carrying a N-terminal strep(II)-tag sequence was cloned into the existing expression plasmids of both wild-type full length and truncated cytoglobin to express the recombinant strep-tagged cytoglobin for pull down assays. Protein expression and purification of the strep-tagged cytoglobin has been described in 2.3.7.

In order to confirm that the N-terminal strep-tag in the strep-tagged cytoglobin is functional, trial expression in *E.coli* and subsequent purifications using “strep-tactin” - an engineered strepavidin coated magnetic beads to “pull down” the target proteins from crude bacterial cell lysates were carried out. Both strep-tagged cytoglobins are expressed in bacteria as shown by the presence of protein bands at their expected sizes (Figure 6.5, lanes #1 and #3). Both strep-tagged cytoglobins are isolated from other bacterial proteins by the magnetic beads (Figure 6.5, lane#2 and #4). Therefore, the trial experiments provide evidence that the engineered cytoglobins contain a functional and intact N-terminal strep-tag which can be used for subsequent purification as well as pull-down assays. However to ensure that the addition of the strep-tag did not impact on other properties of the proteins, further characterisations of the purified proteins were necessary.

Both purified strep-Cgb and strep-Cgb $\Delta$ C proteins were examined by non-reducing SDS-PAGE with or without pre-incubation with DTT to assess the state of the intramolecular disulphide bond as shown in figure 6.6. As is the case for the non-tagged cytoglobin, both strep-tagged forms show a higher mobility when the disulphide bond is intact. The protein bands associated with strep-Cgb and strep-Cgb $\Delta$ C running with apparent molecular weights of approximately 19 kDa and 17 kDa, respectively. When the disulphide bond is reduced with DTT, the protein band of Strep-Cgb appears to run with a higher molecular apparent weight

than its non-tagged counterpart (*ca* 22 vs 23 kDa) which can be accounted for the addition of the strep-tag sequence (approx. 1 kDa). On the other hand, the protein band of strep-Cgb $\Delta$ C appears at approximately 19kDa which agrees as well to the calculated molecular weight of a truncated cytoglobin (Figure 6.6). Notably, in the strep-Cgb $\Delta$ C, a small fraction of disulphide bonds is readily reduced in the absence of DTT. However, this observation is unusual, yet, it is inconclusive to suggest that addition of the N-terminal sequence or deletion of the C-terminal domain would affect the formation of the intramolecular disulphide bond as these experiments were done based on only single batch of purified protein.

Further examinations by a combination of spectroscopies were performed to assess the effect of the addition of the N-terminal strep-tag sequence on biophysical properties of cytoglobin. UV/vis spectra of both non-tagged and strep-tagged cytoglobin in both ferric and ferrous states were compared. The ferric strep-tagged cytoglobin has very similar spectral features with the non-tagged cytoglobin in the ferric state with the Soret absorption maxima at 416nm,  $\alpha$ - and  $\beta$ -bands at 563 nm and 534 nm, respectively. The proteins were then reduced by dithionite. The strep-tagged cytoglobin in the deoxy-ferrous state also displays a similar spectrum to its non-tagged counterpart. In both cases the Soret peak is red-shifted (relative to the ferric state) to 428 nm with well resolved  $\alpha$ - and  $\beta$ -bands in the visible region (Figure 6.7).

The spin and ligation state of the heme iron in both full length and truncated strep-tagged cytoglobin in ferric state were assessed by room-temperature MCD and low-temperature X-band EPR spectroscopies and compared to their non-tagged counterparts described previously (Chapter 3). Compared to the non-tagged cytoglobin, the RT-MCD spectra of the two strep-tagged cytoglobins are broadly similar and consistent with a single low-spin ferric heme which indicate that the additional N-terminal strep-tag has not changed significantly either the oxidation or spin state of the heme iron in cytoglobin. However it is noted that the

MCD signal of the strep-Cgb in the region between 400nm to 420nm is slightly less intense. In comparison, the MCD signal of the strep-Cgb $\Delta$ C in this region is similar to that of the non-tagged cytoglobin. Moreover, the CT band in the strep-tagged cytoglobin is slightly shifted to 577 nm compared to 569 nm in the wild-type non-tagged cytoglobin (Figure 6.8). Since no indication of changing the spin-state is observed in the MCD spectra of the strep-tagged cytoglobin, it is therefore assumed that the effect of the addition of the N-terminal strep-tag is benign.

In the EPR spectra, both forms of strep-tagged cytoglobin also display the same low-spin trio ( $g = 3.21, 2.05$  and  $1.70$ ) that was described for non-tagged wild-type cytoglobin in chapter 3. This is in good agreement with the RT-MCD data and the heme iron being in the low-spin ferric state. Taken together, the RT-MCD and EPR data confirm that the addition of the N-terminal strep-tag has no significant effect on the spin and oxidation state of cytoglobin. However it is interesting to note that in the EPR spectrum of strep-Cgb $\Delta$ C, the minor high-spin signal ( $g = 5.95$ ) is greatly diminished compared to its non-tagged wild-type counterparts (Figure 6.9). Since the removal of the disulphide bond in cytoglobin has been shown to correlate with a disappearance of the sub-population high-spin species in the EPR spectra as described in the cysteine variants (Chapter 4), hence this observation in the EPR spectrum of Strep-Cgb $\Delta$ C is very likely due to the partial reduction of the disulphide bond in the samples as shown in the figure 6.6, although the reason for deletion of C-termini causing partial reduction is not clear. Conclusions should not be made from only one prep of strep-tagged cytoglobin.

Although detailed functional studies of the strep-tagged protein are lacking, it can still be assumed that the additional N-terminal strep-tag appears to have no significant adverse effects on the biochemical and biophysical properties of cytoglobin. Therefore, the strep-

tagged cytoglobins were used in the subsequent pull down assays as a bait protein to search for any cognate interacting partner(s) in RCC4 cells.

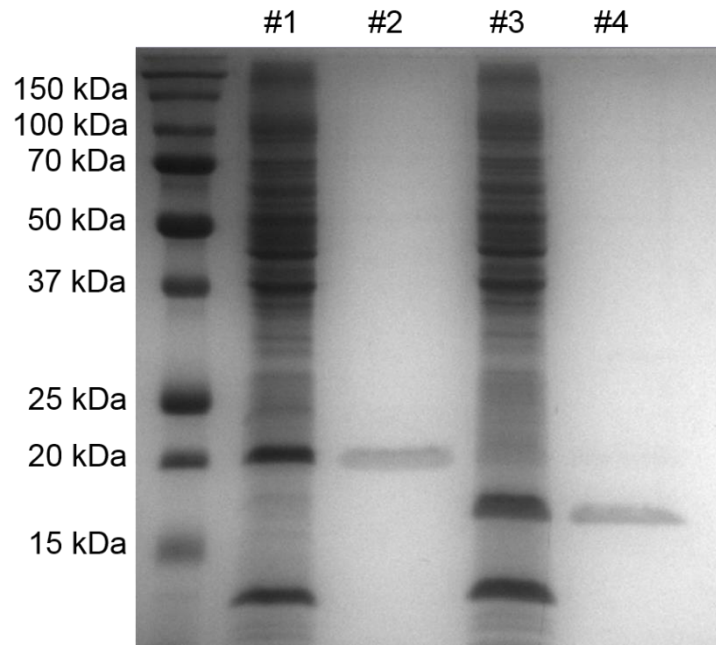


**Figure 6.5 Preliminary expression and purification test for strep-tagged cytoglobin proteins.** #1 = *E.coli* cell lysate containing over-expressed Strep-Cytoglobin, #2 = purified Strep-Cytoglobin eluted from magnetic beads, #3 = *E.coli* cell lysate containing over-expressed Strep-Cytoglobin $\Delta$ C, #4 = purified Strep-Cytoglobin $\Delta$ C eluted from magnetic beads. Samples were run in a 15% no-reducing gel.

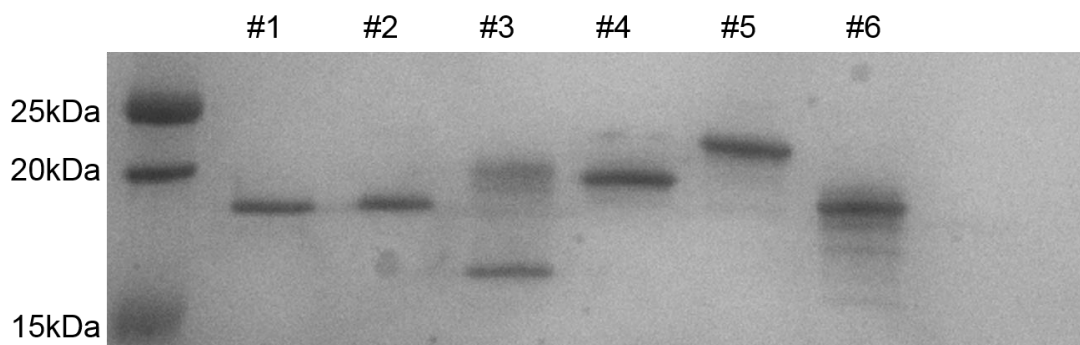


**Figure 6.6 The state of the disulphide bonds of strep-tagged cytoglobin on non-reducing gel.** #1 = wild-type Cytoglobin, #2 = Strep-Cgb, #3 = Strep-Cgb $\Delta$ C, #4 = wild-type Cytoglobin +10mM DTT, #5 = Strep-Cgb + 10Mm DTT, #6 = Strep-Cgb $\Delta$ C + 10mM DTT.

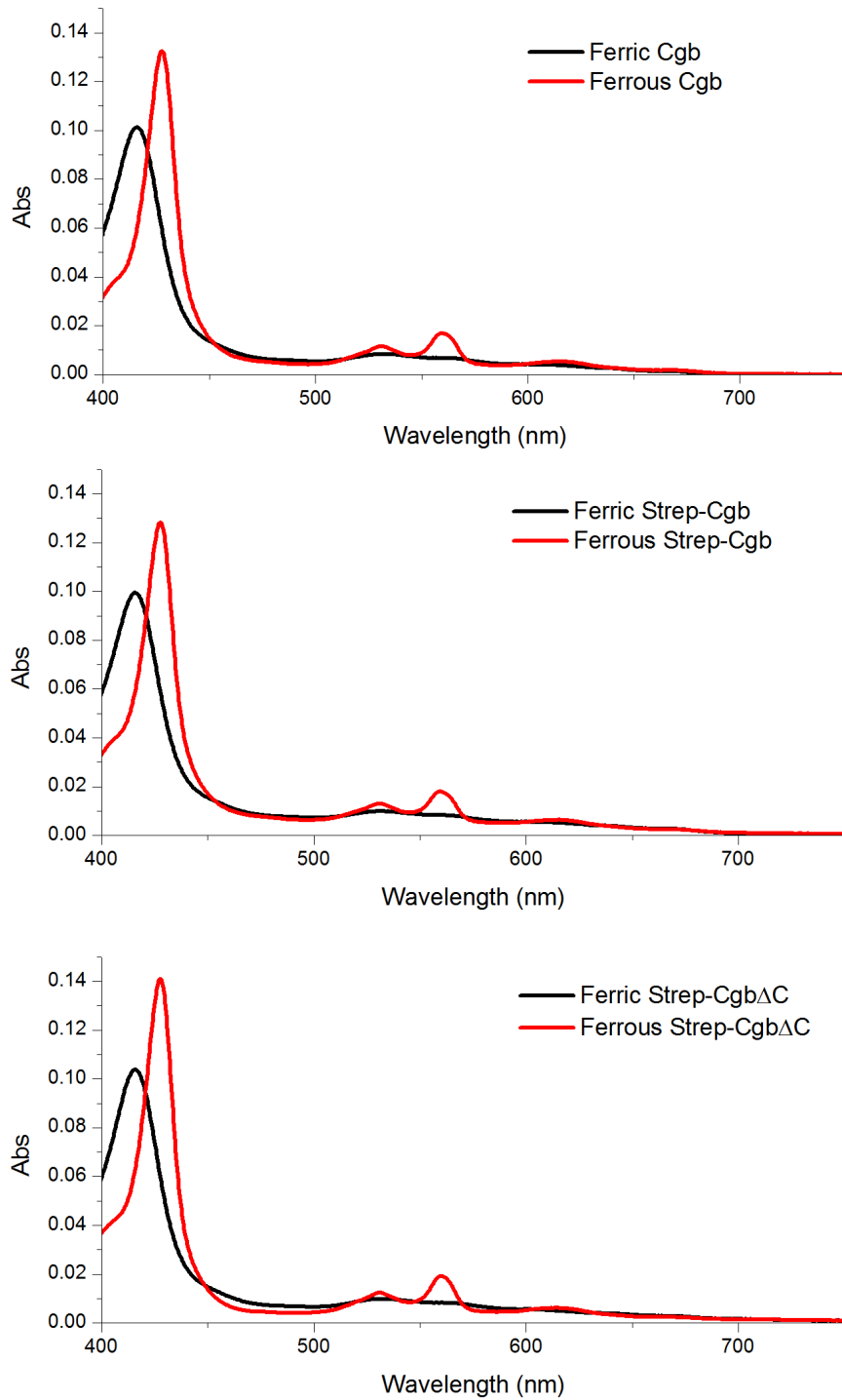


**Figure 6.7 Comparison of the electron absorption spectra of wild-type non-tagged cytoglobin and the strep-tagged cytoglobin in both ferric and ferrous states.** Wild-type cytoglobin and strep-tagged were reduced by mixing with tiny amount of solid sodium dithionite into approx. 5  $\mu$ M of protein solution in 20 mM Tris-HCl pH 8.0

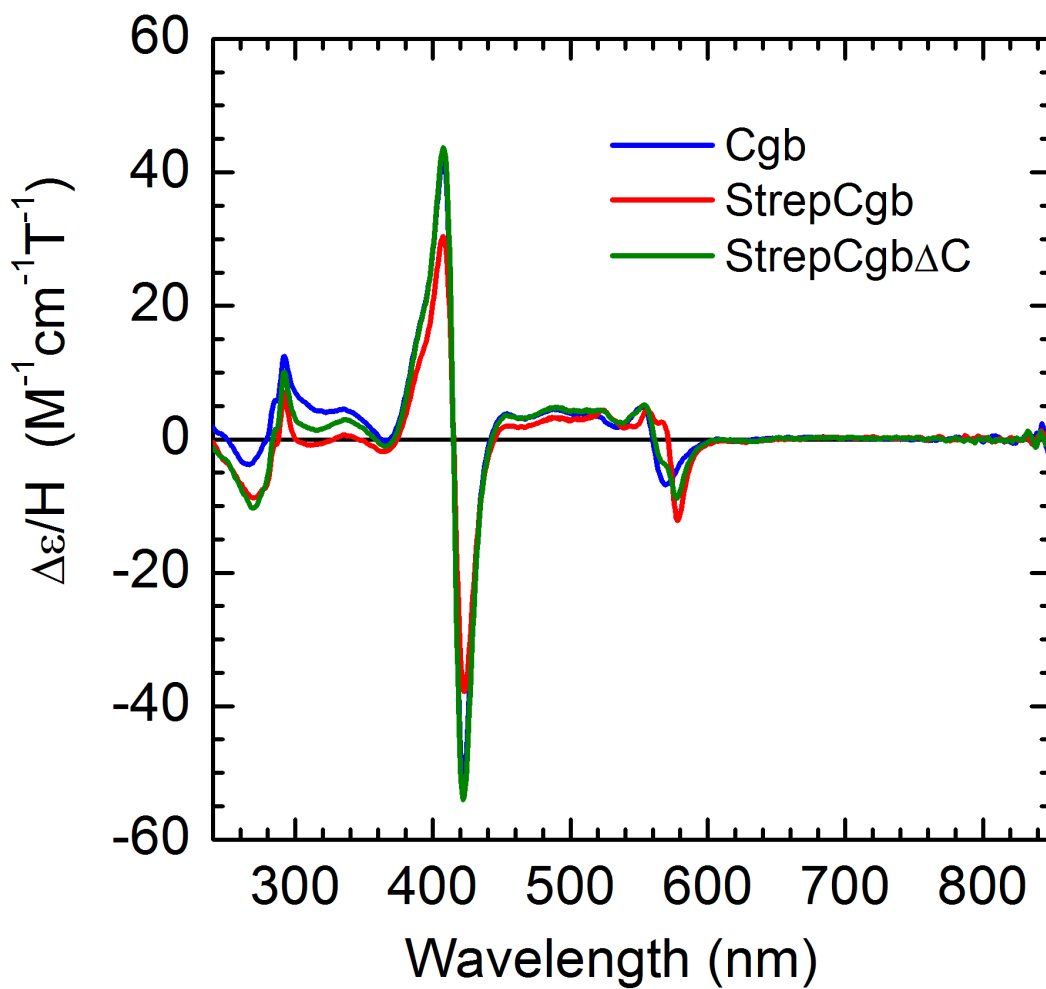


**Figure 6.8 Comparison of the spin and oxidation state of wild-type non-tagged cytoglobin and the Strep-tagged Cytoglobin in the room-temperature MCD spectra.** RT-MCD spectra of 150  $\mu$ M of wild-type cytoglobin (Blue trace), Strep-Cgb (red trace) and Strep-Cgb $\Delta$ C (Green trace) in 20 mM Tris HCl pH 8.0. MCD conditions: 298K 6T

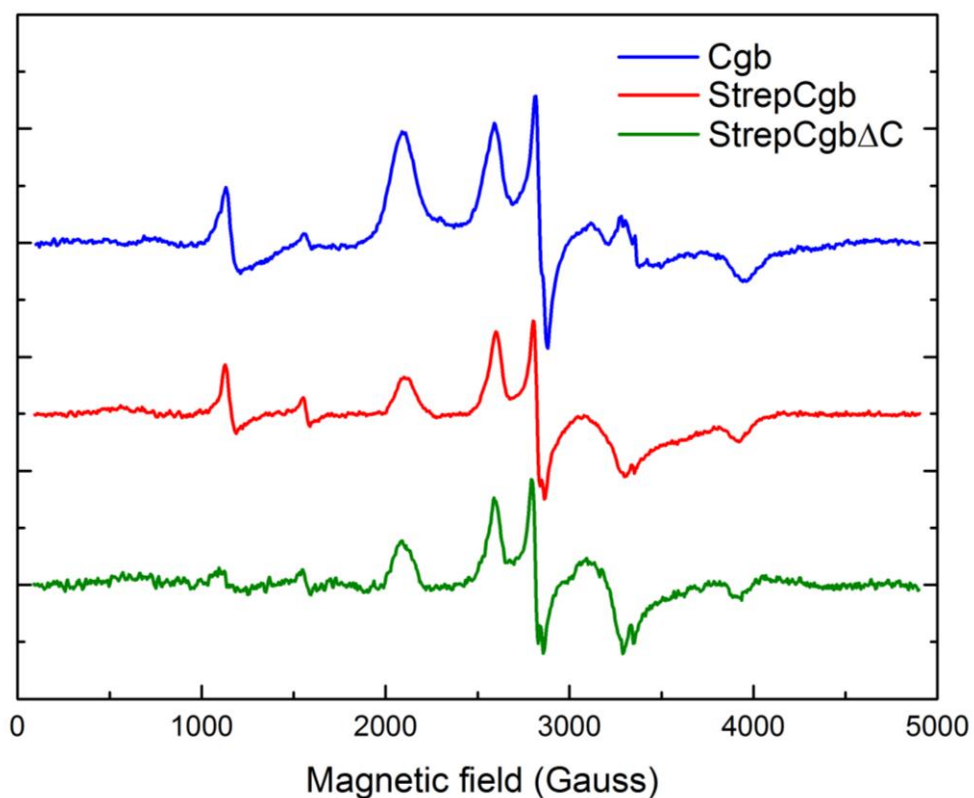


**Figure 6.9 Comparison of the spin state of wild-type non-tagged cytoglobin and strep-tagged cytoglobin proteins in Low-temperature EPR.** EPR spectra of approximately 150  $\mu\text{M}$  of wild-type cytoglobin (Blue trace), Strep-Cgb (Red trace) and Strep-Cgb $\Delta\text{C}$  (Green trace) in 20 mM Tris-HCl pH 8.0. EPR conditions: microwave frequency 9.35 GHz; microwave power 0.5 mW; temperature 11 k; modulation amplitude 10G

#### 6.2.4 Pull Down Assays in RCC4 Cells

A pull down assay was designed using recombinant strep-tagged cytoglobin as a “bait” protein to identify any interacting “prey” protein in the cancer cells which could confer cytoglobin’s tumour suppression activities. Before performing the pull down assay in the presence of RCC4 cell lysates, the binding of strep-Cgb to the magnetic beads and the elution of the strep-Cgb from the beads were first tested under different conditions to ensure that the detergent components in the lysis buffer have no adverse effect on such steps. Comparing the treatments with and without detergents, the addition of detergents only has a minor effect on the binding of the strep-Cgb to the magnetic beads as only a very small amount of strep-Cgb is left unbound in the buffer containing the detergents (Figure 6.10 lane #2 and #6). Regarding the recovery of the strep-Cgb from the magnetic beads (Figure 6.10 lane #3, #4, #7 and #8), the performance of protein elution was not affected by detergents (Figure 6.10). In the subsequent pull down assays in RCC4 cells, the elution of bound protein was achieved by d-biotin, rather than by desthiobiotin to ensure completed elution in one fraction since d-biotin has a much higher binding affinity to the strep-tactin beads than desthiobiotin.

In the pull down assays with RCC4 cells, 2 µg of strep-Cgb protein was added into fresh cell lysates and then incubated for 3 hours at 4 °C with agitation. After the incubation, no degradation of strep-Cgb protein was observed in both RCC4 cell lysates (Figure 6.11A #2; 6.11B #2). However, the identification of potential protein partners was hampered by non-specific binding of cellular proteins to magnetic beads especially at the high molecular weight region (Figure 6.11A #3; 6.11B #3). Comparing the two RCC4 sub cell lines, a faint protein band at ca 18 kDa was observed in the cell lysate of RCC4 + *VHL* cells as indicated by red arrow in the figure (Figure 6.11A #5), however, in RCC4 *VHL* null cells the corresponding band was not observed (Figure 6.11B #5). Hence, only the RCC4 WTHA4 cell line was selected for further investigations.

In order to identify any potential protein bands in the high molecular weight region where a lot of non-specific binding was apparent as shown in the figure 6.11, a better separation of the protein bands at high molecular weight region was achieved by separating proteins on gradient gels. Comparing the protein bands in the control lane (Figure 6.12 #3) to the pull down assay results of strep-Cgb (Figure 6.12 #5), no observable difference in the pattern of the protein bands was observed. Moreover, comparing the pull down assay results using strep-Cgb with the results using the truncated strep-Cgb $\Delta$ C, no observable difference in the pattern of the protein bands was observed as well (Figure 6.12 #5 and #7). However, it is of note that the faint protein band at ca 18 kDa which was observed previously was not observed in the 4-20% gradient gel because of the loss of the resolution at the low molecular region. A similar result was obtained using 8 to 16% gradient gels suggesting that the binding protein(s) were not likely to be in the high molecular weight region.

Since the disulphide bond of strep-tagged cytoglobin is reduced when the protein was incubated with the fresh cell lysates resulting in two protein bands on the gel, to avoid confusion when visualizing the potential binding proteins, the protein samples were run in a reducing gel in the presence of  $\beta$ -mercaptoethanol as shown in the figure 6.13. The faint protein band at ca18 kDa was observed again in the pull down assay (Figure 6.13 #5), and the same band was vaguely observed in the pull down assay using strep-Cgb $\Delta$ C (Figure 6.13 #7) indicated by the red arrows in the figure. Surprisingly, another protein band at ca 15 kDa which had not been seen previously when using non-reducing gels was now observed in the pull down assays indicated by the blue arrows (Figure 6.13 lane #5 and #7). Taken together, two potential proteins in RCC4 WTHA4 (+VHL) cells were found to be interacting with cytoglobin shown in the pull down assays. However, validating the results proved to be difficult due to poor signal-to-noise ratio of the gel imaging which may be due to the moderate detection limit of the Coomassie stain.

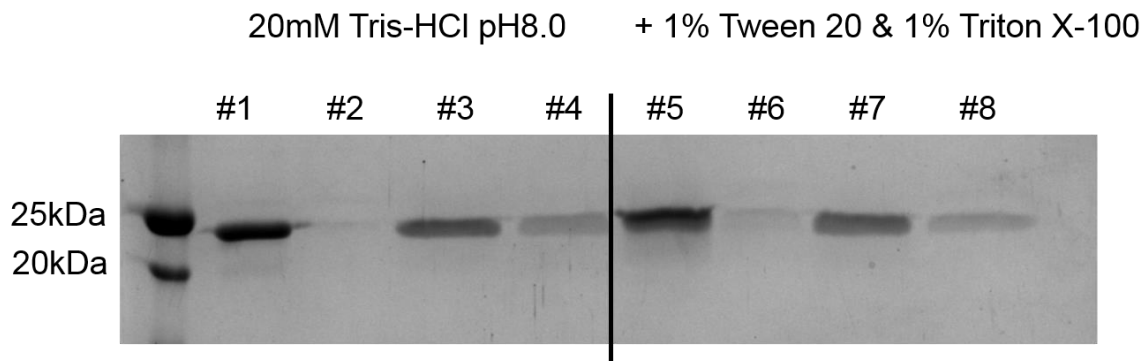


**Figure 6.10 Examining the effect of detergents on the binding and elution of strep-Cgb in pull down assays.** A representative gel showing the effect of the addition of the detergents on the binding and the elution of the strep-Cgb, #1 = 1  $\mu$ g of strep-Cgb in 20 mM Tris-HCl pH 8.0, #2 = unbound protein in the supernatant, #3 = 1<sup>st</sup> fraction of strep-Cgb protein eluted from the Strep-tactin magnetic beads by desthiobiotin, #4 = 2<sup>nd</sup> fraction of strep-Cgb protein eluted from the Strep-tactin magnetic beads by desthiobiotin, #5 1  $\mu$ g of strep-Cgb in 20 mM Tris-HCl pH 8.0 with 1% of tween 20 and Triton X-100, #6 = unbound protein in the supernatant, #7 = 1<sup>st</sup> fraction of strep-Cgb protein eluted from the strep-tactin magnetic beads by desthiobiotin, #8 = 2<sup>nd</sup> fraction of strep-Cgb protein eluted from the Strep-tactin magnetic beads by desthiobiotin.

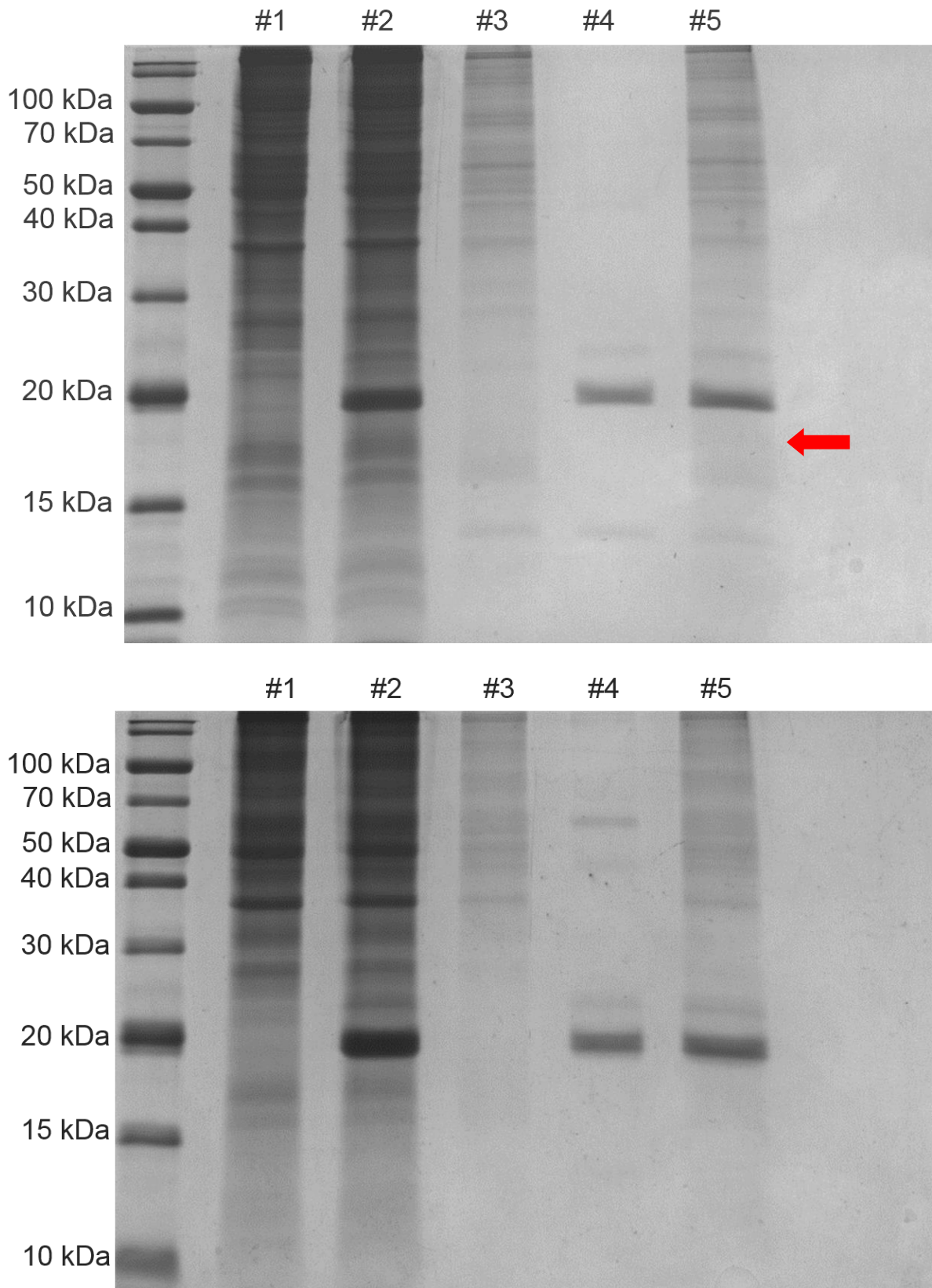


**Figure 6.11 Pull down assays in RCC4 cells. (A)** A representative non-reducing gel showing the results of pull down assay on RCC4 WTHA4 (+VHL) cells; #1 = A fraction of cell lysate, #2

= A same fraction of cell lysate spiked with 2  $\mu\text{g}$  of strep-Cgb, #3 = Eluted fraction (Cell lysate with Strep-tactin magnetic beads – non-specific binding control), #4 = Eluted fraction (2  $\mu\text{g}$  of strep-Cgb with strep-tactin magnetic beads – binding control) and #5 = Eluted fraction (Cell lysate + 2  $\mu\text{g}$  of strep-Cgb with strep-tactin magnetic beads – pull down experiment). The red arrow indicates the position of the protein band observed. **(B)** A representative gel showing the results of pull down assay on RCC4 VHL (VHL null) cells; 1 = A fraction of cell lysate, #2 = A same fraction of cell lysate spiked with 2  $\mu\text{g}$  of strep-Cgb, #3 = Eluted fraction (Cell lysate with Strep-tactin magnetic beads – non-specific binding control), #4 = Eluted fraction (2  $\mu\text{g}$  of strep-Cgb with strep-tactin magnetic beads – binding control) and #5 = Eluted fraction (Cell lysate + 2  $\mu\text{g}$  of strep-Cgb with strep-tactin magnetic beads – pull down experiment)

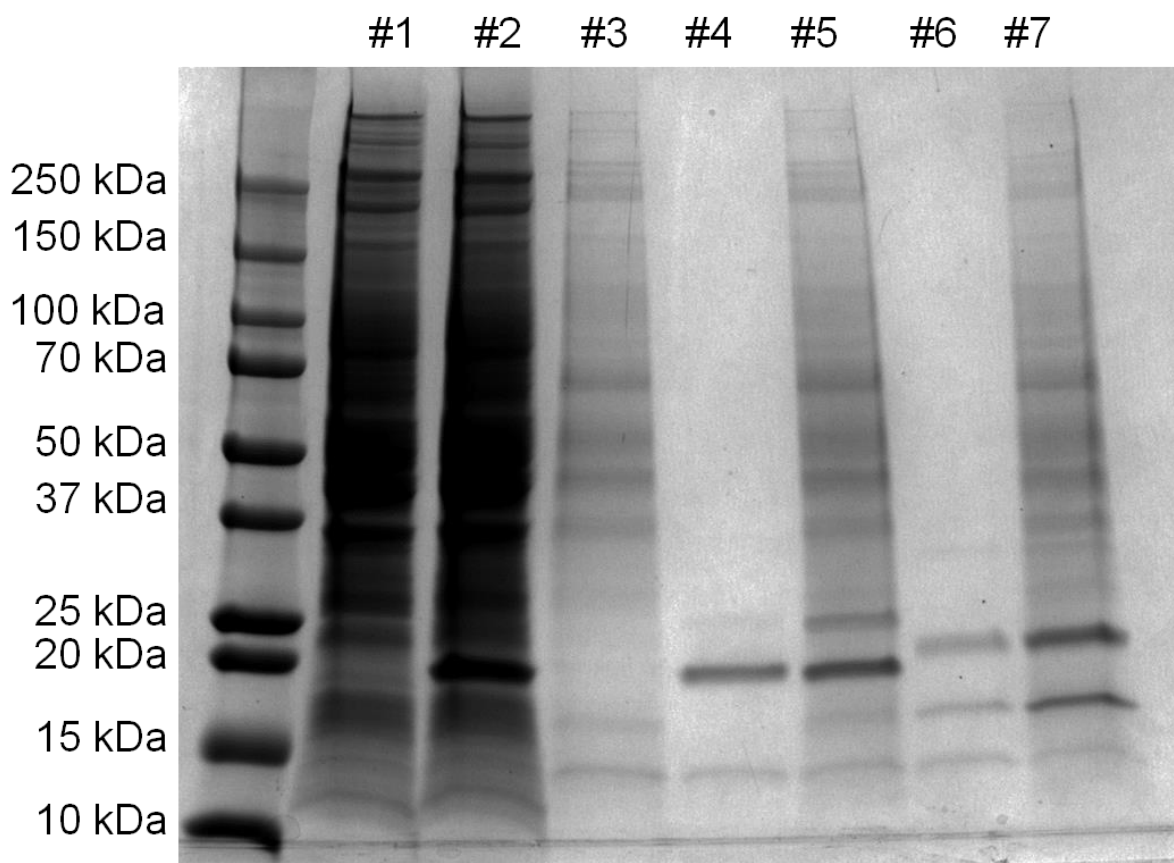


**Figure 6.12 Pull down assays in RCC4 cells in 4-20% gradient gels.** A representative non-reducing 4-20% gradient gel showing the results of pull down assay on RCC4 WTHA4 (+VHL) cells; #1 = A fraction of cell lysate, #2 = A same fraction of cell lysate spiked with 2 µg of strep-Cgb, #3 = Eluted fraction (Cell lysate with Strep-tactin magnetic beads – non-specific binding control), #4 = Eluted fraction (2 µg of strep-Cgb with strep-tactin magnetic beads – binding control), #5 = Eluted fraction (Cell lysate + 2 µg of strep-Cgb with strep-tactin magnetic beads – pull down experiment), #6 = Eluted fraction (2 µg of strep-CgbΔC with strep-tactin magnetic beads – binding control) and #7 = Eluted fraction (Cell lysate + 2 µg of strep-CgbΔC with strep-tactin magnetic beads – pull down experiment).

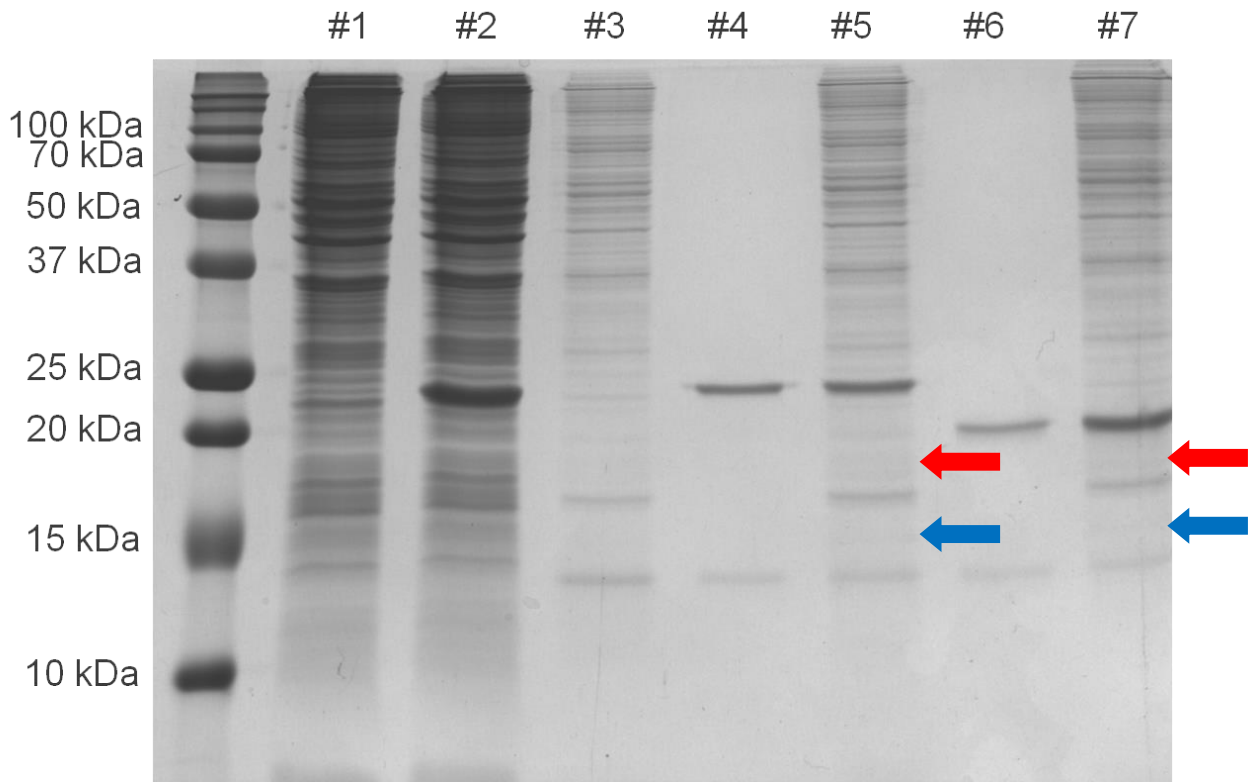


**Figure 6.13 Pull down assay in RCC4 WTHA4 (+VHL) cells in reducing gel.** A representative SDS gel showing the results of pull down assay on RCC4 WTHA4 (+VHL) cells; #1 = A fraction of cell lysate, #2 = A same fraction of cell lysate spiked with 2 µg of strep-Cgb, #3 = Eluted fraction (Cell lysate with Strep-tactin magnetic beads – non-specific binding control), #4 = Eluted fraction (2 µg of strep-Cgb with strep-tactin magnetic beads – binding control), #5 = Eluted fraction (Cell lysate + 2 µg of strep-Cgb with strep-tactin magnetic beads – pull down experiment), #6 = Eluted fraction (2 µg of strep-CgbΔC with strep-tactin magnetic beads – binding control) and #7 = Eluted fraction (Cell lysate + 2 µg of strep-CgbΔC with strep-tactin magnetic beads – pull down experiment). The red arrow and the blue arrow indicate the position of the protein band at ca18 kDa and ca15 kDa, respectively.

### 6.3 Discussion

In this study, the *CYGB* gene was shown to be down-regulated in clear cell renal carcinoma (RCC) cells under an epigenetic control of DNA methylation which could be subsequently restored by applying de-methylation drugs to the cells. This finding confirms and extends previous results in oral tumours (Shaw et al., 2006; Shaw et al., 2009). The 5-fold increase in the steady state mRNA levels for *CYGB* after de-methylation treatment was independent of pVHL status of the cells. Since *CYGB* has been shown to be up-regulated by hypoxia under the control of the HIF signalling pathway (Emara et al. 2010; Gorr et al., 2011; Shaw et al., 2009), one would expect that the expression of *CYGB* gene should be high in RCC4 cells under normal circumstances, especially in the *VHL* null cell line where the HIF-1 $\alpha$  is stabilized due to the loss of functional pVHL. Interestingly, our results do not support such a notion. When the mRNA expression level of *CYGB* gene was normalized against the mRNA expression level in control *VHL* null cells, a significant difference in the basal *CYGB* mRNA level between the two RCC4 cell lines was observed. The mRNA level in the *VHL* null cells is found to be 50% less than that in the RCC4 + *VHL* cells where a functional VHL protein is restored (see Appendix). A similar result showing a difference in the basal mRNA level between the two RCC4 cell lines was also observed in the report published by Gorr and colleagues, although the difference in the level of expression is much greater compared to this study. Such observation on the difference in the basal level of *CYGB* gene expression is unusual which may imply that there is an indirect transcriptional activation of *CYGB* gene caused by the tumour suppressor protein VHL and/or its downstream signalling pathway which contributes to the variation in the basal expression of *CYGB* gene between the two cell lines.

The exact role of cytoglobin in cancer cells is still unclear. Current knowledge on cytoglobin suggested that it may possess a bimodal function in the cancer cells based on the gain-and-loss of function studies under different conditions. Cytoglobin has tumour suppressor

gene properties indicated by inhibition of cell proliferation as well as reduction in migration of tumour cells under normoxia (Shivapurkar et al., 2008; Oleksiewicz et al., 2013). On the other hand, cytoglobin could protect cancer cells from oxidative insults and promote tumourigenesis during stress conditions, such as under hypoxia (Oleksiewicz et al., 2013). Although cytoglobin expression is shown to be up-regulated under hypoxia and anoxia apparently by activated HIF signalling pathway (Fordel et al, 2004 & 2007; Emara et al, 2010; Gorr et al, 2011; Guo et al, 2007), other pathways may be implicated. Singh and colleagues demonstrated that, in cardiomyocytes, there is a more complex transcriptional activation pathway of *CYGB* gene by transcriptional factors other than HIF-1 $\alpha$ , such as nuclear factor of activated T-cell (NFAT) and AP-1 which are under the influence of an action of a phosphatase, called calcineurin during hypoxia (Singh et al., 2009). Whether or not this is also true in the cancer cells would require further investigation. Nonetheless, our data obtained from the RCC model could provide a clue here that activation of *CYGB* gene is not as simple as initially hypothesised since stabilization of HIF-1 $\alpha$  in *VHL* null cells had no promotional effect on *CYGB* gene expression even after de-methylation and also the fact that the highest *CYGB* gene expression is actually found in the cells transfected with VHL protein. Future studies should focus on elucidating the exact molecular mechanism of the activation of *CYGB* gene under different conditions.

Although a correlation between the methylation state and the expression level of *CYGB* gene in cancer has been established in a number of malignancies including the sporadic squamous cell oesophageal cancer cells (McRonald et al., 2006), breast and lung cancer cells (Shivapurkar et al., 2008), and head and neck cancer cell lines (Shaw et al., 2009), the possible interplay between the methylation state of *CYGB* gene and how it might respond to the tumour microenvironment during tumourigenesis, such as tumour hypoxia, has not been examined in details. Interestingly, Vanharanta and colleagues have recently demonstrated in another renal carcinoma cell line (786-O) that several downstream targets of the HIF signalling

pathway are selectively regulated by epigenetic alterations during tumour progression. Some of them are responsible for metastasis and survival of the RCC cancer cells (Vanharanta et al., 2013). One of the VHL-HIF driven pro-metastatic genes examined in the study is cytohesin-1 interacting protein (CYTIP) which has been shown to enhance AP1 transcriptional activities and regulate cell adhesion and migration. Since AP1 has been shown to activate cytoglobin expression under hypoxia (Singh et al., 2009), it would be interesting to postulate that the *CYGB* gene may be down-regulated in primary tumour cells due to epigenetic control by DNA methylation as shown in this chapter, but gradually up-regulated due to changes in the epigenetic alteration which is exploited by the metastatic cancer cells during tumour progression as one of the pro-metastatic genes which would provide the metastatic cells a survival advantage under stress conditions during further tumourigenesis.

A Pull down assay using a recombinant cytoglobin engineered with a strep-tag sequence imbedded in the N-terminal extension of the protein was designed in an attempt to search for potential interacting protein(s) in cancer cells which might provide vitally important information for unravelling the novel cell signalling role of cytoglobin. To date, there is no study examining the possible interacting protein(s) with cytoglobin available in the literature, even though the disordered C-terminal extension has long been hypothesized to be a potential binding site for interacting proteins, for example protein partners that have DNA binding ability (Geuens et al., 2003). Therefore, the significances of this part of the study are mainly two-fold. First, a method was set up and tested for looking at the potential interacting protein(s) of cytoglobin in the culture cells. Second, this study provided some preliminary results for the discovery of potential interacting partner(s).

In the pull down assays, two potential interacting proteins were only observed in the cell lysate of +*VHL* cells that co-eluted with the strep-tagged cytoglobin. While in the *VHL* null cells,

those proteins were not co-eluted with the strep-tagged cytoglobin in the pull down assays. It demonstrates that the interacting partners of cytoglobin may not be constitutively expressed in the RCC4 cells. Instead, given that the presence of the protein bands seems to be dependent on the pVHL status of the cells, the interacting partners could also be under the same cell signalling control of cytoglobin in the case of RCC4 cells. However, the amount of the interacting protein eluted from the pull down assay was very low, such that it could hardly be seen by conventional Coomassie blue staining. It might suggest that either the expression level of the interacting proteins is low or the binding of the interacting proteins to the strep-tagged cytoglobin is weak. In the first case, alternative methods to increase the expression level might be used. For example, adding extra growth factors to the culture cells to boost the protein expression level. While in the latter case, generating covalent interaction between the interacting proteins and the strep-tagged protein by adding cross-linking agents to the cell lysate might help to improve the results in the pull down assay, although some non-specific or undesired interactions may cause false-positive results.

Interestingly, Singh and co-workers reported that the GFP-tagged cytoglobin was found to be in both the nucleus and cytoplasm, while mutations at the two histidines (His81, His113) and the single cysteine (Cys38) abolished the nuclear localization in myogenic progenitor cells (Singh et al., 2013) which implies that one of these amino acid residues could be crucial to the translocation of cytoglobin in the cells. Since the two histidine residues reside in the inner heme pocket and are coordinating to the heme cofactor, it is very unlikely that they are involved in interactions with other proteins. On the other hand, the two cysteines residues in cytoglobin have been shown to respond to changes in the redox potential of solution where they existed as free cysteines, or being reduced, when the redox potential shifts to a more negative side (chapter 3.2.4). A similar observation was observed during the pull-down assay when the strep-tagged cytoglobin was incubated with the cell lysate where the redox state is believed

to be reducing due to a presence of GSH/GSSG couple and other cellular redox couples. Thus, it is plausible to suggest that the free cysteine residue, in particular the Cys38, may play an additional role besides controlling the ligand binding property of cytoglobin by forming intra-molecular disulphide bond with Cys83 residue, but also contributing to the interaction between potential binding partner(s), for example a nuclear translocator, via an inter-molecular disulphide bond. Therefore, it would be interesting to examine whether the free cysteine residue at Cys38 would be involved in the binding to the interacting proteins by pre-incubating the strep-tagged cytoglobin with reducing agents, such as DTT, TCEP and GSH, before the pull down assays or generating a strep-tagged cytoglobin variant with a disrupted disulphide bond (i.e. Strep-CgbC83S).

In summary, several promising and interesting observations regarding cytoglobin in cancer cells were presented in this chapter. *CYGB* gene was shown to be down-regulated in RCC4 cell lines under epigenetic control by DNA methylation which is consistent with its potential TSG role in cancer. Moreover, an interesting initial observation was made regarding the potential degradation of cytoglobin protein in the *VHL* null cells. However, this finding was not reproducible but the possibility remains that under certain conditions cytoglobin may be susceptible to metalloproteinase-mediated degradation and future studies are necessary to explore this further. Finally, two potential protein partners were co-eluted with cytoglobin in the preliminary pull down assays which suggest an existent of putative binding partners. Further study will be needed to improve the detection quality of the gel-based pull down assays and to validate this result to confirm the protein-protein interacting.

## Chapter 7: General discussion

### 7.1 Oligomeric State and Disulphide bond of Cytoglobin

Conventional views on the functions of globins have been changed greatly since the discoveries of a number of new members within the globin superfamily from different organisms over the past fifteen years (reviewed in Burmester and Hankeln, 2014). A lot of efforts have been made by researchers worldwide to delineate different physiological roles of each new member of the globins. Among the newly discovered globins, human cytoglobin, which is the subject of this study, is at the centre of attentions for two reasons. Firstly, it is ubiquitously expressed in a wide range of tissues (Trent and Hargrove, 2002; Burmester et al., 2002). Secondly, it is the first vertebrate globin to be related with pathological conditions, such as organ fibrosis (Nakatani et al., 2004) and certain types of cancer (Shaw et al., 2009; Oleksiewicz et al., 2013) in which cytoglobin may play a crucial role in disease progression. The underlying aims of this study were to investigate a structure-to-function relationship of cytoglobin with the use of advanced biochemical and biophysical methods and also to search for novel interacting partner in cancer cells with the use of pull down assays. Hence, the results presented in this study may provide very useful information about the potential mechanisms of cytoglobin to function as a tumour suppressor protein in cancer cells.

The first research question addressed in this study was about the oligomeric state of human cytoglobin. Although crystallographic studies have shown that cytoglobin exists as a homo-dimer in which the two monomers are linked by an inter-molecular disulphide bond (Sugimoto et al., 2004, Makino et al., 2011), such a prediction of the dimeric state would be of little physiological relevance due to two reasons: First, the formation of inter-molecular disulphide bond would not be favoured by the the presence of high amount of a number of redox couples in the cells, such as GSH/GSSG which could reduce the disulphide bond as

shown in section 3.2.2. Second, a much lower protein concentration in the cells compared to the experimental conditions in crystallography means that any undesirable interaction with other monomeric cytoglobin is prevented and thus it would be conceivable to suggest that formation of an intra-molecular disulphide bond would be more favourable than inter-molecular disulphide bond under this circumstance. Indeed, it has been clearly shown in chapter 3 that the wild-type recombinant cytoglobin purified from the soluble fraction appears to exist as a monomer in non-reducing SDS-PAGE with an intra-molecular disulphide bond formed between Cys38 and Cys83, although an apparent dimer-like molecular weight is observed in analytical gel filtration experiments described in section 3.2.3 which led us to speculate an alternative dimeric interaction exists via other parts of the protein (e.g. the N-termini). This, the physiologically relevant oligomeric state still need to be defined.

Due to the fact that the redox potential in the cells is governed by the relative ratios of the reduced and oxidized species of more than one single redox couple, including GSH/GSSG, cysteine/cystine, thioredoxin, etc, it is therefore impossible to determine a definitive redox potential in the cells. However, for simplicity, since the GSH/GSSG couple is the most abundant redox couple which directly involves in intracellular redox homeostasis in the cells, it could be assumed that the relative ratio of intracellular GSH/GSSG could reflect the ambient redox potential in the cells. According to this assumption, the redox potential of normal cells would be estimated at the region of -240 mV to -200 mV, while redox potential would shift towards a more positive potential, at around -170 mV, when the cells are undergoing apoptosis (Schafer and Buettner, 2001). Furthermore, the redox potential also vary in different compartments within the cells. The redox potentials of the cytoplasm, nucleus and mitochondria, are reported to be -280 mV, -300 mV and -340 mV, respectively based on the relative ratio of the thioredoxin couple (Kemp et al., 2008). Hence, the redox potential of a thiol/disulphide couple has to be near the range of the ambient redox potentials in order to be

considered as physiologically significant. Based on the fact that the redox potential of the thiol/disulphide couple of cytoglobin (-280 mV) falls well into the reported range of the ambient redox potential in the cells, it is plausible to suggest the biological role of the two cysteine residues in cytoglobin to be a redox switch which regulates cytoglobin's function – most likely affecting the ligand accessibility to the heme cofactor which is shown in chapters 4.2.2 and 5.2.8, in response to changes in the cellular redox potential.

Regarding the state of the disulphide bond under the ambient redox potential *in vivo*, it is generally accepted that the disulphide bond should be reduced, or at least partially reduced, as in the free cysteine residue in the cytoplasm. However, there is currently no available data to show the actual state of the disulphide bond of cytoglobin *in vivo*. Therefore, to conclude that the cysteine residues in cytoglobin functions as a redox switch, one should compare the ratio of oxidized (disulphide bond) and reduced (free thiol) cysteine in the cytoglobin under different physiological conditions which exhibit different cellular redox potentials, such as hypoxia and oxidative stress. The measurement of the ratio of oxidized/reduced cysteine residues can be achieved by using isotope-coded affinity tag (ICAT) method to trap the cysteine residues and subsequently quantify the amount of the ICAT labelled oxidized and reduced cysteine by using tandem mass spectroscopy (Ragsdale and Li, 2011)

## **7.2 S-glutathionylation of Cys83 and Oxidative Stress**

A number of studies have demonstrated that expression of cytoglobin in the cells is correlated with the cellular stress conditions, including hypoxia (Fordel et al., 2004; Schmidt et al., 2004; Mammen et al., 2006; Shaw et al., 2009; Emara et al., 2010) and oxidative stress (Chua et al., 2009; Basu et al., 2012). In these circumstances, cytoglobin is reported to play a protective role against cellular damage caused by free radicals, such as reactive oxygen

species including hydrogen peroxide (Fordel et al., 2007; Li et al., 2007; Hodges et al., 2008; McRondal et al., 2012). However, no appreciable enzymatic activity towards the reactive oxygen species has been observed in recombinant cytoglobin (Trandafir et al., 2007) which argues against its physiological role as an effective scavenger for reactive oxygen species. Interestingly, reactive oxygen species have been implicated as secondary signalling molecules which are involved in redox signalling pathways, such as oxidative modification of cysteine residues in redox sensitive proteins (Reviewed in Carter and Ragsdale, 2014). Such a oxidative modification of the cysteine residues may promote a further modification by GSH/GSSG via thiol/disulphide exchange (Grek et al., 2013).

The potential of the two cysteine residues of cytoglobin to respond to changes in the cellular redox environment by forming a disulphide bond *in vitro* was demonstrated in chapter 3. However, in the presence of other complex redox systems, instead of simply forming intramolecular disulphide bond as an immediate response to a change in the cellular redox environment, further modification of the thiol groups, driven by the reactive oxygen species, is also possible, especially if the cysteine residue is surrounded by the basic residues Arg, Lys or His which tend to promote deprotonation of the thiol to form a more reactive thiolate ion (Grek et al., 2013). Interestingly, the cysteine at position 83 (Cys83) in cytoglobin exists in such a basic environment as shown in figure 7.1D.

At the end of chapter 4, it was suggested that GSH could modify the free cysteine residues of cytoglobin which in turn could influence the ligand binding properties of cytoglobin. During the course of this study, I have attempted to further understand the effect of GSH on cytoglobin and this work yielded some unexpected observations. Prolonged incubation of cytoglobin in buffer containing a high concentration of GSH (50 mM) causes a dramatic decrease in the Soret region in the UV/vis spectrum similar with that observed in H81F shown

in chapter 4.2.5 (Figure 7.1A). Such an effect was further explored in the two cysteine variants (C38S and C83S) each of which leaves a single defined cysteine free to react with glutathione. In principle, treating the two cysteine variants with GSH should have no effect unless the thiol group of the cysteine is deprotonated to become reactive. Surprisingly, a similar spectral change was observed in the C38S variant (in which the cysteine at position 83 remains), but not in the C83S variant (Figure 7.1B and C). These observations suggest that the spectral change is not caused by the reduction of a disulphide bond. Instead, it should be an effect exerted on the Cys83 residue by GSH. Since the Cys83 residue is at the proximity of the distal heme pocket (on helix E where it is one residue apart from the distal heme ligand (His81)), such an effect seems to subsequently change a local environment of the heme iron which is reflected on the UV/vis spectrum.

The effect of GSH on the Cys83 residue was further investigated by prolonged treatment of the C38S variant with GSH at different concentrations. Interestingly, the extent of the spectral changes was shown to be dependent on the concentration of GSH (Figure 7.2A to C). The same experiments with the C38S variant were repeated under anaerobic conditions. Surprisingly, the spectral change in the C38S was not observed in the absence of oxygen even with the highest concentration of GSH or extended incubation time with GSH (Figure 7.2D).

To correlate the spectral changes due to the treatment of GSH with the structural change of the cytoglobin, the GSH treated C38S samples were analysed by mass spectrometry (Figure 7.3). Although the data from mass spectrometry show that a peak at 21965 Da, which is equivalent to C38S (21,388) + GSH (307) arises in response to the treatment of GSH indicating a formation of protein mixed disulphide, the intensity of the original peak of C38S variant at 21,388 Da only contributes to a very small fraction of the protein samples in which

it is dominated by four major peaks at 21420, 21524, 21603 and 21707, respectively. Some of the peaks, for example the peak at 21,420 (which is equivalent to Cys38 (21,388) with a persulfide (+32) and the peak at 21603 (which is equivalent to 21420 with an unknown adduct (+183)), reduce in intensity in response to GSH treatment while some of them do not (e.g. the peak at 21,524 Da (which is believed to be a modified C38S (21,388) by monopotassium phosphate (+136); and the peak at 21707 Da (Figure 7.3). Interpretation of the results from mass spectrometry has proven to be problematic with those unknown adducts. Nevertheless, the results suggest that the active species that responds to GSH treatment is the cysteine persulfide rather than free thiol in the cysteine residue. It is not clear whether persulfide formation at the cysteine residue could occur naturally. The modification by GSH still needs to be examined carefully under better controlled conditions, including using an alternative buffer system that does not modify the protein.

Although the detailed mechanism of such modification of the Cys83 residue is not defined yet, it has been widely suggested that the deprotonated thiol (i.e thiolate) could be directly modified by GSSG or by oxidative modification from reactive oxygen or nitrogen species followed by a nucleophilic attack from GSH to form a protein mixed disulphide (Grek et al., 2013). How exactly the consequence of such modification would alter the function of cytoglobin is unknown. However, a significant increase in ligand accessibility is observed when compared with the scenario where the disulphide bond is intact, which implied that the S-glutathionylation of the Cys83 residue would alter the enzymatic properties of cytoglobin.

Therefore, a site specific S-glutathionylation of cytoglobin at the Cys83 residues could still be a possible mechanism to activate cytoglobin as a stress responsive protein under cellular stress conditions. Perhaps, future studies should first optimise the experimental conditions, for examples the buffer systems and the oxygen level, to define the consequence

of such modification to the heme local environment. Also, ligand binding properties of GSH treated cytoglobin in the ferrous state may have to be examined in order to prove the effect of modification of Cys83 residue to the cellular functions of cytoglobin in a more physiological relevant redox state.

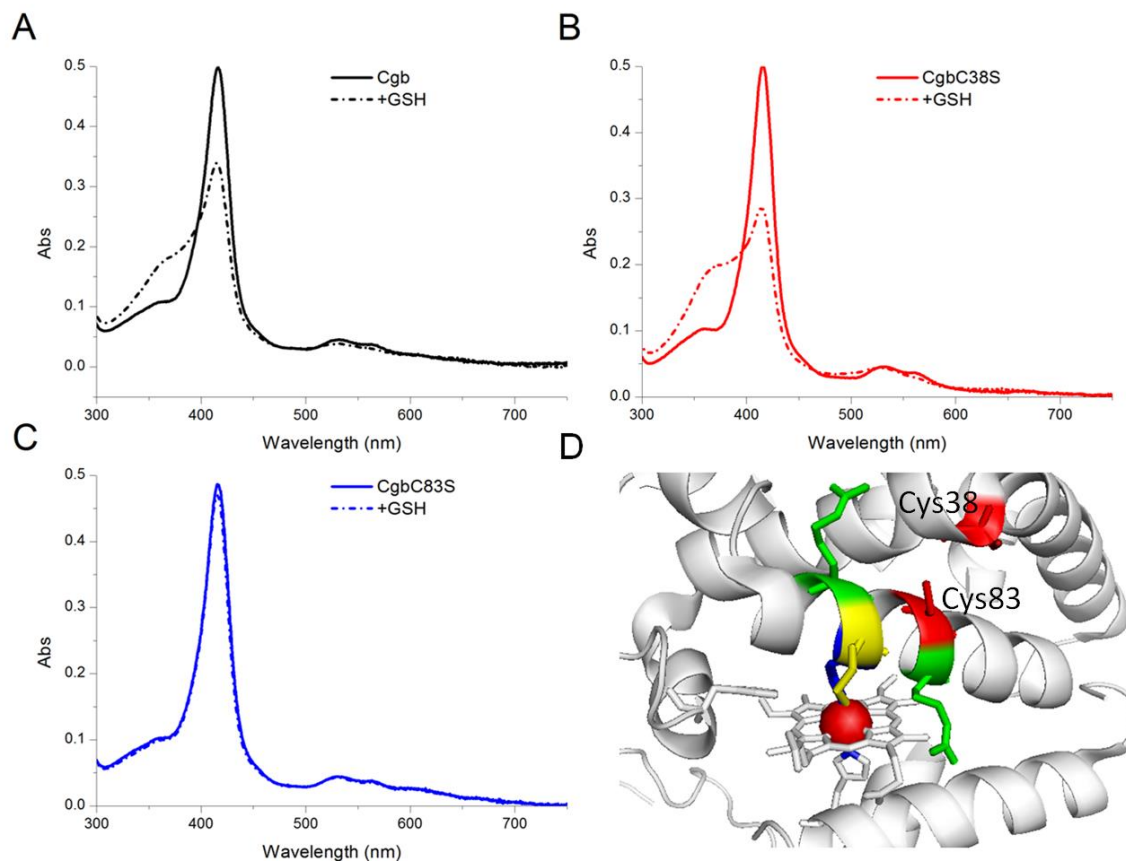


**Figure 7.1 Site-specific modification of cytoglobin by GSH.** (A) 25  $\mu$ M of wild-type cytoglobin was incubated with 50 mM GSH in 20 mM sodium phosphate pH 7.0 (Black trace) (B) 25  $\mu$ M of C38S variant was incubated with 50 mM GSH in 20 mM sodium phosphate pH 7.0 (Red trace) (C) 25  $\mu$ M of C83S variant was incubated with 50 mM GSH in 20 mM sodium phosphate pH 7.0. Spectra were recorded before (solid trace) and 20 minutes after incubation (dot and dash trace). (D) X-ray structure of cytoglobin shows the basic residues - Arginine (green), histidine (blue), and Lysine (yellow), surrounding the cysteine residues (Red). (redrawn from PDB file 2DC3 using Pymol v1.3)

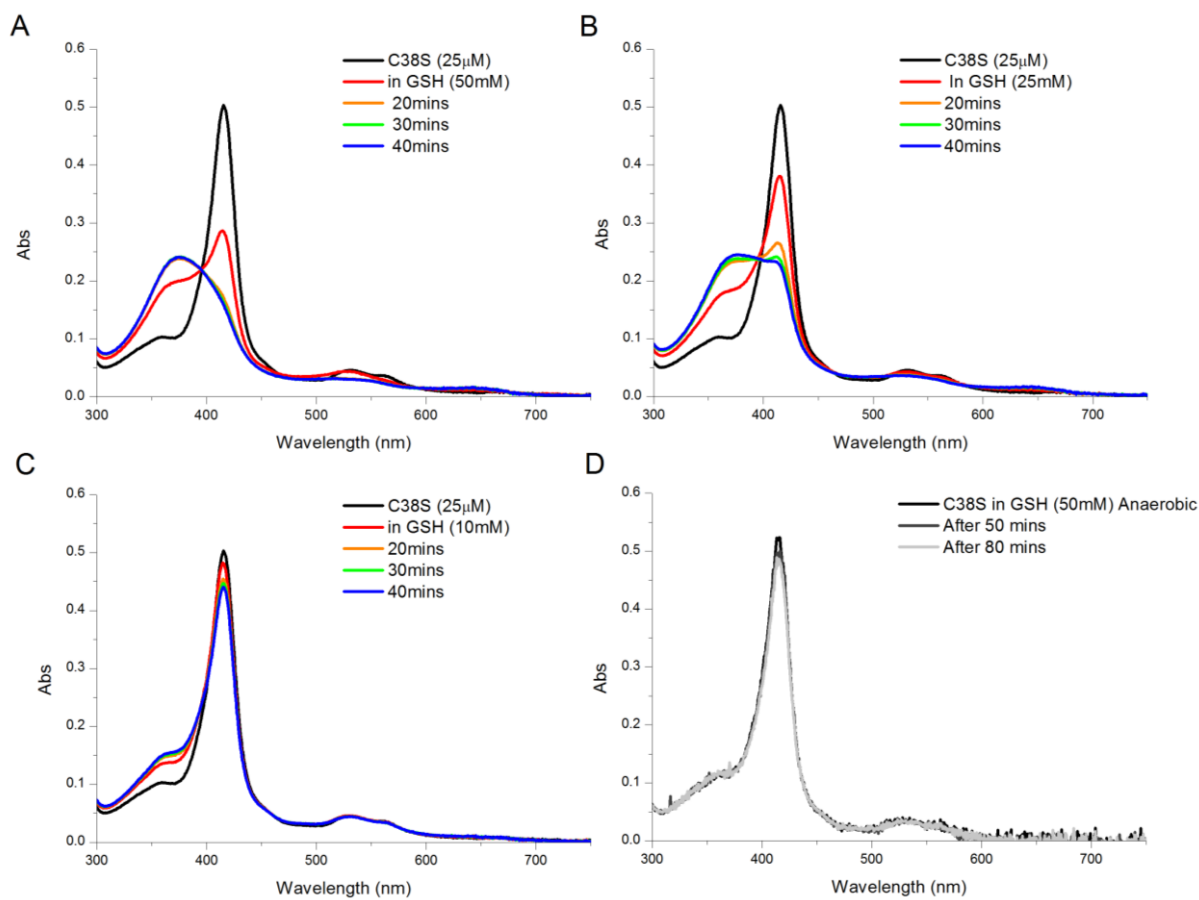


**Figure 7.2 Concentration- and oxygen-dependent modification of the C38S variant by GSH.** 25  $\mu$ M of C38S variant was treated with (A) 50 mM of GSH, (B) 25 mM of GSH, (C) 10 mM of GSH in 20 mM sodium phosphate pH7.0. (D) Same experiment with 50 mM of GSH was repeated in the absence of oxygen The spectrum was recorded every 10 minutes after incubation of the C38S variant with GSH in a total of 40 minutes.

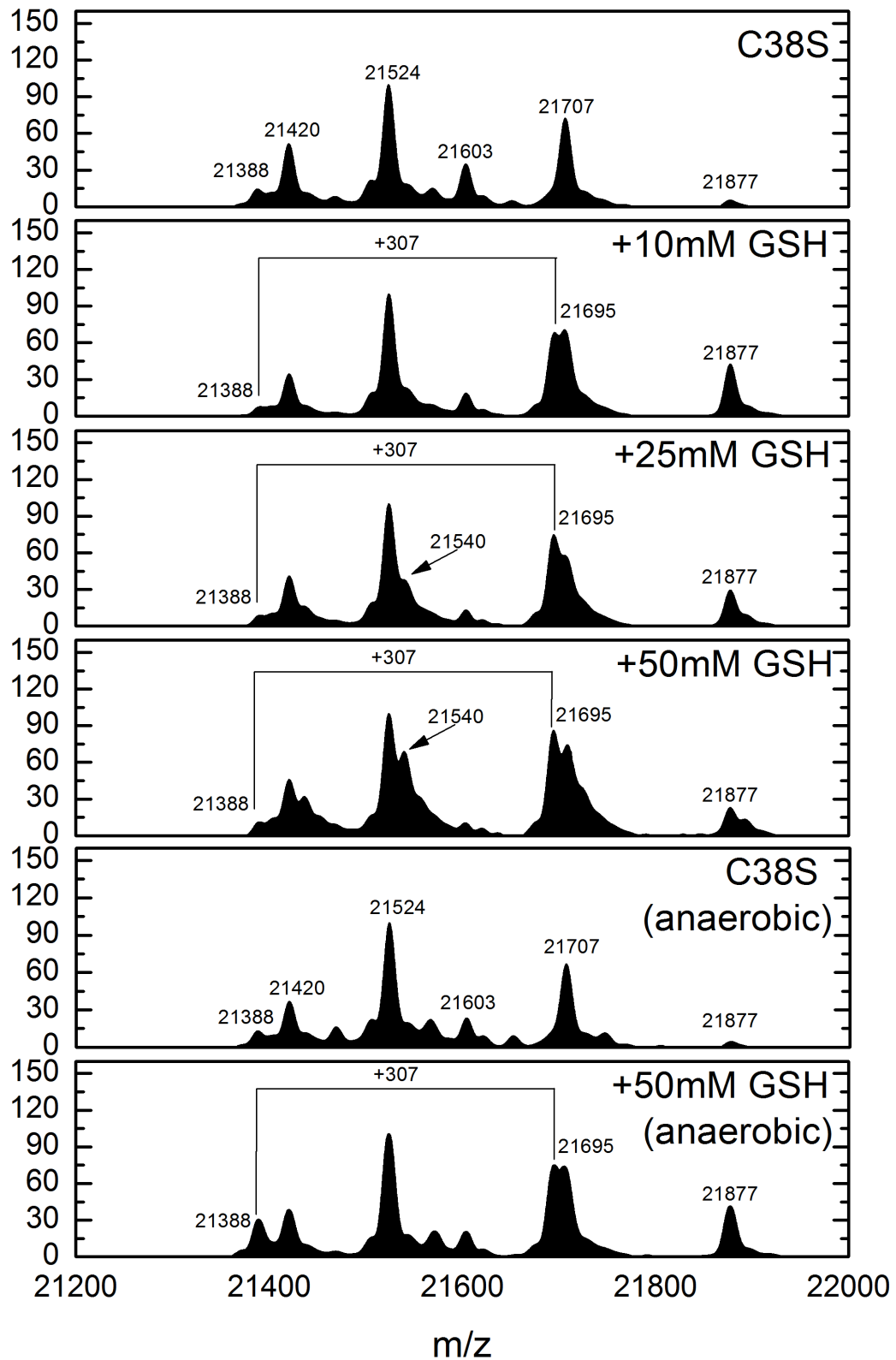


**Figure 7.3 Mass spectrometry of the S-glutathionylation of Cys83 residue.** Samples of C38S variant treated with GSH at various concentrations (10 mM, 25 mM and 50 mM) in the presence or absence of air were analysed by LCMS.

### 7.3 Role of Cytoglobin in Metastasis

The role of cytoglobin in cancer is still not fully understood as it seems to play a role in both tumour suppression and tumour promotion in response to the stress conditions in the cancer cells (Oleksiewicz et al., 2013). It has been well established that *CYGB* gene expression is down-regulated in a number of cancers, including esophageal cancer (McRonald et al, 2006), non small cell lung cancer (Xinarianos et al., 2006), breast cancer (Shivapuraker et al., 2008), head and neck cancer (Shaw et al., 2009) and renal cell carcinoma (Gorr et al., 2011) due to hyper-methylation at its promoter region. Furthermore, *CYGB* gene has been shown to be up-regulated in cancer cells by hypoxia (Shaw et al., 2009) which is in concordance with the proposed role in stress-response in the cells. However, in the context of tumour hypoxia, cytoglobin might exert its function beyond a stress-responsive protein.

Tumour hypoxia is a very common condition in solid tumours and it has also been considered as a crucial driving factor for promoting metastasis (Semenza, 2012). For cancer cells of epithelium origin (i.e. carcinoma) to initiate metastasis, the cells must go through a process called “epithelial-to-mesenchymal transition, or EMT, in order to gain motility, invasiveness for metastasis. One of the important events during the EMT is extracellular matrix remodelling in which the composition of the extracellular matrix where the cancer cells is embedded in is modified to facilitate the migration of the cancer cells (Kalluri and Weinburg, 2009). Hypoxia-driven metastasis has been demonstrated to regulate extracellular remodelling by modulating the expression of procollagen hydroxylase, including prolyl hydroxylase P4HA1 and P4HA2 (Gilkes et al., 2013a) as well as lysyl hydroxylase (Gilkes et al., 2013b), which leads to abnormal collagen deposition in the extracellular matrix.

A relationship has been drawn between cytoglobin and extracellular matrix since it was first discovered in hepatic stellate cells in fibrotic liver where excessive deposition of

extracellular matrix is correlated with disease progression (Kawada et al., 2001). Interestingly, in search for cytoglobin's tumour suppressive role, Shivapuraker and colleagues identified several downstream target genes that are regulated in response to the over-expression of *CYGB* gene which implicates an unexpected gene regulation role in the cytoglobin signalling pathway. One of the genes that is consistently down-regulated upon *CYGB* gene is type-1 collagen alpha-1 chain (*COL 1A1*) which is the major component of type-1 collagen in extracellular matrix. Furthermore, it has been demonstrated by Oleksiewics and colleagues that over-expression of *CYGB* gene in hypoxic lung cancer cells increases their migratory ability. Although the biochemical basis of how cytoglobin is involved in the synthesis of extracellular matrix is missing, it would still be tempting to speculate that cytoglobin could be involved in extracellular matrix remodelling in hypoxic cancer cells during EMT which could facilitate metastasis under hypoxia.

Understanding the mechanism of metastasis is of vital importance not only for the therapeutic purposes, but also for diagnostic and prognostic determination. Therefore, further studies regarding cytoglobin in the context of cancer, as suggested in chapter 6, should focus on examining the relationship between activation of *CYGB* gene and tumour progression and also the impact of targeting *CYGB* gene during metastasis. Moreover, the involvement in extracellular matrix remodelling should also be investigated. It is still unclear how *CYGB* gene is able to regulate gene expression of *COL 1A1* and other genes. It is known that no appreciable DNA-binding motif is found in cytoglobin. Hence, as we hypothesised that DNA binding may be achieved through other binding partner(s), protein-protein interaction studies, such as the one presented in chapter 6.2.4 where we observed a couple of potential interacting partner(s), should be employed to elucidate the molecular mechanisms of such regulation. Finally, the molecular mechanisms of how cytoglobin contributes to extracellular matrix remodelling, whether at the transcriptional level, translation or post-translation level should

also be investigated together with the impact on the composition of the extracellular matrix upon *CYGB* gene up-regulation.

## References:

Antonini, E., Brunori, M. (1971). Hemoglobin and Myoglobin in their reactions with ligands. North Holland Publishing Co., Amsterdam.

Appleby, C.A., Tjepkema, J.D., and Trinick, M.J. (1983). Hemoglobin in a nonleguminous plant, parasponia: possible genetic origin and function in nitrogen fixation. *Science* 220, 951-953.

Astudillo, L., Bernad, S., Derrien, V., Sebban, P., Miksovská, J. (2013). Reduction of the internal disulphide bond between cys38 and 83 switches the ligand migration pathway in cytoglobin. *J Inorg biochem* 129, 23-29

Basu, A., Drame, A., Muñoz, R., Gijssbers, R., Debyser, Z., De Leon, M., and Casiano, C.A. (2012). Pathway specific gene expression profiling reveals oxidative stress genes potentially regulated by transcription co-activator LEDGF/p75 in prostate cancer cells. *Prostate* 72, 597-611

Beckerson, P., Wilson, M.T., Svistunenko, D.A., and Reeder B.J. (2014). Cytoglobin ligand binding regulated by changing haem-coordination in response to intramolecular disulphide bond formation and lipid interaction. *Biochem J* 465, 127-137

Beckerson, P., Reeder, B.J., Wilson, M.T. (2015). Coupling of disulphide bond and distal histidine dissociation in human ferrous cytoglobin regulates ligand binding. *FEBS Letters*.

Bolognesi, M., Bordo, D., Rizzi, M., Tarricone, C., and Ascenzi, P. (1997). Nonvertebrate hemoglobins: structural bases for reactivity. *Prog Biophys Mol Biol* 68, 29-68

Burmester, T., Welch, B., Reinhardt, S., and Hankeln, T. (2000) A vertebrate globin expressed in the brain. *Nature* 407, 520-523

Burmester, T., Ebner, B., Weich, B., and Hankeln, T. (2002). Cytoglobin: a novel globin type ubiquitously expressed in vertebrate tissues. *Mol Biol Evol* 19, 416-421

Burmester, T., Haberkamp, M., Mitz, S., Roesner, A., Schmidt, M., Ebner, B., Gerlach, F., Fuchs, C., and Hankeln, T. (2004). Neuroglobin and cytoglobin: genes, proteins and evolution. *IUBMB Life* 56, 703-707

Burmester, T., Hankeln, T. (2014). Function and evolution of vertebrate globins. *Acta Physiologica* 211, 501-514

Carter, E.L., Ragsdale, S.W. (2014) Modulation of nuclear receptor function by cellular redox poise. *J Inorg Biochem* 133, 92-103

Cao, M., Westerhausen-Larson, A., Niyibizi, C., Kavalkovich, K., Georgescu, H.I., Rizzo, C.F., Hebda, P.A., Stefanovic-Racic, M., Evans, C.H. (1997). Nitric oxide inhibits the synthesis of type-II collagen without altering Col2A1 mRNA abundance: prolyl hydroxylase as a possible target. *Biochem. J* 324, 305-310

Cheesman, M.R., Greenwood, C., Thomon, A.J. (1991). Magnetic circular dichroism of hemoproteins. *Adv. in Inorg. Chem.* 36, 201-255

Cheesman, M.R., Watmough, N., J., Gennis, R.B., Greenwood, C., Thomson, A.J. (1994). Magnetic-circular-dichroism studies of *Escherichia coli* cytochrome bo. Identification of high-spin ferric, low-spin ferric and ferryl [Fe(IV)] forms of heme o. *Eur. J. Biochem* 219, 595-602

Cheesman, M., R. Watmough, N.J., Pires, C.A, Turner, R., Brittain, T., Gennis, R.B., Greenwood, C., Thompson, A.J. (1993). Cytochrome bo from *Escherichia coli*: identification of haem ligands and reaction of the reduced enzyme with carbon monoxide. *Biochem J.* 289, 709-718

Chen, C.A., Wang, T.Y., Varadharaj, S., Reyes, L.A., Hemannm C., Talukder, M.A., Chen, Y.R., Druhan, L.J., and Zweier, J.L. (2010) S-glutahtionylation uncouples eNOS and regulates its cellular and vascular function. *Nature* 468, 1115-1118

Chen, H.Y., Zhao, X., and Meng, D. (2014). Expression and biological role of cytoglobin in human ovarian cancer. *Tumor Biol* 35, 6933-6939

Christman, J.W., Blackwell, T.S., Juurlink, B.H.J. (2000). Redox regulation of nuclear factor kappa B: therapeutic potential for attenuating inflammatory responses. *Brain Pathology* 10, 153-162

Chua, P.J., Yip, G.W., and Bay, B.H. (2009). Cell cycle arrest induced by hydrogen peroxide is associated with modulation of oxidative stress related genes in breast cancer cells. *Exp Biol Med (Maywood)* 234, 1086-1094

Cockman, M.E., Masson, N., Mole, D.R., Jaakkola, P., Chang, G.W., Clifford, S.C., Maher, E.R., Pugh, C.W., Ratcliffe, P.J., and Maxwell, P.H. (2000). Hypoxia inducible factor- $\alpha$  binding and ubiquitylation by the von Hippel-Lindau tumor suppressor protein. *J Biol Chem* 275, 25733-25741

Cox, R. P., Hollaway, M. R. (1977). The reduction by dithionite of Fe(III) myoglobin derivatives with different ligands attached to the iron atom. *Eur. J. Biochem* 74, 575-587

de Sanctis, D., Dewilde, S., Pesce, A., Moens, L., Ascenzi, P., Hankeln, T., Burmester, T., and Bolognesi, M. (2004). Crystal structure of cytoglobin: the fourth globin type discovered in man displays heme hexa-coordination. *J Mol Biol* 336, 917-927

Dewilde, S., Kiger, L., Burmester, T., Hankeln, T., Baudin-Creuzat, V., Aerts, T., Marden, M.C., Caubergs, R., Moens, L. (2001) Biochemical characterization and ligand binding properties of neuroglobin, a novel member of the globin family. *J. Biol. Chem.* 276, 38949-38955

Dhawan, I.K., Shelver, D., Thorsteinsson, M.V., Roberts, G.P., Johnson, M. K. (1999). Probing heme axial ligation in CO-sensing CooA Protein with magnetic circular dichroism spectroscopy. *Biochemistry* 38, 12805-12813

Doyle, M.P., Pickering, R.A., DeWeert, T.M., Hoekstra, J.W., Pate, D. (1981). Kinetics and mechanism of the oxidation of human deoxyhemoglobin by nitrites. *J Biol Chem* 256 (23) 12393-12398

Emara, M., Turner, A.R., and Allalunis-Turner, J. (2010). Hypoxic regulation of cytoglobin and neuroglobin expression in human normal and tumor tissues. *Cancer Cell Int* 10, 33

Esteban, M.A., Tran, M.G., Harten, S.K., Hill, P., Castellanos, M.C., Chandra, A., Raval, R., O'brien, T.S., and Maxwell, P.H. (2006). Regulation of E-cadherin expression by VHL and hypoxia-inducible factor. *Cancer Res* 66, 3567-3575

Fago, A., Hundahl, C., Dewilde, S., Gilany, K., Moens, L., and Weber, R.E. (2004a). Allosteric regulation and temperature dependence of oxygen binding in human neuroglobin and cytoglobin. Molecular mechanisms and physiological significance. *J Biol Chem* 279, 44417-44426

Fago, A., Hundahl, C., Malte, H., and Weber, R.E. (2004b). Functional properties of neuroglobin and cytoglobin. Insights into the ancestral physiological roles of globins. *IUBMB*

Flögel, U., Merx, M.W., Godecke, A., Decking, U.K., and Schrader, J. (2001). Myoglobin: A scavenger of bioactive NO. *Proc Natl Acad Sci U S A* 98, 735-740.

Fordel, E., Geuens, E., Dewilde, S., De Coen, W., and Moens, L. (2004a). Hypoxia/ischemia and the regulation of neuroglobin and cytoglobin expression. *IUBMB Life* 56, 681-687

Fordel, E., Geuens, E., Dewilde, S., Rottiers, P., Carmeliet, P., Grooten, J., and Moens, L. (2004b). Cytoglobin expression is upregulated in all tissues upon hypoxia: an in vitro and in vivo study by quantitative real-time PCR. *Biochem Biophys Res Commun* 319, 342-348

Fordel, E., Thijs, L., Martinet, W., Schrijvers, D., Moens, L., and Dewilde, S. (2007). Anoxia or oxygen and glucose deprivation in SH-SY5Y cells: a step closer to the unraveling of neuroglobin and cytoglobin functions. *Gene* 398, 114-122

Forsythe, J.A., Jiang, B.H., Iyer, N.V., Agan, F., Leung, S.W., Koos, R.D., Semenza, G.L. (1996). Activation of vascular endothelial growth factor gene transcription by hypoxia-inducible factor 1. *Mol Cell Biol* 16, 4604-4613

Gabba, M., Abbruzzetti, S., Spyrakis, F., Forti, F., Bruno, S., Mozzarelli, A., Luque F.J., Viappiani, C., Cozzini, P., Nardini, M., Germani, F., Bolognesi, M., Moens, L., Dewilde, S. (2013). CO rebinding kinetics and molecular dynamics simulations highlight dynamic regulation of internal cavities in human cytoglobin. *PLOS One* 8(1), e49770

Gardner, A.M., Cook, M.R., and Gardner, P.R. (2010). Nitric-oxide dioxygenase function of human cytoglobin with cellular reductants and in rat hepatocytes. *J Biol Chem* 285, 23850-23857

Gardner, P.R., Martin, L.A., Hall, D., and Gardner, A.M. (2001). Dioxygen-dependent metabolism of nitric oxide in mammalian cells. *Free Radic. Biol Med.* 31, 191-204.

Geuens, E., Brouns, I., Flamez, D., Dewilde, S., Timmermans, J.P., Moens, L. (2003). A globin in the nucleus! *J Biol Chem* 278, 30417-30420

Gorr, T.A., Wichmann, D., Pilarsky, C., Theurillat, J.P., Fabrizius, A., Laufs, T., Bauer, T., Koslowski, M., Horn, S., Burmester, T., *et al.* (2011). Old proteins - new locations: myoglobin, haemoglobin, neuroglobin and cytoglobin in solid tumours and cancer cells. *Acta Physiol (Oxf)*

202, 563-581

Gilkes, D.M., Chaturvedi, P., Bajpai, D., Wong, C.C., Wei, H., Pitcairn, S. et al. (2013a). Collagen prolyl hydroxylases are essential for breast cancer metastasis. *Cancer Res* 73, 3285-3296

Gilkes, D.M., Bajpai, D., Wong, C.C., Chaturvedi, P., Hubbi, M.E., Wirtz, D. et al. (2013b). Procollagen lysyl hydroxylase 2 is essential for hypoxia-induced breast cancer metastasis. *Mol Cancer Res* 11, 456-466

Gilmore, T.D. (2006). Introduction to NF- $\kappa$ B: players, pathways perspectives. *Oncogene* 25, 6680-6684

Grek, C.L., Zhang, J., Manevich, Y., Townsend, D.M., Tew, K.D. (2013). Cause and consequences of cysteine s-glutathionylation. *J Biol Chem* 288, 26497-26504

Guo, X., Philipsen, S., and Tan-Un, K.C. (2006). Characterization of human cytoglobin gene promoter region. *Biochim Biophys Acta* 1759, 208-215

Guo, X., Philipsen, S., and Tan-Un, K.C. (2007). Study of the hypoxia-dependent regulation of human CYGB gene. *Biochem Biophys Res Commun* 364, 145-150

Halligan, K.E., Jourd'heuil, F.L., and Jourd'heuil, D. (2009). Cytoglobin is expressed in the vasculature and regulates cell respiration and proliferation via nitric oxide dioxygenation. *J Biol Chem* 284, 8539-8547

Hamdane, D., Kiger, L., Dewilde, S., Green, B.N., Pesce, A., Uzan, J., Burmester, T., Hankeln, T., Bolognesi, M., Moens, L., et al. (2003). The redox state of the cell regulates the ligand binding affinity of human neuroglobin and cytoglobin. *J Biol Chem* 278, 51713-51721

Hardison, R. (1998). Hemoglobins from bacteria to man: evolution of different patterns of gene expression. *J Exp Biol* 201, 1099-1117

Hardison, R.C. (1996). A brief history of hemoglobins: plant, animal, protist, and bacteria. *Proc Natl Acad Sci U S A* 93, 5675-5679

Hayashi, M., Sakata, M., Takeda, T., Yamamoto, T., Okamoto, Y., Sawada, K., Kimura, A., Minekawa, R., Tahara, M., Tasaka, K., Murata, Y. (2004). Induction of glucose transporter 1

expression through hypoxia-inducible factor 1 $\alpha$  under hypoxic conditions in trophoblast-derived cells. *J Endocrinol* 183, 145-154

Hodges, N.J., Innocent, N., Dhanda, S., and Graham, M. (2008). Cellular protection from oxidative DNA damage by over-expression of the novel globin cytoglobin in vitro. *Mutagenesis* 23, 293-298

Huang, Z., Shiva, S., Kim-Shapiro, D.B., Patel, R.P., Ringwood, L.A., Irby, C.E., Huang, K.T. et al. (2005). Enzymatic function of hemoglobin as a nitrite reductase that produces NO under allosteric control. *J. Clin. Invest.* 115, 2099-2107

Hunt, P.W., Klok, E.J., Trevaskis, B., Watts, R.A., Ellis, M.H., Peacock, W.J., and Dennis, E.S. (2002). Increased level of hemoglobin 1 enhances survival of hypoxic stress and promotes early growth in *Arabidopsis thaliana*. *Proc Natl Acad Sci U S A* 99, 17197-17202

Kakar, S., Hoffman, F. G., Storz, J. F., Fabian, M., Hargrove, M. S. (2010). Structure and reactivity of hexacoordinate hemoglobins. *Biophysical chemistry* 152, 1-14

Kalluri, R. Weinberg, R.A. (2009) The basics of epithelial-mesenchymal transition. *J. Clin. Invest.* 119, 1420–1428

Kawada, N., Kristensen, D.B., Asahina, K., Nakatani, K., Minamiyama, Y., Seki, S., and Yoshizato, K. (2001). Characterization of a stellate cell activation-associated protein (STAP) with peroxidase activity found in rat hepatic stellate cells. *J Biol Chem* 276, 25318-25323

Kemp, M., Go, Y., Jones, D.R. (2008). Nonequilibrium thermodynamics of thiol/disulphide redox systems: A perspective on redox systems biology. *Free Radic. Biol. Med.* 44, 921-937

Kil, I.S., Shin, S.W., and Park, J.W. (2012). S-glutathionylation regulates GTP-binding of Rac2. *Biochem. Biophys. Res. Commun.* 425, 892-896

Kundu, S., Trent, J.T., and Hargrove, M.S. (2003). Plants, humans and hemoglobins. *Trends Plant Sci* 8, 387-393

Lando, D., Peet, D.J., Gorman, J.J., Whelan, D.A., Whitelaw, M.L., and Bruick, R.K. (2002). FIH-1 is an asparaginyl hydroxylase enzyme that regulates the transcriptional activity of hypoxia-inducible factor. *Genes Dev* 16, 1466-1471

Langan, J.E., Cole, C.G., Huckle, E.J., Byrne, S., McDonald, F.E., Rowbottom, L., Ellis, A., Shaw, J.M., Leigh, I.M., Kelsell, D.P., *et al.* (2004). Novel microsatellite markers and single nucleotide polymorphisms refine the tylosis with oesophageal cancer (TOC) minimal region on 17q25 to 42.5 kb: sequencing does not identify the causative gene. *Hum Genet* 114, 534-540

Lechauve, C., Chauvierre, C., Dewilde, S., Moens, L., Green, B.N., Marden, M.C., Célier, C., and Kiger, L. (2010). Cytochrome conformations and disulphide bond formation. *FEBS J* 277, 2696-2704

Li, D., Chen, X.Q., Li, W.J., Yang, Y.H., Wang, J.Z., and Yu, A.C. (2007). Cytochrome up-regulated by hydrogen peroxide plays a protective role in oxidative stress. *Neurochem Res* 32, 1375-1380

Li, H., Hemann, C., Abdelghany, T.M., El-Mahdy, M.A., Zweier, J.L. (2012). Characterization of the mechanism and magnitude of cytochrome-mediated nitrite reduction and nitric oxide generation under anaerobic conditions. *J. Biol Chem* 287, 36623-36633

Li, R.C., Lee, S.K., Pouranfar, F., Brittan, K.R., Clair, H.B., Row, B.W., Wang, Y., and Gozal, D. (2006). Hypoxia differentially regulates the expression of neuroglobin and cytochrome in rat brain. *Brain Res* 1096, 173-179

Liu, X., Follmer, D., Zweier, J.R., Huang, X., Hemann, C., Liu, K., Druhan, L.J., and Zweier, J.L. (2012). Characterization of the function of cytochrome as an oxygen-dependent regulator of nitric oxide concentration. *Biochemistry* 51, 5072-5082

Liu, X., Tong, J., Zweier J.R., Follmer, D., Hemann, C., Ismail R.S. and Zweier, J.L. (2013). Differences in oxygen-dependent nitric oxide metabolism by cytochrome and myoglobin account for their differing functional roles. *FEBS J* 280, 3621-3631

Loboda, A., Jozkowicz, A., and Dulak, J. (2010). HIF-1 and HIF-2 transcription factors--similar but not identical. *Mol Cells* 29, 435-442

Makino, M., Sawai, H., Shiro, Y., Sugimoto H. (2011). Crystal structure of the carbon monoxide complex of human cytochrome. *Proteins: Structure, Function and Bioinformatics* 79, 1143-1153

Makino, M., Sugimoto, H., Sawai, H., Kawada, N., Yoshizato, K., and Shiro, Y. (2006). High-

resolution structure of human cytoglobin: identification of extra N- and C-termini and a new dimerization mode. *Acta Crystallogr D Biol Crystallogr* 62, 671-677

Mammen, P.P., Shelton, J.M., Ye, Q., Kanatous, S.B., McGrath, A.J., Richardson, J.A., and Garry, D.J. (2006). Cytoglobin is a stress-responsive hemoprotein expressed in the developing and adult brain. *J Histochem Cytochem* 54, 1349-1361

Man, K.N., Philipsen, S., and Tan-Un, K.C. (2008). Localization and expression pattern of cytoglobin in carbon tetrachloride-induced liver fibrosis. *Toxicol Lett* 183, 36-44

Maxwell, P.H., Wiesener, M.S., Chang, G.W., Clifford, S.C., Vaux, E.C., Cockman, M.E., Wykoff, C.C., Pugh, C.W., Maher, E.R., and Ratcliffe, P.J. (1999). The tumour suppressor protein VHL targets hypoxia-inducible factors for oxygen-dependent proteolysis. *Nature* 399, 271-275

Mayhew, S.G. (1978). The redox potential of dithionite and SO<sub>2</sub>; from equilibrium reactions with flavodoxins, methyl viologen and hydrogen plus hydrogenase. *Eur. J. Biochem* 85, 535-547

McLysaght, A., Hokamp, K., and Wolfe, K.H. (2002). Extensive genomic duplication during early chordate evolution. *Nat Genet* 31, 200-204

McDonald, F.E., Liloglou, T., Xinarianos, G., Hill, L., Rowbottom, L., Langan, J.E., Ellis, A., Shaw, J.M., Field, J.K., and Risk, J.M. (2006). Down-regulation of the cytoglobin gene, located on 17q25, in tylosis with oesophageal cancer (TOC): evidence for trans-allele repression. *Hum Mol Genet* 15, 1271-1277

McDonald, F.E., Risk, J.M., and Hodges, N.J. (2012). Protection from intracellular oxidative stress by cytoglobin in normal and cancerous oesophageal cells. *PLoS One* 7, e30587

Mimura, I., Nangaku, M., Nishi, H., Inagi, R., Tanaka, T., and Fujita, T. (2010). Cytoglobin, a novel globin, plays an antifibrotic role in the kidney. *Am J Physiol Renal Physiol* 299, F1120-1133

Nakatani, K., Okuyama, H., Shimahara, Y., Saeki, S., Kim, D.H., Nakajima, Y., Seki, S., Kawada, N., and Yoshizato, K. (2004). Cytoglobin/STAP, its unique localization in splanchnic fibroblast-like cells and function in organ fibrogenesis. *Lab Invest* 84, 91-101

Oikawa, T. (2004) ETS transcription factors: Possible target for cancer therapy. *Cancer Sci* 95, 626-633

Oleksiewicz, U., Liloglou, T., Field, J.K., and Xinarianos, G. (2011). Cytoglobin: biochemical, functional and clinical perspective of the newest member of the globin family. *Cell Mol Life Sci* 68, 3869-3883

Oleksiewicz, U., Liloglou, T., Tasopoulou, K., Daskoulidou, N., Bryan, J., Gosney, J.R., Field, J.K., Xinarianos, G. (2013). Cytoglobin has bimodal: tumour suppressor and oncogene functions in lung cancer cell lines. *Hum Mol Genet* 22(16): 3207-3217

Ostojčić, J., Sakaguchi, D.S., de Lathouder, Y., Hargrove, M.S., Trent, J.T., Kwon, Y.H., Kardon, R.H., Kuehn, M.H., Betts, D.M., and Grozdanić, S. (2006). Neuroglobin and cytoglobin: oxygen-binding proteins in retinal neurons. *Invest Ophthalmol Vis Sci* 47, 1016-1023

Perissionotti, L., Matri, M. A., Doctorovich, F., Luque, F.J., Estrin, D.A. (2008). A Microscopic study of the deoxyhemoglobin-catalyzed generation of nitric oxide from nitrite anion. *Biochemistry* 47, 9793-9802

Perutz M.F. (1979). Regulation of oxygen affinity of hemoglobin: influence of structure of the globin on the heme iron. *Annu Rev Biochem* 48, 327–386

Perutz, M.F. (1990). Mechanisms regulating the reactions of human hemoglobin with oxygen and carbon monoxide. *Annu Rev Physiol* 52, 1–25

Pesce, A., Bolognesi, M., Bocedi, A., Ascenzi, P., Dewilde, S., Moens, L., Hankeln, T., and Burmester, T. (2002). Neuroglobin and cytoglobin. Fresh blood for the vertebrate globin family. *EMBO Rep* 3, 1146-1151

Quillin, M.L., Arduini, R.M., Olson, J.S., Philips, G. N., Jr (1993). High-resolution crystal structures of distal histidine mutants of sperm whale myoglobin. *J. Mol. Biol.* 234, 140–155

Ragsdale, S.W. and Li, Y. (2011). Thiol/disulphide redox switches in the regulation of heme binding to proteins. *Antioxidants & redox signaling* 14, 1039-1047

Sawai, H., Kawada, N., Yoshizato, K., Nakajima, H., Aono, S., and Shiro, Y. (2003). Characterization of the heme environmental structure of cytoglobin, a fourth globin in humans.

Schafer, F.Q., Buettner, G.R. (2001). Redox environment of the cell as viewed through the redox state of the glutathione disulphide/glutathione couple. *Free Radic. Biol. Med.* 30, 1191-1212

Schmidt, M., Gerlach, F., Avivi, A., Laufs, T., Wystub, S., Simpson, J.C., Nevo, E., Saaler-Reinhardt, S., Reuss, S., Hankeln, T., *et al.* (2004). Cytoglobin is a respiratory protein in connective tissue and neurons, which is up-regulated by hypoxia. *J Biol Chem* 279, 8063-8069

Schmidt, M., Giessl, A., Laufs, T., Hankeln, T., Wolfrum, U., and Burmester, T. (2003) How does the eye breathe? Evidence for neuroglobin-mediated oxygen supply in the mammalian retina. *J Biol Chem* 278, 1932-1935

Semenza, G.L. (2000). HIF-1 and human disease: one highly involved factor. *Genes Dev* 16, 1983-1991

Semenza, G.L. (2013). Hypoxia-inducible factors: mediators of cancer progression and targets for cancer therapy. *Trend Pharmacol Sci* 33, 207-214

Semenza, G.L., Neifelt, M.K., Chi, S.M., Antonarakis, S.E. (1991). Hypoxia-inducible nuclear factors bind to an enhancer element located 3' to the human erythropoietin gene. *Proc Natl Acad Sci USA* 88, 5680-5684

Shaw, R.J., Omar, M.M., Rokadiya, S., Kogera, F.A., Lowe, D., Hall, G.L., Woolgar, J.A., Homer, J., Liloglou, T., Field, J.K., *et al.* (2009). Cytoglobin is upregulated by tumour hypoxia and silenced by promoter hypermethylation in head and neck cancer. *Br J Cancer* 101, 139-144

Shigematsu, A., Adachi, Y., Matsubara, J., Mukaide, H., Koike-Kiryama, N., Minamino, K., Shi, M., Yanai, S., Imamura, M., Taketani, S., *et al.* (2008). Analyses of expression of cytoglobin by immunohistochemical studies in human tissues. *Hemoglobin* 32, 287-296

Shiva, S., Huang, Z., Grubina, R., Sun, J., Ringwood L.A, MacArthur P.H., Xu, X., Murphy, E., Darley-Usmar, V.M., Gladwin M.T., (2007). Deoxymyoglobin is a nitrite reductase that generates nitric oxide and regulates mitochondrial respiration. *Circ Res* 100, 654-661

Shivapurkar, N., Stastny, V., Okumura, N., Girard, L., Xie, Y., Prinsen, C., Thunnissen, F.B., Wistuba, I.I., Czerniak, B., Frenkel, E., *et al.* (2008). Cytoglobin, the newest member of the globin family, functions as a tumor suppressor gene. *Cancer Res* 68, 7448-7456

Silaghi-Dumitrescu, R., Svistunenko, D.A., Cioloboc, D., Bishchin, C., Scurtu, F., Cooper, C.E. (2014). Nitrite binding to globins: Linkage isomerism, EPR silence and reductive chemistry. *Nitric Oxide* 42, 32-39

Singh, S., Canseco, D.C., Manda, S.M., Shelton, J.M., Chirumamilla, R.R., Goetsch, S.C., Ye, Q., Gerard, R.D., Schneider, J.W., Richardson, J.A., Rothermel, B.A., and Mammen, P.P. (2014). Cytoglobin modulates myogenic progenitor cell viability and muscle regeneration. *Proc Natl Acad Sci USA* 111, E129–E138

Singh, S., Manda, S.M, Sikder, D., Birrer, M.J., Rothermel, B.A., Garry, D.G., and Mammen, P.P. (2009). Calcineurin activates cytoglobin transcription in hypoxic myocytes. *J Biol chem* 284, 10409-10421

Solomon, S.S., Majumdar, G., Martinez-Hernandez, A., Raghov, R. (2008). A critical role of Sp1 transcription factor in regulating gene expression in response to insulin and other hormones. *Life Science* 83, 305-312

Sowa, A.W., Duff, S.M., Guy, P.A., Hill, R.D. (1998). Altering hemoglobin levels changes energy status in maize cells under hypoxia. *Proc Natl Acad Sci USA* 95, 10317-10321

Sturms, R., DiSpirito, A.A., Hargrove, M.S. (2011). Plant and cyanobacterial hemoglobins reduce nitrite to nitric oxide under anoxic conditions. *Biochemistry* 50, 3873-3878

Springer, B.A. (1994). Mechanisms of ligand recognition in myoglobin. *Chemical reviews* 94, 699-714

Stagner, J.I., Parthasarathy, S.N., Wyler, K., and Parthasarathy, R.N. (2005). Protection from ischemic cell death by the induction of cytoglobin. *Transplant Proc* 37, 3452-3453

Sugase, K., Dyson, J.H., and Wright, P.E. (2007). Mechanism of coupled folding and binding of an intrinsically disordered protein. *Nature* 447, 1021–1025

Sugimoto, H., Makino, M., Sawai, H., Kawada, N., Yoshizato, K., and Shiro, Y. (2004). Structural basis of human cytoglobin for ligand binding. *J Mol Biol* 339, 873-885

- Tanaka, C., Coling, D.E., Manohar, S., Chen, G.D., Hu, B.H., Salvi, R., and Henderson, D. (2012). Expression pattern of oxidative stress and antioxidant defense-related genes in the aging Fischer 344/NHsd rat cochlea. *Neurobiol Aging* 33, 1842.e1841-1814
- Tejero, J., Sparacino-Watkins, C.E., Ragireddy, V., Frizzell, S., Gladwin, M.T. (2015). Exploring the mechanisms of the reductase activity of neuroglobin by site-directed mutagenesis of the heme distal pocket. *Biochemistry* 54, 722-733
- Tiso, M., Tejero, J., Kenney, C., Frizzell, S., Gladwin, M.T. (2012). Nitrite reductase activity of nonsymbiotic hemoglobins from *Arabidopsis thaliana*. *Biochemistry* 51, 5285-5292
- Tiso, M., Tejero, J., Basu, S., Azarov, I., Wang, X., Simplaceanu, V., Frizzell, S., Jayaraman, T., Geary, L., Shapiro, C. et al., (2011). Human neuroglobin functions as a redox-regulated nitrite reductase. *J. Biol Chem* 286, 18377-18289
- Trandafir, F., Hoogewijs, D., Altieri, F., Rivetti di Val Cervo, P., Ramser, K., Van Doorslaer, S., Vanfleteren, J.R., Moens, L., Dewilde, S. (2007). Neuroglobin and cytoglobin as potential enzyme or substrate, *Gene* 398, 103-113
- Trent, J.T., III., Hvitved, A.N., and Hargrove, M. S. (2001). Model for ligand binding to hexacoordinate hemoglobins. *Biochemistry* 40, 6155-6163
- Trent, J.T., III., and Hargrove, M.S. (2002). A ubiquitously expressed human hexacoordinate hemoglobin. *J Biol Chem* 277, 19538-19545
- Tsujino, H., Yamashita, T., Nose, A., Kukino, K, Sawai, H., Shiro, Yoshitsugu. and Uno, T. (2014). Disulphide bonds regulate binding of exogenous ligand to human cytoglobin. *J Inorg Biochem* 135, 20-27
- Vanharanta, S., Shu, W., Brenet, F., Hakimi, A.A., Heguy, A., Viale, A., Reuter V.E., Hsieh, J.J., Scandura J.M., and Massague, J. (2013). Epigenetic expansion of VHL-HIF signal output drives multiorgan metastasis in renal cancer. *Nat Med* 19, 50-56
- Vinck, E., Van Doorslaer, S., Dweilide, S. and Moens, L. (2004) Structural change of heme pocket due to disulphide bridge formation is significantly larger for neuroglobin than for cytoglobin. *J. Am. Chem. Soc* 126, 4516-4517

Vinogradov, S.N., and Moens, L. (2008). Diversity of globin function: enzymatic, transport, storage, and sensing. *J Biol Chem* 283, 8773-8777

Wanat, A., Gdula-Argasinska, J., Rutkowska-Zbik, D., Witko, M., Stochel, G., van Eldik, R. (2002). Nitrite binding to metmyoglobin and methemoglobin in comparison to nitric oxide binding. *Journal of biological inorganic chemistry : JBIC : a publication of the Society of Biological Inorganic Chemistry* 7, 165-176.

Wang, G.L., Jiang, B.H., Rue, E.A., and Semenza, G.L. (1995). Hypoxia-inducible factor 1 is a basic-helix-loop-helix-PAS heterodimer regulated by cellular O<sub>2</sub> tension. *Proc Natl Acad Sci U S A* 92, 5510-5514

Weber, R.E., and Fago, A. (2004). Functional adaptation and its molecular basis in vertebrate hemoglobins, neuroglobins and cytoglobins. *Respir Physiol Neurobiol* 144, 141-159

Weber, R.E., and Vinogradov, S.N. (2001). Nonvertebrate hemoglobins: functions and molecular adaptations. *Physiol Rev* 81, 569-628

Wittenberg, B.A., and Wittenberg, J.B. (1989). Transport of oxygen in muscle. *Annu Rev Physiol* 51, 857-878

Wystub, S., Ebner, B., Fuchs, C., Weich, B., Burmester, T., and Hankeln, T. (2004). Interspecies comparison of neuroglobin, cytoglobin and myoglobin: sequence evolution and candidate regulatory elements. *Cytogenet Genome Res* 105, 65-78

Xinarianos, G., McDonald, F.E., Risk, J.M., Bowers, N.L., Nikolaidis, G., Field, J.K., and Liloglou, T. (2006). Frequent genetic and epigenetic abnormalities contribute to the deregulation of cytoglobin in non-small cell lung cancer. *Hum Mol Genet* 15, 2038-2044

Xu, R., Harrison, P.M., Chen, M., Li, L., Tsui, T.Y., Fung, P.C., Cheung, P.T., Wang, G., Li, H., Diao, Y., *et al.* (2006). Cytoglobin overexpression protects against damage-induced fibrosis. *Mol Ther* 13, 1093-1100

Yi, J., Heinecke, J., Tan, H., Ford, P.C., Richter-Addo, G.B. (2009). The distal pocket histidine residues in horse heart myoglobin directs the o-binding more of nitrite to the heme iron. *J. Am. Chem. Soc.* 131, 18119-18128

Yi, J. Richter-Addo, G.B. (2012). Unveiling the three-dimensional structure of green pigment of nitrite-cured meat. *Chem Commun* 48, 4172-4174

Zhou, H., Zarubin, B., Ji, Z., Min, Z., Zhu, W., Downey, J.S., Lin, S., Han, J. (2005). Frequency and distribution of AP-1 sites in the human genome. *DNA Research* 12, 139-150

## Appendix

**Ct values of gene expressions in RCC4 cells treated with demethylation drugs measured by qRT-PCR**

### 1. *CYGB*

Sample Name	Ct Value	Ct - 18s Ct
RCC4 WTHA4 (1)	32.27887	20.34508705
RCC4 WTHA4 (2)	31.64279	19.92982006
RCC4 WTHA4 (3)	32.09498	20.45559883
RCC4 WTHA4 (4)	31.94003	20.36570645
RCC4 WTHA4 + 5uM Decatabine (1)	29.4586	17.65101719
RCC4 WTHA4 + 5uM Decatabine (2)	29.48165	17.95264817
RCC4 WTHA4 + 5uM Decatabine (3)	29.35726	17.79550362
RCC4 WTHA4 + 5uM Decatabine (4)	29.47258	18.27307606
RCC4 VHA (1)	32.47266	21.18318271
RCC4 VHA (2)	32.24973	21.0293026
RCC4 VHA (3)	32.46342	21.21097183
RCC4 VHA (4)	32.69966	21.6065855
RCC4 VHA + 5uM Decatabine (1)	30.55797	19.30465221
RCC4 VHA + 5uM Decatabine (2)	30.67647	18.8248396
RCC4 VHA + 5uM Decatabine (3)	30.48902	19.0405159
RCC4 VHA + 5uM Decatabine (4)	31.10179	18.702178

### 2. *VHL*

Sample Name	CT Value	CT - 18s CT
RCC4 WTHA4 (1)	33.8781	21.94431114
RCC4 WTHA4 (2)	28.86222	17.14924907
RCC4 WTHA4 (3)	29.88231	18.24293137
RCC4 WTHA4 (4)	28.79623	17.22190762
RCC4 WTHA4 + 5uM Decatabine (1)	27.52378	15.71620464
RCC4 WTHA4 + 5uM Decatabine (2)	27.14435	15.61534882
RCC4 WTHA4 + 5uM Decatabine (3)	27.4621	15.90034867
RCC4 WTHA4 + 5uM Decatabine (4)	27.31911	16.11959935
RCC4 VHA (1)	27.68136	16.39188099

RCC4 VHA (2)	27.39564	16.17520523
RCC4 VHA (3)	27.36579	16.11334038
RCC4 VHA (4)	27.11923	16.02615452
RCC4 VHA + 5uM Decatabine (1)	28.63802	17.38470363
RCC4 VHA + 5uM Decatabine (2)	27.95303	16.10140324
RCC4 VHA + 5uM Decatabine (3)	27.55621	16.10770416
RCC4 VHA + 5uM Decatabine (4)	29.14828	16.74866962

### 3. HIF-1 $\alpha$

Sample Name	CT Value	CT - 18s CT
RCC4 WTHA4 (1)	21.93691	10.00312615
RCC4 WTHA4 (2)	22.20408	10.49111461
RCC4 WTHA4 (3)	22.12986	10.49048233
RCC4 WTHA4 (4)	22.22961	10.65528965
RCC4 WTHA4 + 5uM Decatabine (1)	22.11476	10.30718136
RCC4 WTHA4 + 5uM Decatabine (2)	21.9542	10.42519188
RCC4 WTHA4 + 5uM Decatabine (3)	21.65179	10.09003449
RCC4 WTHA4 + 5uM Decatabine (4)	21.93015	10.73063755
RCC4 VHA (1)	23.11402	11.82453823
RCC4 VHA (2)	22.92858	11.70815278
RCC4 VHA (3)	22.37663	11.12417793
RCC4 VHA (4)	22.5813	11.4882288
RCC4 VHA + 5uM Decatabine (1)	22.67742	11.42410564
RCC4 VHA + 5uM Decatabine (2)	22.92299	11.07135678
RCC4 VHA + 5uM Decatabine (3)	23.07391	11.62540817
RCC4 VHA + 5uM Decatabine (4)	23.96527	11.56566143

### 4. GLUT-1

Sample Name	CT Value	CT - 18s CT
RCC4 WTHA4 (1)	34.67446	22.74067116
RCC4 WTHA4 (2)	28.91272	17.19975566
RCC4 WTHA4 (3)	28.58825	16.94887352
RCC4 WTHA4 (4)	27.82149	16.24716664
RCC4 WTHA4 + 5uM Decatabine (1)	27.2303	15.42271709

RCC4 WTHA4 + 5uM Decatabine (2)	27.01131	15.48230934
RCC4 WTHA4 + 5uM Decatabine (3)	26.93119	15.36943627
RCC4 WTHA4 + 5uM Decatabine (4)	27.27244	16.07293034
RCC4 VHA (1)	28.18745	16.89797687
RCC4 VHA (2)	28.50368	17.28325272
RCC4 VHA (3)	28.62141	17.36896133
RCC4 VHA (4)	27.98374	16.8906622
RCC4 VHA + 5uM Decatabine (1)	27.73214	16.47882747
RCC4 VHA + 5uM Decatabine (2)	28.00006	16.14843083
RCC4 VHA + 5uM Decatabine (3)	27.87942	16.43091583
RCC4 VHA + 5uM Decatabine (4)	28.17877	15.77915859

### 5. 18s (internal control)

Sample Name	CT Value
RCC4 WTHA4 (1)	11.93379
RCC4 WTHA4 (2)	11.71297
RCC4 WTHA4 (3)	11.63938
RCC4 WTHA4 (4)	11.57432
RCC4 WTHA4 + 5uM Decatabine (1)	11.80758
RCC4 WTHA4 + 5uM Decatabine (2)	11.529
RCC4 WTHA4 + 5uM Decatabine (3)	11.56176
RCC4 WTHA4 + 5uM Decatabine (4)	11.19951
RCC4 VHA (1)	11.28948
RCC4 VHA (2)	11.22043
RCC4 VHA (3)	11.25245
RCC4 VHA (4)	11.09308
RCC4 VHA + 5uM Decatabine (1)	11.25332
RCC4 VHA + 5uM Decatabine (2)	11.85163
RCC4 VHA + 5uM Decatabine (3)	11.44851
RCC4 VHA + 5uM Decatabine (4)	12.39961